Investigation of the role of mTORC1 and MAPK/ERK pathways in cellular responses to amino acid deprivation

Thesis submitted in accordance with the requirements of the University of Liverpool for the degree of Doctor in Philosophy (PhD)

by

Xiaomeng Wang

July 2018

Abstract

Sustaining proliferative signalling is one of the hallmarks of cancer. Cancer cells universally have high demands for nutrients to support their rapid proliferation. Studies presented in this thesis are focused on mTORC1 and MAPK/ERK signalling pathways, both of which promote cell growth and proliferation and are frequently found over-active in a wide range of cancer types, and their role in response to amino acid deprivation. mTORC1 activation requires GTP-bound Rheb and Rag GTPase-mediated lysosomal translocation. TSC2 inhibits mTORC1 by deactivating Rheb and it also undergoes lysosomal translocation. GCN2, a kinase that senses amino acid deficiency, has been identified as a novel regulator of mTORC1 signalling potentially by promoting the lysosomal translocation of TSC2, which inhibits mTORC1 additionally by preventing RagA from associating with lysosomes. We demonstrate that Rheb not only activates the catalytic activity of mTORC1 but also lysosomal translocation of both mTORC1 and TSC2. Therefore, these data suggest an alternative model of mTORC1 inhibition by amino acid deprivation. In addition, we demonstrate that the MAPK/ERK cascade contributes to ferroptosis, an oxidative non-apoptotic cell death, in response to deprivation of the amino acid cystine, via downregulating GPX4 and upregulating NOX4, enzymes known to scavenge and produce lipid ROS respectively. Based on this, amino acid cystine has been identified as a synthetic lethal target in NSCLC cells expressing an activated EGFR mutant, and pharmacological depletion of intracellular cystine using an engineered cystine-degrading enzyme efficiently suppresses tumour growth in a NSCLC xenograft model. These data therefore provide an approach that can be potentially exploited for cancer therapeutics.

Final word count: 42144

Acknowledgements

First and foremost, I would like to express my sincere gratitude to my supervisor Dr Nikolina Vlatković for the continuous support of my PhD study, for her patience, motivation, and immense knowledge. It was a great honour to have her as my supervisor after my previous supervisor Dr Richard Lamb left the University in May 2016. Her valuable guidance helped me in all the time of writing of this thesis. Her advice on both research as well as on my career have been priceless. I could not have imagined having a better supervisor for my PhD study. I would also like to thank my co-supervisor Prof Mark Boyd and my previous supervisor Dr Richard Lamb for their insightful comments and constructive suggestions, which were determinant for the accomplishment of the work presented in this thesis. I would specially like to thank Dr Ioannis Poursaitidis, my colleague and also my friend, for being a "big brother" to me both in the lab and in life, who had always encouraging words and was always ready to help me. I also want to thank Drs Carlos Rubbi, Shankar Varadarajan and Rebecca Lamond for their kind help and support with experiments.

I gratefully acknowledge the financial support for my PhD study from the North West Cancer Research Committee and the Institute of Translational Medicine.

A special thanks to my family, my parents and my sister for their unconditional support, encouragement and love, without which I would not have come this far. I would also like to thank my close friends for their unconditional friendship, support and patience throughout these years.

Declaration

This thesis is a result of my own work performed during the course of studies in the Department of Molecular and Clinical Cancer Medicine, Institute of Translational Medicine, University of Liverpool, between November 2014 and July 2018. All work described was performed by me unless clearly indicated. The thesis was written wholly by me under the valued guidance of my supervisor Dr Nikolina Vlatković.

List of Contents

List of Figures and Tables

List of Abbreviations

AGC	protein kinase A/protein kinase G/protein kinase C
AIF	apoptosis-inducing factor
AML	acute myeloid leukaemia
AMP	adenosine monophosphate
AMPK	AMP-activated protein kinase
Apaf1	apoptotic protease activating factor 1
APS	ammonium persulfate
Atg13	autophagy-related gene 13
ASS1	argininosuccinate synthetase 1
ATF4	activating transcription factor 4
ATM	ataxia-telangiectasia mutated
ATP	adenosine triphosphate
BH domain	Bcl-2 homology domain
BSA	albumin from bovine serum
BSO	buthionine sulfoximine
BRCA1	breast cancer 1
BRCA2	breast cancer 2
CAD	caspase-activated DNase
CNH	citron homology
COX2	cyclooxygenase-2
CST	Cell Signaling Technology
CRC	colorectal cancer
DA	DFG motif to AFG
delE746-A750	deletion of Leu-Arg-Glu at positions 747 to 749
Deptor	DEP-domain-containing mTOR-interacting protein
d.FBS	dialysed FBS
DFO	deferoxamine
DISC	death-inducing signalling complex
DMEM	Dulbecco's modified Eagle's medium
DMSO	dimethylsulfoxide
DNA	deoxyribonucleic acid

dNTP	deoxynucleotide
DPBS	Dulbecco's PBS
DTT	dithiothreitol
DsRed	red fluorescent protein
4E-BP1	eIF-4E-binding protein 1
ECL	enhanced chemilumescent
eEF2K	eukaryotic elongation factor 2 kinase
EF3	Elongation factor 3
EGF	epidermal growth factor
EGFR	epidermal growth factor receptor
eIF2	eukaryotic initiation factor 2
EIF2AK4	eIF2 alpha kinase 4 gene
eIF4B	eukaryotic translation initiation factor 4B
eIF4E	eukaryotic initiation factor 4E
Endo G	endonuclease G
ER	endoplasmic reticulum
ERK	extracellular-signal-regulated kinase
FACS	fluorescence-activated cell sorting
FADD	Fas-associating protein with death domain
Fas	first apoptosis signal receptor
FasL	Fas ligand
FBS	fetal bovine serum
FGF	fibroblast growth factor
Fip200	focal adhesion kinase family-interacting protein of 200kDa
FKBP	FK506-binding protein
FRAP	FKBP-rapamycin-associated protein
GAP	GTPase activating protein
GATOR	GAP activity toward Rags complexes
GCK	germinal-center kinase
GCN2	general control nonderepressible 2
GDP	guanosine diphosphate
GEF	guanine nucleotide exchange factor
GFP	green fluorescent protein

GLK	GCK)-like kinase
β-GP	β-Glycerophosphate disodium salt hydrate
G protein	guanine nucleotide-binding protein
GPX	glutathione peroxidase
Grb2	growth factor receptor-bound protein 2
GSH	reduced glutathione
GSSG	oxidized glutathione
GST	glutathione S-transferase
GTP	guanosine triphosphate
HA	haemagglutinin
HBXIP	C7orf59 and hepatitis B X-interacting protein
HEK	human embryonic kidney
HIF1α	hypoxia-inducible factor 1-alpha
HisRS	histidyl-tRNA synthetases
HME	human mammary epithelial
HO•	hydroxyl radicals
H_2O_2	hydrogen peroxide
HPLC	high-performance liquid chromatography
HRP	horseradish peroxidase
HtrA2	high temperature requirement protein A2
ICAD	inhibitor of CAD
IF	immunofluorescence
IP	Immunoprecipitation
IRS1	insulin receptor substrate 1
JACoP	Just Another Colocalisation Plugin
JNK	c-Jun amino-terminal kinase
LAMP2	lysosomal associated membrane protein 2
LAMTOR	MAPK and mTOR activator
LB	lysogeny broth
LC-MS	liquid chromatography-mass spectrometry
LDS	Lithium dodecyl sulfate
LiCl	lithium chloride
L-O•	lipid free radicals

LOOH	lipid peroxides
MAPK	mitogen-activated protein kinase
MAP4K3	Mitogen-activated protein kinase kinase kinase kinase 3
MBP	myelin basic protein
β-ME	β-Mercaptoethanol
MEF	mouse embryonic fibroblasts
MEM	minimum essential medium
MDCK	Madin-Darby Canine Kidney
MDM2	mouse double minute 2 homolog
mLST8	mammalian lethal with Sec13 protein 8
MP1	MAPK binding partner 1
mSin1	mammalian stress-activated protein kinase interacting protein
mTOR	mechanistic target of rapamycin
mTORC1	mTOR complex 1
mTORC2	mTOR complex 2
MBP	myelin basic protein
NaCl	sodium chloride
NEB	New England BioLabs
NF-kB	nuclear factor kappa-light-chain-enhancer of activated B cells
NOX	NADPH oxidases
NSCLC	non-small cell lung cancer
O_2	oxygen
$O_2^{\bullet-}$	superoxide anions
O.A.	okadaic acid potassium salt
PA	phosphatidic acid
PARP	poly(ADP-ribose) polymerase
PBS	phosphate buffered saline
PCD	programmed cell death
PCR	polymerase chain reaction
Pen strep	penicillin streptomycin
PEST	proline, glutamic acid, serine, and threonine
PDGF	platelet-derived growth factor
PDI	protein disulfide isomerase

PDK1	3-phosphoinositide-dependent protein kinase-1
PFA	paraformaldehyde
PH domain	pleckstrin-homology domain
PKB	protein kinase B
PKC	protein kinase C
PI3K	phosphatidylinositol-4,5-bisphosphate 3-kinase
PIKK	PI3K-related kinase
PIP_2	phosphatidylinositol (4,5)-bisphosphate
PIP_3	phosphatidylinositol (3,4,5)-trisphosphate
PLD1	phospholipase D 1
PR core	proline-rich core
PRAS40	proline-rich Akt substrate 40kDa
Protor1/2	protein observed with Rictor-1 or 2
PTEN	phosphatase and tensin homolog
PUFA	polyunsaturated fatty acid
PVDF	polyvinylidene difluoride
Rag	Ras-related small GTPase
Raptor	regulatory-associated protein of mTOR
Rictor	rapamycin-insensitive companion of mTOR
ROS	reactive oxygen species
RSK	p90 ribosomal S6 kinase
RTK	receptor tyrosine kinases
SD	standard deviation
SDS	sodium dodecyl sulfate
SDS-PAGE	SDS-polyacrylamide gel electrophoresis
SH2 domain	Src homology 2 domain
siRNA	small interfering RNA
Smac	second mitochondria-derived activator of caspase
S6K1	p70S6 Kinase 1
SOS	son of sevenless
SREBP	sterol responsive element binding protein
TBC1D7	Tre2-Bub2-CDC16 (TBC) 1 domain family member 7
Tel2	telomere maintenance 2

TFR	transferrin receptor
TKD	tyrosine kinase domain
TNF	tumour necrosis factor
TSC	tuberous sclerosis complex
Tti1	Tel2-interacting protein 1
Ulk1	unc-51-like kinase 1
UV	ultraviolet
v-ATPase	vacuolar H+-ATPase
VEGF	vascular endothelial growth factor
WB	western blotting

List of Publications

*Poursaitidis, I., ***Wang, X.** (co-first author), Crighton, T., Labuschagne, C., Mason, D., Cramer, S.L., Triplett, K., Roy, R., Pardo, O.E., Seckl, M.J., Rowlinson, S.W., Stone, E., Lamb, R.F. (2017) "Oncogene-Selective Sensitivity to Synchronous Cell Death following Modulation of the Amino Acid Nutrient Cystine." *Cell Rep.* 18(11): p. 2547-2556.

*These authors contributed equally to this publication by generating figures and providing results about the inhibitor and siRNA treatment, viability assays, FACS analyses, immunoblotting experiments, intracellular metabolites extraction, NSCLC experiments and analysis of tumour tissue samples.

Chapter 1

Introduction

Chapter 1- Introduction

1.1 Role of oncogenic signalling pathways in cancer development

The latest data (1 February 2018) from World Health Organization (WHO, http://www.who.int/en/news-room/fact-sheets/detail/cancer) suggest that cancer is the second leading cause of death worldwide (8.8 million deaths in 2015), with lung cancer being the most prevalent cause of cancer death (1.69 million deaths). Cancer is a group of diseases involving abnormal cell growth with the potential of metastasis. Many cancers form solid tumours (abnormal masses of tissue) with malignancy that can invade nearby and distant tissue, such as lung, liver and breast cancers, whilst hematologic cancers, such as leukaemia, generally do not form solid tumours and they affect the circulation and immune systems.

Cancer cells differ from normal cells in a variety of ways that allow them to grow without restraint and become invasive (reviewed in reference [1]) (Figure 1). Sustaining proliferative signalling is one of the most fundamental traits of cancer cells. Production and release of growth-promoting signals, which are mainly conveyed by growth factors that stimulate cell growth and cell cycle progression, are under precise control in normal tissues to ensure a homeostasis of cell number and thus maintenance of normal tissue architecture and function. These signals, however, become deregulated in cancer cells and endow them with unrestrained growth and division. Growth factors, such as insulin and epidermal growth factor (EGF), bind to their corresponding transmembrane receptor tyrosine kinases (RTKs), which transduce the signals to the branched downstream intracellular signalling pathways that promote cell growth, division and survival [2, 3]. Cancer cells, by upregulating the activity of these signalling pathways, become capable of proliferating in a sustained manner. Such hyperactive growth-promoting signals in cancer cells can result from ligand-dependent and –independent mechanisms. The former includes enhanced production and release of growth factor ligands and the elevated expression of RTKs that render cancer cells hyper-responsive to the ligands. Alternatively, constitutive activation of RTKs and the downstream signalling components, due to structural alterations, may facilitate the ligand-independent proliferation and growth in cancer cells. For example, activation of EGF receptor

(EGFR) oncogene, either by overexpression or mutation, has been implicated in a number of cancers including a large proportion of non-small cell lung cancer (NSCLC) cases [4-6]. Likewise, activating mutations in RAS and RAF oncogenes are prevalent in about 30% and 8% of all human cancers respectively [7, 8]. Such alterations render the phosphatidylinositol-4,5-bisphosphate 3-kinase (PI3K)/Akt (also known as protein kinase B), mitogen-activated protein kinase (MAPK)/extracellular-signal-regulated kinase (ERK) and the mechanistic (formerly mammalian) target of rapamycin complex 1 (mTORC1) signalling pathways constitutively active in cancer cells and ultimately lead to sustained proliferation and growth (Figure 2), as described in Chapters 1.2, 1.3 and 1.4 respectively.

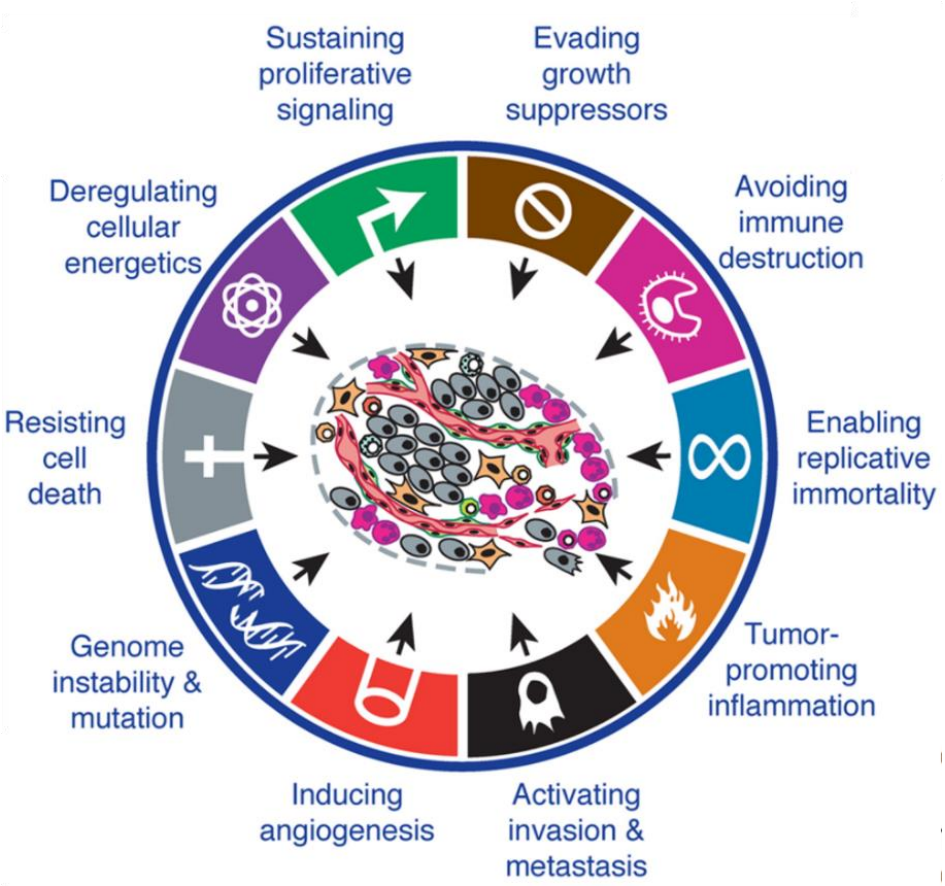

Figure 1. Overview of the hallmarks of cancer.
Ten hallmarks of cancer have been proposed, based on current knowledge of the mechanisms underlying cancer development, to characterize the distinctions between cancer and normal cells. Cancer cells have acquired the capabilities of persistent cell growth (increase of cell size) and proliferation (increase of cell number), and the involved hallmarks include the continuously active growth-promoting signalling pathways, replicative immortality, evasion of growth suppressors, repression of programmed cell death apoptosis and avoidance of immune destruction. In addition, cancer cells are capable of inducing angiogenesis and reprogramming energy and

nutrient metabolism, which fuels their rapid proliferation and growth. Moreover, genomic instability, resulting from alteration in genes involved in DNA repair process such as the tumour repressor BRCA1, is the most prominent enabling characteristic of the above acquired capabilities of cancer cells. Furthermore, cancer cells are able to invade and colonize other parts of the body, which is the process of metastasis. Cancer development is also accompanied by inflammation that contributes to the tumour-promoting microenvironment [1].

Defects in the negative regulation of the aforementioned signalling pathways are also important in promoting cancer development [1]. There are many negative-feedback loops that normally operate to dampen the growth-promoting signalling and thereby maintain a homeostatic flux of signals that flow through the proliferative signalling circuit. For example, the tumour suppressor phosphatase and tensin homolog (PTEN), which is the most important negative regulator of PI3K/Akt signalling pathway, functions to degrade the PI3K product PIP_3, thereby counteracting the signalling (Figure 5) [9]. Loss-of-function mutations of PTEN result in upregulation of the PI3K/Akt signalling and are associated with 15 human cancer types, such as head and neck, lung and prostate cancers [10]. Moreover, there are also negative-feedback loops between the three proliferative signalling pathways. Growth factor-induced activation of the PI3K/Akt and MAPK/ERK signalling pathways leads to activation of mTORC1 signalling, which in turn promotes inhibition of both PI3K/Akt and MAPK/ERK pathways [11] (Figure 2). In addition, active Akt phosphorylates and inhibits RAF, counteracting the MAPK/ERK signalling [12].

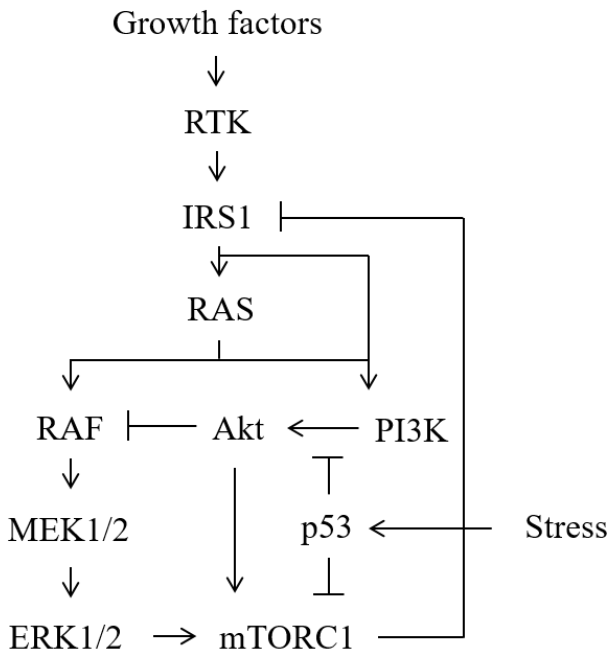

Figure 2. Crosstalk between PI3K/Akt, MAPK/ERK and mTORC1 pathways. Insulin receptor substrate 1 (IRS1) can be activated by insulin and insulin-like growth factor 1 (IGF1) receptors, which are RTKs that bind to growth factor ligands. Activated IRS1 stimulates the activation of RAS, leading to activation of the PI3K/Akt and MAPK/ERK signalling pathways. IRS1 also directly activates PI3K. Both Akt and ERK1/2 are capable of promoting activation of mTORC1 signalling pathway, which in turn causes repression of these two pathways by inhibiting IRS1. In addition, activated Akt counteracts the MAPK/ERK signalling by restraining the activity of RAF. Moreover, stress-activated p53 promotes the inhibition of both PI3K/Akt and mTORC1 signalling pathways. Regular arrows represent activation and blunt arrows inhibition, the same for all figures in this thesis where applicable. This figure is modified from reference [11].

1.2 The PI3K/Akt signalling pathway

The PI3K/Akt signalling pathway regulates a number of essential cellular processes, including cell cycle progression, apoptosis and metabolism, and aberrant activation of this pathway is commonly found in solid tumours and hematologic malignancies, such as breast cancer, melanomas and leukaemia [13, 14]. The PI3K/Akt signalling pathway mediates the process of signal transduction from cell membrane to intracellular corresponding effectors, and involves growth receptor RTKs and the small G protein RAS amongst other components [14].

1.2.1 RTKs are a group of transmembrane receptors

RTKs are a group of transmembrane glycoproteins that act to receive extracellular signals and mediate cellular responses [3]. RTKs include the insulin receptor and the receptors for many growth factors including EGF, fibroblast growth factor (FGF), platelet-derived growth factor (PDGF) and vascular endothelial growth factor (VEGF). Abnormal changes in the activity, cellular abundance and subcellular distribution of RTKs, resulting from genetic mutations or amplification and/or increase of the ligands, leads to aberrant activation of the corresponding signalling pathways, which is causally linked to numerous diseases and notably cancer [2, 3]. RTKs share the typical structure that is required to transduce extracellular signals into the intracellular mediators (Figure 3): the ligand binding domain within the extracellular region, a single transmembrane α helix and the intracellular regions that contain a tyrosine kinase domain (TKD), juxtamembrane regulatory and C-terminal regions [3].

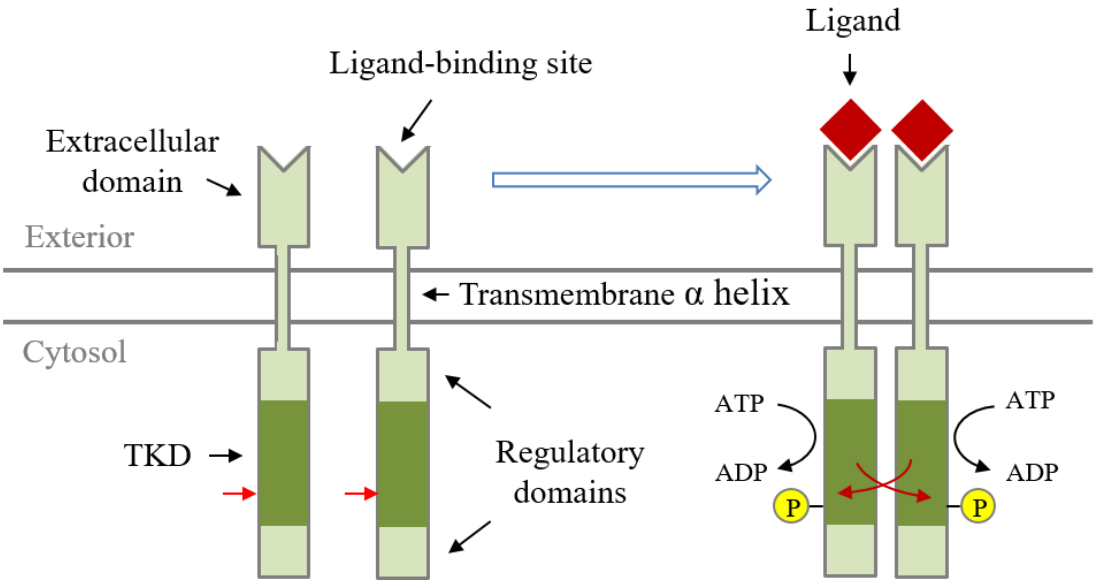

Figure 3. Schematic representation of RTK structure.
A typical transmembrane receptor RTK consists of the extracellular region containing the ligand-binding site, the transmembrane α helix and the intracellular domains containing TKD and regulatory domains. Growth factor ligands bind to the extracellular region of RTKs, which stimulates the dimerization and subsequent trans-autophosphorylation of RTKs. This figure is based on description of RTK structure in reference [3]. The most common EGFR mutations delE746-A750 and L858R in the TKD, as indicated by red arrow, activate the kinase activity of EGFR via a ligand-independent mechanism [4, 15].

In the inactive state, RTKs are monomeric and auto-inhibited by the key tyrosine in the intracellular regions contacting the active site which is otherwise phosphorylated by TKD [3]. Such configuration renders RTKs inaccessible by adenosine triphosphate (ATP) and substrates. Generally, a bivalent ligand simultaneously binds to the extracellular fragments of two corresponding RTK molecules, which induces dimerization and trans-phosphorylation (phosphorylation by its partner) of the two tyrosine residues [3]. This event disrupts the auto-inhibitory contacts and enables auto-phosphorylation of the active site, which then acts as a docking site for assembly and activation of the specific downstream molecules in signalling pathways including PI3K/Akt and MAPK/ERK [3, 16].

1.2.2 Aberrant activation of EGFR in cancer

Overexpression of EGFR has been identified in a number of cancer types, including head and neck, breast, ovarian, cervical bladder, endometrial and colorectal cancers [17]. Particularly, EGFR is found overexpressed in 62% of NSCLC [4], which accounts for about 85% of all lung cancers [8]. Overexpression of EGFR causes increased local concentration of the receptor and leads to overwhelming activation of the downstream signalling pathways [16]. This type of abnormal activation mainly results from genetic amplification and is linked with poor prognosis [16]. In addition to being amplified, EGFR is often mutated in cancer. The most common mutations found are a deletion of three amino acid residues at positions 747 to 749 (Leu-Arg-Glu, referred to as delE746-A750) and a missense mutation EGFR L858R, which account for 46% and 39% of EGFR mutations respectively [5, 6]. These two mutations render EGFR active independently of ligands by disrupting the auto-inhibitory interactions (Figure 3) [4, 15].

Small compounds called EGFR tyrosine kinase inhibitors have been developed to specifically inhibit EGFR activity by competitively binding the ATP-binding pocket within TKD, such as erlotinib and gefitinib (also known as tarceva and iressa respectively) [5]. 10% of NSCLC patients possess activating EGFR mutations and response to EGFR inhibitor therapy [18]. However, a majority of these patients acquire inhibitor resistance after 9-11 months of treatment [4, 19], and

approximately 50% of acquired resistance results from the second activating EGFR mutation T790M that affects the ATP-binding pocket of TKD [20].

1.2.3 The small G protein RAS

The RAS proteins, which consist of HRAS, NRAS, and KRAS isoforms [21], belong to the small guanine nucleotide-binding protein (G protein) family. These proteins are guanosine triphosphate (GTP)ases that are capable of hydrolyzing GTP and act as molecular switches in transmitting signals within the cell [22]. GTPases switch between two states, the active GTP-bound and the inactive guanosine diphosphate (GDP)-bound form, which are tightly regulated by their corresponding guanine nucleotide exchange factors (GEFs) and GTPase activating proteins (GAPs) [22]. GEFs bind to GDP-bound GTPases and catalyze dissociation of GDP, which allows GTP to bind the GTPases; whilst GAPs interact with GTP-bound GTPases and stimulate their GTPase activity that hydrolyzes GTP, returning them to the inactive GDP-bound state (Figure 4).

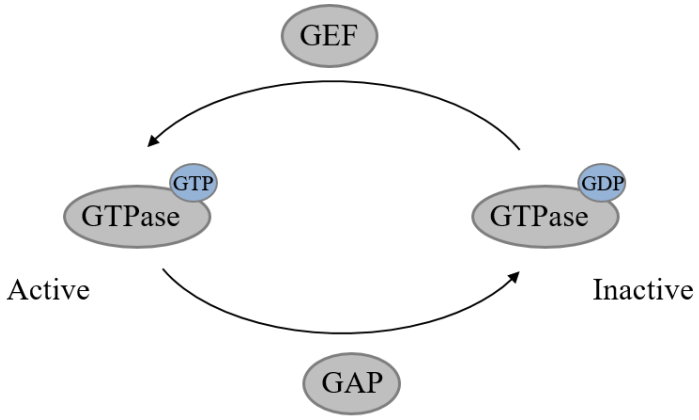

Figure 4. Regulation of GTPase by GEF and GAP.
GEF activates GTPase by inducing its dissociation from GDP and thus association with GTP, whereas GAP inactivates GTPase by stimulating its hydrolysis of GTP.

RAS proteins are critical signal transducers of RTKs, and the isoforms KRAS and HRAS are the main activators of MAPK/ERK and PI3K/Akt signalling pathways respectively [23]. Activating mutations in RAS genes are present in 30% of all human cancers [7]. KRAS is the most frequently mutated isoform that accounts for 85% of all RAS mutations [21], and KRAS mutations are found in 22% of all human cancers [24]. Notably, KRAS mutations are present in about 90% of pancreatic

cancers, 45% of colorectal cancer (CRC) and 35% of lung cancers [25]. The most frequent mutations occur on amino acid glycine at the position 12 (G12) with single base substitutions, such as G12D, G12V and G12C, all of which render KRAS defective in GAP-mediated GTP hydrolysis, leading to accumulation of GTP-bound KRAS and constitutively activated downstream signalling [21].

1.2.4 Activation of the PI3K/Akt signalling pathway

The family of PI3Ks can be divided into three classes based on the primary structure and substrate specificity, and Class IA PI3K is mainly associated with cancer (hereafter also called PI3K for brevity) [26]. PI3K is a heterodimer that consists of the p85 regulatory and the p110 catalytic subunits [14]. PI3KCA is the gene that encodes the p110 subunit and the mutation PI3KCA H1047R, where a histidine is substituted by an arginine at the position 1047, renders PI3K constitutively active, and is the most frequent PI3K mutation found in cancer [27]. The lipid kinase PI3K phosphorylates the phosphatidylinositol (4,5)-bisphosphate (PIP_2) and converts it into phosphatidylinositol (3,4,5)-trisphosphate (PIP_3), which acts to recruit specific substrates containing the pleckstrin-homology (PH)-domain onto plasma membrane for activation [14]. Akt is a serine/threonine kinase and is the major downstream effector of PI3K [9]. PIP_3 is maintained at low levels in un-stimulated cells by the action of phosphatases, mainly PTEN that hydrolyzes PIP_3 to PIP_2 [9], antagonizing the PI3K/Akt signalling. In addition, stress-activated p53 upregulates the cellular level of PTEN, resulting in inhibition of the PI3K/Akt signalling [28].

The PI3K/Akt signalling pathway is activated by RTKs (Figure 5). Interaction of RTKs with ligands induces auto-phosphorylation of tyrosines that allows binding to specific substrates containing the Src homology 2 (SH2) domain, such as growth factor receptor-bound protein 2 (Grb2) [26]. Grb2 then interacts with and activates the protein son of sevenless (SOS), thereby recruiting it to the plasma membrane. SOS is a GEF for RAS that converts it into the active GTP-bound state. Membrane-localized GTP-bound RAS interacts with the p85 regulatory subunit of PI3K, which stimulates the kinase activity of the p110 subunit [29]. Activated PI3K generates the lipid second messenger PIP_3 that binds to Akt. Membrane-localized Akt is then activated through phosphorylation on Thr308 and Ser473 by membrane protein 3-

phosphoinositide-dependent protein kinase-1 (PDK1) [30] and mTOR complex 2 (mTORC2) respectively [31]. Activated Akt phosphorylates several components involved in regulation of cell survival and apoptosis [27]. Akt phosphorylates and inhibits pro-apoptotic proteins Bad and protease caspase-9 (see Chapter 1.6.1), thereby inhibiting apoptosis. In addition, Akt phosphorylates mouse double minute 2 homolog (MDM2), which increases its affinity for p53 and ultimately leads to enhanced degradation of p53 (see Chapter 1.5) and thus repression of apoptosis [32]. Furthermore, Akt phosphorylates and inhibits the tumour suppressor TSC2, leading to mTORC1 activation that promotes protein synthesis [33].

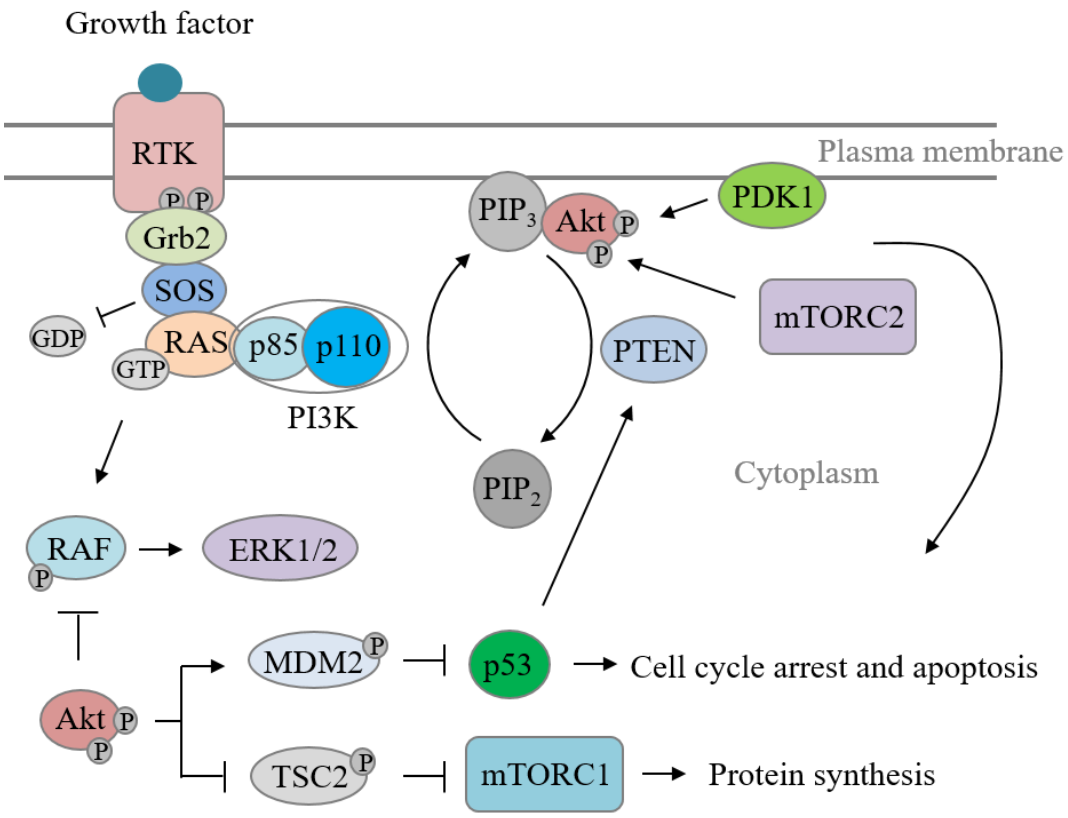

Figure 5. Schematic representation of the PI3K/Akt pathway.
Upon activation by ligand-bound RTKs and GTP-bound RAS, PI3K phosphorylates PIP_2 into PIP_3, which binds to and recruits Akt onto cell membrane, allowing for its activation by membrane protein PDK1 and mTORC2. Activated Akt in turn phosphorylates multiple substrates including the p53 binding partner MDM2 and the mTORC1 inhibitor TSC2, leading to cell cycle progression, repression of apoptosis, and activation of the mTORC1 signalling. PIP_3 is dephosphorylated by PTEN, thereby antagonizing the PI3K/Akt signalling. P53 binds to PTEN and stimulates its transcription, resulting in inhibition of the PI3K/Akt signalling. RTKs and RAS are also activators of the MAPK/ERK signalling pathway by stimulating activation of RAF. Notably, activated Akt also phosphorylates and inhibits RAF, counteracting the MAPK/ERK signalling. This figure is modified from reference [14].

1.3 The MAPK/ERK cascade

MAPKs are a group of serine/threonine kinases involved in transduction of signals from the cell surface to the intracellular effectors (reviewed in reference [34]). They are critical in regulating various cellular processes, such as differentiation, cell cycle progression, migration, angiogenesis and apoptosis. MAPKs comprise three families: ERK, p38 isoforms and c-Jun amino-terminal kinases (JNKs). The RAS-RAF-MEK1/2-ERK1/2 pathway, also termed MAPK/ERK pathway, is central in controlling cell proliferation and survival. Overexpression and mutations of the members within this pathway, particularly RAS and RAF, are one of the most common sources for cancer transformation and progression [35, 36].

1.3.1 The serine/threonine kinase RAF

RAF proteins, ARAF, BRAF, CRAF (also called RAF-1), are serine/threonine kinases and core downstream effectors of RAS [35]. Membrane-localized GTP-bound RAS interacts with RAF and stimulates its activation. Once activated, RAF binds to and phosphorylates MEK1 and MEK2, which in turn activate and phosphorylate ERK1 and ERK2. Activated ERKs regulate a wide range of substrates and ultimately promote cell proliferation and survival [35] (Figure 6). Of the three RAF isoforms, BRAF is the main activator of the MAPK/ERK signalling pathway [37], and is the most frequently mutated RAF isoform in cancer [35]. BRAF mutations have been found in 8% of all human cancers [8]. Particularly, the mutant BRAF V600E, where a valine is substituted by a glutamic acid at position 600, renders BRAF constitutively active and constitutes 90% of all BRAF mutations [38]. This mutation has been found in 70-80% of melanoma [35], as well as 1-2% of NSCLC [8].

1.3.2 MEK and ERK

MEK isoforms, MEK1 and MEK2 (referred to as MEK1/2), are tyrosine and serine/threonine dual-specificity kinases that are capable of phosphorylating tyrosine, serine and threonine residues. They are predominantly activated by BRAF phosphorylating on Ser218/222 of MEK1 and Ser222/226 of MEK2 [39]. Activated

MEK1/2 in turn specifically activate ERK1 and ERK2 by phosphorylating Thr202/Tyr204 of ERK1 and Thr185/Tyr187 of ERK2 [34, 40].

ERK1 and ERK2 (referred to as ERK1/2) are two isoforms with 84% amino acid sequence identity [40]. The two isoforms are activated in parallel and share many biological functions. ERK1/2 are ubiquitously expressed serine/threonine kinases and have a variety of substrates comprising cytoplasmic regulators and nuclear transcription factors (Figure 6). Once activated, a large portion of ERK1/2 undergo nuclear translocation, interact with and activate several transcription factors including c-myc, which promote expression of proteins involved in regulating cell proliferation and differentiation [34, 41]. Some of ERK1/2 are localized in the cytoplasm and phosphorylate several cytosolic regulators, such as TSC2 and p90 ribosomal S6 kinase (RSK). ERK1/2 phosphorylates the mTORC1 inhibitor TSC2 on Ser664, which leads to inhibition of TSC2 and thus activation of the mTORC1 signalling as described in Chapter 1.4 [42]. Phosphorylation of RSK on Thr359 and Ser363 by ERK1/2 activates RSK, which on one hand stimulates cell cycle progression through phosphorylation of transcriptional regulators; on the other hand, phosphorylates and inhibits SOS, resulting in reduced concentration of GTP-bound RAS and thus antagonizing the MAPK/ERK signalling [43]. In addition, activated RSK phosphorylates and inhibits TSC2, leading to activation of mTORC1 signalling pathway [44].

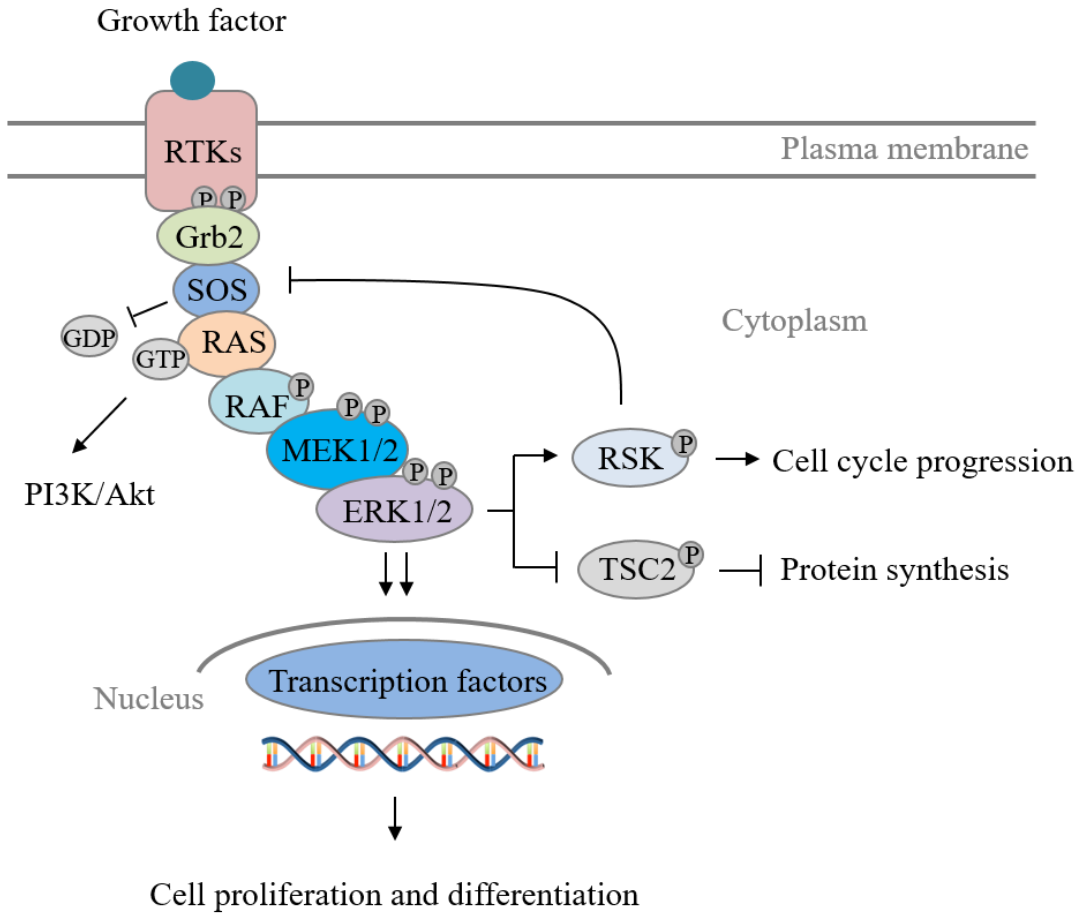

Figure 6. Activation of the MAPK/ERK cascade.
GTP-bound RAS stimulates the activation of RAF, which binds to and phosphorylates MEK1/2. Activated MEK1/2 interact with and catalyze dual phosphorylation of ERK1/2. Upon activation, a large portion of ERK1/2 accumulate to nucleus and activate several transcription factors, leading to cell proliferation and differentiation. Some ERK1/2 phosphorylate cytoplasmic regulators including RSK and TSC2, promoting cell cycle progression and protein synthesis respectively. In addition, RSK phosphorylates and inhibits the RAS activator SOS, which performs a negative feedback regulation of the MAPK/ERK signalling. This figure is adapted from reference [14].

1.4 The mTOR signalling pathways

mTOR, also named FK506-binding proteins (FKBP)-rapamycin-associated protein (FRAP) [45], belongs to the serine/threonine kinase family termed PI3K-related kinase (PIKK) with sequence homology to PI3K (reviewed in reference [46]). mTOR has a central role in regulating cell growth and proliferation by acting as the catalytic subunit of two complexes, termed mTORC1 and mTORC2. These two complexes are composed of distinct subunits (Figures 8 and 9) and have distinct

cellular functions via different signalling pathways (Figure 10). The mTOR signalling pathways are frequently found over-active in many cancer types due to mutations in Akt and TSC2, which are upstream regulators of the mTOR kinase [10, 47] (Figure 10).

1.4.1 mTORC1 and mTORC2 possess multiple subunits

1.4.1.1 mTOR structure

mTOR is a large protein kinase with a molecular weight of 289kDa. It is constituted of multiple domains: the amino-terminal HEAT (Huntington, Elongation factor 3 (EF3), A subunit of protein phosphatase-2A, and TOR) repeats, a central FAT (FRAP, ATM, TRAP, which are PIKK members) domain, the FRB (FKBP12-rapamycin binding) region, the carboxyl-terminal catalytic and FAT (FATC) domains (reviewed in [48]), as shown in Figure 7. Rapamycin is a small compound with antifungal, immunosuppressive and antitumor properties, and it inhibits mTOR signalling through forming complexes with a group of immunophilin molecules termed FKBP12 (molecular weight of 12kDa).

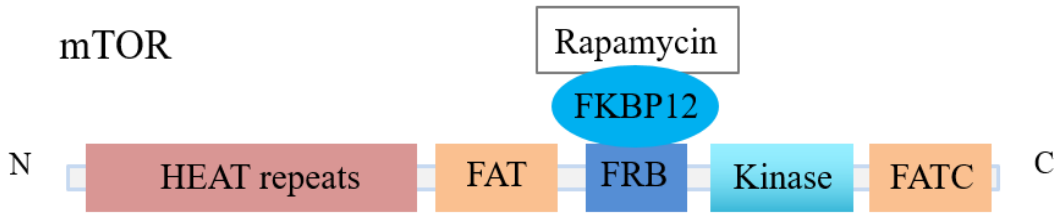

Figure 7. Linear schematic representation of mTOR structure.
mTOR is a multi-domain protein that consists of the multiple (at least 20) HEAT repeats, a central FAT domain, FRB that binds to the rapamycin-FKBP12 complex, a kinase domain which shares sequence identity to that of PI3K and a second FAT domain at its carboxyl terminus (FATC). This figure is adapted from reference [48].

1.4.1.2 mTORC1 and mTORC2 subunits

Common subunits

In addition to mTOR, mTORC1 and mTORC2 contain multiple subunits that regulate its kinase activity and substrate specificity (Figures 7 and 8). They share three additional subunits: mLST8 (the positive regulator mammalian lethal with Sec13 protein 8) that binds to the kinase domain of mTOR [49], Deptor (DEP-

domain-containing mTOR-interacting protein) that interacts with the central FAT region and negatively regulates the activity of both complexes [50], and the Tti1 (telomere maintenance 2 (Tel2)-interacting protein 1)-Tel2 complex that associates with the HEAT repeats domain and stabilizes complex assembly [51].

Distinct subunits of mTORC1

In addition to the common subunits, mTORC1 also contains Raptor (the regulatory-associated protein of mTOR) that binds the HEAT repeats region of mTOR [52-54], and PRAS40 (the proline-rich Akt substrate 40kDa) that interacts with Raptor [55-57] (Figures 8 and 9). Activation of mTORC1 signalling requires that mTOR is catalytically active and that mTOR interacts with the downstream substrates, which together allow the substrates to be phosphorylated. Raptor is the defining subunit for mTORC1 due to its role to interact with downstream mTORC1-specific substrates [52, 53]. In addition, Raptor is critical for lysosomal localization of mTORC1 as described in Chapter 1.4.3. The association of Raptor with substrates, however, is disrupted by PRAS40 that competitively binds to Raptor [57]. Interaction of PRAS40 with Raptor dislocates the substrates away from mTOR and thus deactivates the mTORC1 signalling. Likewise, the mTOR inhibitor rapamycin inhibits mTORC1 activity by acting on Raptor [58]. The rapamycin-FKBP12 complex interacts with the FRB domain of mTOR (Figure 8) and interrupts its association with Raptor, rendering mTOR unable to phosphorylate substrates even when it is kinase-active.

Distinct subunits of mTORC2

mTORC2 possesses three additional subunits (Figures 8 and 9), Rictor (the rapamycin-insensitive companion of mTOR) [31, 59], mSin1 (mammalian stress-activated protein kinase interacting protein) [60, 61] and Protor1/2 (protein observed with Rictor-1 or 2) [62]. Similar to Raptor and PRAS40 in mTORC1, Rictor interacts with the HEAT repeats of mTOR and is the characteristic component for mTORC2; both mSin1 and Protor1/2 interact with Rictor. mTORC2-specific Rictor has similar function as mTORC1-specific Raptor that regulates complex assembly and acts as a scaffolding partner to recruit mTORC2-specific substrates. mSin1

seems to stabilize the assembly of mTORC2 and the role of Protor1/2 remains unknown.

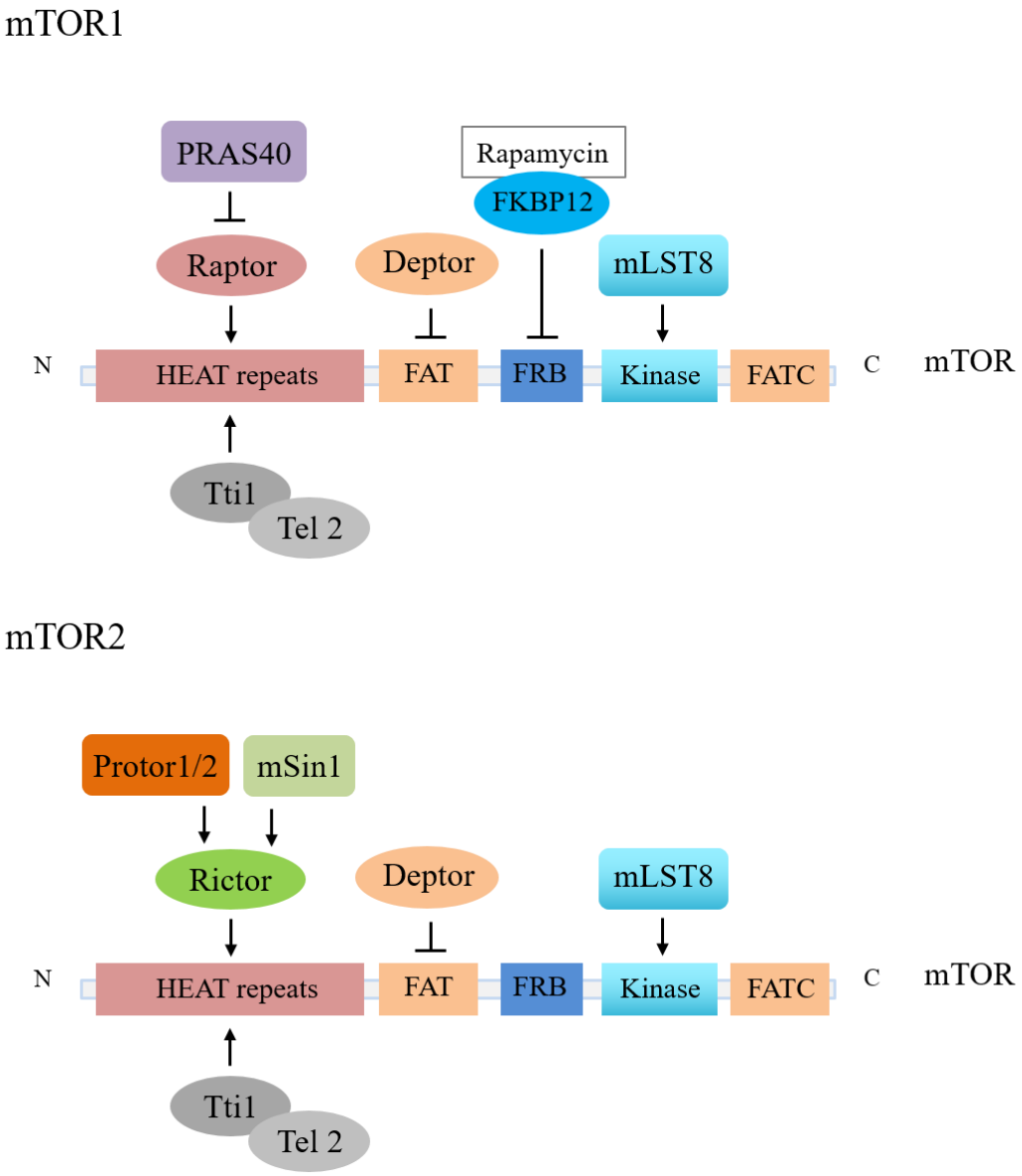

Figure 8. mTORC1 and mTORC2 subunits.
In addition to the kinase mTOR itself, three subunits are common to mTOR complexes 1 and 2: the complex of Tti1 and Tel2, Deptor and mLST8, and they respectively bind the HEAT repeats, central FAT and kinase domains of mTOR. mTORC1 additionally comprises Raptor and PRAS40 while mTORC2 additionally possesses Rictor, mSin1 and Protor1/2. Raptor and Rictor both interact with the HEAT repeats of mTOR. PRAS40 interacts with Raptor whilst mSin1 and Protor1/2 bind to Rictor. The mTOR inhibitor rapamycin forms a complex with FKBP12, which binds to the FRB domain of mTOR, leading to dissociation of Raptor from mTOR and thus inhibition of mTORC1 signalling. This figure is adapted from reference [48].

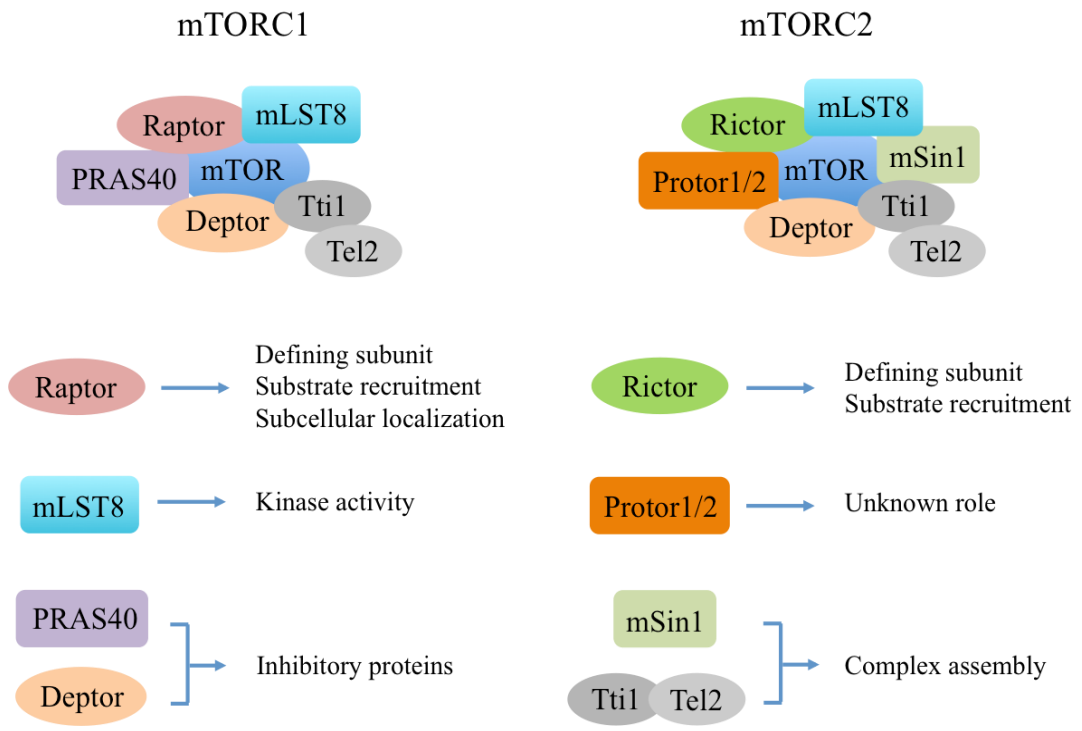

Figure 9. Regulation of mTORC1 and mTORC2 by their subunits.
The common subunits, Deptor and mLST8, are respectively negative and positive regulators of mTOR catalytic activity, whilst the Ttil-Tel2 complex regulates the complex assembly. Raptor and Rictor regulate substrate specificity and thus are respectively the characteristic components of mTORC1 and mTORC2. Raptor also regulates mTORC1 subcellular localization by binding to lysosomal proteins. The inhibitory subunit of mTORC1, PRAS40, competes with substrates to bind Raptor, which shifts them away from mTOR and thus deactivates the mTORC1 signalling. mSin1 enhances complex assembly and the role of Protor1/2 remains unknown. This figure is modified from reference [63].

1.4.2 Downstream of the mTOR signalling network

Although mTORC1 and mTORC2 share the mTOR kinase and other three subunits, they exhibit distinct features in terms of sensitivity to rapamycin inhibition [64] and cellular functions [65]. Rapamycin treatment acutely diminishes mTORC1 activity, whereas inhibition of mTORC2 by rapamycin requires prolonged treatment [64], likely due to the disruption of mTORC2 assembly by rapamycin-bound mTOR [66]. mTORC1 and mTORC2 phosphorylate distinct substrates and therefore regulate different cellular processes (Figure 10).

1.4.2.1 mTORC1 promotes synthesis of proteins, lipids and nucleotides

mTORC1 simultaneously integrates multiple upstream signals, such as growth factors and nutrients, to regulate the synthesis of essential macromolecules including proteins, nucleotides and lipids, as well as to regulate autophagy, contributing to control of cell growth and proliferation [67] (Figure 10). Aberrant activation of mTORC1 signalling has been implicated in various diseases, such as cancer, type II diabetes and neurodegenerative diseases [47, 67].

Protein synthesis

When cells are exposed to growth-promoting stimuli, such as sufficient nutrients, mTORC1 is activated and stimulates the anabolic processes by acting on two critical translational regulators, ribosomal protein p70S6 Kinase 1 (S6K1) and eukaryotic initiation factor-4E (eIF-4E)-binding protein 1 (4E-BP1) (reviewed in reference [46]) (Figure 10). mTORC1 directly phosphorylates S6K1 on residue Thr389, which allows for its subsequent phosphorylation and activation by PDK1. Activated S6K1 phosphorylates and activates an array of substrates involved in mRNA translation initiation and elongation [68], such as ribosomal protein S6, eukaryotic elongation factor 2 kinase (eEF2K) and the eukaryotic translation initiation factor 4B (eIF4B) [68]. 4E-BP1 interacts with eIF-4E and prevents the latter from binding to the cap (a modified guanosine at the 5` end) structure of mRNA that is required for translation initiation. Phosphorylation of 4E-BP1 on residues Thr37/46/70 and Ser65 by mTORC1 disrupts its association with eIF-4E [69], relieving the inhibitory effect and thus upregulating mRNA translation.

Lipid and nucleotide synthesis, ribosome biogenesis and glucose metabolism

In addition to promoting protein synthesis, activated mTORC1 also upregulates the synthesis of lipids and nucleotides that are required for new membrane formation and DNA replication respectively [46]. mTORC1 and its key effector S6K1 promote lipogenesis through positively regulating the transcription factor sterol responsive element binding protein (SREBP), which upregulates the synthesis of enzymes involved in cholesterol and fatty acid biosynthesis [70, 71]. Moreover, mTORC1 stimulates the synthesis of purine and pyrimidine respectively by upregulating the activating transcription factor 4 (ATF4)-dependent expression of MTHFD2, a

metabolic enzyme involved in the mitochondrial tetrahydrofolate cycle that provides one-carbon units for purine synthesis [72]; and through S6K1 that phosphorylates caspase-activated DNase (CAD), a key enzyme for pyrimidine synthesis [73]. Importantly, mTORC1 also promotes ribosome biogenesis required for protein synthesis, via regulating ribosomal RNA transcription and synthesis of ribosomal proteins and other components required for ribosome assembly [74]. Furthermore, mTORC1 facilitates anabolic processes by promoting glycolysis, an oxygen-independent glucose metabolic process that provides intermediates for the synthesis of essential macromolecules [71]. mTORC1 stimulates the transcription of hypoxia-inducible factor 1-alpha (HIF1α), which upregulates the glucose transporters and increases the expression of glycolytic enzymes.

1.4.2.2 mTORC1 represses the catabolic process autophagy

Autophagy is the catabolic process in which excessive or damaged organelles are degraded in lysosomes and the resulting products are reused for energy generation, protein synthesis, so that cell can survive nutrient scarcity [75]. One of the critical functions of mTORC1 is to suppress autophagy [67]. In the presence of amino acids, mTORC1 is activated and it phosphorylates two essential autophagy factors, autophagy-related gene 13 (Atg13) and unc-51-like kinase 1 (Ulk1), resulting in repression of their interaction with the third autophagy factor, focal adhesion kinase family-interacting protein of 200kDa (Fip200) [76]. Upon amino acid withdrawal, mTORC1 is inhibited, releasing Ulk1 and Atg13 to form a complex with Fip200 that is required for formation of autophagosome and initiation of autophagy [76-78]. Another mechanism underlying regulation of autophagy by mTORC1 involves the energy sensor adenosine monophosphate (AMP)-activated protein kinase (AMPK) [79]. Glucose deficiency activates AMPK, which directly phosphorylates and activates Ulk1 on Ser317/777 [79]. Activated Ulk1 phosphorylates downstream substrates and promotes autophagy induction, conversely nutrient-activated mTORC1 directly phosphorylates Ulk1 on Ser757, which disrupts its interaction with AMPK and thus prevents autophagy initiation [79].

1.4.2.3 mTORC2 indirectly affect mTORC1 through Akt

In contrast to mTORC1, the role of mTORC2 is not so well described in the literature. mTORC2 appears to regulate cell growth and cytoskeleton by phosphorylating and activating a series of AGC (protein kinase A/protein kinase G/protein kinase C) kinases, such as Akt [31], SGK1 (serum- and glucocorticoid-induced protein kinase 1) [80] and PKC (protein kinase C) [49] (Figure 10). As mentioned in Chapter 1.2.4, Akt plays a critical role in regulating a variety of cellular processes, including metabolism, migration and proliferation [81]. Phosphorylation of residues Ser473 and Thr308 by mTORC2 and PDK1 respectively is required for Akt activation [31]. Akt further activates the mTORC1 signalling by acting on the mTORC1 inhibitor TSC2 [82, 83], connecting mTORC2 to mTORC1. mTORC2 also regulates sodium transport and cytoskeleton by phosphorylating SGK1 on Ser422 [80] and PKCα subunit on Ser657 respectively [49].

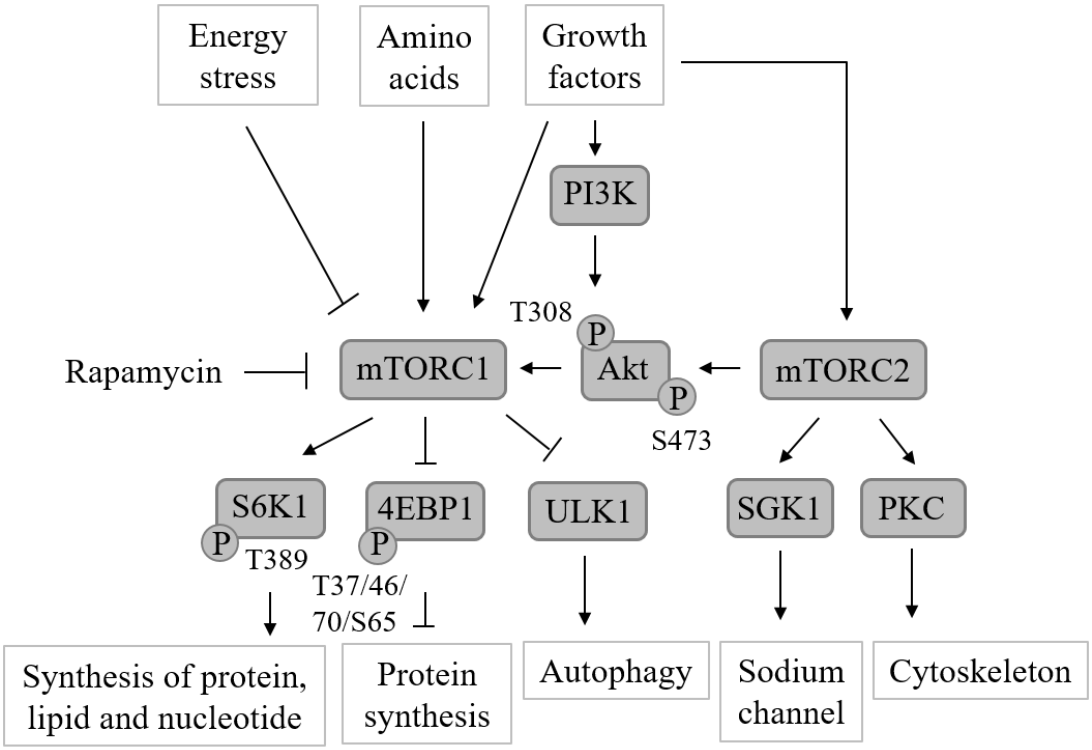

Figure 10. The mTOR signalling network.
mTORC1 is activated by growth-promoting signals including growth factors and amino acid nutrients. Upon activation, mTORC1 phosphorylates S6K1 on Thr389, which stimulates S6K1 activation. Activated S6K1 promotes synthesis of proteins, lipids and nucleotides. mTORC1 also phosphorylates 4EBP1 on Thr37/46/70 and Ser65, leading to upregulation of protein synthesis. In addition, mTORC1 suppresses autophagy by phosphorylating and inactivating autophagy factor Ulk1. Instead of

integrating multiple signal inputs, mTORC2 solely senses and is activated by growth factors. Activated mTORC2 phosphorylates and activates Akt on Ser473. Akt is also activated indirectly by PI3K in response to growth factors. Activated Akt indirectly activates mTORC1, connecting mTORC2 to mTORC1. mTORC2 also contributes to the regulation of cytoskeleton and membrane sodium channels through PKC and SGK1 respectively. This figure is based on description of mTOR signalling in reference [46].

1.4.3 Upstream of mTORC1 signalling network

1.4.3.1 The TSC/Rheb axis is a master regulator of mTORC1 signalling

Since mTORC1 senses various stimuli, the mTORC1 signalling components are rather complex and are strictly regulated to ensure that cell growth only occurs when the cellular environment is favourable. The most critical regulator of this signalling pathway is the TSC/Rheb (Ras homolog enriched in brain) axis. TSC a trimeric tumour suppressor complex that consists of TSC1 (also known as hamartin), TSC2 (also known as tuberin) and TBC1D7 (Tre2-Bub2-CDC16 (TBC) 1 domain family member 7) [84, 85]. Mutations of the tumour suppressors TSC1 and TSC2 predispose patients to tuberous sclerosis, a genetic disorder with benign tumours in multiple organs [86]. TSC2 contains a C-terminal GAP-like domain and functions as a GAP for the small Ras-related GTPase Rheb, a critical activator of mTORC1 [84]. Association of TSC2 with TSC1 stabilizes and prevents TSC2 from degradation and ubiquitination, and TBC1D7 stabilizes the association of TSC2 with TSC1 [85, 87].

Rheb predominantly binds GTP and has low GTPase activity [87]. Although Rheb interacts with the two subunits of mTORC1, mTOR and mLST8, regardless of its GTP-bound state [88], only GTP-bound Rheb is capable of activating the catalytic activity of mTOR and thus the mTORC1 signalling [88]. Notably, activation of mTORC1 by GTP-bound Rheb seems to be required for all upstream signal inputs, though the mechanism underlying this event remains elusive [46]. Under conditions of low energy or nutrients, TSC2 directly inactivates Rheb by stimulating its GTP hydrolysis, switching off the mTORC1 signalling [84, 87]. Therefore, the TSC/Rheb axis acts as a master switch that integrates all of the upstream signal inputs toward mTORC1.

Like many other kinases including mTOR and S6K1, the activity of TSC2 is either positively or negatively regulated by posttranslational modifications. For example, growth factor-activated MAPK/ERK and PI3K/Akt signalling pathways inhibit TSC2 by phosphorylation on residues Ser939/664/1798 and Thr1462 [42, 44, 83], conversely cellular stress such as energy scarcity stimulates AMPK, which activates TSC2 via phosphorylating Thr1227 and Ser1345 residues [89].

1.4.3.2 mTORC1 responds to growth factors

Activation of mTORC1 in response to growth factors primarily involves the PI3K/Akt and MAPK/ERK signalling pathways, which act both upstream and downstream of mTORC1 (Figure 11). Growth factors stimulate these pathways, leading to activation of Akt [33, 81-83], ERK1/2 [42] and RSK [44], which phosphorylate TSC2 on Ser939/Thr1462, Ser664 and Ser1798 respectively. Phosphorylation of these resides disrupts the association of TSC2 and TSC1, which destabilizes TSC2 and leads to activation of Rheb and thus mTORC1 [84, 88]. In addition, phosphorylation of TSC2 by Akt promotes the dissociation of TSC2 from lysosomal surface [90], thereby preventing GTP hydrolysis of Rheb, as described in Chapter 1.4.3.4. PI3K/Akt and MAPK/ERK also promote mTORC1 activation independently of TSC2, through acting on the distinct subunits of mTORC1. For example, Akt phosphorylates PRAS40 on Thr246, which dissociates PRAS40 from Raptor and thus relieves its inhibitory effect on mTORC1 [55]. RSK phosphorylates Raptor on residues Ser719/ 721/722, leading to elevated mTORC1 activity [91]. Moreover, the mTORC1 effector S6K1 in turn directly phosphorylates and inhibits IRS1, an upstream activator of MAPK/ERK cascade and PI3K/Akt [92] (Figure 11), although it is unclear whether S6K1 inhibits other RTK substrates. Through S6K1, mTORC1 stimulates a negative feedback regulation of both MAPK/ERK and PI3K/Akt signalling pathways. This negative feedback loop possibly explains why patients with tuberous sclerosis do not develop malignant tumours. It also has significant implication in cancers that are resistant to mTOR inhibitors [48], in that suppression of mTORC1 activity results in adaptive activation of MAPK/ERK and PI3K/Akt signalling pathways that contribute to proliferation of cancer cells.

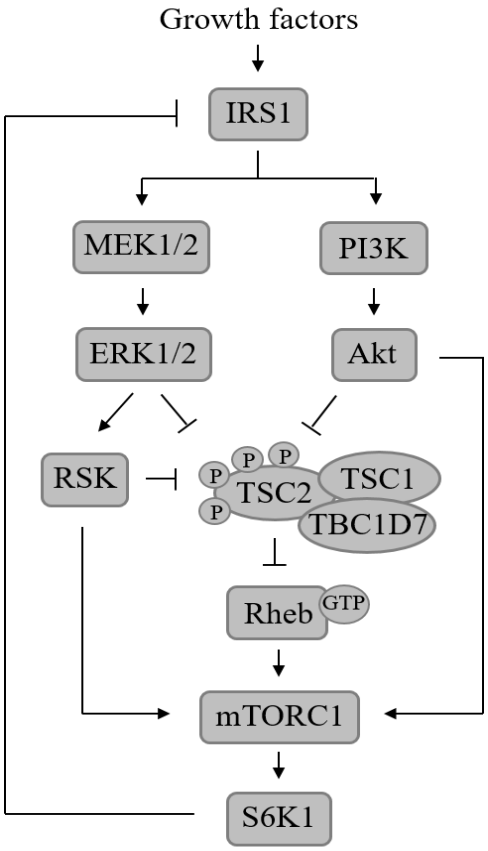

Figure 11. TSC/Rheb regulates mTORC1 activity.
In the presence of growth factors, the MAPK/ERK cascade and PI3K/Akt are activated by RTK and the corresponding substrates. Activated ERK1/2, RSK and Akt phosphorylate TSC2 on multiple sites and inhibit its GAP activity toward Rheb. GTP-bound Rheb then binds to and activates mTORC1, which further stimulates S6K1 activation. S6K1 in turn phosphorylates and inhibits the insulin receptor substrate 1 (IRS1), resulting in repression of the MAPK/ERK, PI3K/Akt and mTORC1 signalling pathways. This figure is based on description of mTORC1 signalling in reference [92].

1.4.3.3 mTORC1 responds to energy, oxygen and DNA damage

AMPK is the major regulator of mTORC1 signalling in response to energy stress. Reduction in energy or oxygen levels decreases the ATP/AMP ratio, which activates AMPK [79]. Activated AMPK represses mTORC1 activity indirectly through phosphorylation and activation of TSC2 and directly through phosphorylation of the defining mTORC1 subunit Raptor [89, 93]. AMPK phosphorylates TSC2 on Thr1227 and Ser1345, which stabilizes TSC2 [89] and results in inhibition of mTORC1 [84, 88]. Phosphorylation of Raptor on Ser722/792 by AMPK disassociates it from mTOR [93] and thereby destabilizes the mTORC1 assembly

[52, 53]. In addition, AMPK and TSC2 are both upregulated by p53 in response to DNA-damaging stress, resulting in mTORC1 inhibition [94].

1.4.3.4 mTORC1 responds to amino acid availability

Amino acids seem to be the indispensable stimulus for mTORC1 activation [46], since, for example, growth factors fail to fully stimulate mTORC1 activity when amino acids are removed. mTORC1 activation requires both lysosomal translocation and GTP-bound Rheb [88, 95]. The first process is controlled by amino acid availability [95] and the second by already described TSC2 [88]. The Ras-related small GTPase (Rag) proteins [96, 97] and Ragulator [95, 98] are critical mediators that recruit mTORC1 onto lysosomes in response to amino acid sufficiency.

Rag proteins interact with Ragulator

Mammalian cells contain four Rag GTPases (hereinafter referred to as Rags), RagA, B, C and D. RagA and B share approximately 90%, whilst RagC and D share 81% sequence homology [96]. The guanine nucleotide-binding state of Rags is essential for their function and is regulated by amino acid availability. Rags function as heterodimers, which switch between the active and inactive conformations in response to amino acid sufficiency and deficiency respectively [96]. The active Rag heterodimer consists of either GTP-bound RagA or RagB and GDP-bound RagC or RagD, while the inactive heterodimer is constituted of either GDP-bound RagA or RagB and GTP-bound RagC or RagD (Figure 12). Rags have been found to localize on lysosomes by associating with the lysosomal protein complex, Ragulator, regardless of amino acid availability [95]. Ragulator is a complex composed of five subunits: p18, p14, MP1 (MAPK binding partner 1), C7orf59 and HBXIP (hepatitis B X-interacting protein [95, 98]. These subunits are alternatively termed LAMTOR (late endosomal/lysosomal adaptor and MAPK and mTOR activator) 1-5 respectively.

Rags interact with mTORC1 and recruit it onto lysosomes

Both mTOR and Raptor, the defining subunit of mTORC1, are found to co-localize with lysosomes under the condition of amino acid sufficiency and they become diffused and cytosolic upon amino acid removal, as detected by immunofluorescence

staining [95, 97]. Such amino acid availability-controlled lysosomal recruitment and release are critical for mTORC1 activation and inactivation, and these processes are found to be mediated by the Rag heterodimers [95, 97] (Figure 12). In the presence of amino acids, the Rag heterodimer is dominant in the active conformation and interacts with Raptor, which recruits mTORC1 onto lysosomal surface [95, 97]. Once localized on lysosomes, mTORC1 is in proximity to Rheb, which allows it to interact with and be activated by GTP-bound Rheb [88, 95]. In the absence of amino acids, Rag heterodimer is switched into the inactive conformation and Rheb binds GDP due to TSC2 activity, leading to release of mTORC1 into cytosol and its inactivation [95, 97, 99] (Figure 12).

Rags interact with TSC and recruit it onto lysosomes

The master inhibitor of mTORC1, TSC2, is also found to undergo lysosomal translocation, however, in an opposite manner [99]. Unlike mTORC1 that co-localizes with lysosomes in the presence of amino acid, TSC2 moves to lysosomal surface under the condition of amino acid deficiency. The subcellular localization of the other two subunits of TSC, TSC1 and TBC1D7, follows the same pattern as that of TSC2 [85]. Like mTORC1, the lysosomal translocation of TSC2 is also found to be mediated by the Rag heterodimers. When amino acids are present, TSC2 is diffused in the cytoplasm and as such unable to bind and inactivate Rheb [99]. Upon amino acid withdrawal, TSC2 interacts with the inactive Rag heterodimer and thus is recruited onto lysosomal surface. Once localized on lysosomes, TSC2 binds to GTP-bound Rheb and induces its GTP hydrolysis, resulting in inhibition of Rheb and mTORC1 [99] (Figure 12). In a recent publication, it is also suggested that TSC2 lysosomal translocation is a universal response to all the upstream stimuli and is required for mTORC1 inactivation [100].

Subcellular localization of Rheb

The subcellular localization of Rheb is still a controversial subject. For many years it has been thought that Rheb is localized on lysosomes where it could meet and activate mTORC1, regardless of the presence of amino acids [95, 101, 102]. Such data were obtained from analysis of overexpressed green fluorescent protein (GFP) tagged Rheb (GFP-Rheb) due to lack of antibody detecting endogenous Rheb by

immunofluorescence at that time. However, more recently it has been suggested that Rheb binds Golgi apparatus, which is in proximity to lysosomes [103]. In addition, an earlier report in 2013 suggests that GFP-Rheb associates with Rab7, a marker to late endosome [97]. Considering that molecules are transported from Golgi apparatus, to late endosome and continue to lysosomes, it is likely that the subcellular distribution of Rheb is highly dynamic. This is supported by studies showing that red fluorescent protein (DsRed) tagged Rheb was present in late endosome 8 hours post transfection in Madin-Darby Canine Kidney (MDCK) cells, and in lysosomes 40 hours later [102]. Considering this discrepancy in Rheb subcellular distribution, it has been positioned in the proximity of lysosomes in the model displayed in Figure 12. In addition to being an activator of mTORC1, Rheb has also been found to activate nucleotide synthesis by binding to CAD protein, an enzyme required for pyrimidine biosynthesis [104].

GAP and GEF for Rags

In addition to regulating the lysosomal localization of Rags, Ragulator also acts as a GEF for RagA and B [98]. Ragulator preferentially binds GDP-bound RagA and B, and stimulates them to switch into the active GTP-bound state. In contrast, GATOR1 (GAP activity toward Rags complexes 1) functions as a GAP towards RagA and B, and converts them into the inactive GDP-bound state [105]. The activity of GATOR1 is regulated by GATOR2 and is sensitive to amino acid conditions [105]. When amino acids are present, Ragulator is active while GATOR1 is inhibited by GATOR2, and thereby Rags form the active heterodimer, recruiting mTORC1 onto lysosomal surface [95, 97, 98]. Upon amino acid withdrawal, Ragulator becomes inhibited and GATOR1 is active, which renders Rags inactive and unable to recruit mTORC1.

①

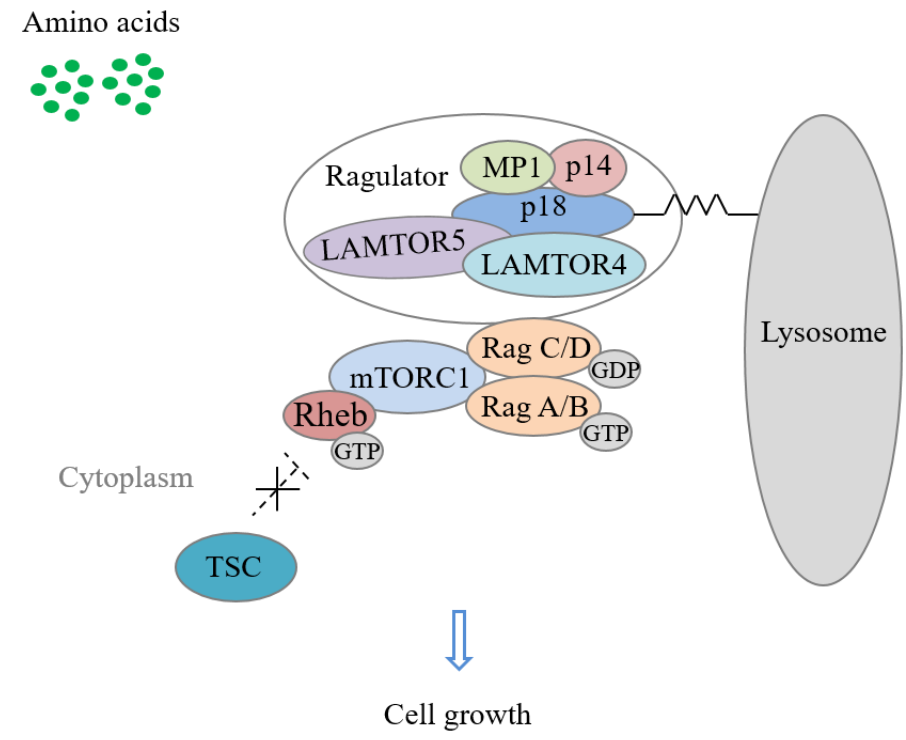

Cell growth

②

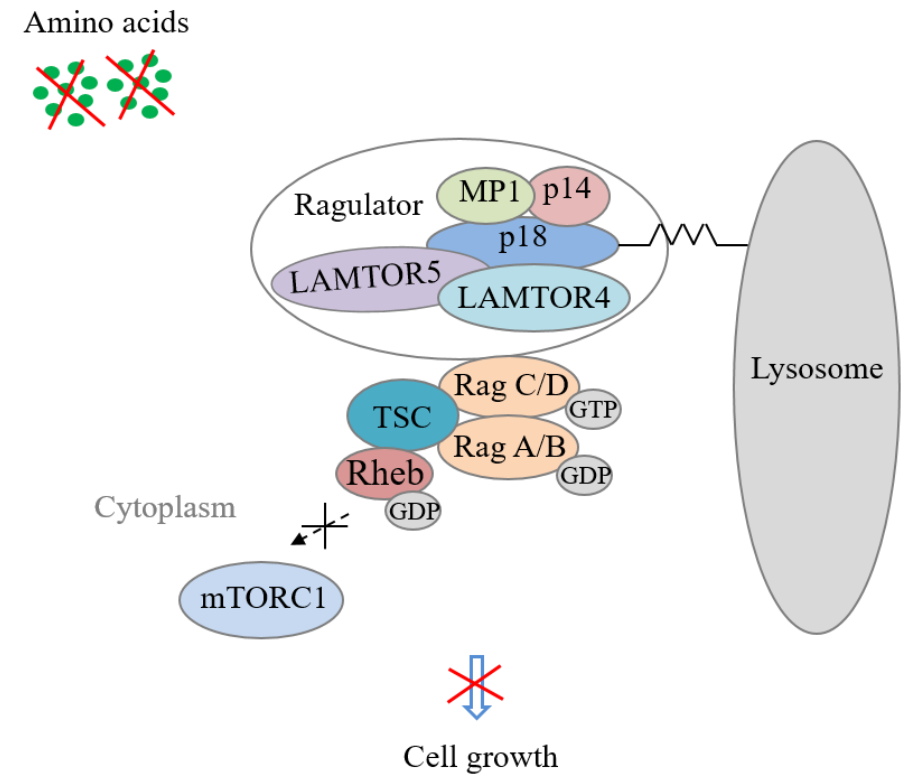

Cell growth

Figure 12. A currently proposed model of mTORC1 regulation by amino acids.
The Rag heterodimer (RagA/B or RagC/D) associates with the lysosomal protein complex Ragulator regardless of amino acid availability. Rheb is positioned in the vicinity of lysosomes in this model. **Panel 1**, in the presence of amino acids, the active Rag heterodimer ($RagA/B^{GTP}$ and $RagC/D^{GDP}$) recruits mTORC1 to lysosomal membrane, which allows it to be activated by GTP-bound Rheb. **Panel 2**, in the absence of amino acids, the inactive Rag heterodimer ($RagA/B^{GDP}$ and $RagC/D^{GTP}$) recruits the complex TSC onto lysosomes. Lysosome-localized TSC2 inactivates Rheb, resulting in inhibition of mTORC1 activity and its dissociation from lysosomes. This figure is adapted from reference [106].

Upstream activators and inhibitors

Several activators that transduce amino acid stimulus to mTORC1 have been identified, which include vacuolar H+-ATPase (v-ATPase) [107], mitogen-activated protein kinase kinase kinase kinase 3 (MAP4K3) [108, 109] and phospholipase D 1 (PLD1) [110] as shown in Figure 13. V-ATPase promotes mTORC1 by interacting with Ragulator. Both MAP4K3 and PLD1 are activated by amino acid sufficiency and stimulate mTORC1 activity. PLD1-mediated activation of mTORC1 requires the Class III PI3K called hVps34 [110] whilst no mediator of MAP4K3 activity towards mTORC1 has been described. In addition to TSC2, general control nonderepressible 2 (GCN2), a kinase that is activated by amino acid deficiency, has been recently demonstrated to inhibit mTORC1 activity [111].

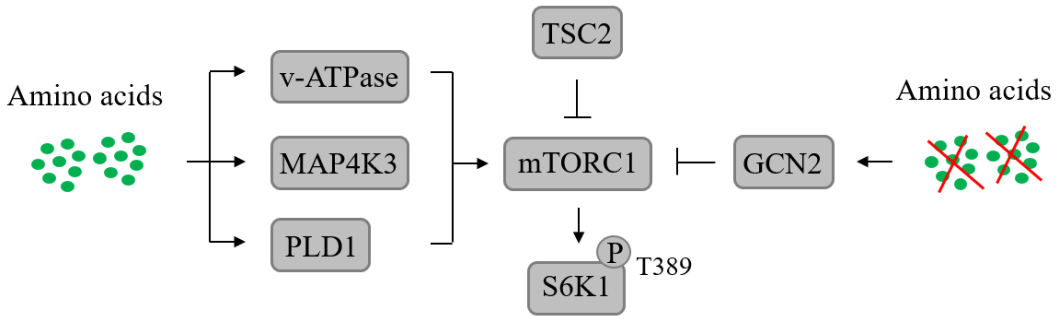

Figure 13. Proposed activators and inhibitors of mTORC1 in response to amino acids.
Three activators, v-ATPase, MAP4K3 and PLD1, have been proposed to sense amino acid sufficiency and activate mTORC1. TSC2 is the master inhibitor of mTORC1 in response to all upstream signals. GCN2 that senses amino acid deficiency has been recently demonstrated to regulate mTORC1 inactivation.

Unsolved puzzles

Of all the upstream stimuli inputs toward mTORC1, the amino acids stimulus is the most interesting, in that it is indispensable for mTORC1 activation [112] and sensing amino acids seems to be a unique function of mTORC1 since other proliferative signalling pathways including MAPK/ERK and PI3K/Akt do not respond to amino acids [112]. In addition, cancer cells demonstrate high demands for certain amino acids, in addition to glucose [113], thereby targeting the mechanism underlying amino acids-mediated activation of mTORC1 might be a promising approach for cancer therapeutics. In spite of many intensive studies that have been conducted, there are still puzzles in the amino acid-mediated mTORC1 signalling. These puzzles include the compartment where endogenous Rheb exactly localizes and whether its localization is regulated by amino acids or growth factors, the mechanism of how exactly GTP-bound Rheb activates mTORC1, regulators of lysosomal translocation of TSC2 in addition to Rags, mechanisms underlying activation and inhibition of mTORC1 signalling by GCN2 and MAP4K3 respectively.

1.4.4 GCN2 senses amino acid deficiency and represses protein synthesis

GCN2, encoded by *eukaryotic initiation factor 2 (eIF2) alpha kinase 4* (*EIF2AK4*) gene, is a protein kinase that represses protein synthesis via phosphorylation of eIF2 alpha subunit (eIF2α), which is the only described substrate of GCN2 [114]. GCN2 possesses five domains [115] (Figure 13): a N-terminal GCN1 and GCN20-binding region (GCN1/GCN20), a degenerate protein kinase domain with unknown function; a serine/threonine protein kinase domain, a regulatory domain homologous to histidyl-tRNA synthetases (HisRS-like) that binds deacylated (uncharged) tRNA [116, 117] and the C-terminal region (Cterm) that is required for its kinase activity.

Deficiency in amino acids results in elevated concentration of uncharged tRNAs, which bind to the HisRS-like region of GCN2 [116, 117]. This stimulates the transition of GCN2-GCN2 dimer from inhibited to catalytically active conformation. Activated GCN2 phosphorylates eIF2α on Ser51 [118-120], which converts eIF2 into an inhibitor of its GEF eIF2B [121] (Figure 14). eIF2 is thereby sequestered in the GDP-bound state, which interferes with formation of the eIF2-GTP and Met-tRNA complex that is required for protein translation initiation [121]. eIF2α

phosphorylation by GCN2 results in general inhibition of protein synthesis, but also upregulation of the transcription factor ATF4 [122], which stimulates expression of amino acid transporters [123] and amino acid synthetases [124] to restore amino acid homeostasis during amino acid deprivation.

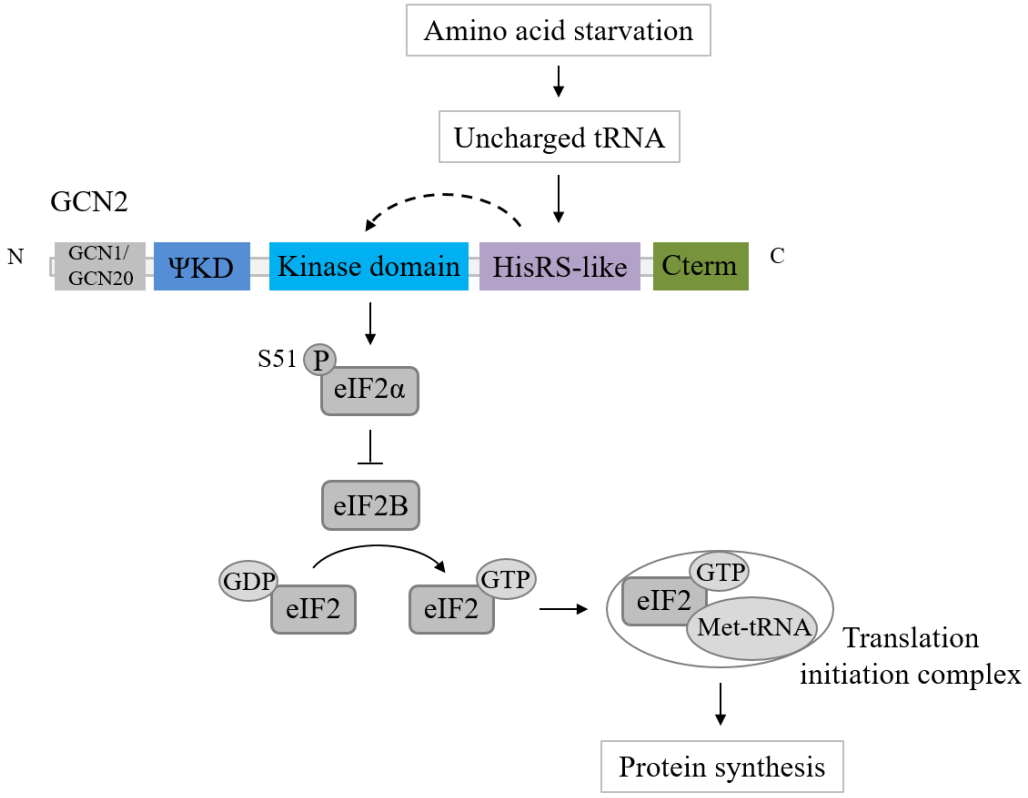

Figure 14. GCN2 senses amino acid deficiency and inhibits protein synthesis. GCN2 consists of a GCN1 and GCN20-binding region (GCN1/GCN20), a degenerate protein kinase domain (ψKD), a serine/threonine protein kinase domain (Kinase domain), a regulatory domain homologous to histidyl-tRNA synthetases (HisRS-like) and the C-terminal region (Cterm). Amino acid starvation increases the level of uncharged tRNAs, which bind to the HisRS-like region of GCN2, leading to its activation. Activated GCN2 phosphorylates eIF2α on Ser51, which inhibits eIF2B, a GEF for eIF2. Under normal-nutrient condition, GTP-bound eIF2 and Met-tRNA form a complex that is required for translation initiation. Inhibition of eIF2B renders eIF2 sequestered in the GDP-bound state and unable to initiate translation, resulting in protein synthesis repression. This figure is adapted from reference [115].

1.4.5 MAP4K3 senses amino acid sufficiency and activates mTORC1

MAP4K3, also known as germinal-centre kinase (GCK)-like kinase (GLK), is involved in various cellular processes, such as amino acid signalling [108, 109], inflammatory response [125], migration [126] and apoptosis [127, 128]. MAP4K3 consists of eleven kinase domains, two PEST (rich in proline, glutamic acid, serine,

and threonine) sequences, a proline-rich core and a regulatory domain [128] (Figure 15). The proline-rich core is composed of three proline-rich sequence motifs, and regulates protein-protein interaction [109, 129]. Two PESTs are associated with rapid protein degradation [127]. Ser170 residue in the kinase domain is a trans-autophosphorylation site that can be phosphorylated by another MAP4K3 kinase [109]. It has been demonstrated that phosphorylation of Ser170 can be induced by amino acids and is required for MAP4K3 to activate mTORC1 [108, 109].

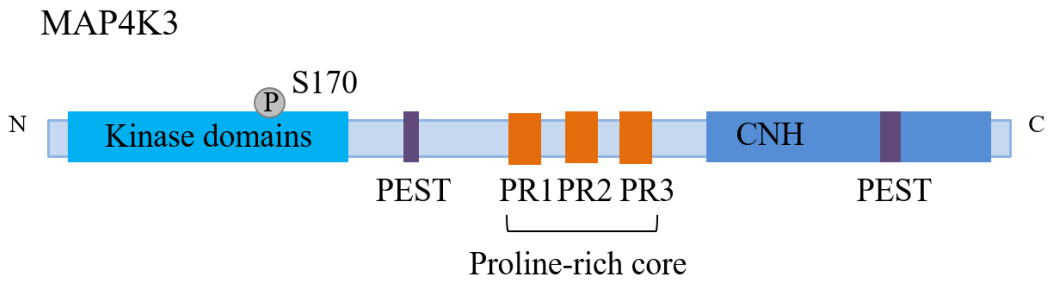

Figure 15. Linear schematic representation of MAP4K3 structure.
MAP4K3 from N- to C-terminus consists of eleven kinase domains containing the trans-autophosphorylation site Ser170, a PEST sequence rich in proline (P), glutamic acid (E), serine (S), and threonine (T), a proline-rich (PR) core composed of three PR sequence motifs, a second PEST and the citron homology (CNH) regulatory domain. This figure is based on description of MAP4K3 structure in reference [128].

MAP4K3 seems to play complicated roles in cellular signalling (Figure 16). On one hand, MAP4K3 can promote apoptosis by activating the JNK signalling pathway, suggesting a tumour suppressor role [128]. In accordance with this, reduced expression of MAP4K3 is associated with pancreatic cancer [127]. On the other hand, MAP4K3 contributes to cell proliferation by activating PKC and mTORC1 [108, 109, 125]. PKC activates the transcription factor nuclear factor kappa-light-chain-enhancer of activated B cells (NF-kB), which promotes cell survival under conditions of cellular stress [125]. MAP4K3 activates mTORC1 in response to amino acid sufficiency, though the mechanism remains elusive [108, 109]. In consistent with its tumour-promoting role, high levels of MAP4K3 are associated with metastasis, invasion and poor survival in NSCLC patients [126, 130].

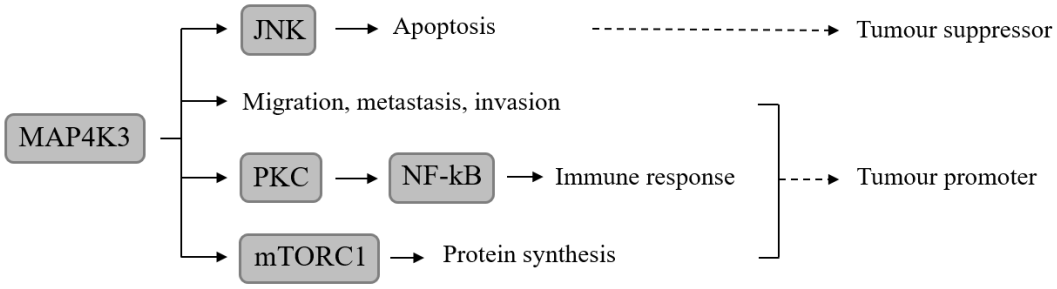

Figure 16. MAP4K3 is a putative tumour suppressor and promoter.
MAP4K3 acts as an apoptosis inducer by activating the JNK signalling, suggesting a tumour suppressor role; on the other hand, it promotes cell growth and survival by activating PKC and mTORC1, indicating that it might contribute to tumorigenesis.

1.5 Role of tumour suppressor p53 in cancer development

The tumour suppressor p53 (tumour protein 53), encoded by the *TP53* gene, is a transcription factor that has been found to regulate expression of more than 500 genes [131]. Among these genes are important regulators of apoptosis, DNA repair, metabolism and growth factors signalling including PI3K/Akt and mTORC1. P53 has a pivotal role in regulating a wide range of cellular responses to different types of stress, including DNA damage, hypoxia and oncogene activation [132] (Figure 17). The role of p53 being a tumour suppressor is predominantly attributed to its ability to promote apoptosis and induce cell cycle arrest, which contribute to elimination of cancer cells and suppression of tumorigenesis [133]. Most common tumour-associated mutations of p53 are within the DNA binding domain, rendering p53 transcriptionally inactive. As a results of these mutations, cells become unresponsive to pro-apoptotic signals and therefore evade cell death [132]. P53 also has a role in regulating senescence and differentiation, which inhibit proliferation and pluripotency of cancer stem cells [134, 135]. Activation of p53 does not necessarily results in cell death. When the DNA-damaging stress is moderate, p53 promotes cell cycle arrest and DNA repair by upregulating cell cycle regulator p21 and also DNA repair pathways such as DNA repair protein poly(ADP-ribose) polymerase 1 (PARP1) [132]. Therefore, the normal function of p53 is critical for maintaining the genetic fidelity and thus the whole genomic stability, and it is not surprising that p53 has been called “the guardian of the genome” [136]. In addition, p53 prevents tumorigenesis also via suppressing glycolysis [137]. Cancer cells universally re-direct the oxidative phosphorylation to aerobic glycolysis, presumably

because the glycolytic pathway provides intermediates that are required for cell growth and division, and also the oxidative phosphorylation produces more reactive oxygen species (ROS) that cancer cells are not well equipped to deal with [138]. P53, by inhibiting key glycolytic enzymes, suppresses glycolysis and inhibits cell growth and proliferation. Therefore, loss of p53 expression or function, due to mutations or viral oncoproteins, results in high rates of mutations and evasion of cell death, leading to cancer progression, and indeed, p53 is the most frequently mutated gene in all human cancers [139, 140].

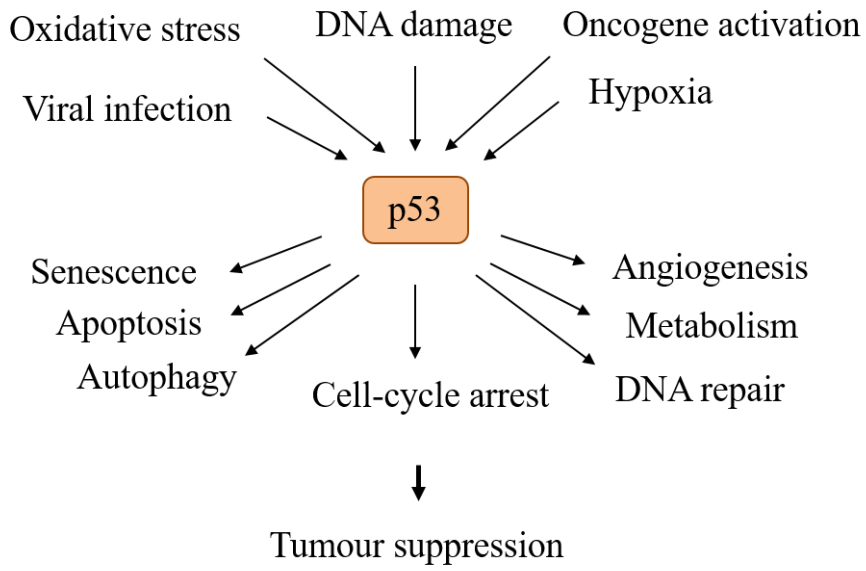

Figure 17. Overview of p53 in cellular responses.
P53 regulates various aspects of cell behaviour in response to a different forms of stress, including DNA damage, oxidative stress, hypoxia, viral infection and oncogene activation, to ensure gene fidelity, normal cell growth and to suppress tumorigenesis. P53 promotes cell-cycle arrest and DNA repair in response to DNA-damaging insults. P53 also stimulates the apoptotic pathway, senescence and autophagy to eliminate dangerous cells and inhibit proliferation. Induction of p53 during immune response promotes angiogenesis for cell survival. Suppression of glycolysis by p53 also contributes to inhibition of cell proliferation. This figure is based on description of the role of p53 in reference [132]

P53 is subject to a variety of post-translational modifications, including phosphorylation, ubiquitination, methylation and farnesylation, which together with its binding partners modulate the subcellular localization, stability and conformation of p53 [132]. One of the central mechanisms that regulate p53 function is regulation of its stability by the ubiquitin ligase MDM2, which targets p53 for degradation as well as directly inhibits its activity by binding to the transcriptional activation

domain [141]. Upon DNA damage, p53 is phosphorylated on Ser15 by the serine/threonine kinase ATM (ataxia-telangiectasia mutated), which disrupts the interaction of p53 with MDM2 and leads to activation of p53 [142]. Activated p53 can induce the expression of MDM2, generating a negative auto-regulatory feedback loop between these two proteins [143]. P53 also has tight links with the growth factor signalling pathways, including PI3K/Akt and mTORC1 (Figure 18), so that a balance between cell growth and stress responses can be achieved and cells proliferate without accumulating damaged DNA [28, 94].

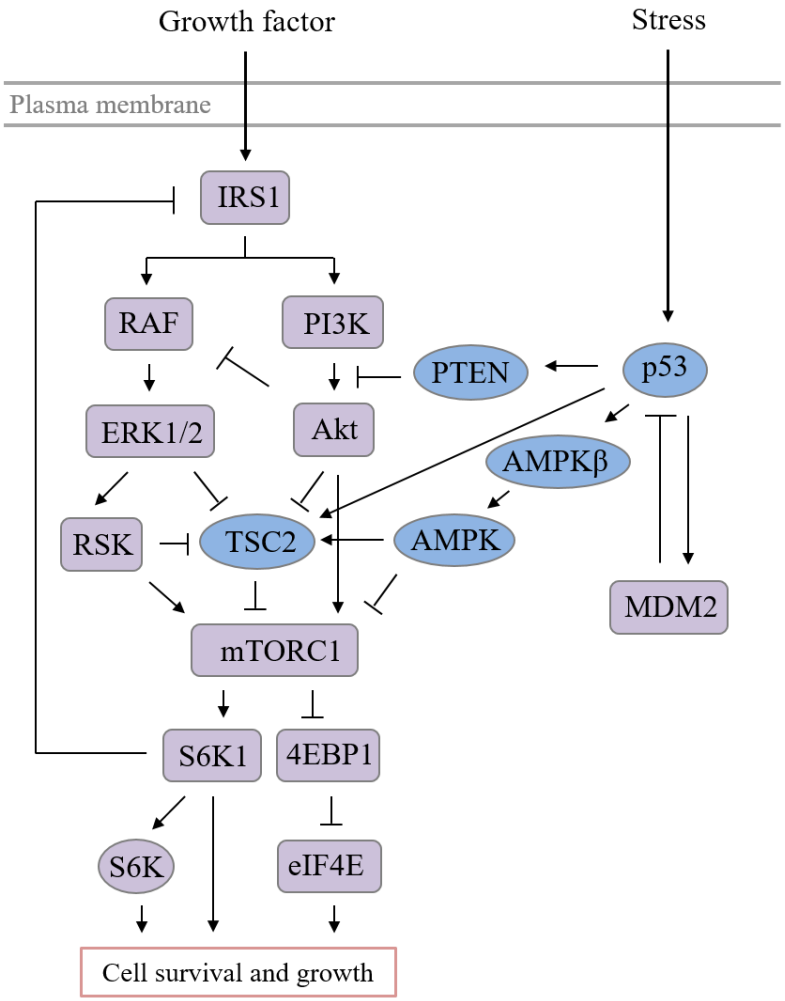

Figure 18. Crosstalk between p53 and PI3K/Akt and mTORC1 pathways. Growth factors stimulate activation of PI3K/Akt, MAPK/ERK and mTORC1 signalling pathways. Moderate stress-activated p53 upregulates the expression of PTEN and AMPKβ, which are the inhibitors of PI3K/Akt and mTORC1 respectively, leading to suppression of the downstream signalling effectors. This figure is modified from reference [144].

1.6 Role of programmed cell death (PCD) in cancer development

PCD is a process during which cells are eliminated in a genetically-determined fashion and is essential for maintaining cell number and homeostasis within the tissue [145]. The three forms of PCD, apoptosis, autophagic cell death and necroptosis (programmed necrosis) can be distinguished by their morphological and biochemical features [146] (Figure 19 and Table 1). Ferroptosis is an emerging form of PCD, characterized by iron (ferrous) dependence and is a type of oxidative cell death that is distinct from other forms of PCD [147]. Morphological features of ferroptosis have not been well established yet, but it has been suggested that ferroptosis is accompanied by mitochondrial shrinkage [147] (Table 1). Apoptosis is the major form of PCD and dysregulation of apoptosis is associated with a wide variety of pathological conditions, such as neurodegenerative diseases, ischemic damage and notably cancer.

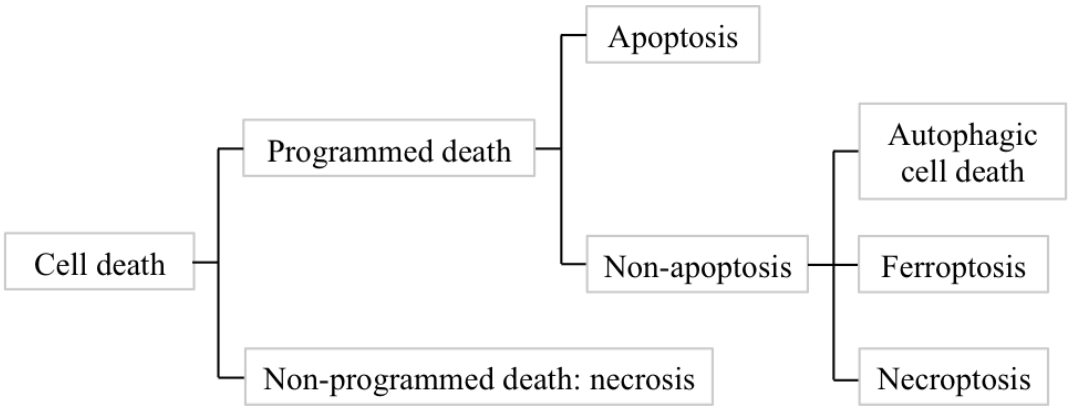

Figure 19. Main forms of cell death.
Cell death can be divided into two groups, programmed and non-programmed death. The former comprises apoptosis and non-apoptosis, and the latter is necrosis. Non-apoptotic cell death includes ferroptosis, necroptosis and autophagic cell death. This figure is based on description of cell death classification in reference [145].

Table 1. Morphological changes during different types of cell death
Necrosis. Irreversible cellular damage resulting from external factors such as injury and infection, with rupture of plasma membrane and organelles swelling.
Necroptosis. A regulated form of necrosis as a result of inflammatory response.
Apoptosis. A precisely regulated form of cell death in response to both intra- and extra-cellular stimuli, with cell shrinkage, chromatin condensation, formation of apoptotic bodies containing intact organelles.

Ferroptosis: An iron-dependent oxidative cell death that is induced by excessive accumulation of lipid ROS and inhibition of GPX4, and is accompanied by mitochondrial shrinkage.

Autophagic cell death. A form of cell death in response to nutrient insufficiency, with massive double-membrane vacuoles containing deteriorate organelles.

1.6.1 Apoptosis

Apoptosis is the major type of cell death [146], and is vital for a number of essential processes including embryonic development and immune response [145]. Apoptosis is accurately controlled under physiological conditions to ensure appropriate development of the system. It is also induced as a part of the defence system to eliminate damaged cells resulting from infection or cytotoxic agents [145]. Inappropriate apoptosis is associated with many diseases, such as neurodegenerative diseases due to upregulation of apoptosis, and conversely many types of cancer owing to downregulation of apoptosis.

Apoptosis is characterized by a sequence of morphological alterations that ultimately leads to degradation of the cellular components, and these alterations include shrinkage of the cell and the nucleus, condensation and margination of nuclear chromatin, destructive fragmentation of the nucleus, cell detachment from the surrounding tissue, formation of apoptotic bodies that contain cellular organelles and fragments of nucleus, and final phagocytosis of these apoptotic bodies into neighbouring cells [148].

On genetic and biochemical levels, apoptosis is tightly controlled by the Bcl-2 family and caspases [149, 150]. The Bcl-2 family comprises more than 20 members that can be divided into three groups based on the presence of conserved Bcl-2 homology (BH) regions (Figure 20): the anti-apoptotic members with all four BH regions including Bcl-2, Bcl-XL, Bcl-w, Mcl-1; two pro-apoptotic subsets which are the BH3-only proteins (share the BH3 region only) including Bid, Bim, Bad and others, and the death effectors Bax, Bak and Bok that share BH 1-3 regions [150]. Caspases are a class of cysteine protease enzymes that act as apoptosis executioners

[146]. They are constitutively synthesized as inactive procaspases, and are activated by pro-apoptotic signals in a self-amplifying and proteolytic manner [145].

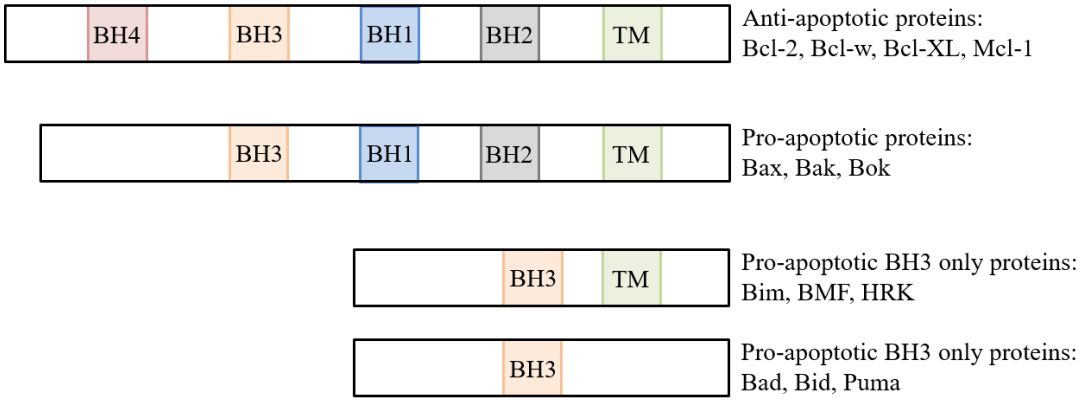

Figure 20. Structural and functional classification of the Bcl-2 proteins.
Bcl-2 proteins are subdivided into three groups according to conserved Bcl-2 homology (BH) domains. Abbreviation: TM, transmembrane domain. This figure is adapted from reference [151].

Apoptosis occurs mainly through the extrinsic death receptor and intrinsic mitochondrial pathways depending the sources of stimuli and biochemical mechanisms (reviewed in references [145, 146]) (Figure 21). The extrinsic pathway is stimulated as a part of immune responses through extracellular ligands that bind to and activate the membrane death receptors. The best characterized ligands and corresponding receptors include first apoptosis signal receptor (Fas) ligand (FasL)/Fas and tumour necrosis factor (TNF)-α/TNFR1 [145]. Activated Fas interacts with and activates the adapter protein Fas-associating protein with death domain (FADD), which associates with pro-caspase-8, leading to formation of death-inducing signalling complex (DISC) and activation of caspcase-8 [146]. Upon activation, caspase-8 promotes the activation of the apoptosis executioner caspase-3 and the Bcl-2 family member Bid [145, 152]. Bid then binds to Bim and induces activation of Bax and Bak [152], initiating the intrinsic pathway.

The intrinsic pathway is initiated by intracellular stimuli such as deprivation of growth factors or hormone [145] (Figure 21). These stimuli activate BH3-only proteins including Bad and Bim, which further inhibit anti-apoptotic proteins and activate pro-apoptotic proteins [152], particularly Bax and Bak, leading to permeabilization of the mitochondrial outer membrane and thus release of two

groups of pro-apoptotic factors into cytoplasm [145, 153]. The first group comprises cytochrome c, second mitochondria-derived activator of caspase (Smac) and the serine protease high temperature requirement protein A2 (HtrA2), all of which promote the caspase-3 activation [145]. Cytoplasmic cytochrome c, apoptotic protease activating factor 1 (Apaf1) and pro-caspase-9 forms the complex called apoptosome, leading to activation of caspase-9, which in turn promotes activation of caspase-3 [145]. Caspase-3 then cleaves various substrates including inhibitor of caspase-activated DNase (ICAD) and poly(ADP-ribose) polymerase (PARP), which ultimately causes DNA fragmentation. The second group of pro-apoptotic factors are apoptosis-inducing factor (AIF), endonuclease G (Endo G) and CAD [146], which translocate to the nucleus and promote DNA fragmentation. This pathway is also stimulated by cytotoxic agents and irradiation that cause DNA damage and activation of p53. Activated p53 binds to and activates Bax and Bak, leading to further apoptotic response [152]. Moreover, apoptosis is accompanied by elevated accumulation of mitochondrial ROS. ROS is a natural by-product of oxygen metabolism (see Chapter 1.6.2.1) and can induce oxidative modification of proteins including the mitochondrial permeability transition complex, leading to hyperpolarization of mitochondrial membranes and thus initiation of the intrinsic apoptotic pathway [154, 155].

Apoptosis is considered as the natural barrier to cancer development [1] and defects in apoptosis are frequently found in cancer [156]. It seems that these defects do not originate from the apoptotic machinery, in that mutations or overexpression of the Bcl-2 family and caspases are not common in cancer. Instead, evasion of cell death in cancer usually results from mutations of the upstream mediators, such as the tumour suppressor p53 that drives the apoptotic response [145].

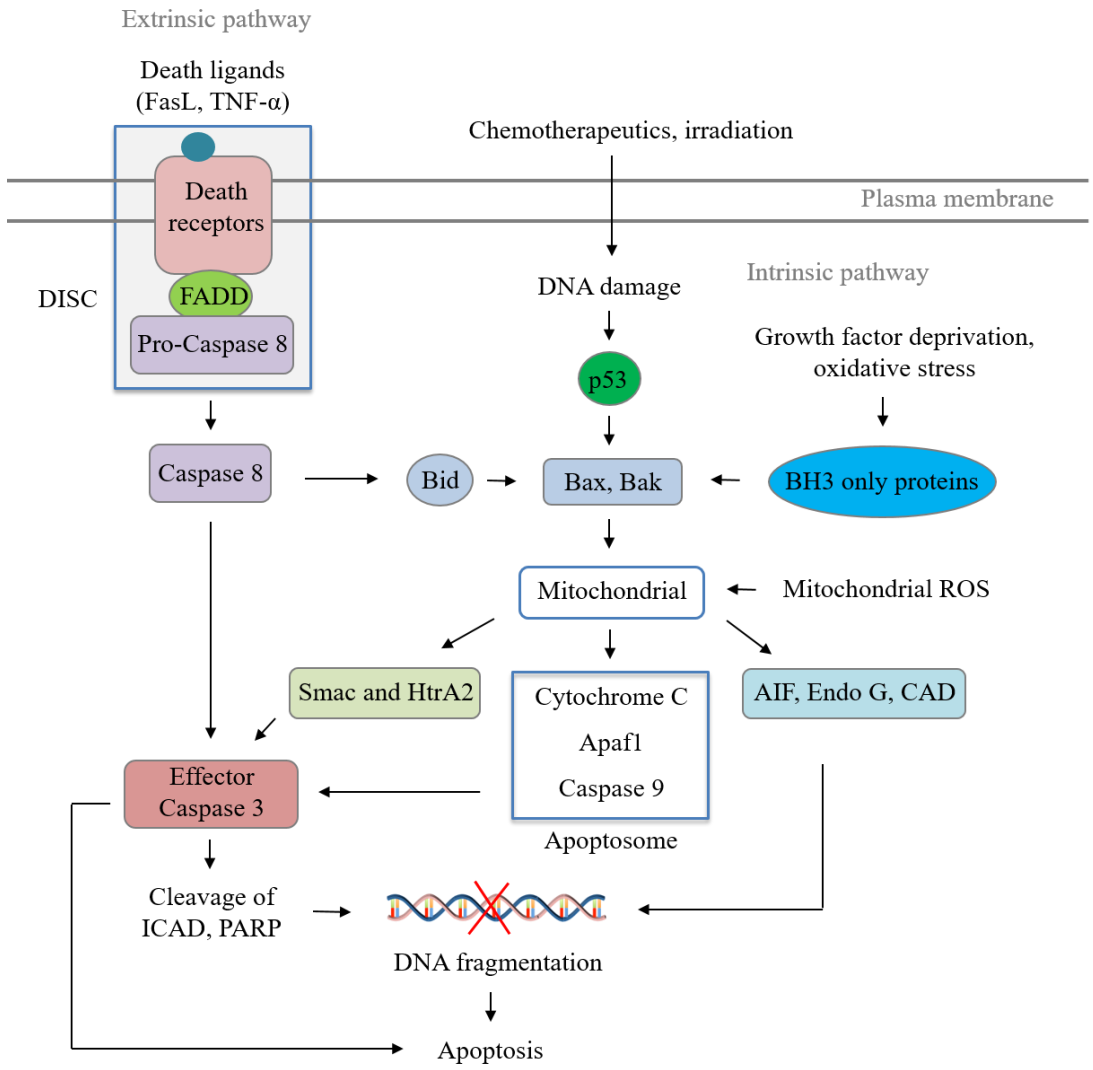

Figure 21. Extrinsic and intrinsic apoptotic pathways.
Extrinsic pathway: inflammation-stimulated death ligands, such as FasL and TNF-α, bind to the transmembrane death receptor, which stimulates the activation of caspase-8 and thus the apoptosis executioner caspase-3. Activated caspase-3 cleaves and inhibits ICAD and PARP, leading to DNA fragmentation and thereby apoptosis. The intrinsic pathway can be induced by three groups of stimuli, the growth factor deprivation and hypoxia that activate BH3 only proteins, cytotoxic agents and irradiation that cause DNA damage and subsequent activation of p53, and mitochondrial ROS that induce oxidative modification of mitochondrial proteins. These stimuli cause permeabilization of the mitochondrial outer membrane and consequently cytosolic translocation of pro-apoptotic factors including cytochrome c, Smac, HtrA2 and CAD, leading to activation of caspase-3 and DNA fragmentation. This figure is modified from reference [146].

1.6.2 Ferroptosis is an oxidative non-apoptotic form of cell death

1.6.2.1 Oxidative stress and antioxidant systems

Reactive oxygen species (ROS) definition and function

ROS are highly reactive molecules derived from oxygen (O_2) and they are divided into two groups: free radicals that contain unpaired electrons such as hydroxyl radicals (HO•) and superoxide anions ($O_2^{\bullet-}$); and non-radicals that do not contain unpaired electrons such as hydrogen peroxide (H_2O_2) [157, 158]. HO•, $O_2^{\bullet-}$ and H_2O_2 are the three major ROS in cells and have significant cellular functions. $O_2^{\bullet-}$ is converted into H_2O_2 by superoxide dismutase and it also reacts with H_2O to generate HO• [158]. ROS act as second messengers to mediate diverse cellular processes, including MAPK/ERK and PI3K/Akt signalling pathways that regulate cell growth and proliferation, immune and hypoxic responses [157, 159-162]. ROS can promote cell growth through two mechanisms: ROS 1) induce auto-phosphorylation of growth factor receptors including EGFR and PDGFR independently of growth factor ligands; 2) activate RAS through oxidative modification that inhibits its GDP/GTP exchange, both of which activate the MAPK/ERK and PI3K/Akt pathways [160]. Moreover, H_2O_2 can activate transcription factor NF-KB that regulates immune response [161]. Moderate cellular levels of ROS are counterbalanced by antioxidant defence systems, however, excessive ROS induce oxidative modification and thus degradation of essential cell structures including lipids, proteins and DNA [158, 159, 163-166]. Among these ROS, HO• is most reactive and induces 1) DNA breakage by oxidizing all four nucleotide bases [164]; 2) protein damage by oxidizing the protein polypeptide backbone [165]; and 3) lipid peroxidation by oxidizing polyunsaturated fatty acids (PUFAs) whereby the membrane lipid bilayer arrangement is disrupted [166]. $O_2^{\bullet-}$ and H_2O_2 indirectly damage DNA, protein and lipid by generating HO•. Furthermore, ROS initiate the intrinsic apoptotic cascade by inducing hyperpolarization of mitochondrial membrane and hence cytochrome c release and mitochondrial translocation of Bax and Bad [155].

Sources of ROS

ROS can originate from exogenous and intracellular sources. Exogenous sources include toxic agents such as cigarette smoke that contains oxidants and free radicals,

hyperoxia and ionizing radiation [158]. Most intracellular ROS are formed in mitochondria as a by-product of the respiratory chain reactions that reduce oxygen to water [167]. Intracellular ROS can also be produced in other cellular compartments, such as lipid membranes, peroxisomes, cytoplasm, mitochondria, endoplasmic reticulum (ER) and lysosomes, by the action of membrane-bound NADPH oxidases (NOX) that convert O_2 to $O_2^{\bullet-}$ and H_2O_2 [158, 159, 168] (Figure 22). Five isoforms of NOX have been identified in humans and they are encoded by different genes [169]. NOX3 is mainly expressed in foetal tissues whilst the other NOXs (1, 2, 4 and 5) are ubiquitously expressed in many cell types.

Antioxidant systems

Antioxidants act as scavengers of ROS and effectively remove their oxidative effects [158]. They can be grouped into enzymatic and non-enzymatic categories. Non-enzymatic antioxidants are a group of low-molecular-weight compounds and molecules containing a thiol group, capable of being oxidized by ROS, such as vitamins C and E, and the amino acid glutathione [158]. Glutathione is highly abundant in all cellular compartments and exists in reduced (GSH) and oxidized (GSSG) forms (Figure 22). GSH is a tripeptide composed of cysteine, glycine and glutamate, and it is the major soluble antioxidant in cells. The amino acid cysteine is unstable and reduced from cystine following uptake by the cystine/glutamate antiporter system x_c^- consisting of SLC3A2 and SLC7A11 [170]. Because intracellular cystine is much less abundant than glycine and glutamate, cystine/cysteine is the rate-limiting precursor in GSH synthesis. One of the major enzymatic antioxidants is the glutathione peroxidase (GPX) family [171, 172]. Four GPX isoforms have been described and they vary in subcellular location and substrate specificity. Cytoplasmic GPX1 and membrane-bound GPX4 are ubiquitous and target H_2O_2 and lipid hydroperoxides (lipid-H_2O_2) respectively (Figure 22). GPX2 is expressed in gastrointestinal epithelial cells and acts on dietary peroxides whilst GPX3 is localized in extracellular compartment. GPX catalyses the oxidation of GSH to GSSG whereby harmful H_2O_2 and lipid-H_2O_2 are reduced to harmless water and alcohol (Figure 22) [172]. GSH thus donates an electron to neutralize H_2O_2, whilst the resulting GSSG accepts an electron from NADPH and converts into

GSH. Glutathione and GPX4 are therefore particularly important in protecting lipid membranes from oxidative damage of lipid ROS.

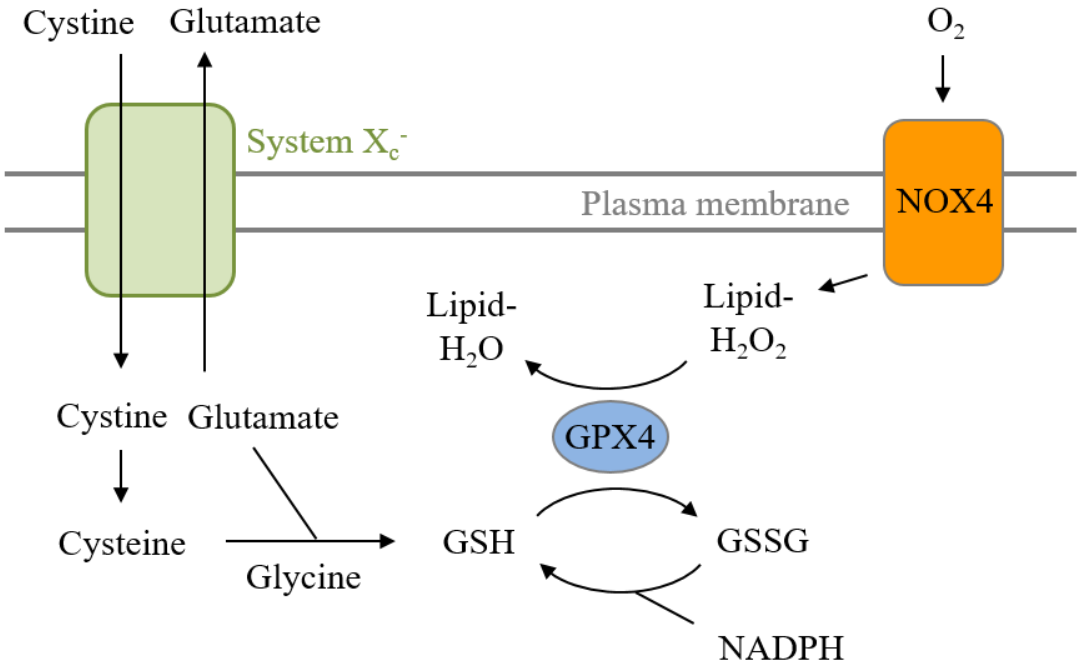

Figure 22. The GSH/GPX4 antioxidant system.
Extracellular amino acid cystine is imported into cells via the cystine/glutamate antiporter system x_c^- that concomitantly exports glutamate. Cystine is the oxidized, more stable form of cysteine. Once inside the cell, two cystine molecules are reduced to form one cysteine molecule. Glutathione is synthesized from cysteine, glutamate and glycine, and cysteine is the rate-limiting precursor due to its low intracellular concentration. The lipid repair enzyme GPX4 catalyses oxidation of GSH (reduced form of glutathione) into GSSG (oxidized form of glutathione), in which GSH donates an electron to lipid hydroperoxides (lipid-H_2O_2) and reduces the latter into corresponding alcohols (lipid-H_2O). GSSG is then recycled into GSH by glutathione reductase, using an electron from NADPH. This figure is adapted from reference [173].

1.6.1.2 Ferroptosis

Ferroptosis was first described in 2012 by the research group of Professor Brent Stockwell as a unique form of non-apoptotic cell death with extreme dependence on the divalent iron (ferrous) [147]. In their experiments that led to the discovery of ferroptosis, the cell death was induced by the small molecule erastin that depletes the intracellular cystine pool by inhibiting the cystine/glutamate antiporter system x_c^-. Subsequent study has demonstrated that ferroptosis is in fact an ancient form of cells death driven by peroxidation of PUFAs in lipids [174]. PUFAs incorporated into

cellular membranes enhance membrane fluidity, which is essential for the function of membrane-associated proteins and other biomolecules. However, the composition of PUFAs within membranes renders the lipids susceptible to oxidative damage [174], in that PUFAs can react with lipid ROS, which induces oxidative degradation of lipids (lipid peroxidation). Ferroptosis is morphologically, biochemically and genetically distinct from other forms of cell death and is implicated in neurodegenerative diseases [175] and cancer [147].

Biochemical features

The process of ferroptotic cell death involves a variety of biochemical reactions including metabolisms of iron, amino acids, and PUFAs, and biosynthesis of glutathione and NADPH (reviewed in [173, 176]). Ferroptosis is induced by ROS, particularly lipid ROS, since this form of cellular death can be suppressed by lipophilic antioxidants such as ferrostatin-1 [147] and α-tocopherol (vitamin E) [177, 178] (Figure 23). Notably, the level of mitochondrial ROS has been demonstrated to remain unchanged during ferroptosis [147], whereas apoptotic cell death is accompanied by elevated mitochondrial ROS. Moreover, induction of ferroptosis by lipid ROS is highly dependent on iron abundance, in that knockdown of transferrin and transferrin receptor (TFR) that import iron inhibits ferroptosis [179, 180]. Ferroptosis is also suppressed by treatment with iron chelators, such as deferoxamine (DFO), which competitively bind iron and remove it from reactions [147]. The precise mechanism of iron promoting ferroptosis remains elusive, although it is likely that iron interacts with lipid peroxides, which converts them into lipid free radicals that are destructive to lipids and cells [181].

The antioxidants glutathione and GPX4 are critical in suppressing ferroptosis due to their capability of detoxifying lipid ROS [173, 182, 183]. The first discovered ferroptosis inducer, erastin [147], is an inhibitor of the glutamate/cystine antiporter in the plasma membrane [182]. Inhibition of the antiporter blocks uptake of cystine, thereby depletes the glutathione pool. Likewise, buthionine sulfoximine (BSO) is found to induce ferroptosis by inhibiting glutathione biosynthesis [184]. Depletion of intracellular glutathione causes excessive accumulation of lipid ROS [185] and renders the cells vulnerable to oxidative damage. Another initially identified

ferroptosis inducer is RSL3, a Ras-selective lethal compound [147], which is an inhibitor of the phospholipid enzyme GPX4 [183]. As described previously, GPX4 converts lipid hydroperoxides into lipid alcohols, thereby protects cells from oxidative damage [186], conversely inhibition of GPX4 results in elevated accumulation of lipid ROS and thus ferroptotic cell death.

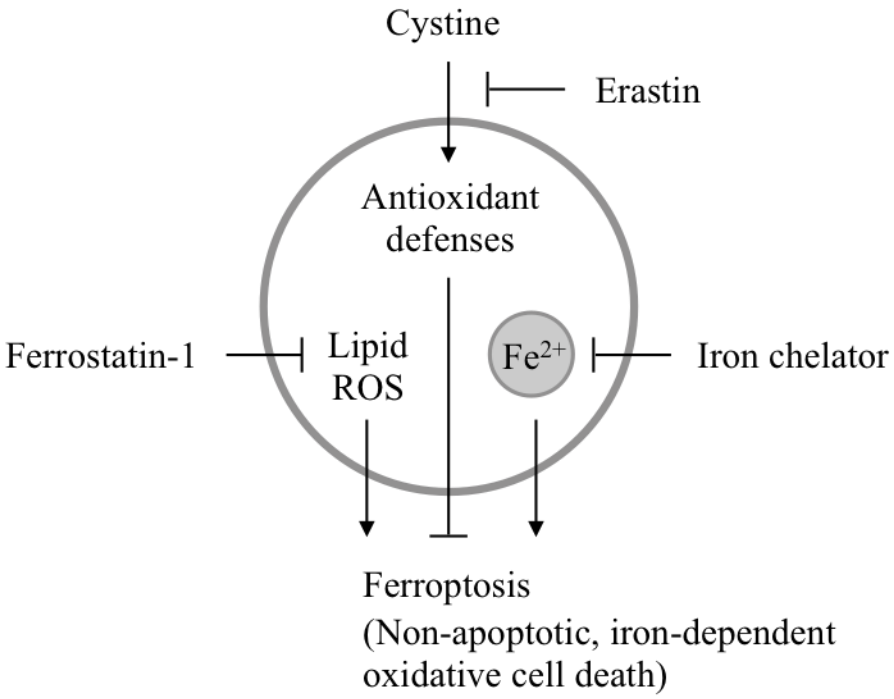

Figure 23. Ferroptosis is an iron-dependent oxidative non-apoptotic cell death. Ferroptosis is induced by excessive accumulation of lipid ROS and is highly dependent on iron abundance. The small compounds, erastin (an inhibitor of system x_c^-) and ferrostatin-1 (a lipophilic antioxidant), are respectively inducer and inhibitor of ferroptosis. Erastin prevents uptake of cystine, leading to depletion of antioxidant glutathione. Cellular antioxidants and ferrostatin-1 eliminate lipid ROS and thus supress ferroptosis. Iron chelating agents such as deferoxamine bind to iron and remove it from reactions, leading to inhibition of ferroptosis. This figure is based on description of ferroptosis in reference [147].

Whilst it is unclear whether there are any genetic factors contributing to ferroptosis, the susceptibility to ferroptosis appears to be tightly linked to certain genetic contexts. Ferroptosis has been reported to occur in RAS (NRAS, KRAS or HRAS) mutated cancer cells [147], however, mechanisms of how the downstream signalling pathways such as MAPK/ERK regulate ferroptosis remain elusive. Regardless, cells expressing the RAS mutations that sensitize them to ferroptosis are found to harbour increased levels of transferrin receptor (reviewed in [187]). In addition, p53 has been

demonstrated to promote ferroptosis by repressing expression of the glutamate/cystine antiporter and thus inhibiting cystine uptake [182, 188]. mTORC1 has been reported to promote ferroptosis [189] possibly through regulating iron metabolism [190].

1.7 Synthetic lethality is a promising approach for cancer therapeutics

For decades, radiation and toxic chemicals were the most commonly used therapies for cancer patients, both of which also cause dramatic damages to normal tissues. Although discoveries of small-molecule and antibody-based inhibitors that target oncogenes have personalised cancer therapies, resistance to these therapies arises and loss-of-function tumour suppressors remain un-targetable (reviewed in [191]). Identification of cancer-specific vulnerabilities or dependencies has emerged as a promising therapeutic strategy that selectively induces lethality in cancer cells while leaving normal cells undamaged or little damaged. Synthetic lethality screens have provided such an approach to distinguish genetic dependencies associated with the driver mutation in cancer cells. The American geneticist Calvin Bridges first reported synthetic lethality in 1922 when he observed in the fruit fly *Drosophila melanogaster* that mutations in two genes lead to cell death, although neither of these genes are individually required for viability [192]. Geneticist Theodore Dobzhansky also observed the similar genetic interaction and coined it as “synthetic lethality” [193]. Synthetic lethality thus describes genetic interactions where simultaneous disruption of two genes induces cell lethality, whereas disruption of either gene alone is viable. In the context of cancer, synthetic lethality creates a second-site gene target for a cancer-driving mutation (reviewed in [194]) (Figure 24). This overcomes the limitations of the conventional chemotherapy and expands the repertoire of anticancer therapeutic agents. Firstly, targeting the gene synthetic lethal to the cancer-driving mutation selectively kills cancer cells and spare normal cells, which should be efficacious with fewer side effects. Secondly, by targeting the second-site gene instead of the loss-of-function mutation itself, synthetic lethality opens the opportunities to certain cancer types with loss of tumour suppressor genes that are non-druggable by the conventional chemotherapy. For example, inhibitors targeting poly (ADP-ribose) polymerase (PARP) have been clinically approved for therapies

of cancer patients carrying mutations in the tumour suppressor genes BRCA1 or BRCA2 that functions to repair damaged DNA when normally expressed [195]. BRCA1 or BRCA2 mutations render patients defective in one specific DNA repair process, and PARP inhibitors, by targeting the PARP-mediated DNA repair process, have become lethal to cells with these mutations.

The concept of synthetic lethality has been extended to identify metabolic vulnerabilities of cancer cells that undergo metabolic re-programming and are addicted to certain metabolites. Such metabolic alterations in cancer cells include increased glucose uptake and glycolysis [196], nucleotide biosynthesis [197] and uptake of certain specific amino acids such as glutamine, serine, glycine, proline and arginine [198, 199]. Identification of the specific metabolic pathways is likely to offer opportunities for effective cancer-specific treatments and for treatments of cancers that are resistant to inhibitory agents.

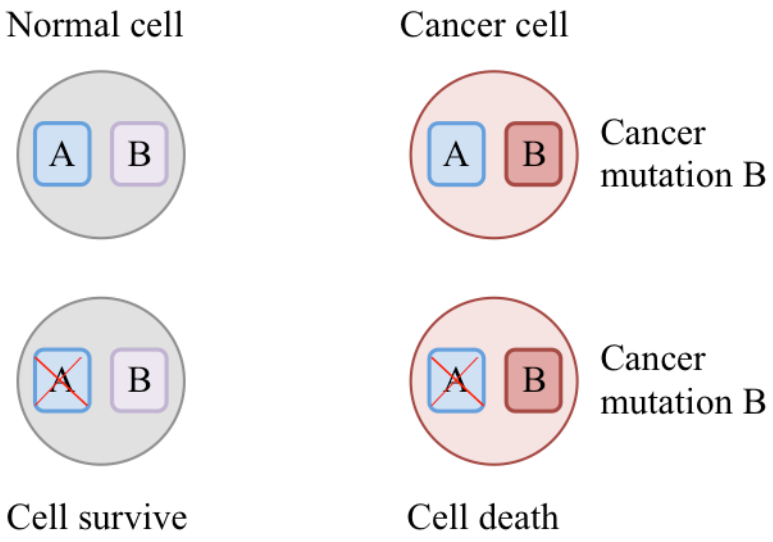

Figure 24. Schematic representation of synthetic lethality.
Targeting gene A causes lethality in cancer cells expressing the mutation B whereas normal cells survive. This figure is modified from reference [200].

1.8 Project strategies and aims

In this study, we focused on the proliferative signalling pathways, mTORC1, PI3K/Akt and MAPK/ERK, and their association with nutrient amino acids, the building blocks of proteins. The work presented in this thesis is mainly divided into

two parts, identification of mechanisms involved in mTORC1 inhibition in response to amino acid deprivation (Results Chapter 3.1) and identification of amino acid-associated vulnerabilities specific to the common mutations in oncogenes PI3K, EGFR, KRAS and BRAF (Chapter 3.3). In addition, this thesis also contains two minor parts, investigation of MAP4K3 as a tumour promoter and tumour suppressor (Chapter 3.2), and investigation of association of the tumour suppressor p53 with amino acids and mTORC1 (Chapter 3.4), which are present in the Results Chapter but not included in the Discussion Chapter due to lack of consistency to the main work.

The study on mTORC1 aimed to identify novel regulators and mechanisms involved in mTORC1 signalling in response to amino acid deprivation by centring on the recent findings that TSC2 undergoes lysosomal translocation and Rag GTPases mediates the lysosomal translocation of both mTORC1 and TSC2. To identify novel mediators of TSC2 subcellular localization, which would potentially reveal the additional mechanisms of its inhibition on mTORC1, a high-throughput quantitative cell imaging siRNA was performed. The resulting candidates were selected based on their association with amino acids and the relationship with TSC2 was examined using independent siRNAs and specific inhibitors. It has been demonstrated that the Rag GTPases regulate TSC2 lysosomal localization, we further investigated whether TSC2 affected Rag GTPases, by examining the localization of RagA and RagC in cells lacking TSC2. Rheb is critical for mTORC1 activation due to its ability to activate the catalytic activity of mTORC1. We then explored the role of Rheb in the lysosomal translocation of both mTORC1 and TSC2, via siRNA-induced suppression of Rheb. Since lysosomal translocation of mTORC1 and TSC2 is stimulated by amino acid sufficiency and deficiency respectively and is important for mTORC1 activation and inactivation, media shift treatment, which is switch from medium containing amino acids (the normal culture medium) to medium lacking amino acids (reconstituted medium according to the formulation of culture medium but omit all amino acids, see Material Chapter 2.1.10), was utilized throughout this work and also work on MAP4K3 and p53.

EGFR delE746-A750, KRAS G13D, BRAF V600E and PIK3CA H1047R are frequently found in multiple cancer types. To identify amino acid-associated vulnerabilities specific to these mutations, we have taken advantages of the hTERT human mammary epithelial (HME) cell lines established by the group of Professor Alberto Bardelli [201], and also an amino acid dropout screen. The four mutations have been knocked into the HME cell lines and demonstrated to activate the corresponding signalling pathways. These isogenic HME cell lines therefore provide a genetic context that is significantly less complicated than that in the cancer cell lines, which presumably allows the properties specific to these mutations to be characterized. By reconstituting media omitting one specific amino acid, an amino acid dropout screen could be performed. Based on the observation that depletion of which specific amino acid would cause lethality only in the mutant cells but not wild type, a cancer-specific vulnerability could be potentially established. Inhibitors specific to the mutations and downstream signalling effectors were also utilized to verify which pathway exactly was associated with the lethality caused by deprivation of the specific amino acid. To investigate the mechanisms involved in the distinct responses between mutant and wild type cells, the level of intracellular amino acids was examined and the specific amino acid-associated subcellular response was investigated. A panel of nine NSCLC cell lines were utilized so that the study in these isogenic HME cells could be expanded into the heterogeneous context of cancer cells, and the cell line that was susceptible to deprivation of the specific amino acid was selected for further engrafted tumour study in a mouse model. To mimic the media shift treatment, an engineered enzyme that degrades the specific amino acid was also utilized in both cell culture and the mouse model.

The work presented in this thesis has been re-directed several times due to unforeseen circumstances, however, the molecules that were studied, without exception, contribute to cancer development, and all the work centred on the cellular responses to amino acid conditions.

Chapter 2

Materials and Methods

Chapter 2 - Materials and Methods

2.1 Materials

2.1.1 Chemicals

- Acetonitrile (HPLC) *(Fisher Scientific, A998-1)*
- Acrylamide (30%) *(Geneflow, A2-0072)*
- Adenosine 5'-triphosphate (ATP) *(Cell signaling, 9804)*
- Agar *(Invitrogen, 30391-049)*
- Agarose *(Sigma, A9539)*
- Albumin from bovine serum (BSA) *(Sigma, A3059)*
- Ammonium persulfate (APS) *(Sigma, A3678)*
- ATP, [γ-32P]- 3000Ci/mmol 10mCi/ml, 250 µci *(PerkinElmer, BLU002A250UC)*
- Bacto-peptone *(BD Biosciences, 211677)*
- Bio-Rad protein assay dye reagent *(Bio-Rad Laboratories, 500-0006)*
- C11-BODIPY581/591 *(Thermo Fisher, D3861)*
- CellTiter-Glo reagent *(Promega, G7571)*
- Complete protease inhibitor cocktail tablets *(Roche Diagnostics, 11873580001)*
- Dako faramount aqueous mounting medium *(Dako North America, S3025)*
- ddH_2O (lab supplied through a Millipore Q 0.22µM filter system)
- Deoxynucleotide (dNTP) solution mix *(New England BioLabs, N0447S)*
- D-Glucose *(Fischer Scientific, G/0500/53)*
- Digitonin *(Sigma, D141)*
- Dimethylsulfoxide (DMSO) *(Sigma, D8418)*
- Dithiothreitol (DTT) *(Sigma, 43817)*
- 1kb DNA ladder *(New England BioLabs, N3232S)*
- Dried skimmed milk *(Marvel)*
- Dulbecco's phosphate buffered saline (DPBS) *(Invitrogen, 17104)*
- Dulbecco's Modified Eagle Medium (DMEM) *(Life Technologies, 31966021)*
- DMEM low glucose, w/o amino acids, pyr (powder) *(USBiological, D9800-13)*
- ECL western blotting detection reagents *(Fisher Scientific, RPN2106)*
- EDTA *(Fisher Scientific, 1021-3570)*
- EGTA *(Sigma, E3889)*
- Ethanol *(Fischer Scientific, E/0056DF/P17)*

- Etoposide *(Sigma, E1383)*
- Fetal bovine serum (FBS) *(Life Technologies, 10270106)*
- Glycerol *(Sigma, G3664-500UN)*
- β-Glycerophosphate disodium salt hydrate (β-GP) *(Sigma, G9422)*
- Glycine *(Fischer Scientific, 10080160)*
- Goat serum *(Sigma, G9023*)
- Hydrochloric acid (37%) *(Sigma, 320331)*
- Hydrocortisome (25mg/ml) *(Sigma, H0888)*
- Hydrogen peroxide, 30% in water *(Fisher Scientific, 10386643)*
- Hyperfilm ECL *(GE Healthcare Life Sciences, 28-9068-37)*
- Immersion oil immersol 518F fluorescence free *(Carl Zeiss, 444962-0000-000)*
- Insulin solution from bovine pancreas *(Sigma, I0516)*
- Isoproponal *(Fisher scientific, 11805725)*
- L-Amino acids *(Sigma, LAA21)*
- L-Buthionine-sulfoximine *(Sigma, B2515)*
- L-Glutamic acid *(Sigma, G1251)*
- Lipofectamine 2000 Transfection Reagent *(Life Technologies, 11668019)*
- Lithium chloride (LiCl) *(Sigma, 203637)*
- Lithium dodecyl sulfate (LDS) sample buffer *(Life Technologies, NP0007)*
- Luminol *(Sigma, A8511)*
- Magnesium chloride hexahydrate *(Sigma, M2670)*
- Methanol (HPLC) *(Fisher Scientific, 10675112)*
- β-Mercaptoethanol (β-ME) *(Sigma, M3148)*
- Minimum essential medium (MEM) amino acids solution *(Invitrogen, 11130-051)*
- NEB 10-β competent E. coli *(New England Biolabs, C3019I)*
- Okadaic acid potassium salt (O.A.) *(Sigma, O7885)*
- Paraformaldehyde (PFA) *(Sigma, 158127)*
- p-Coumaric acid *(Sigma, C9008)*
- Penicillin streptomycin (Pen strep) *(Life Technologies, 15140122)*
- Phosphate buffered saline solution *(Fisher Scientific, 10649744)*
- Phosphate buffered saline (PBS) for cell culture *(Thermo Fisher, 10010023)*
- Polyvinylidene difluoride (PVDF) membrane *(Millipore, IPVH00010)*
- Ponceau S solution *(Sigma, P7170)*

- Protein marker *(Fisher Scientific, RPN800E)*
- Purple DNA loading buffer *(New England BioLabs, B7024S)*
- Qiagen Plasmid Maxiprep Kit *(Qiagen, 12163)*
- QIAprep Spin Miniprep Kit *(Qiagen, 27104)*
- QuikChange Site-Directed Mutagenesis Kit *(Agilent Technologies, 200521)*
- Recombinant human EGF *(PeproTech House, AF-100-15)*
- RG x-ray Developer *(Jet X-Ray, RTU Developer)*
- RG x-ray Fixer *(Jet X-Ray, RTU Fixer)*
- RPMI 1640 medium *(Life Technologies, 61870010)*
- SafeView nucleic acid stain *(NBS Biologicals, NBS-SV)*
- Snakeskin dialysis tubing, 3.5K MWCO *(Fisher Scientific, 88244)*
- SOC growth medium *(BioLabs, B9020S)*
- Sodium chloride (NaCl) *(Fisher Scientific, 10428420)*
- Sodium dodecyl sulfate (SDS) *(Sigma, L6026)*
- Sucrose *(Sigma, S0389)*
- TEMED *(Sigma, T9281)*
- Tris-acetate-EDTA (TAE) solution *(Fisher Scientific, 10490264)*
- Tris base *(Fischer Scientific, 10376743)*
- Triton X-100 *(Sigma, T8787)*
- Trypsin 0.25% EDTA *(Life Technologies, 25200072)*
- Tryptone microbial media *(Fisher chemical, F24965)*
- Tween 20 *(Fisher Scientific, 10485733)*
- Ultrapure DNAse/RNAse-free Water *(Life Technologies, 10977035)*
- Water HPLC *(Fisher Scientific, 1070-6501)*
- XL-10-GOLD competent cell *(Agilent Technologies, 220314)*
- Yeast extract powder *(Fisher Scientific, 10697612)*

2.1.2 Antibodies

The specificity of antibodies had been established by the lab group using corresponding siRNAs. Primary antibodies for western blotting (WB) were purchased from Cell Signaling Technology (CST) unless otherwise indicated.

- Actin goat pAb *(Santa Cruz Biotechnology, CK1705)*
- Akt rabbit pAb *(Merck, 07-416)*

- Cyclooxygenase-2 (COX2) (CX229) mouse mAb *(Cayman Chemical, 160112)*
- EGFR rabbit pAb *(2232)*
- EIF2α rabbit pAb *(9722)*
- ERK1/2 (K-23) rabbit pAb *(Santa Cruz Biotechnology, C2410)*
- Flag (M2) mouse mAb *(Sigma, F3165)*
- GCN2 rabbit pAb *(3302)*
- Glutathione peroxidase 1 (GPX1) goat pAb *(Biotechne, AF3798)*
- Glutathione peroxidase 2 (GPX2) (496010) mouse mAb *(Biotechne, MAB5470)*
- Glutathione peroxidase 3 (GPX3) goat pAb *(Biotechne, AF4199-SP)*
- Glutathione peroxidase 4 (GPX4) (EPNCIR144) rabbit mAb *(Abcam, ab125066)*
- GST (B-14) mouse mAb *(Santa Cruz Biotechnology, sc-138)*
- Hemagglutinin (HA)-tag (6E2) mouse mAb *(2367)*
- MAP4K3 rabbit (Institute of Cancer Research, London, U.K.)
- mTOR (7C10) rabbit mAb *(2983)*
- Myc-tag (9E10) mouse mAb *(Cedarlane/Millipore, 05-419)*
- NADPH oxidase 1 (NOX1) rabbit pAb *(Abcam, ab55831)*
- NADPH oxidase 4 (NOX4) (N3C3) rabbit mAb *(Abcam, ab133303)*
- Phospho-Ser15 p53 rabbit pAb *(9284)*
- Phospho-Ser51 eIF2α (D9G8) rabbit mAb *(3398)*
- Phospho-Ser170 MAP4K3 goat *(Ctiakrks Figtpy)*
- Phospho-Ser473 Akt (11E6) rabbit mAb *(9271)*
- Phospho-Thr147 PLD1 rabbit pAb *(3831)*
- Phospho-Thr202/Tyr204 ERK (D13.14.4E) rabbit mAb *(4370)*
- Phospho-Thr359 p90RSK (D1E9) rabbit mAb *(8753)*
- Phospho-Thr389 p70S6 Kinase rabbit pAb *(9205)*
- Phospho-Thr899 GCN2 rabbit pAb *(Cedarlane/Epitomics, 2425-1)*
- Phospho-Tyr1068 EGFR (D7A5) rabbit mAb *(3777)*
- p53 (DO-1) mouse mAb *(Merck, MABE327)*
- PLD1 (F-12) mouse mAb *(Santa Cruz Biotechnology, sc-28314)*
- S6K1 (16/p70) mouse mAb *(BD Transduction Laboratories, 611261)*
- RagA (D8B5) rabbit mAb *(4357)*
- RagC (D8H5) rabbit mAb *(9480)*
- Rheb (3H6) mouse mAb (Institute of Cancer Research, London, U.K.)

- RSK1/RSK2/RSK3 (32D7) rabbit mAb *(9355)*
- TSC2 (D93F12) rabbit mAb *(4308)*

Primary antibodies for immunofluorescence (IF) staining were purchased from CST unless otherwise indicated.

- HA-tag (6E2) mouse mAb *(2367)*
- Hoechst fluorescent DNA dye *(4082)*
- LAMP2 (H4B4) mouse mAb *(Abcam, ab25631)*
- LAMP2 (GL2A7) rat mAb (*Abcam, ab13524)*
- mTOR (7C10) rabbit mAb *(2983)*
- PLD1 (F-12) mouse mAb *(Santa Cruz Biotechnology, sc-28314)*
- RagC (D8H5) rabbit mAb *(9480)*
- Rheb (3H6) mouse mAb (Institute of Cancer Research, London, U.K.)
- RhoA (1B12) mouse mAb *(Abnova, H00000387-M04)*
- TSC2 (D93F12) rabbit mAb *(4308)*

Secondary antibodies for WB were purchased from Fisher Scientific.

- Goat anti-rabbit IgG, HRP conjugate *(31460)*
- Goat anti-mouse IgG, HRP conjugate *(31430)*
- Rabbit anti-goat IgG, HRP conjugate *(31402)*
- Rabbit anti-sheep IgG, HRP conjugate *(31480)*

Secondary antibodies for IF were purchased from Invitrogen.

- Alexa Fluor 488 goat anti-mouse IgG *(A11029)*
- Alexa Fluor 546 goat anti-mouse IgG *(A11030)*
- Alexa Fluor 594 goat anti-mouse IgG *(A11032)*
- Alexa Fluor 488 goat anti-rabbit IgG *(A11034)*
- Alexa Fluor 555 goat anti-rabbit IgG *(A21429)*
- Alexa Fluor 488 goat anti-rat IgG *(A11006)*
- Alexa Fluor 546 goat anti-rat IgG *(A11081)*

Antibody-coupled agarose beads Flag M2 (A2220), glutathione (G4510), HA (A2095) and protein G (11243233001) for immunoprecipitation (IP) were purchased from Sigma.

2.1.3 Molecular cloning enzymes

DNA polymerases Q5 (M0493S) and OneTaq (M0481S) were purchased from New England BioLabs (NEB), and Pfu (M7741) was purchased from Promega. Restriction enzymes AgeI (R3552S), BamHI (R3136S), DpnI (R0176S), EcoRI (R3101S), HindIII (R3104S), KpnI (R3142S), NotI (R3189S), SmaI (R0141S), SalI (R3138S), XbaI (R0145S), XhoI (R0146S) and XmaI (R0180S) were purchased from NEB.

2.1.4 Antibiotics

Gentamicin (G1397), ampicillin (A9518) and kanamycin (60615) were purchased from Sigma. They were prepared in ddH_2O at 50mg/ml, filtered through a 0.22μm membrane filter for sterilization, stored at -20°C, and used at 1:1000 dilution for bacterial culture selection.

2.1.5 Kinase inhibitors

Kinase inhibitors were prepared in DMSO and stored at -20°C. Final concentration in the culture media for each inhibitor is shown in Table 3.

Table 2. Kinase inhibitors

Kinase	Inhibitor	Concentration (μM)	Source
GCN2	MSC2524505	5	Merck Serono, T0077791
	MSC2526779	5	Merck Serono, T0077794
mTORC1	Rapamycin	0.1	Millipore, 553210
EGFR	Iressa	1	Tocris, 3000
PI3K	Wortmannin	1	Sigma, W1628
MEK	Selumetinib	5	Selleckchem, S1008
	UO126	10	Calbiochem, 109511-58-2
	PD184352	10	Sigma, PZ0181
	PD0325901	1	Selleckchem, S1036

ERK	GDC0994	5	Selleckchem, S7553
	SCH772984	5	Cayman, 942183-80-4

2.1.6 Small interfering RNA (siRNA)

siRNAs were resuspended in RNase-free siRNA buffer at 20µM. Non-targeting siRNA pool control siRNA (D-001206-13), siRNAs targeting human MAP4K3 (D-003588-05, J-003588-05), RagA (L-016070-00-0005), PLD1 1-2 (custom, GCGUCUACAUCCCAACAUAAAUU, CCACUAGAAGACACACGUUUAUU), GCN2 1-2 (GGAAAUUGCUAGUUUGUCA, GACCAUCCCUAGUGACUUA) were purchased from Dharmacon. Human PLD1 siRNAs 3-5 (SI00686357, SI04369316, SI04166134) were purchased from Qiagen. siRNA targeting human Rheb (custom, UUUUUCUUCUGUUAACCUGAAdTdT) was purchased from Fisher Scientific.

2.1.7 Primers

Primers were resuspended in ddH_2O at 1µg/µl and were designed for mutagenesis of human MAP4K3 (sequence is shown in Appendix 1) and for subsequent sequencing. Primers were purchased from Sigma and are listed in Appendix 2.

2.1.8 Plasmid constructs

Plasmids were dissolved in ddH_2O and DNA fragments were verified on an agarose gel (see 2.1.13). pRK5-Myc, pRK5-Myc-GCN2, pRK5-S6K1-GST, pEGFP-TSC1, pRK7-Flag-TSC2, HA-PLD1, pRK5-Flag-MAP4K3, pRK5-Flag-MAP4K3 DA (DFG motif to AFG, kinase inactive [108]) were from laboratory storage. Nine MAP4K3 point mutations (D54N, V182F, E209G, N290I, E351K, Q473K, T669A, D715Y and R753Q) were generated using pRK5-Flag-MAP4K3 as a template and using the Site-Directed Mutagenesis Kit (see Methods 2.2.2).

2.1.9 Cell lines

Mammalian cell lines were used in this study. Hela, human embryonic kidney (HEK)293T, mouse embryonic fibroblasts (MEF) wild type, GCN2 knockout, EIF2α S51A and TSC2 knockout cell lines, HCT116 wild type and p53 knockout cell lines

were from the laboratory storage. The hTERT-HME (human mammary epithelial) isogenic cell lines including wild type, EGFR delE746-A750, KRAS G13D, BRAF V600E and PI3KCA H1047R [201] were a kind gift from Prof Alberto Bardellia. NSCLC cell lines (Table 3) were from the Liverpool cell line repository.

Table 3. NSCLC cell lines	
	Mutations in the MAPK/ERK cascade or PI3K
A549	KRAS G12S
Calu 6	KRAS Q61K
NCI-NH1650	EGFR delE746-A750, L858R, T790M
H1975	EGFR L858R, T790M
H727	KRAS G12V
H460	KRAS, PIK3CA
H322	WT
H3255	EGFR L858R
PC 9	EGFR delE746-A750

2.1.10 Media

Media for bacteria growth were prepared in ddH_2O and autoclaved at 121°C for 20min using the liquid cycle. Antibiotics were added appropriately.

- Lysogeny broth (LB) medium: 10g/l bacto-tryptone, 5g/l yeast extract powder, 5g/l NaCl.
- LB agar plates: 7.5g/l agar in LB medium.

Laboratory-formulated media used for media switch treatments were prepared in ddH_2O, according to the components of commercial media. Both dialysed FBS and formulated media were filtered through 0.22μm membrane filters.

- Dialysed FBS (d.FBS): prepared by dialysing 50ml FBS against SnakeSkinTM dialysis membrane 3.5K MWCO in 4L 1X PBS at 4°C with stirring for overnight.
- Freezing medium: 90% FBS, 10% DMSO.
- Amino acid (AA)-free DMEM: 8.32g/l of DMEM low glucose, w/o amino acids, w/o pyruvic acid powder, 3.5g/l glucose (final concentration was 4.5g/l), 3.7g/l

sodium bicarbonate, 1mM sodium pyruvate, 1% Pen strep, pH 7.4, according to the USBiological recipe. 10% d.FBS was added prior to use.

- Individual 50X amino acid solution: amino acids (Sigma) constituting original DMEM were formulated individually at 50X concentrations, according to the Sigma recipe.
- AA-free HME medium: AA-free DMEM supplemented with 20ng/ml EGF, 10µg/ml insulin, and 100µg/ml hydrocortisone.
- HME complete medium: 50X amino acid solutions were added at 1X concentration to AA-free HME medium.
- Cystine-free HME medium: HME complete medium lacking cystine.

2.1.11 Solutions

Solutions were prepared in ddH_2O and stored at -20°C unless otherwise indicated.

- Homemade enhanced chemilumescent (ECL) reagents were used for detection of horseradish peroxidase (HRP) enzyme activity and the recipes are displayed in Tables 5 and 6. Stock solutions of luminol and p-coumaric acid were made in DMSO. Equivalent volumes of reagents 1 and 2 were added to the membrane prior to detection.

Table 4. Homemade ECL reagent 1 recipe

Chemicals	Stock	Working
Luminol	250mM	2.5µM
P-coumaric acid	90mM	405µM
Tris-HCl pH 8.5	1M	100µM

Table 5. Homemade ECL reagent 2 recipe

Chemicals	Stock	Working
Tris-HCl pH 8.5	1M	100µM
Hydrogen peroxide	30%	0.018%

- Digitonin was prepared in PBS at 5% as stock solution and used at a final concentration of 0.01% in PBS.

- 4% Paraformaldehyde (PFA) was prepared by dissolving PFA in pre-heated PBS.
- Okadaic acid (O.A.) is an inhibitor of phosphatases and was used for routine cell lysis. Stock solution was 200μM in DMSO and was added at a final concentration of 60nM to Jośe buffer (see 2.1.12) prior to use.
- Metabolite extraction solution: 50% methanol, 30% acetonitrile, 20% water.

2.1.12 Buffers

Buffers were prepared in ddH_2O unless otherwise indicated.

- Jośe buffer was used to lyse cells. It was stored at -20°C for long-term and 4°C for short-term use. The compositions of Jośe buffer are shown is Table 7.

Table 6. Jośe buffer recipe

	Stock concentration (M)	Working concentration (mM)
Tris-HCl pH 7.6	1	50
EDTA	0.5	1
EGTA	0.2	1
Na_3VO_4	1	1
NaF	1	50
β-GP	1	50
β-ME (v/v)	100%	0.1%
Triton X-100 (v/v)	100%	1%
Sucrose		270
Complete protease inhibitor cocktail tablets		1 tablet/50ml

- PBST: 0.2% Tween 20 in 1X PBS.
- 10X Tris-glycine buffer: 144g/l glycine, 30g/l Tris, pH 8.4.
- SDS running buffer: 1X Tris-glycine buffer, 0.1% SDS.
- Western blot blocking buffer: 5% dried skimmed milk in PBST.
- Western blot stripping buffer: 62.5mM Tris pH 6.8, 2% SDS.
- Western blot transfer buffer: 1X Tris-glycine buffer, 20% methanol.
- Ste20 kinase assay buffer: 20mM Tris-HCl pH 7.2, 25mM β-GP, 5mM EGTA, 1mM Na_3VO_4, 0.1% β-ME, 15mM $MgCl_2$ [108].

2.1.13 Gel electrophoresis systems

Two types of gel electrophoresis were used: agarose gel for DNA fragment analysis and SDS-PAGE for protein analysis.

- 1% Agarose gel: 1% agarose in TAE buffer was microwaved for 2.5min at 50% power to dissolve. Solution was mixed with 0.005% Safeview nucleic acid stain and set in the cassette. DNA samples were prepared using 6X DNA loading dye and loaded into wells in the agarose gel. An additional well was loaded with 0.5µg 1kb DNA ladder (NEB). Gels were run at 130V for 40min before visualization under ultraviolet (UV) light.
- SDS-PAGE is a common technique for separation of proteins based on their molecular weight. Typically a 10% resolving gel was used. Resolving gel: 3.8ml ddH_2O, 2ml 40% acrylamide, 2ml 1.5M Tris pH 8.8, 80µl 10% SDS, 80µl 10% APS, 8µl TEMED. Stacking gel (6%): 2.9ml ddH_2O, 0.75ml 40% acrylamide, 1.25ml 0.5M Tris pH 6.8, 50µl 10% SDS, 50µl 10% APS, 5µl TEMED. Gels were run at 120V for 90-120min.

2.2 Methods

Procedures were performed at room temperature unless otherwise indicated.

2.2.1 Bacterial culture

Bacterial culture was used to amplify plasmid DNA, which were then extracted and purified using the Qiagen Kits and used for transfection. Bacterial culture work was performed using aseptic techniques.

- Glycerol stock of bacterial culture: 800µl LB culture was mixed with 200µl absolute glycerol, snap frozen in liquid nitrogen and stored at -80°C.
- Bacterial inoculation: glycerol stock or a single colony was inoculated into LB medium containing antibiotic, and the culture was incubated at 37°C with shaking at 225 rpm for overnight.
- Transformation: 30µl chemically competent *E. coli* were incubated with 5ng plasmid for 30min on ice, heat shocked at 42°C for 45sec and immediately placed on ice for 2min. Bacteria were resuspended in 900µl SOC medium and incubated at 37°C with shaking at 225 rpm for 1 hour before centrifuged at 1,000 xg for 1min. 800µl supernatant was discarded and pellet was resuspended in the

remaining 100µl media, and spread onto LB agar plates containing antibiotics to form colonies at 37°C for overnight.

2.2.2 Molecular cloning

- Site-directed mutagenesis was performed to generate point-mutations of human MAP4K3 inserted in the pRK5-Flag vector. Primers were designed to introduce intentional mutations, and the protocol of polymerase chain reaction (PCR) in the Site-Directed Mutagenesis Kit (Agilent) was followed. PCR reaction was conducted at 95°C, 60°C and 68°C in the sequence shown in Appendix 3 for denaturation, annealing and extension respectively. Amplification was confirmed by running 10µl out of 50µl PCR product on a 1% agarose gel. Mutations were verified by DNA sequencing from Source Biosience Company.
- Plasmid DNA digestion: diagnostic restriction enzyme digestion was performed to verify plasmid DNA, based on their molecular weight and conformations. Typically 500ng of plasmid DNA were incubated with or without (uncut, control) single or double restriction enzymes in compatible buffer at 37°C for 1 hour before heat-inactivation at 65°C for 20min and agarose gel analysis.
- Plasmid DNA isolation: Qiagen plasmid DNA purification kits of miniprep and maxiprep were used to analyze bacterial clones and obtain large-scale purified plasmid DNA respectively. Purified plasmid DNA was then quantified using Nanodrop and verified on an agarose gel. Maxiprep: briefly 500ml LB culture was pelleted at 6000 xg for 15min at 4°C and pellets were resuspended in 10ml Buffer P1 containing RNase A. Cellular contents were extracted by incubating in 10ml Buffer P2 for 3min and plasmid DNA was separated from genomic DNA and proteins by adding 10ml Buffer N3 and centrifuging at 20,000 xg for 30min at 4°C. Supernatant containing plasmid DNA was subjected to column purification which selectively binds DNA. Plasmid DNA was then eluted from the column by adding 8ml Buffer QF and precipitated by adding 4ml isopropanol and incubating at -20°C for 1 hour. DNA pellet was collected by centrifuging at 15,000 xg for 30min at 4°C and washed twice with 70% ethanol. The pellet was then left to air-dry for 10min and dissolved in 300µl ddH_2O. Miniprep: briefly 2ml LB culture was pelleted at 6000 xg for 3min and pellets were resuspended in 100µl Buffer P1. 100µl Buffer P2 and 150µl Buffer N3 were sequentially added

and the resulting mixture was centrifuged at 16,000 xg for 10min. Supernatant was transferred into the small column, which was then washed once by adding Buffer PE and centrifuging for 1min. DNA was eluted in 50µl warm ddH_2O by centrifuging for 1min.

2.2.3 Cell culture

Cell culture flasks were maintained at 37°C in a humidified incubator in an atmosphere of 5% CO_2-95% air and passaged at a 1:5 ratio using trypsin every 3-5 days. Fresh culture medium was warmed at 37°C water bath for 30min prior to use. Cell culture manipulations were performed in a Class II laminar flow cabinet using aseptic techniques. All culture media were supplemented with 10% FBS and 1% Pen strep except for HCT116 cell lines. Specifically, Hela, HEK293T and MEF cell lines were cultured in DMEM, HME cell lines in DMEM additionally supplemented with 20ng/ml EGF, 10µg/ml insulin, and 100µg/ml hydrocortisone, and NSCLC cell lines in RPMI 1640 medium. HCT116 cell lines were cultured in RPMI 1640 medium supplemented with 10% d.FBS.

2.2.4 Media switch treatments

In order to investigate the effects of amino acid deprivation on protein translocation and cell proliferation, all treatment media were supplemented with 10% dialysed FBS. Cells were cultured in commercial media containing FBS and amino acids prior to media switch treatments. Three types of media switch were performed. Differences between treatments were amino acid compositions in media and times of treatments.

- Amino acid deprivation and re-stimulation treatment: cells in duplicate wells were washed twice using and incubated in AA-free DMEM medium for 1 or 4 hours. One of the two wells was stimulated for 15min with minimum essential medium (MEM) amino acids by adding 50X MEM amino acid solution (Invitrogen) to a final 1X concentration.
- Amino acid dropout screen for HME cell lines: to deprive individual or all amino acids, cells were washed twice using AA-free HME medium and incubated in HME complete medium lacking specific amino acid for 72 hours (related to Figure 44).

- Cystine deprivation treatment for HME cell lines: cells in duplicate wells were washed twice using AA-free HME medium, and one was incubated in cystine-free HME medium and the other one in HME complete medium. Treatment times were 12 and 16 hours for FACS and cell viability analysis respectively.

2.2.5 Transient vector transfection

Lipofectamine 2000 (Invitrogen) was used as a transfection reagent to introduce plasmid DNA and siRNA into cells for transient gene overexpression and suppression respectively. Briefly, cells were seeded at a required density (300,000 cells/well for overexpression and 100,000 cells/well for siRNA transfection) in 6-well plates (the well contained two coverslips when IF staining was required) for overnight. For each well, two portions of 250µl DMEM were prepared, with one incubated with 5µl lipofectamine 2000 for 5min, and the other mixed with plasmid DNA (the amount varied depending on experiment) or siRNA (a final concentration of 67pM). The two portions were then mixed and incubated for 40min before 1ml of 20% FBS was added. Each well was washed once using DMEM medium without FBS and antibiotics, and incubated in the 1.5ml transfection mixer for overnight. Pen strep was added 1-2 hours post transfection at a final concentration of 1%. Cells were harvested the following day for overexpression transfection or switched to fresh DMEM medium supplemented with 10% FBS and 1% Pen strep the next day and harvested 72 hours post siRNA transfection.

2.2.6 Bradford assay

Bradford assay is a quick and accurate spectroscopic analytical procedure to determine protein concentrations. Cell lysates in Jośe buffer were scraped off plates and centrifuged at 16,000 xg for 10min at 4°C. Supernatants were collected and concentration of total protein was determined by incubating 1µl of cell lysates with 200µl Bradford reagent blue dye in a 96-well plate for 1min with vortexing at 600 rpm and measuring absorbance at A595nm using Spectra Max Plus plate reader with the SoftMax Pro 6 software. 1µl of Jośe buffer and bovine serum albumin (BSA) standards made in Jośe buffer at concentrations of 0.25, 0.5, 1, 2, 4, 8µg/µl were used for blank and standard curve respectively. Since absorbance was proportional to

the amount of bound dye and hence to the amount of protein present, concentrations of protein in cell lysates were quantified against the standard curve.

2.2.7 Western blotting

Western blotting was mostly used in this study to examine protein expression and phosphorylation levels.

- SDS-PAGE: typically 20-25μg protein were prepared using 4X LDS sample buffer containing 5% β-ME, heated at 97°C for 5min and subjected to SDS-PAGE resolving. 5μl of protein ladder were loaded on both sides.
- Electrophoretic transfer enables protein from a gel matrix to bind and be transferred to a membrane. The SDS-PAGE gel was assembled with methanol-activated PVDF membrane in transfer buffer, and transferred at 100V for 1 hour at 4°C by wet electroblotting (tank transfer). Membrane was then rinsed with ddH_2O and stained with Ponseau S solution to detect general protein bands.
- Immunoblotting: membrane was incubated in blocking buffer for 1 hour with shaking prior to incubation with primary antibody in blocking buffer overnight at 4°C with rotating. Membrane was then washed for 15min in PBST and incubated with secondary antibody in blocking buffer for 1 hour, followed by wash in PBST for 30-60min.
- Detection: membrane was incubated with ECL solutions for 2min. Protein bands were visualized using the x-ray films or Bio-Rad ChemiDoc Imager.
- Membrane stripping for re-probing: membrane was incubated in stripping buffer containing fresh 0.7% β-ME at 60°C for 25-30min.

2.2.8 Immunoprecipitation (IP)

Immunoprecipitation (IP) was used to examine interactions between proteins. Briefly 800,000 HEK293T cells/dish in 60mm dishes were transfected with plasmid DNA containing an HA or Flag tags, and lysed in 500μl Jośe buffer 40 hours post transfection. Tagged protein was purified by incubation of cell lysates with HA or Flag-agarose (alternatively protein G-agarose and HA or Flag antibodies) for 2-4 hours at 4°C with rotating, and beads were washed three times with Jośe buffer

containing 0.5M LiCl. Plasmids used for different IP experiments are listed in Table 8.

Table 7. Transfection conditions for IP		
IP antibodies	Plasmid DNA	Amounts (μg)/dish
HA	pRK5-Flag MAP4K3 WT or DA	2.5
	HA-PLD1	0.25
Flag	pRK5-Myc-GCN2	2
	pEGFP-TSC1	2
	pRK7-Flag-TSC2	4

2.2.9 S6K1 reporter assay

800,000 HEK293T cells/well in 6-well plates were transfected with 2.5μg pRK5-Myc vector (mock), pRK5-Flag-MAP4K3 wild-type (WT), kinase-inactive (DA) or the nine pRK5-Flag MAP4K3 mutant constructs (see **2.1.8**), co-transfected with 100ng pRK5-S6K1-GST. 24 hours post transfection, two mock transfected wells were switched to DMEM lacking FBS (serum starvation) for 16 hours, and one was re-stimulated with FBS at a final concentration of 10% for 30min before cell lysis.

2.2.10. *In vitro* kinase assay

2000,000 HEK293T cells/dish in 60mm dishes were transfected with 8μg pRK5-Flag MAP4K3 WT, DA or mutations, and lysed in 500μl Jośe buffer 40 hours post transfection. Flag-tagged MAP4K3 was isolated using the Flag-IP procedure and washed once with Ste20 kinase assay buffer prior to kinase assay. The kinase assay was performed at 30°C in 50μl kinase buffer supplemented with 100μM ATP, 3μCi of [γ-32P]ATP and 5μg of myelin basic protein (MBP), and terminated after 30min by adding 2X LDS sample buffer [108]. Samples were subjected to SDS-PAGE and transfer, and ^{32}P incorporated into MBP and MAP4K3 (autophosphorylation) were detected by x-ray films.

2.2.11 Immunofluorescence (IF)

Cells on coverslips were fixed in 4% PFA for 15min, permeabilized in 0.01% digitonin for 10min and blocked with 10% goat serum in PBS for 30min, prior to sequential incubation with primary and secondary antibodies for 1 hour. Coverslips were washed in PBS for 15min with shaking before and after secondary antibody incubation, and once with ddH_2O prior to mounting onto slides with mounting medium. Confocal immunofluorescence micrographs were acquired using the 3i Marianas fluorescence microscope with SlideBook 6 software. Identical exposure times were used for comparative analysis. The co-localization efficiency was quantified from 20-50 cells using the software ImageJ Just Another Colocalisation Plugin (JACoP).

2.2.12 Intracellular amino acid extraction

5,000,000 wild type and EGFR mutant HME cells/dish were seeded in seven 100mm dishes. On the third day cells were washed twice with DPBS and three dishes of each cell line were incubated in cystine-free and complete HME media for 4 hours. Cells in the last dish were trypsinized and counted, and the cell count was used to calculate the volume of extraction solution so that the final cell concentrations in the extraction solution were around 1,000,000 cells/ml. Cells were washed three times with cold PBS and incubated with extraction solution for 5min at 4°C with shaking. The extraction solution containing cells was collected into eppendorf tubes, shaken in Thermomixer (Eppendorf AG) at 1,400 rpm for 10min at 4°C to extract intracellular metabolites, and centrifuged at 16,000 xg for 10min at 4°C to precipitate any proteins present. The supernatants were transferred into glass HPLC vials and stored at -80°C prior to liquid chromatography-mass spectrometry (LC-MS) quantification of free amino acids, which was conducted by Dr Christiaan Labuschagne at the University of Glasgow (related to Figure 47).

2.2.13 Cell viability assay

Cell viability was determined using the CellTiter-Glo assay (Promega) that uses ATP as an indicator of metabolic active cells. ATP is a co-factor of the luciferase reaction and the resulting luminescence is proportional to the amount of ATP present, which is an indicator of cellular metabolic activity. Briefly 50,000 cells/well in triplicate

wells in a 96-well plate (NUNC, Thermofisher) were mixed with 20µl medium (the medium used for cell treatment) and 20µl CellTiter-Glo reagent (mixture of CellTiter-Glo buffer and substrate) for 2min with shaking at 1,000 rpm to allow cell lysis. Plates were incubated for another 10min on bench to stabilize luminescent signal and the emitted luminescence was then detected using a plate reading luminometer (Tecan Genios). Three additional wells containing medium and reagent without cells were used to obtain a value for background luminescence.

2.2.14 Flow cytometry (FACS analysis)

The level of cellular lipid ROS was quantified using the C11-BODIPY581/591 dyes which is a lipid peroxidation sensor, and using flow cytometry. 200,000 cells/well were seeded in a 6-well plate and switched to cystine-free or complete HME media for 12 hours prior to flow cytometry analysis. Following cystine deprivation, cells were washed once with PBS and sequentially incubated with 2µM C11-BODIPY581/591 dyes in DPBS for 30min, trypsinized with 0.25% Trypsin-EDTA and resuspended in PBS containing 1% FBS. Resuspended cells were collected into 1.5ml eppendorf tubes and analysed using the Attune NxT flow cytometer (Thermo Fisher). A minimum of 5,000 cells were loaded and the dyes were excited using a blue 488nm laser, and emission was recorded on channel BL1 (530/30).

2.2.15 Statistical analysis

The ImageJ software was used to quantify immunoblotting bands, and ImageJ JACoP to quantify the percentage of co-localization [202, 203]. Images of immunoblots, phase-contrast and IF confocal microscopy, are representative of at least two independent experiments. Quantification data were analyzed using Microsoft Excel and are presented as mean values ± standard error of the mean (SEM) of three biological replicates. Statistical significance was set at $p<0.05$ and p value was calculated using two-tailed Student's T test.

Chapter 3

Results

Chapter 3-Results

3.1 Mechanisms involved in amino acid regulation of mTORC1

The mTORC1 signalling pathway coordinates various environmental signals to control cell growth via regulating synthesis of proteins, lipids and nucleotides, as well as the catabolic process autophagy [46]. Activation of mTORC1 is promoted by the Rheb GTPase and is associated with translocation to late-endosomal/lysosomal membrane [88, 95]. S6K1 is the critical downstream effector of mTORC1 and phosphorylation of S6K1 on residue Thr389 by mTORC1 stimulates the activation of S6K1, which then promotes the synthesis of the enumerated macromolecules [68, 71, 73]. TSC2, by deactivating GTP-bound Rheb which is the crucial activator of mTORC1, functions as the master inhibitor of the mTORC1 signalling [84]. Among all of the growth-promoting stimuli, amino acids seem to be indispensable for mTORC1 activation [46]. In the presence of amino acids, mTORC1 translocates to lysosomal membrane, which allows it to be activated by GTP-bound Rheb; whilst upon amino acid removal, mTORC1 is released from lysosomes and becomes inactive [95, 97]. In contrast to mTORC1, TSC2 complexed with TSC1 and TBC1D7 has been found to associate with lysosomes under the condition of amino acid deficiency and becomes cytosolic when amino acids are present [99]. Recruitment of mTORC1 and TSC2 appears to be mediated by the Rag GTPase heterodimer (RagA/B-RagC/D) [96, 97], however, the exact mechanisms of their lysosomal translocation and dissociation remain elusive. The aim of the studies presented in this section was to investigate the molecular mechanisms underlying TSC2 subcellular localization by exploring recent findings on the Rag GTPases.

3.1.1 GCN2 inhibits mTORC1 potentially by regulating TSC2 lysosomal translocation

3.1.1.1 GCN2 promotes TSC2 lysosomal translocation

To identify mediators of TSC2 subcellular localization, Dr Richard Lamb and his colleagues in Dr Chris Bakal's group at the Institute of Cancer Research have performed a high-throughput quantitative cell imaging siRNA screen of around 975 protein kinases/phosphatases in Hela cells under normal-nutrient and amino acid-

deprived conditions (Figure 25). This screen revealed an array of potential regulators of TSC2 lysosomal localization, among which GCN2 kinase (red box in Figure 25C) was of particular interest in that it is known to sense amino acid deficiency and repress protein synthesis.

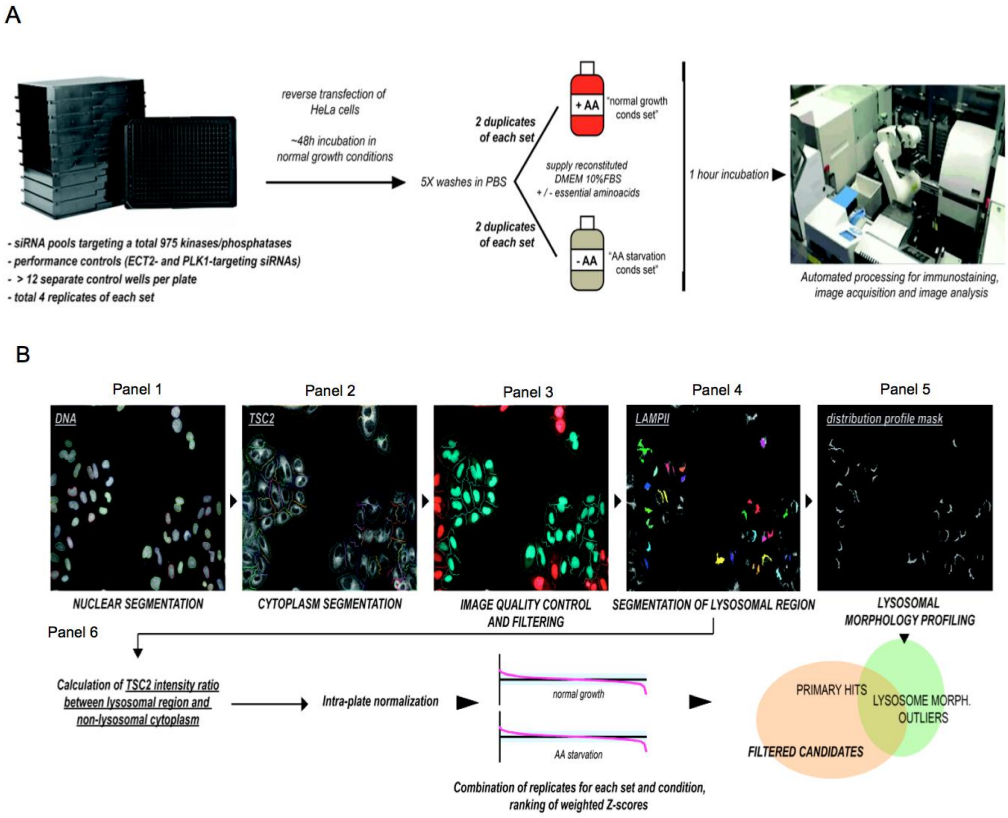

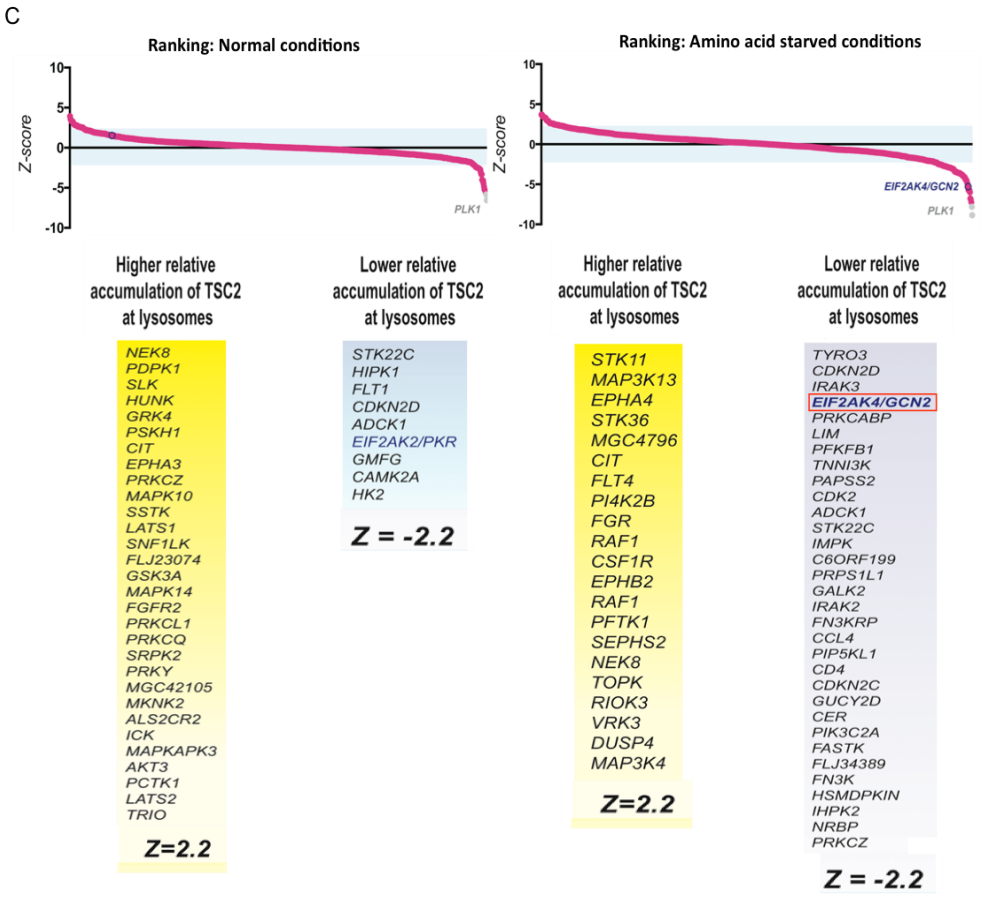

Figure 25. Image-based screening for regulators of TSC2 subcellular distribution.
A. Hela cells were transfected with a siRNA library targeting all human kinases in four equal replicates on 384-well plates. After 48h two of the four replicates were washed in PBS and switched to reconstituted DMEM media with 10% d.FBS either containing or lacking amino acids (AA) for 1 hour, and stained against nuclear, TSC2 and LAMP2 (a lysosome marker). Confocal microscope images were sequentially acquired and simultaneously analyzed using Acapella 2.5 software (PerkinElmer). **B.** Examples of images acquired from **A**. Panel 1, nuclear channel; panel 2, TSC2 channel; panel 3, filtering of incomplete, border cells, mitotic cells, late apoptotic cells and artefacts based on morphological properties of the initially segmented cells, and out-of-focus objects; panel 4, segmentation of lysosomes; panel 5, systematic morphological profiling of lysosomes; panel 6, gathering of basic phenotypic parameters and calculation of TSC2 lysosome/cytoplasmic ratio based on panel 4. **C.** Normalizations/ranking calculations of TSC2 lysosome/cytoplasmic ratio. EIF2AK4/GCN2 kinase (red box) is one of the candidates that potentially regulate the lysosomal localization of TSC2. Z score shows normalized percentage of TSC2-lysosome co-localization. Experiments shown in this figure were performed by Drs Richard Lamb and Chris Bakal's group at The Institute of Cancer Research.

In order to investigate whether GCN2 regulates TSC2 lysosomal localization in response to amino acid deprivation, GCN2 was knocked-down in Hela cells using

two independent siRNAs targeting GCN2 (GCN2 siRNA1 and 2, distinct from those used in the screen) and the effects on TSC2 lysosomal localization was examined using a rabbit monoclonal antibody (TSC2 clone D93F12 from CST) that specifically recognizes the endogenous TSC2 and also a mouse monoclonal antibody (LAMP2, clone H4B4 from Abcam) that detects LAMP2 (lysosomal associated membrane protein 2), a marker of late-endosomes/lysosomes (henceforward referred to as lysosomes) [85]. Hela cells were treated with medium lacking amino acid (-AA) for 30min following siRNA transfection and were then fixed and stained with the two antibodies and the corresponding fluorescently-labelled anti-rabbit and anti-mouse secondary antibodies for co-localization analysis. The staining results were captured using a confocal microscope and the individual monochrome (grey) and merge (green and red) micrographs were displayed in Figure 26A. The efficiency of TSC2-lysosome co-localization was quantified from the confocal micrographs using the software ImageJ the Just Another Colocalisation Plugin (JACoP) and was displayed in Figure 26B. As shown in Figure 26A, TSC2 (stained in green) rapidly accumulated on lysosomes (stained in red) within 30min following amino acid (AA) withdrawal in cells transfected with control (Ctrl) siRNA. The co-localization of TSC2 with lysosomes was demonstrated by the yellow clusters in the merge channel, which were eliminated in cells transfected with GCN2 siRNAs. The quantification results were consistent with the image data, showing that knockdown of GCN2 remarkably decreased the co-localization of TSC2 with lysosomes under the condition of amino acid withdrawal, to a similar extent in the control group (Ctrl siRNA) cultured in medium containing amino acids (+AA). These results suggested that GCN2 was required for TSC2 lysosomal localization and were in agreement with the siRNA screen data.

A

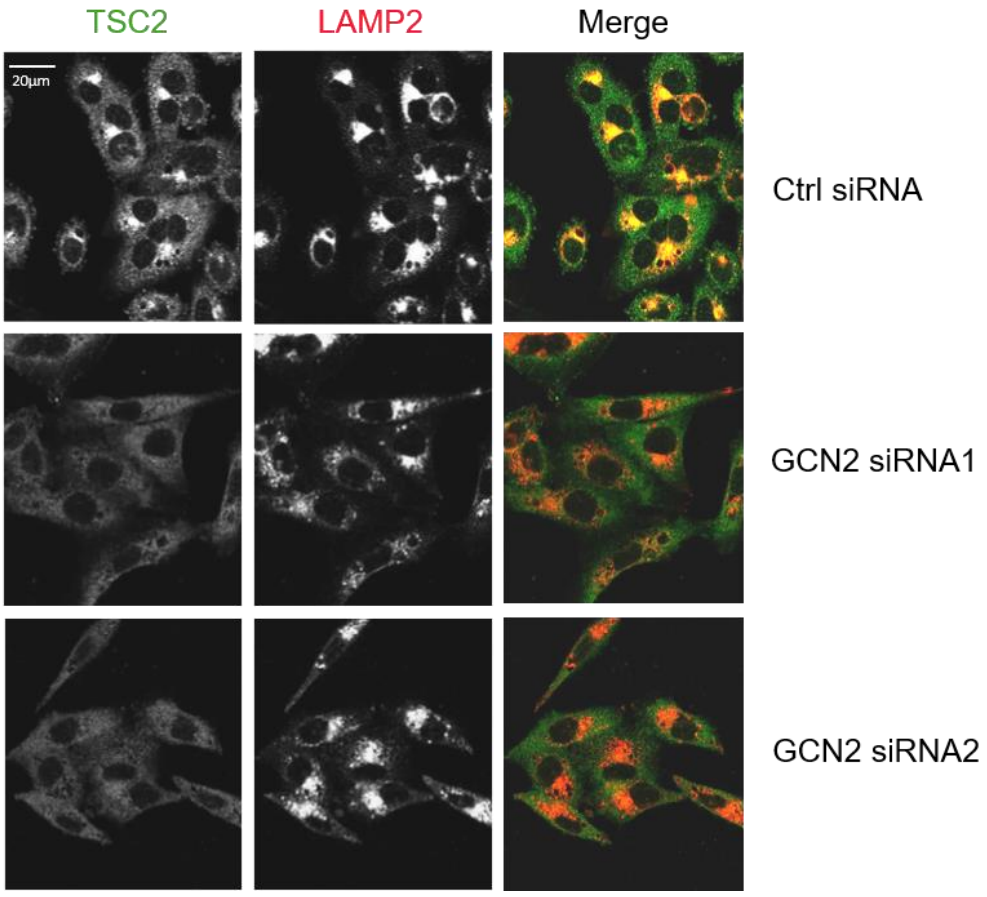
IF confocal images of Hela cells -AA 30min
TSC2
LAMP2
Merge
20μm
Ctrl siRNA
GCN2 siRNA1
GCN2 siRNA2

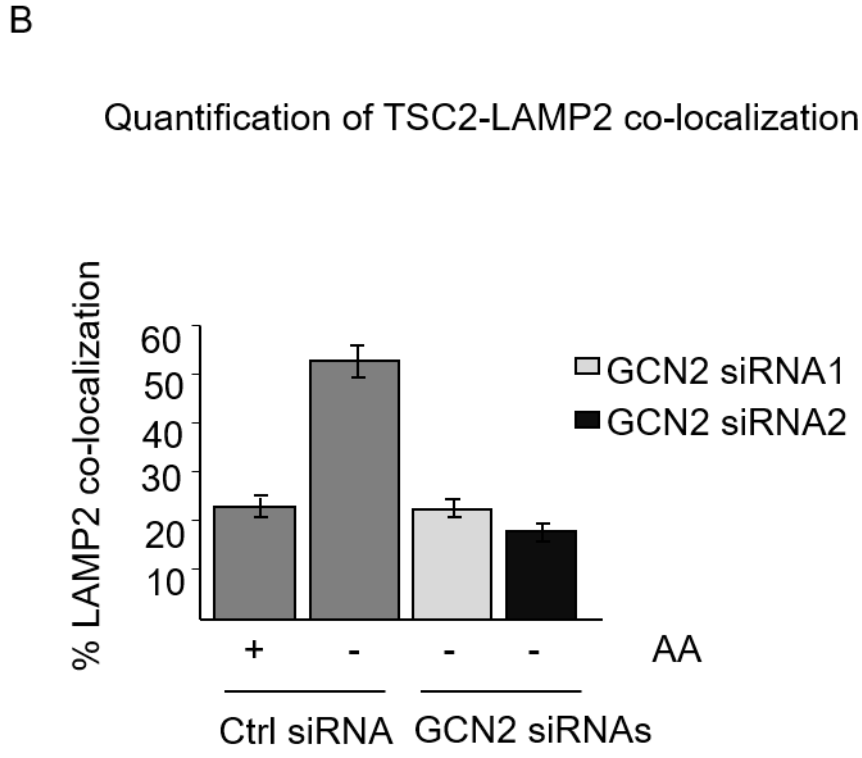

Figure 26. GCN2 promotes TSC2 lysosomal translocation upon amino acid removal.
Hela cells were subjected to amino acid deprivation (-AA) for 30min following transfection with control (Ctrl) or two GCN2-specific siRNAs. **A.** Monochrome (grey) and merge confocal immunofluorescence (IF) micrographs of cells stained with antibodies detecting endogenous TSC2 (green) and LAMP2 (red). **B.** Co-localization analysis of TSC2 with lysosomes. Y-axis represents the percentage of LAMP2-positive TSC2 over the total TSC2. Experiments displayed in this figure were performed by Drs Richard Lamb and Rebecca Lamond.

3.1.1.2 GCN2 promotes inhibition of mTORC1 in response to amino acid deprivation

Following data showing that GCN2 positively regulates TSC2-lysosome translocation, which is critical for mTORC1 inhibition, we asked if GCN2 contributes to mTORC1 inactivation upon amino acid removal. We firstly tested whether GCN2 activation induced by amino acid depletion correlates with down-regulation of mTORC1 activity in Hela cells (Figure 27A). Hela cells were treated with medium lacking amino acids (-AA) for different times from 5min up to 30min (left panel) or for 10min followed by amino acid re-addition for up to 15min (right panel). Cell lysates were analyzed by western blot and the activity of GCN2 and mTORC1 was indicated by auto-phosphorylated Thr899 of GCN2 (pGCN2 T899)

and mTORC1-phosphorylated Thr389 of S6K1 (pS6K1 T389), respectively. The level of total GCN2 and S6K1 was also analyzed so that the relative activity under different conditions was comparable. Upon amino acid withdrawal (-AA), inhibition of mTORC1 activity was seen in HeLa cells as soon as within 10min, with a complete inhibition after 30min, as demonstrated by S6K1 phosphorylation on Thr389 (left panel). The decreased mTORC1 activity caused by amino acid deprivation for 10min was restored immediately by adding amino acids back for 2 minutes (right panel). In contrast, GCN2 was rapidly activated and auto-phosphorylated on Thr899 following removal of amino acids (within 10min) and the activity was significantly reduced within re-addition of amino acids for 2min after deprivation for 10min (right panel), suggesting an immediate response of GCN2 activation to amino acid deprivation. Thus, the activation of mTORC1 and GCN2 is respectively regulated by the presence and absence of amino acids.

Whether GCN2 was required for mTORC1 inhibition was then examined in GCN2 wild-type (WT) and knockout (KO) MEF (mouse embryonic fibroblasts) cells (Figure 27B). The level of S6K1 phosphorylation on T389 was barely detectable following deprivation of leucine (-Leu), arginine (-Arg) or all amino acids (-AA) for 30 minutes in control MEF cells (GCN2 WT), and was significantly increased by re-addition of leucine (+Leu), arginine (+Arg) or MEM (minimum essential medium) amino acids (+AA) for 30 minutes. However, this pattern that mTORC1 activity was inhibited in response to amino acid deprivation has disappeared in cells lacking GCN2. mTORC1 became constitutively active and unresponsive to amino acid deprivation in GCN2 KO cells, suggesting an inhibitory function of GCN2 on mTORC1 activity. Together, these data demonstrated that GCN2, potentially by regulating TSC2 lysosomal localization, acts as an upstream inhibitor of the mTORC1 signalling pathway in response to amino acid depletion.

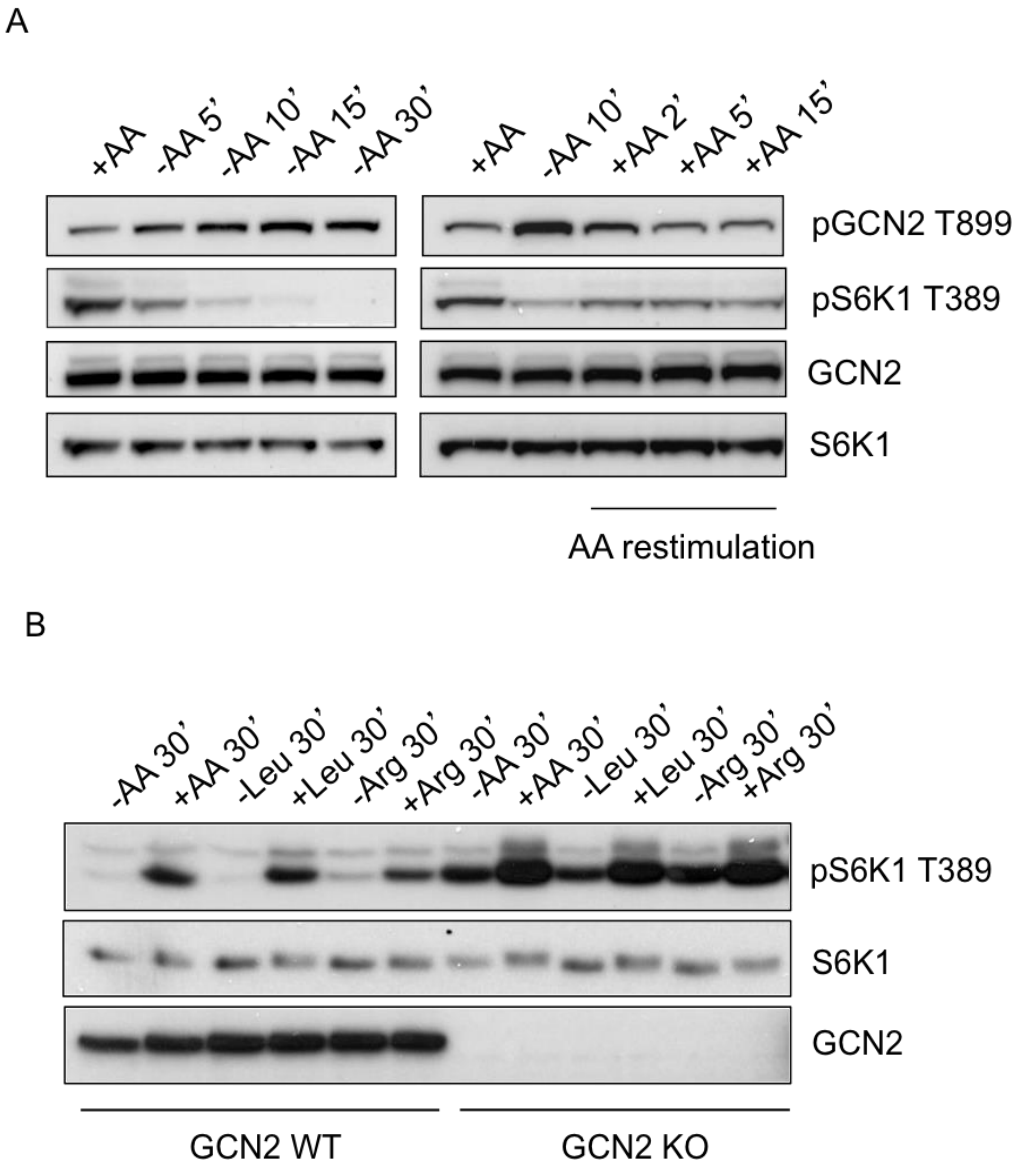

Figure 27. GCN2 senses amino acid deficiency and inhibits mTORC1 activation.

A. Amino acid deprivation activates GCN2. Immunoblot analysis of lysates from Hela cells treated with amino acid-free (-AA) medium for up to 30min (left panel) or for 10min followed by amino acid re-addition for up to 15min (right panel). Immunoblots were probed with antibodies detecting auto-phosphorylated Thr899 of GCN2 (pGCN2 T899) and phosphorylated Thr389 of S6K1 (pS6K1 T389), as well as detecting total GCN2 and S6K1. **B.** GCN2 is required for mTORC1 inactivation following amino acid deprivation. GCN2 wild type (WT) and knock out (GCN2 KO) MEF cells were treated with media lacking amino acids (-AA), leucine (-Leu) or arginine (-Arg) for 30min, or were deprived and stimulated with MEM amino acids (+AA), leucine (+Leu) or arginine (+Arg) for 30min. Immunoblots were probed for pS6K1 T389, total S6K1 and GCN2. Experiments displayed in this figure were performed by Dr Richard Lamb's group at University of Alberta.

3.1.1.3 The kinase activity is required for GCN2 to regulate TSC2 localization

We further examined whether the kinase activity of GCN2 was required for TSC2 lysosomal translocation using two recently developed GCN2-specific inhibitors (Merck Company). One of the GCN2 siRNAs used in the experiment displayed in Figure 26 was also used in this experiment to serve as a positive control for the disruption of TSC2 lysosomal translocation (Figure 28). Control siRNA transfected Hela cells were pre-treated with GCN2 inhibitors for 30min and switched to medium lacking amino acids for 60min in the continued presence of inhibitors (GCN2 inhibitor 1 and 2). The inhibition of GCN2 activity by the specific inhibitors was confirmed by western blot analysis showing the disappearance of auto-phosphorylated GCN2 (Figure 28A, pGCN2 T899). Likewise, the level of total GCN2 was much lower in cells transfected with GCN2 siRNA, confirming the decent level of suppression. As shown in Figure 28B, TSC2 (stained in green) displayed a diffused pattern in the presence of amino acids in control siRNA transfected cells, and switched to a lysosome-associated pattern upon amino acid deprivation as demonstrated by the yellow clusters in the merge channel (Ctrl siRNA -AA). Consistent with the previous experiment (Figure 26), TSC2-lysosome association was diminished in cells transfected with GCN2 siRNA (Figure 28 B and C, GCN2 siRNA, –AA). The GCN2 inhibitor treatment has decreased TSC2-lysosome association to similar extents, suggesting that kinase activity of GCN2 seemed to be required for regulation of TSC2 lysosomal localization. Since eIF-2α is the only known substrate of GCN2, GCN2 might regulate the TSC2 lysosomal translocation through eIF-2α. The different patterns of GCN2 auto-phosphorylation affected by amino acid conditions in Figure 28A and Figure 27A might be due to different times of amino acid deprivation treatment. GCN2 autophosphorylation somehow appeared decreased following amino acid deprivation for 1 hour in Figure 28A.

A

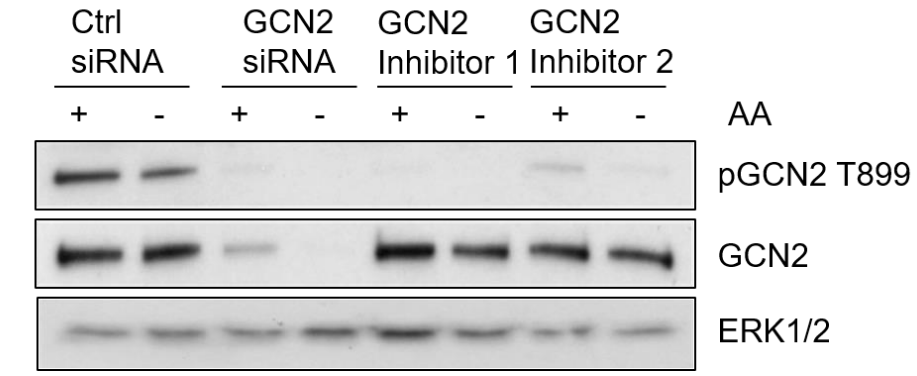
Ctrl siRNA
GCN2 siRNA
GCN2 Inhibitor 1
GCN2 Inhibitor 2
+ - + - + - + -
AA
pGCN2 T899
GCN2
ERK1/2

B

IF confocal images of Hela cells

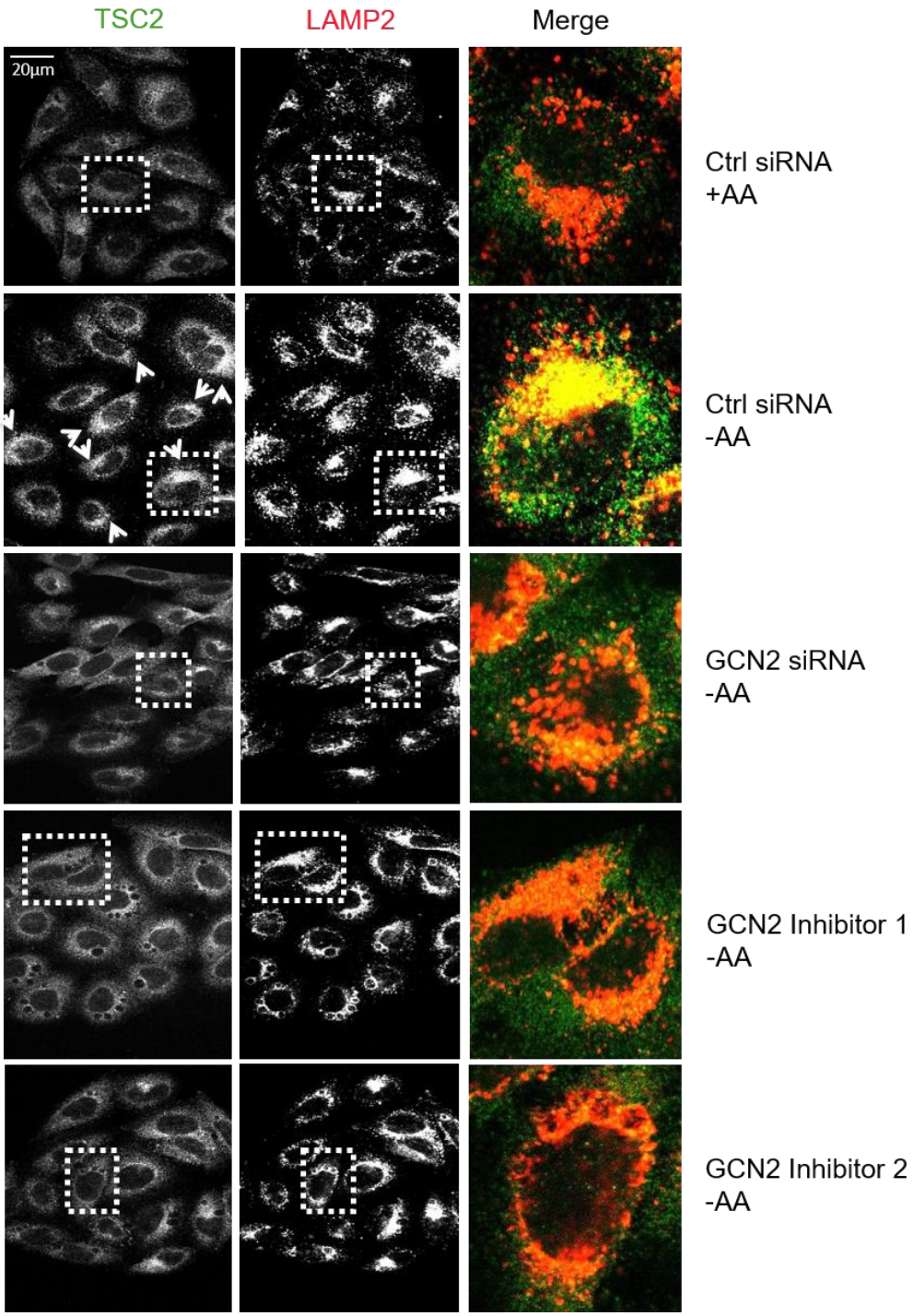

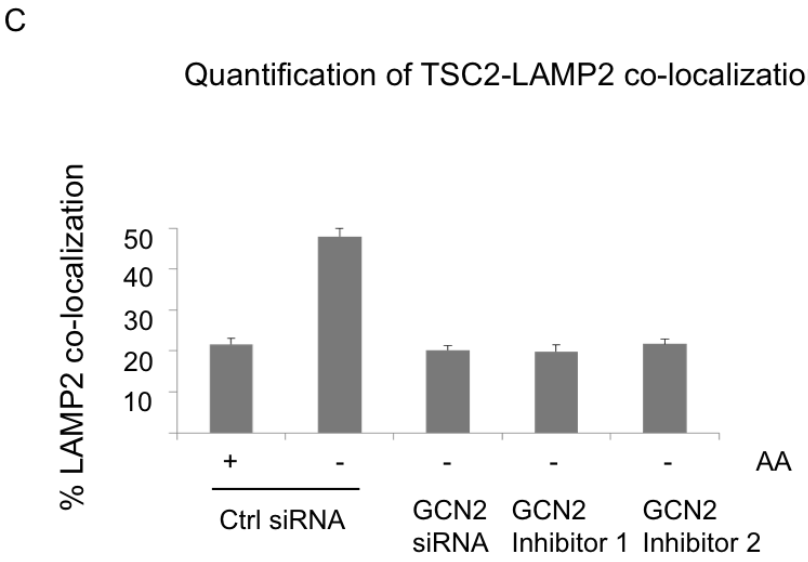

Figure 28. GCN2 activity is required for TSC2 translocation to lysosomes. Control (Ctrl) or GCN2-specific siRNA transfected Hela cells were washed in DPBS and switched to reconstituted DMEM media with 10% d.FBS lacking amino acids for 60 minutes (-AA), or deprived and stimulated with MEM amino acids for 30min (+AA). For inhibitor treatment, Ctrl siRNA transfected cells were pre-treated with 5μM GCN2-specific inhibitors 1 and 2 for 30 minutes prior to amino acid deprivation/stimulation in the continued presence of inhibitors. **A.** Immunoblots of cell lysates probed for pGCN2 T899, total GCN2 and ERK1/2 as a loading control. **B.** Confocal immunofluorescence micrographs of cells stained to TSC2 (green) and LAMP2 (red). Images in the merge channel are amplified from areas in the white dotted boxes in the monochrome images to display more details. **C**. Quantitative analysis of co-localization of TSC2 with LAMP2-positive lysosomes. Y-axis represents the percentage of LAPM2-positive TSC2 over the total TSC2.

3.1.1.4 GCN2 regulates TSC2 translocation to lysosomes independently of eIF2α

The data presented above support a model whereby GCN2 inhibits mTORC1 signalling potentially through regulating the lysosomal translocation of TSC2, and the kinase activity of GCN2 seems to be required for the regulation. We therefore asked whether eIF2α, the only known substrate of GCN2 kinase [116, 204], mediated the effect of GCN2 on TSC2 translocation. GCN2 controls translational repression via phosphorylation of the initiation factor eIF2α on Ser51, which was found to correlate with decrease in tRNA charging resulting from amino acid deprivation [205]. To determine whether GCN2 was affecting TSC1/2 via similar mechanism, we examined TSC2 translocation in MEF cells expressing a non-phosphorylatable knock-in mutant of eIF2α, eIF2α S51A where serine at position 51 was substituted by alanine [118]. As shown in Figure 29A, TSC2 was diffused in the

presence of amino acids (+AA) in all the four MEF cells lines, GCN2 wild type, eIF2α wild type, GCN2 knockout and eIF2α S51A, in a pattern that was not concentrated on lysosomes. Following amino acid deprivation (-AA), TSC2 accumulated on lysosomes in three cell lines, GCN2 wild type, eIF2α wild type and eIF2α S51A, but not GCN2 knockout (Figure 29B). Surprisingly, eIF2α S51A did not reduce the TSC2-lysosome association under the condition of amino acid deprivation, in contrast to that in GCN2 knockout cells, suggesting that GCN2 regulates TSC2 lysosomal translocation independently of eIF2α phosphorylation. Therefore, there are likely to be other cellular substrates of the GCN2 kinase that might play a role in mediating TSC2 lysosomal translocation.

A

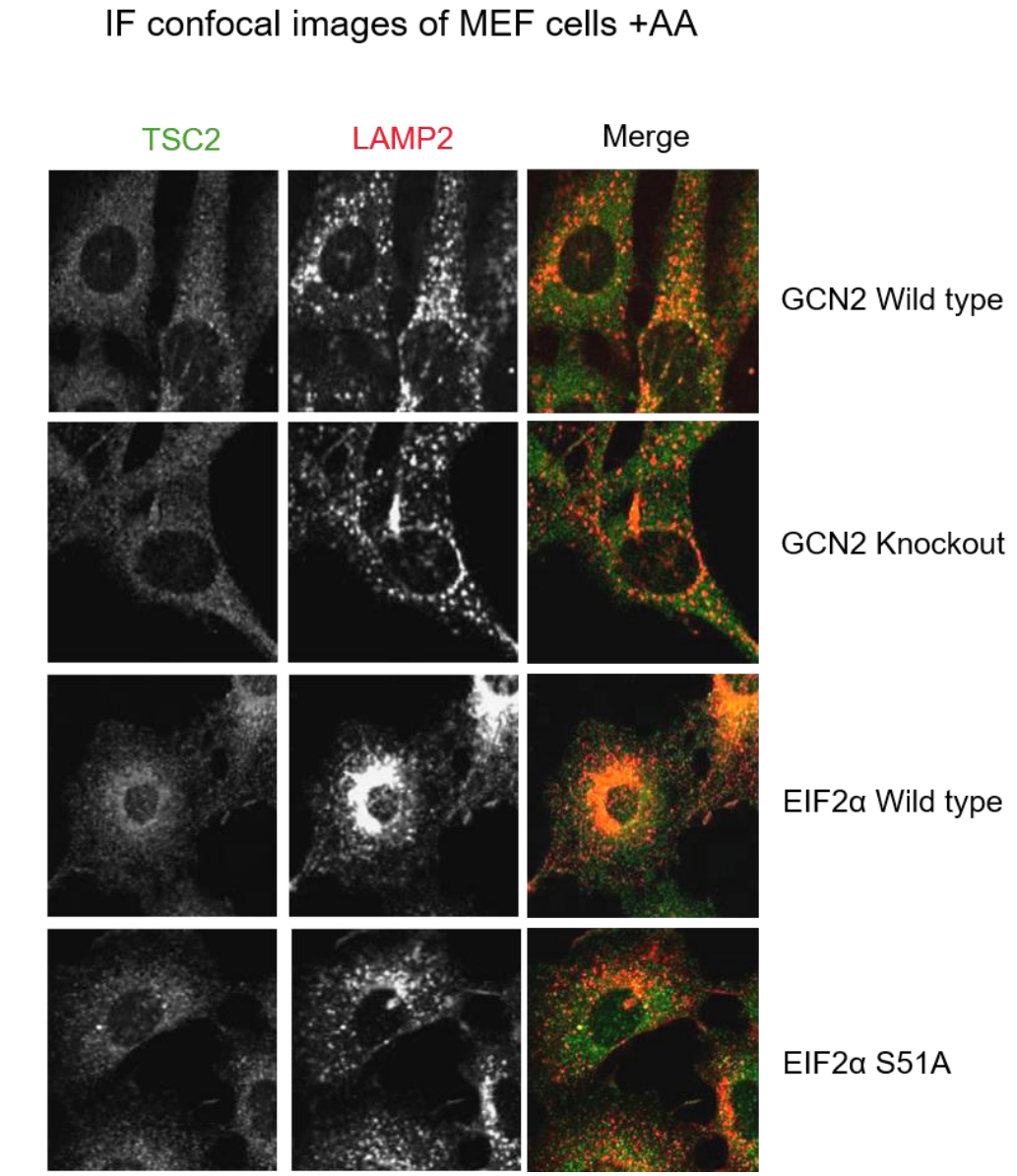

B

IF confocal images of MEF cells -AA 4h

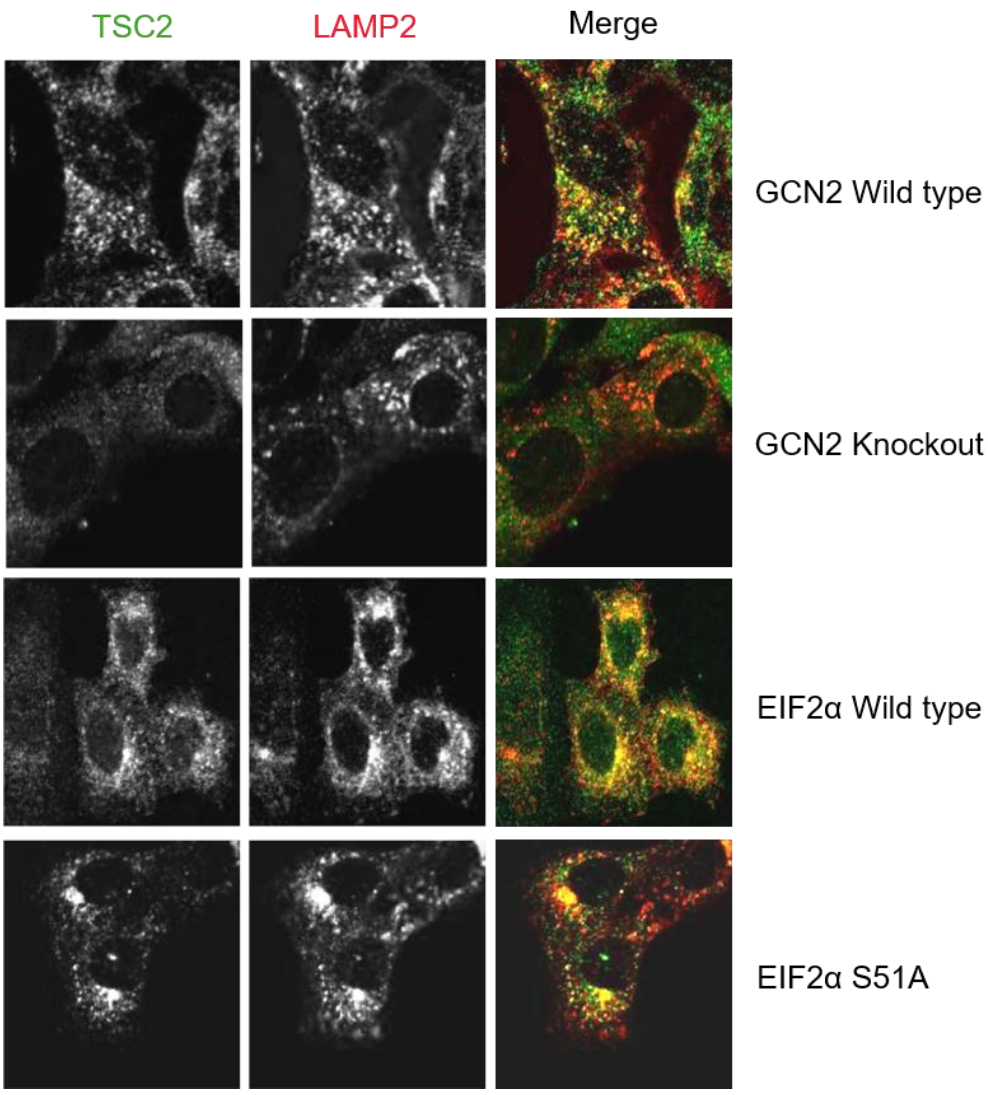

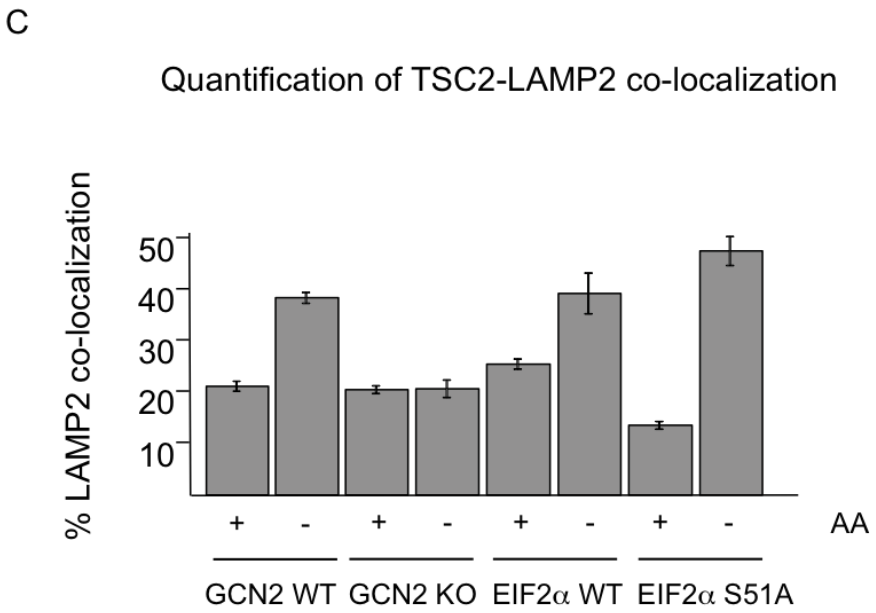

Figure 29. GCN2 regulates TSC2 lysosomal translocation independently of eIF2α.
Four MEF cells lines, GCN2 wild type, eIF2α wild type, GCN2 knockout and eIF2α S51A were treated with normal medium (**A**.) or medium lacking amino acids (**B**.) for 4 hours. **A** and **B.** Confocal immunofluorescence micrographs of MEF cells stained to TSC2 (green) and LAMP2 (red). **C.** Quantitative analysis of co-localization of TSC2 with LAMP2-positive lysosomes in the absence (-AA) or presence (+AA) of amino acids. Y-axis represents the percentage of LAPM2-positive TSC2 over the total TSC2. Experiments displayed in this figure were performed by Drs Richard Lamb and Rebecca Lamond.

3.1.1.5 TSC2 is unlikely a substrate of GCN2

We then examined whether TSC2 itself was a substrate of GCN2 via co-immunoprecipitation (co-IP) of extracts from HEK293T cells simultaneously overexpressing myc-GCN2, Flag-TSC2 and GFP-TSC1. As shown in Figure 30, although TSC1 was pulled down with Flag-IP, no GCN2 was detected in the IP samples, demonstrating that TSC2 does not interact with GCN2 or their interaction is too weak that had been interrupted during the lysis and IP procedures.

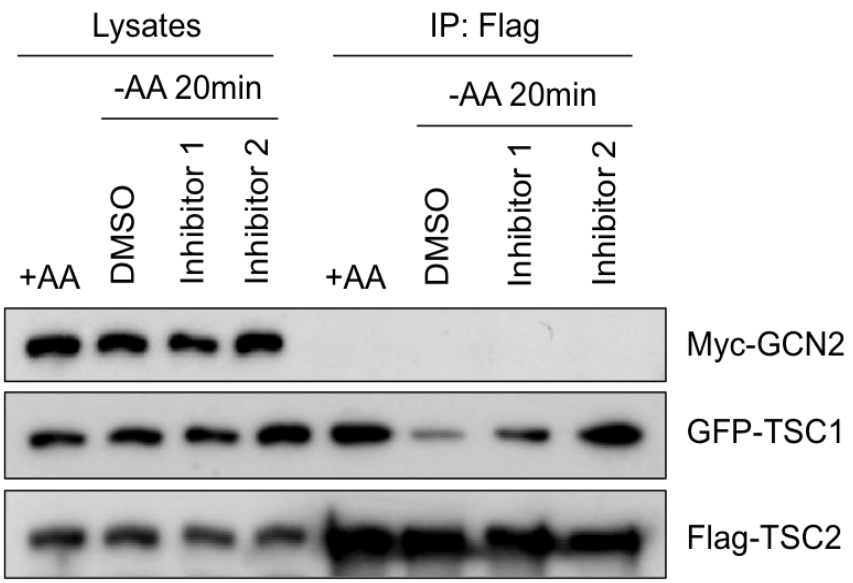

Figure 30. GCN2 does not interact with TSC2.
HEK293T cells were simultaneously transfected with plasmids containing Myc tagged GCN2, GFP tagged TSC1 and Flag tagged TSC2, and pre-treated with the vehicle control DMSO or GCN2 inhibitors for 30min prior to amino acid deprivation (-AA) for 20min in the continuous presence of the inhibitors. Cell lysates were subjected to Flag-IP and subsequent immunoblots probed with antibodies against Myc, GFP and Flag.

3.1.2 RagA and Rheb promotes TSC2 lysosomal translocation

It has been demonstrated that Rheb and the Rag GTPases are required for recruitment of TSC2 to the lysosomal surface [90, 99], we wanted to examine whether this was repeatable in our cell culture system. Hela cells were subjected to amino acid deprivation treatment following transfection with siRNAs designed to target human Rheb and RagA. The suppression efficiency by siRNAs was confirmed by immunoblot analysis (Figure 31A) and the effects on TSC2-lysosome co-localization was analyzed by immunofluorescence staining. Indeed, suppression of Rheb or RagA resulted in a diffused and non-lysosomal pattern for TSC2 localization in Hela cells deprived of amino acids for 1 hour, in contrast to that in control siRNA transfected cells (Figure 31B). The co-localization efficiencies of TSC2 with lysosomes, as demonstrated in the quantification analysis in Figure 30C, were considerably reduced following suppression of Rheb or RagA. Therefore, both Rheb and RagA are required for TSC2 to localize on lysosomes.

A

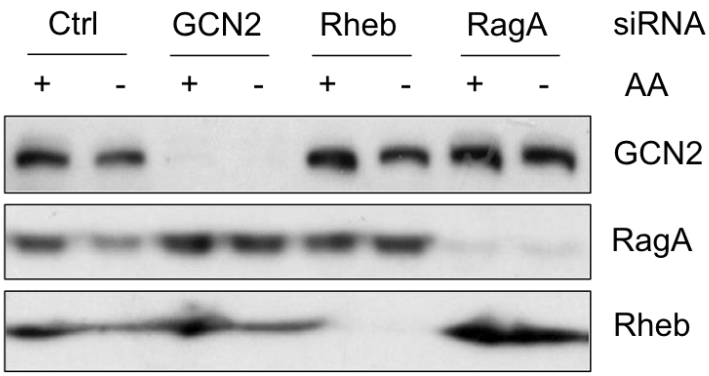

B

IF confocal images of Hela cells -AA 1h

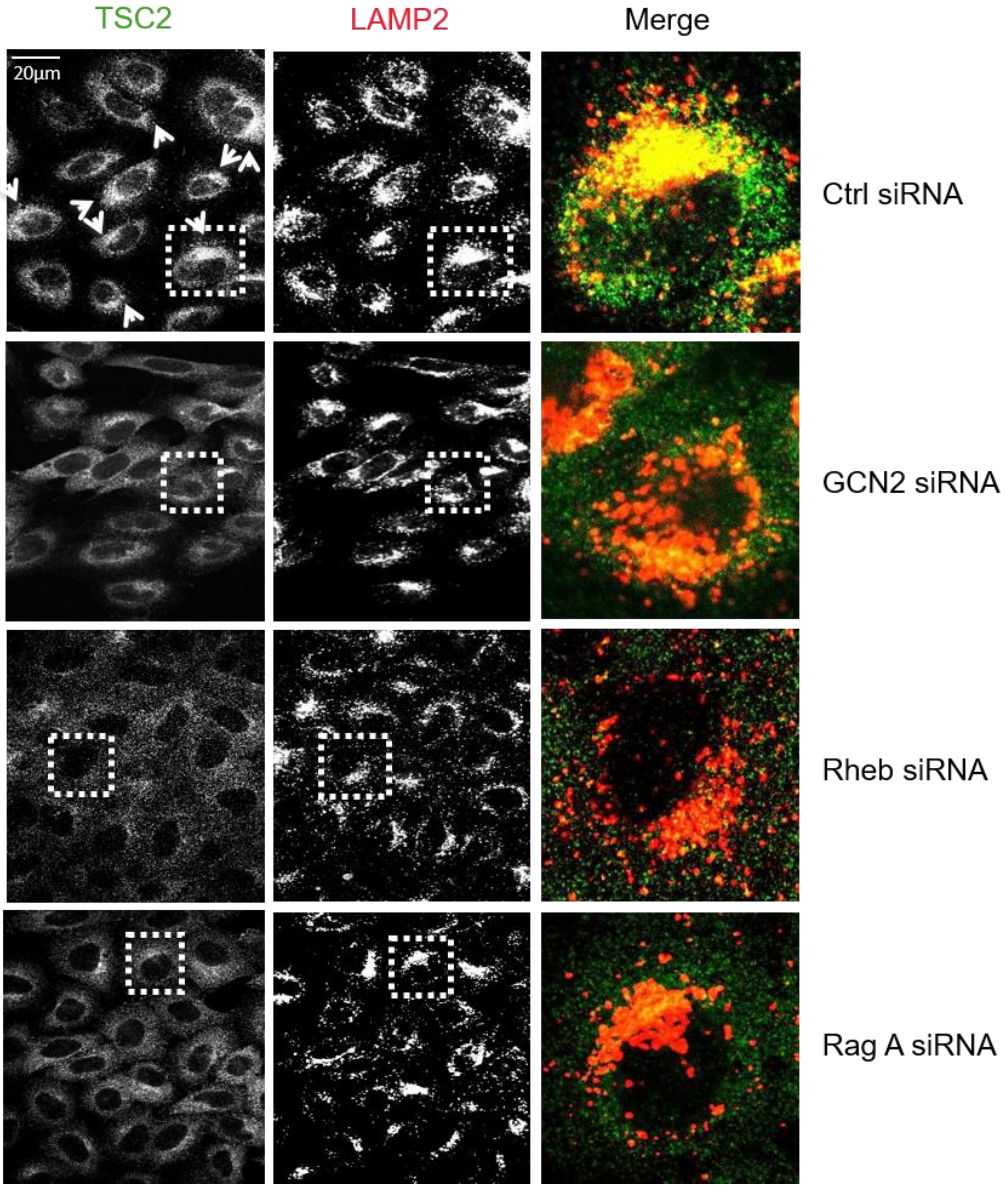

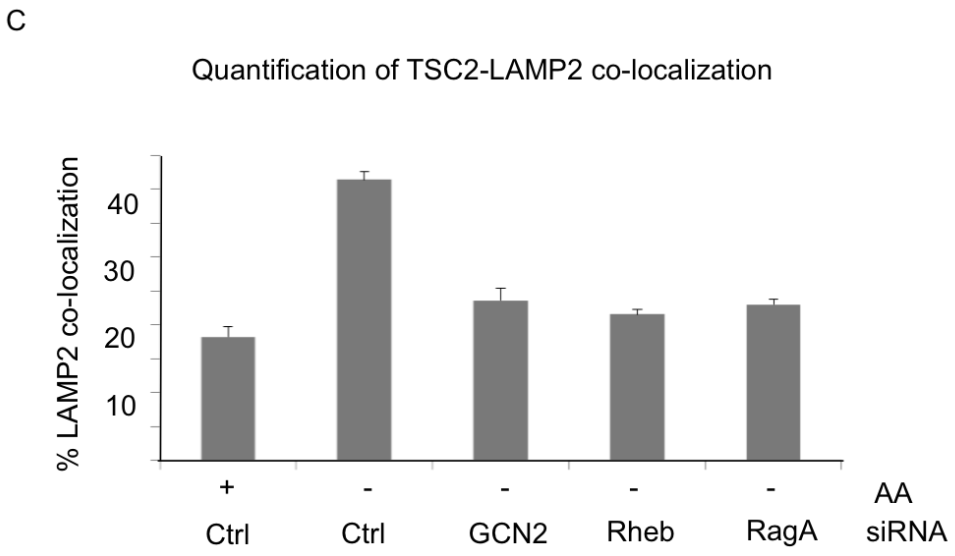

Figure 31. Rheb and RagA promote TSC2 translocation to lysosomes.
Hela cells were treated with medium lacking amino acids (-AA) for 60min or deprived and stimulated with MEM amino acids for 30min (+AA) following transfection with siRNAs that target none (Ctrl), human GCN2, Rheb or RagA. **A.** Immunoblots of cell extracts probed with antibodies to GCN2, Rheb and RagA. **B.** Confocal immunofluorescence micrographs of cells stained with antibodies to TSC2 (green) and LAMP2 (red). **C.** Quantitative analysis of co-localization of TSC2 with LAMP2-positive lysosomes. Y-axis represents the percentage of LAPM2-positive TSC2 over the total TSC2.

3.1.3 TSC2 preferentially binds RagC

Recruitment of mTORC1 and TSC2 to lysosomal membrane seems to be mediated through their interaction with the Rag GTPase heterodimer [95, 99]. Hence, we sought to investigate whether TSC2 interacted with Rag GTPases and which Rag GTPase via GST pull down assay. As shown in Figure 32, GST-tagged RagC alone or the RagA/C heterodimer, but not RagA alone, co-immunoprecipitated with endogenous TSC2 in HEK293T cells following amino acid deprivation (-AA) for 60min. To verify that the interaction of TSC2 with Rag GTPase was specific, we have used a control protein, Rap2A that also belongs to the Ras-related small G protein family, and it did not bind TSC2. In addition, the interaction of TSC2 with RagC and RagC/RagA heterodimer seemed to decrease following re-addition of amino acids (+AA) for 30min. Therefore, it is likely that RagC interacts with TSC2 and recruits it to lysosomal membrane in response to amino acid deprivation.

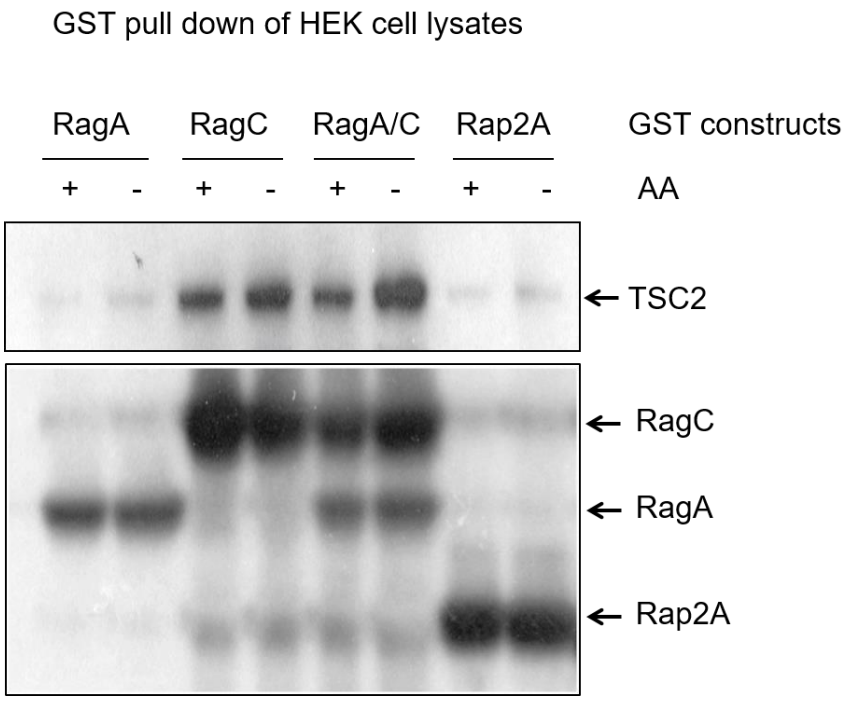

Figure 32. TSC2 preferentially interacts with RagC.
GST pull down assay of extracts from HEK293T cells treated with medium lacking amino acid for 60min (-AA) or deprived and stimulated with MEM amino acids for 30min (+AA) following transfection with plasmids containing GST tagged proteins as indicated on the top. Immunoblots were probed with antibodies detecting endogenous TSC2, GST tagged RagC, RagA and the control protein Rap2A. The molecular weights of these proteins are indicated in the brackets. Experiment displayed in this figure was performed by Drs Richard Lamb and Rebecca Lamond.

3.1.4 Rheb does not associate with lysosomes

We next investigated if endogenous Rheb itself associated with lysosomes using an antibody verified as specifically detecting Rheb (clone 3H6, mouse monoclonal antibody that was generated at Institute of Cancer Research) by immunofluorescence. The specificity of this antibody had been established using the Rheb siRNAs. However, although TSC2 associated with lysosomes following amino acid depletion (Figure 33A, -AA), Rheb does not exhibit lysosomal localization in the presence or absence of amino acids (Figure 33B, +AA and -AA), in a similar pattern with that of RhoA, a cytosolic GTPase (Figure 33C).

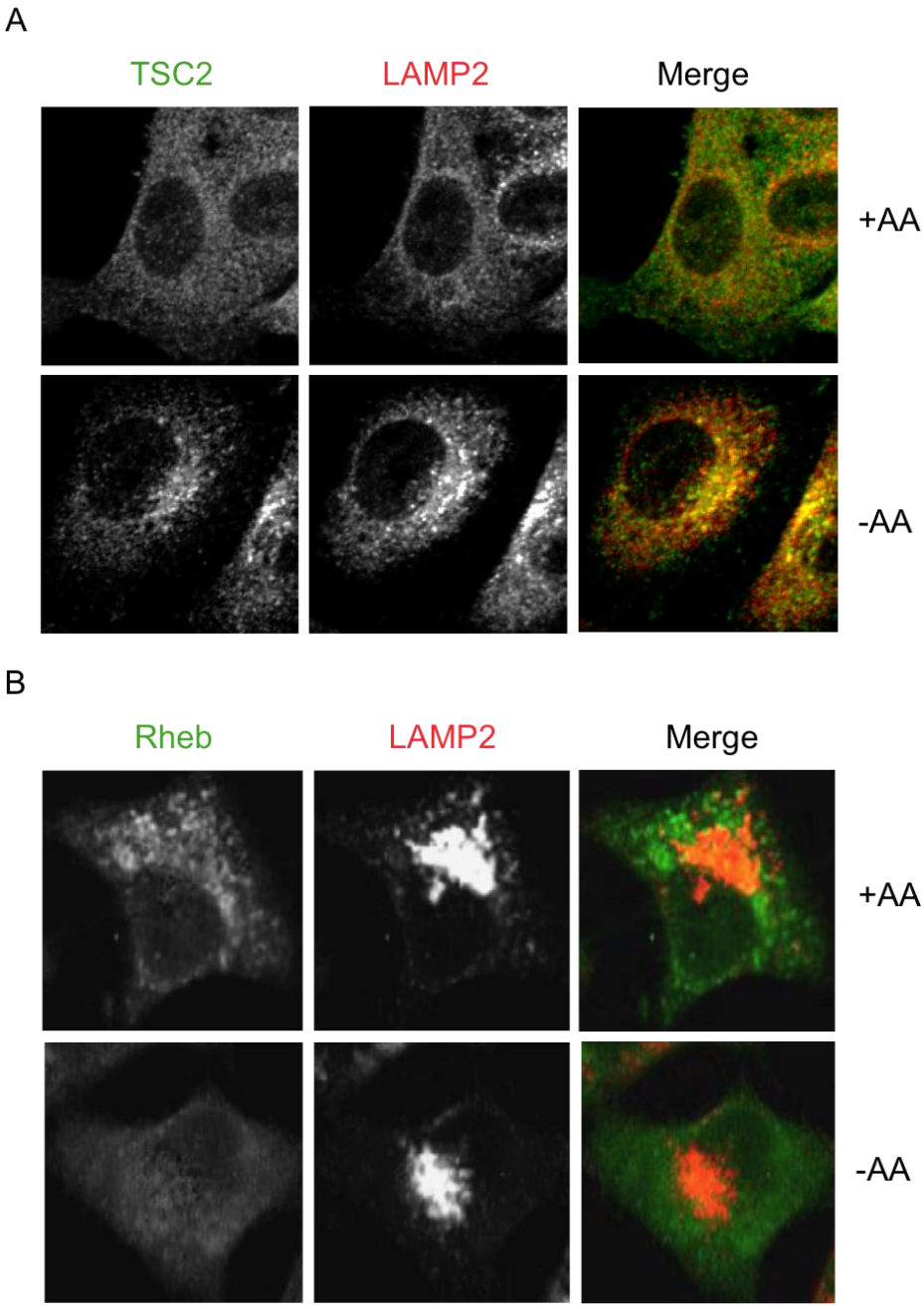
A
TSC2
LAMP2
Merge
+AA
-AA
B
Rheb
LAMP2
Merge
+AA
-AA

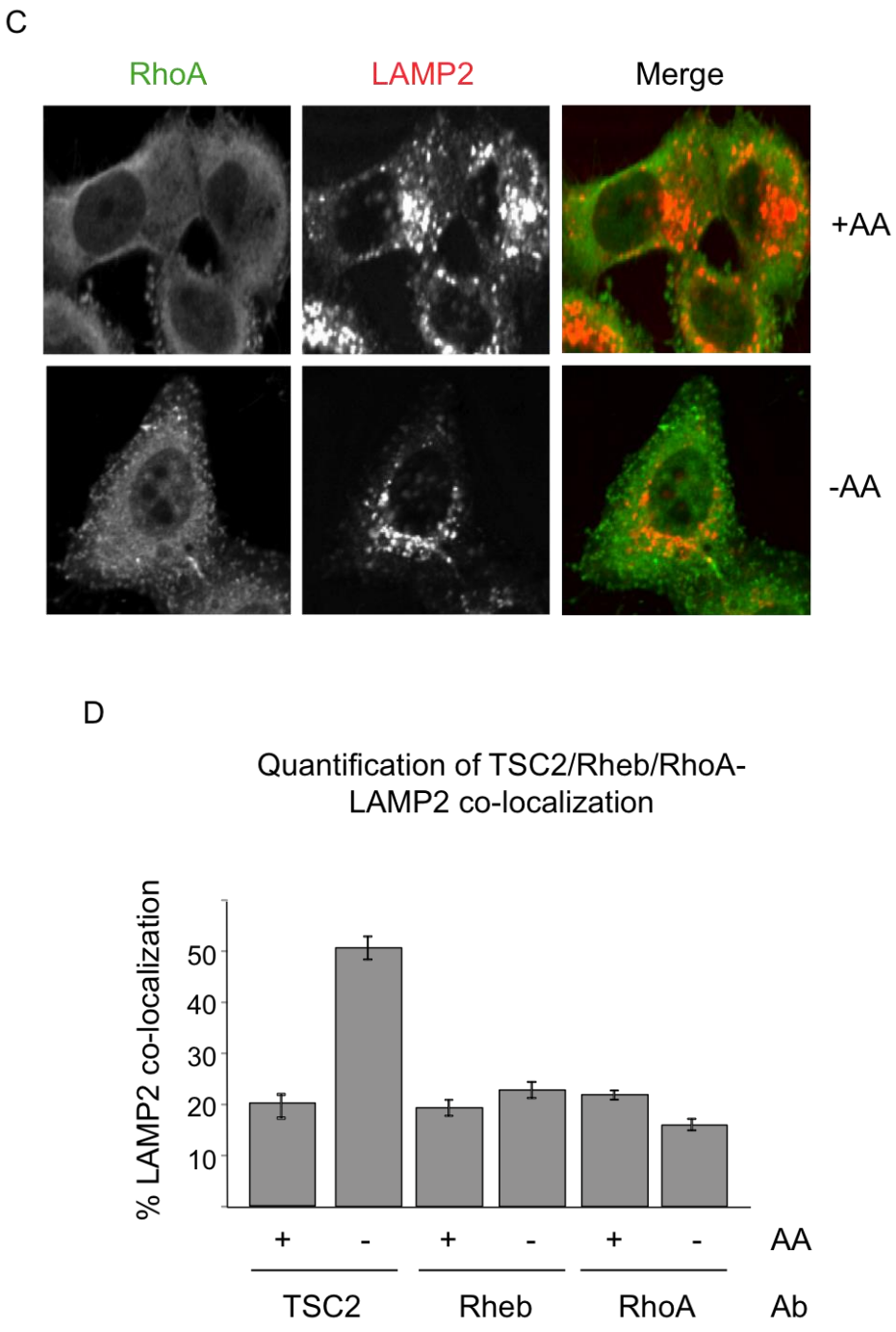

Figure 33. Rheb does not associate with lysosomes.
Confocal immunofluorescence analysis of TSC2, Rheb and RhoA localization in the absence (-AA, 60min) or presence (+AA, 30min) of amino acids in Hela cells. TSC2, Rheb and RhoA were stained in green in panel **A**, **B** and **C** respectively and LAMP2 in red. **D.** Quantitative analysis of co-localization of TSC2 with LAMP2-positive lysosomes. Y-axis represents the percentage of LAPM2-positive TSC2 over the total TSC2. Experiments displayed in this figure were performed by Drs Richard Lamb and Rebecca Lamond.

3.1.5 Rheb promotes lysosomal localization of mTOR and RagC

The data presented so far suggest that amino acid deficiency-induced translocation of TSC2 to lysosomes requires both Rheb and RagA, whilst TSC2 appears to bind preferentially to RagC. In addition, the sub-cellular localisation of Rheb is found to be cytoplasmic. Based on these findings, it is possible that Rheb promotes the association of the TSC2 with lysosomes indirectly by affecting the lysosomal localisation of the Rag GTPases. To investigate whether Rheb played a role in the lysosomal localization of RagC, Rheb was suppressed in HeLa cells using siRNA and the resulting co-localization of RagC/mTOR was analyzed by immunofluorescence staining. As shown in Figure 34A, suppression of Rheb led to a dramatic reduction of mTORC1 activity as demonstrated by the ratio of relative pS6K1 T389 to total S6K1, which is in support of Rheb being the critical activator of mTORC1. In control siRNA transfected cells, mTOR accumulated on lysosomes under normal nutrient condition (+AA) and dissociated from lysosomes upon amino acid withdrawal (-AA) (Figure 34B and C), as expected. In contrast, RagC was localised on lysosomes under both conditions (+AA and –AA) (Figure 34D and E). Interestingly, neither mTOR nor RagC accumulated on lysosomes following suppression of Rheb (Figure 34B. D and E). The quantitative analysis (Figure 34F) accords with the confocal micrographs data, demonstrating that Rheb regulates lysosomal localization of both mTOR and RagC. In addition, the reduction of mTORC1 activity caused by suppression of Rheb is consistent with dissociation of mTOR from lysosomes following Rheb suppression.

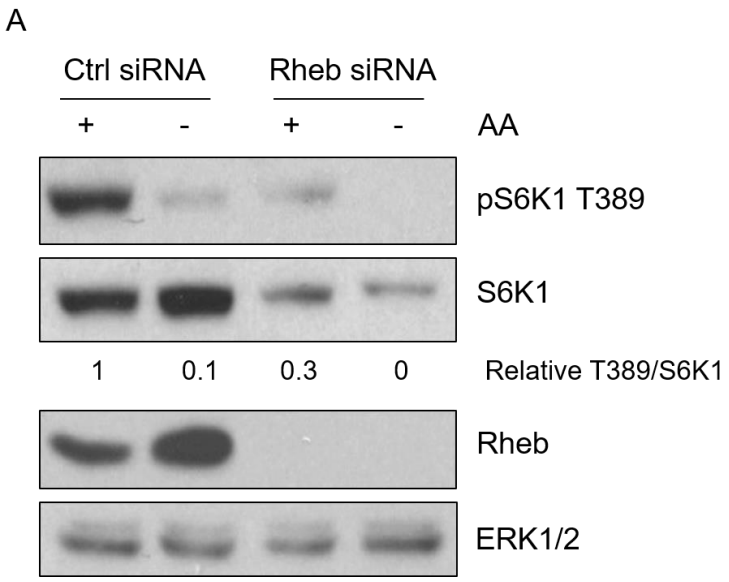

B

IF confocal images of Hela cells +AA

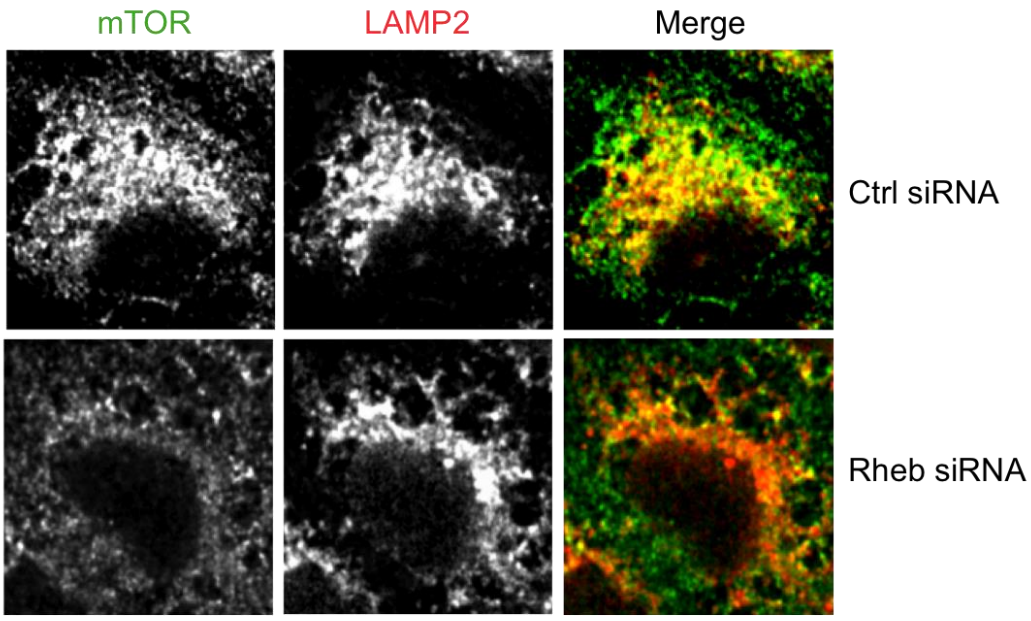

C

IF confocal images of Hela cells -AA 1h

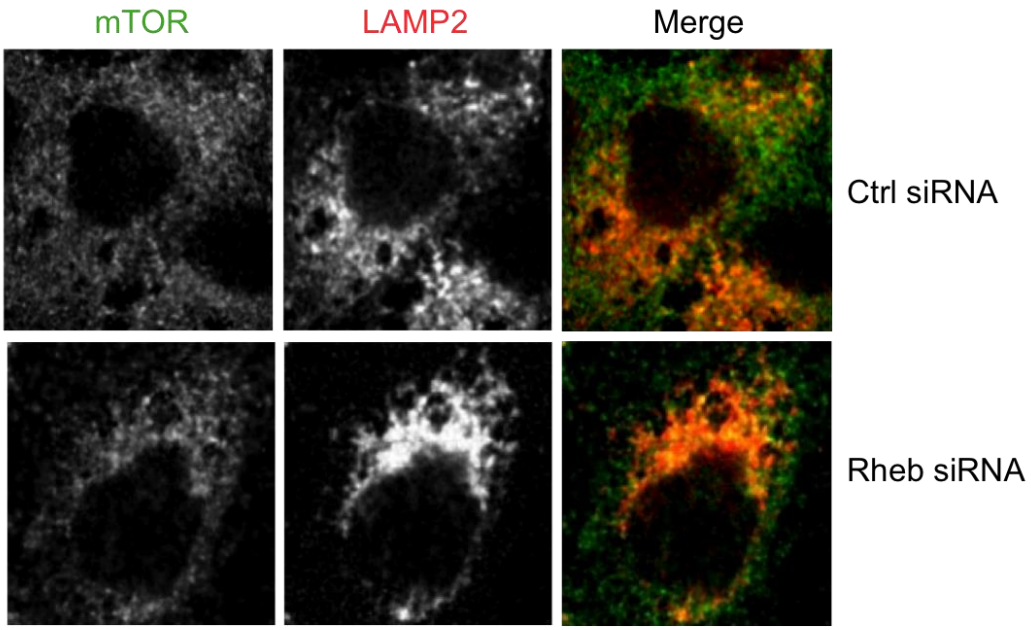

D

IF confocal images of Hela cells +AA

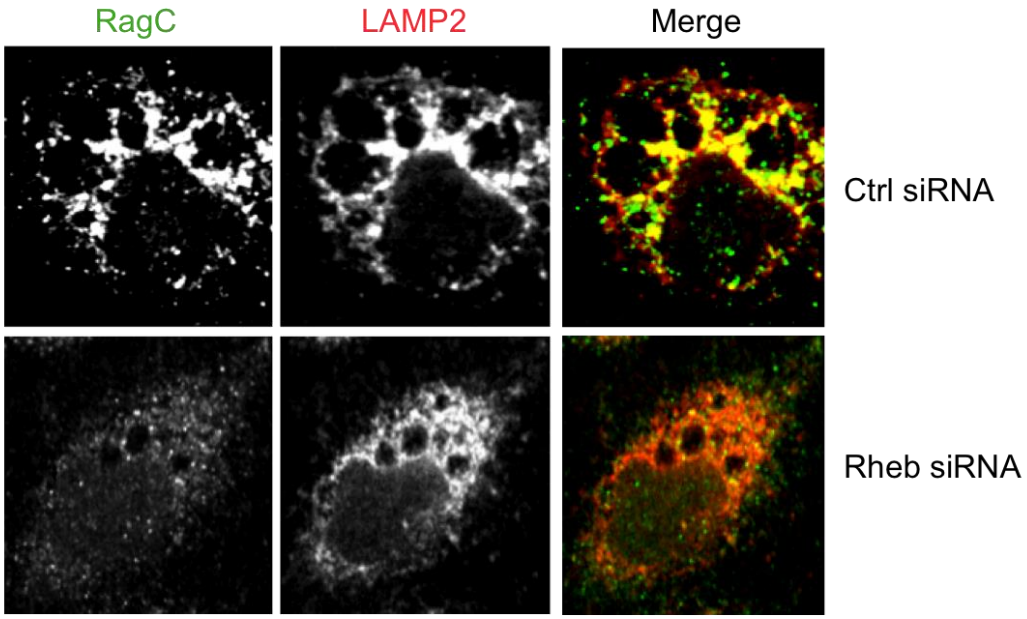

E

IF confocal images of Hela cells -AA 1h

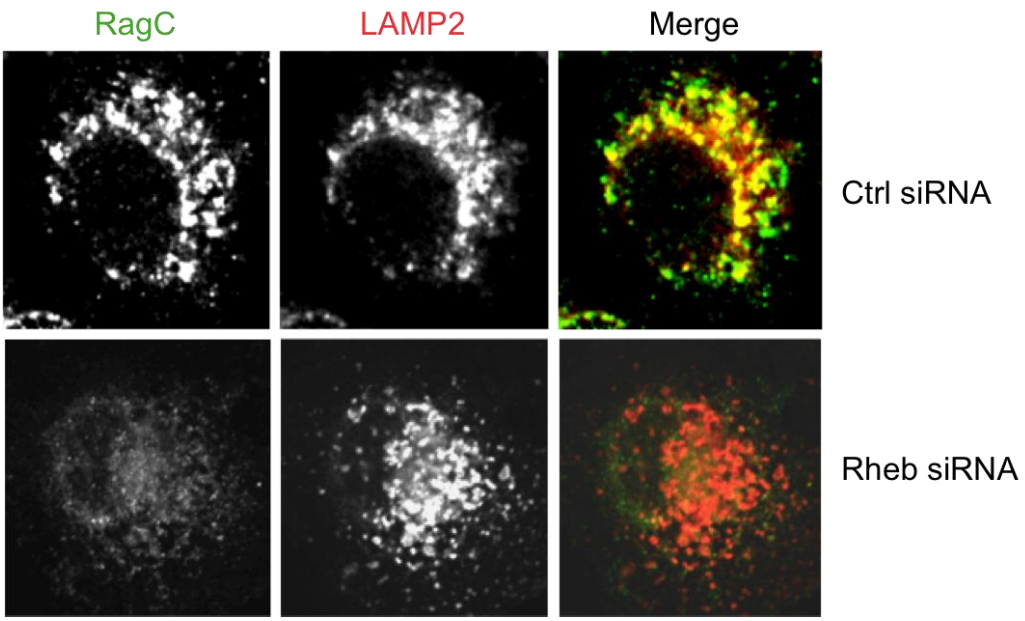

F

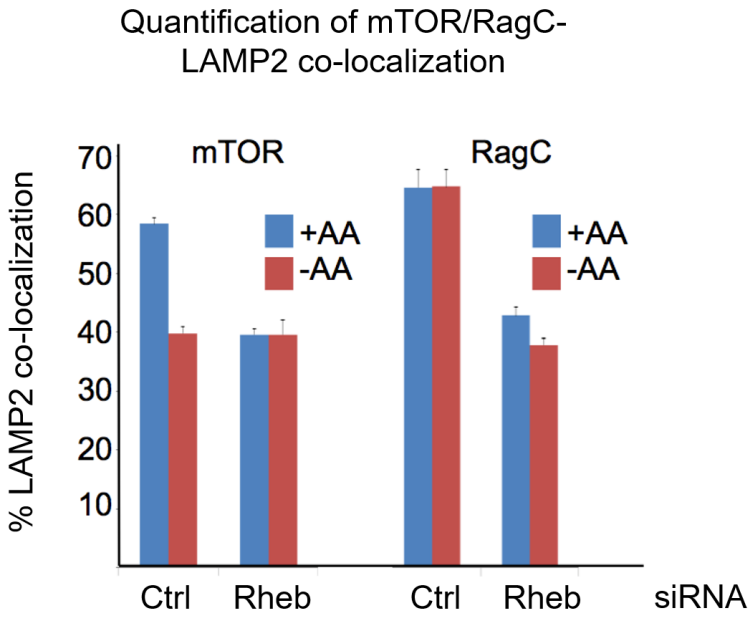

Figure 34. mTOR and RagC localize with lysosomes in a Rheb-dependent mechanism.
Hela cells were treated with medium lacking amino acids for 60min (-AA) or deprived and stimulated with MEM amino acids for 15min (+AA) following transfection with control (Ctrl) or Rheb-specific siRNAs. **A.** Immunoblots of cell extracts probed with antibodies to pS6K1 T389, total S6K1, Rheb and ERK1/2. Relative T389/S6K1 ratio was the average value from three biological repeats and was calculated using the ImageJ software from scanned autoradiographs, with the ratio in control siRNA-transfected cells in the presence of amino acid (Ctrl siRNA +AA) assigned the value of 1. **B-E.** Confocal immunofluorescence micrographs of cells stained to mTOR (green in **B** and **C**) or RagC (green in **D** and **E**) and LAMP2 (red). Amplified micrographs were shown in this figure to display more details. The original micrographs were shown in the supplementary figure Appendix 4. **F.** Quantitative analysis of co-localization of mTOR or RagC with LAMP2-positive lysosomes**.** Y-axis represents the percentage of LAPM2-positive mTOR/RagC over the total mTOR/RagC.

3.1.6 Rheb promotes the association of RagA and lysosomes

Previously published data suggest that Rag GTPases interact with the lysosomal protein Ragulator, which together mediate the recruitment of mTORC1 to lysosomal surface [95, 98]. We therefore asked whether Rheb mediated the association of RagA with lysosomes. Due to lack of immunofluorescence antibody detecting endogenous RagA, we have examined the interaction of RagA with LAMTOR1, a component of the Ragulator complex, via co-IP analysis following Rheb suppression; we also

examined whether Rheb affected the localization of transiently overexpressed HA tagged RagA via immunofluorescence staining against HA.

3.1.6.1 Interaction of RagA with LAMTOR1 requires Rheb

As shown in Figure 35, endogenous RagA was co-immunoprecipitated with LAMTOR1-IP, but not the control IgG-IP, and the interaction has been eliminated by suppression of Rheb using siRNA. Immunoblots were also probed for LAMTOR3, another component of the Ragulator complex, which bound LAMTOR1 regardless of the presence of Rheb and served as a positive control for interaction with LAMTOR1. Therefore, Rheb seems to promote the interaction of RagA with LAMTOR1.

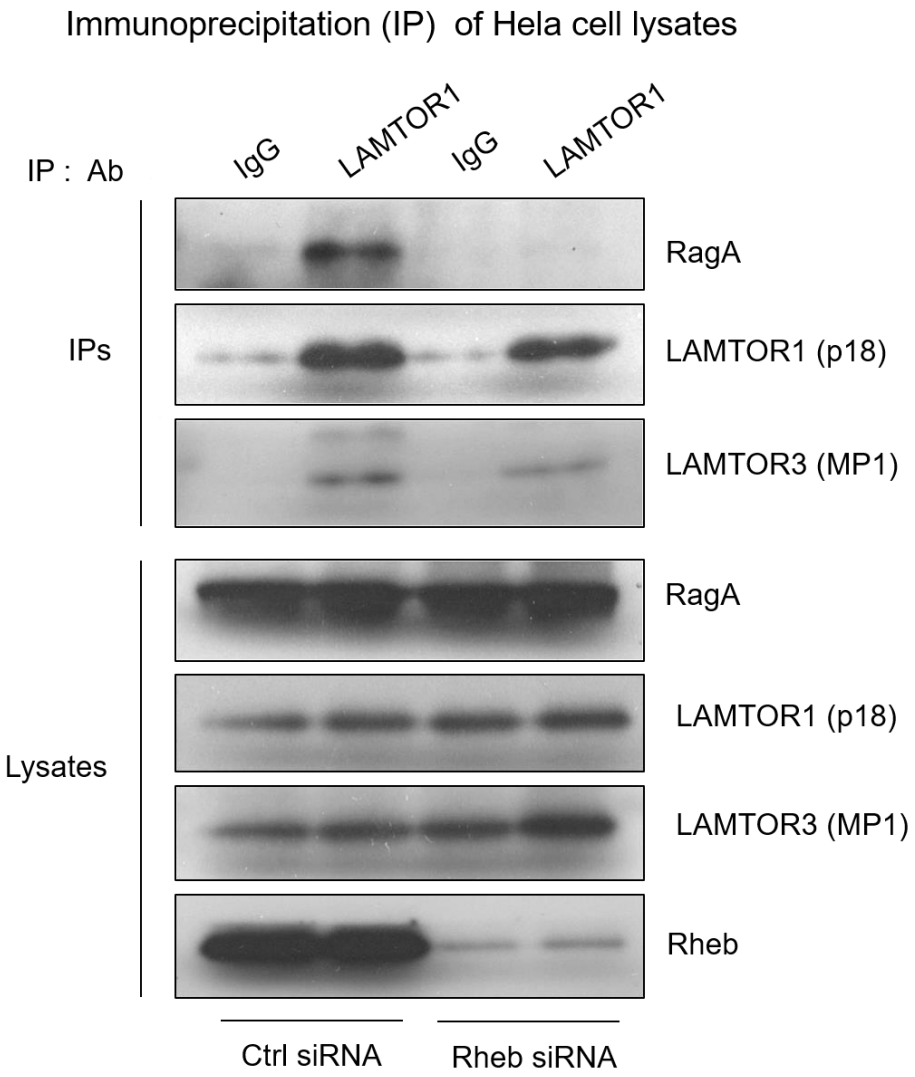

Figure 35. Interaction of RagA with LAMTOR1 requires Rheb.

Co-IP analysis of Hela cell extracts subjected to LAMTOR1- or control IgG-IPs and probed with antibodies detecting endogenous RagA, LAMTORs 1 and 3. Cell lysates (Lysates) were probed with the same antibodies and an additional antibody to Rheb to show siRNA knockdown. Experiment displayed in this figure was performed by Drs Richard Lamb and Rebecca Lamond.

3.1.6.2. TSC2 inhibits the interaction of RagA with lysosomes

We have further examined whether the TSC2/Rheb axis played a role in regulating the lysosomal localization of RagA and RagC by transiently expressing HA tagged RagA or RagC in MEF TSC2 knockout (KO) cells (Figure 36A). Following amino acid deprivation, HA tagged RagA exhibited a pattern that did not concentrate on lysosomes in cells expressing TSC2, but it was found to almost completely associate with lysosomes in cells lacking TSC2, suggesting that TSC2 may promote the dissociation of RagA from lysosomes during amino acid deprivation. This is also in accordance with the conclusion that Rheb promotes the RagA-lysosome/Ragulator association (Figure 35), in that Rheb is predominantly in the active GTP-bound state in TSC2 knockout cells. In contrast to RagA, HA tagged RagC was found to associate with lysosomes independently of TSC2 (Figure 36B).

A

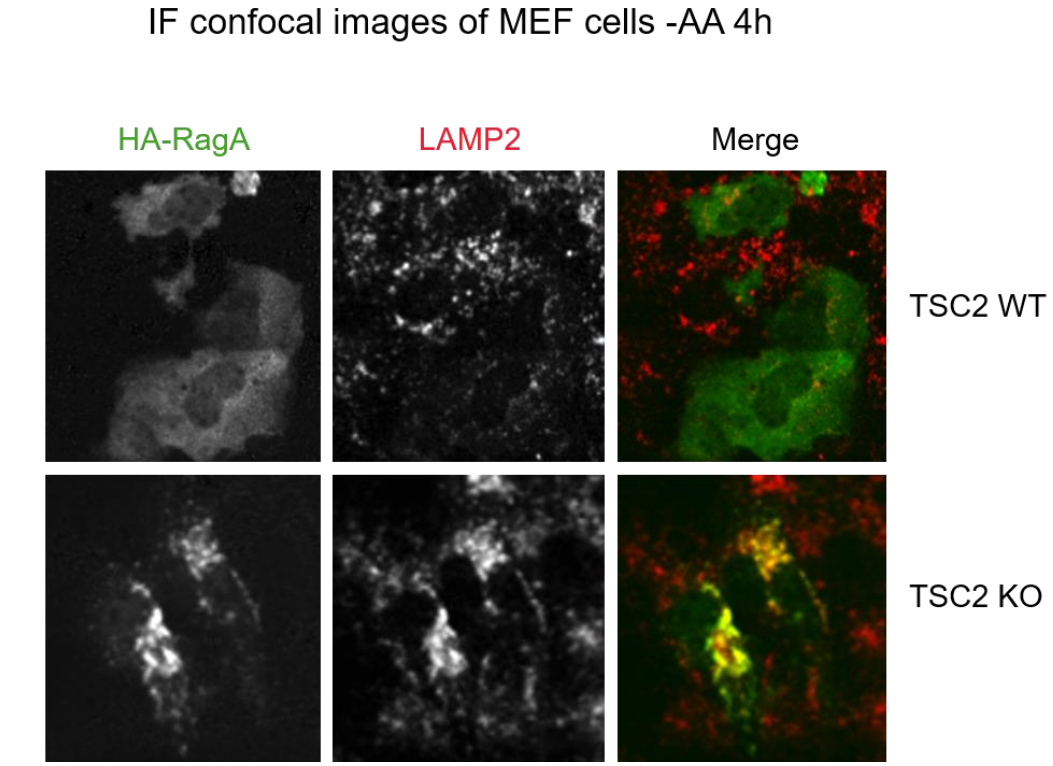

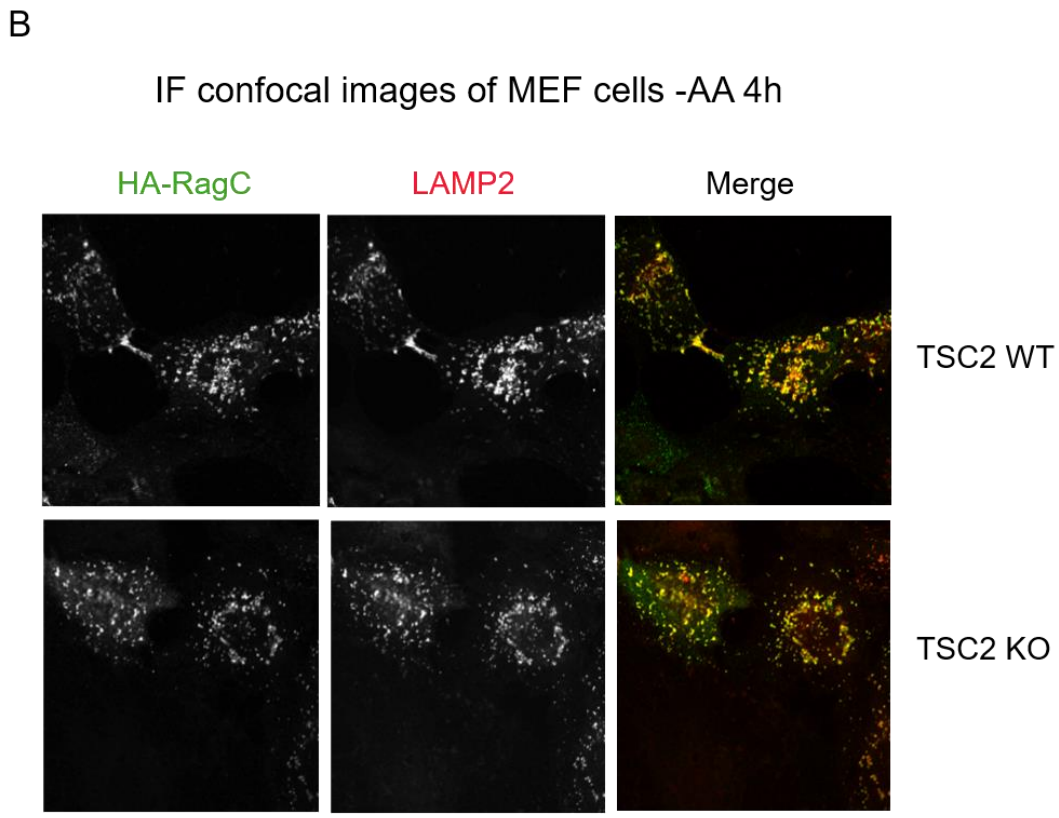

Figure 36. TSC2 promotes dissociation of RagA from lysosomes in response to amino acid deprivation.
Confocal immunofluorescence micrographs of MEF cells expressing (TSC2 WT) or lacking (TSC2 knockout, KO) TSC2. Cells were subjected to deprivation of amino acids for 4 hours (-AA) following transfection with plasmids containing HA-tagged RagA or RagC. Cells were stained with antibodies to HA (green) and LAMP2 (red) to respectively mark overexpressed RagA (**A**) or RagC (**B**) and endogenous lysosomes. Experiments displayed in this figure were performed by Drs Richard Lamb and Rebecca Lamond (Panel B), and me (Panel A).

3.2. MAP4K3 is an activator of mTORC1

MAP4K3 plays a complex role in cellular signalling. On one hand, it can activate mTORC1 in response to amino acids [108], suggesting a cancer-promoting function; on the other hand, MAP4K3 can induce apoptosis through the JNK pathway [128], which suppresses cancer progression. The aim of this section is to investigate the mechanism of MAP4K3-mediated activation of mTORC1, and to characterize nine MAP4K3 mutants identified in Cosmic Sanger Database.

3.2.1. PLD1 is a downstream effector of MAP4K3

3.2.1.1 Preliminary work: PLD1 is a potential mediator between MAP4K3 and mTORC1

MAP4K3 has been demonstrated by Dr Richard Lamb's group in 2007 to activate mTORC1 signalling in response to amino acid sufficiency and the kinase activity of MAP4K3 is required [108] (Figure 37A). Thus it had been proposed that the substrate of MAP4K3 might act as a mediator to activate mTORC1. To identify potential substrates of MAP4K3, Dr Richard Lamb and his colleagues at Yale University have initially established the substrate specificity of MAP4K3, and revealed a particularly interesting candidate, the substrate site (Thr147) within the PX domain of PLD1 (Figure 37B), in that PLD1 and its metabolic product, phosphatidic acid (PA), had been implicated as the upstream activators of mTORC1 [206-211]. To investigate whether MAP4K3 indeed regulated PLD1, the expression of MAP4K3 was suppressed in Hela cells using two independent siRNAs (MAP4K3-1 and MAP4K3-2) targeting distinct sites of MAP4K3, and the effects on phosphorylation of PLD1 was examined by western blot. Due to lack of an antibody detecting endogenous phosphorylated Thr147 of PLD1 (the antibody used in this study only detects overexpressed PLD1 Thr147), the phosphorylation state of PLD1 was evaluated by its SDS-PAGE migration, in which slow migrating bands were presumably indicative of phosphorylated PLD1 due to additional phosphoryl groups. As shown in Figure 37C, suppression of MAP4K3 has indeed caused the disappearance of the slow-migrating phospho-PLD1 band on SDS/PAGE, compared to that of control siRNA transfected cells (left panel). In accordance with this,

overexpression of wild type (WT) but not the kinase-inactive mutant of MAP4K3 (DA, where the kinase-active DFG motif is mutated to inactive AFG [108]) resulted in a significant increase in phospho-PLD1 (Thr147-P) (right panel). Therefore, MAP4K3 seems to act as an upstream kinase that stimulates the phosphorylation of PLD1 and the stimulation is dependent on its kinase activity. Based on this, a model has been proposed where PLD1 has been positioned downstream of MAP4K3 and upstream of mTORC1.

A

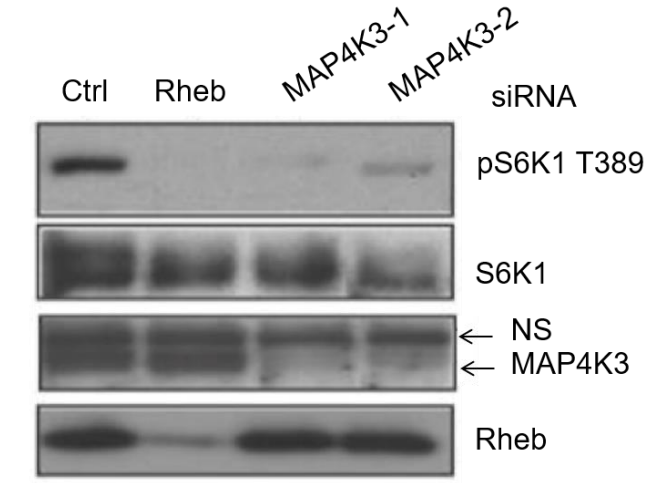

B

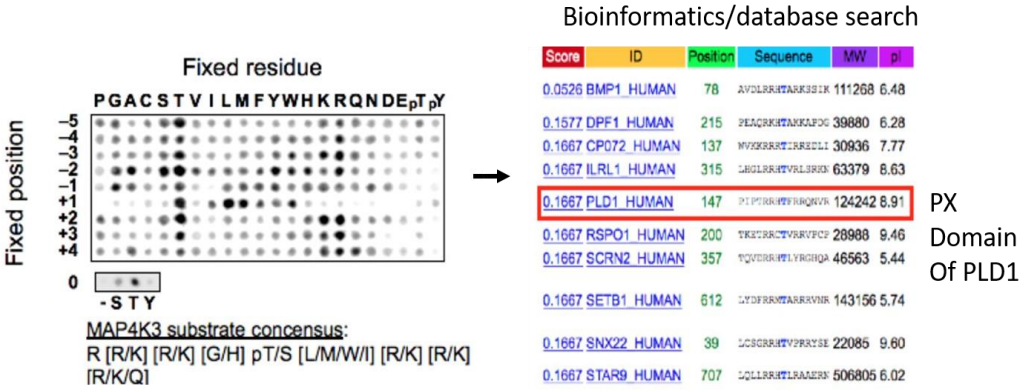

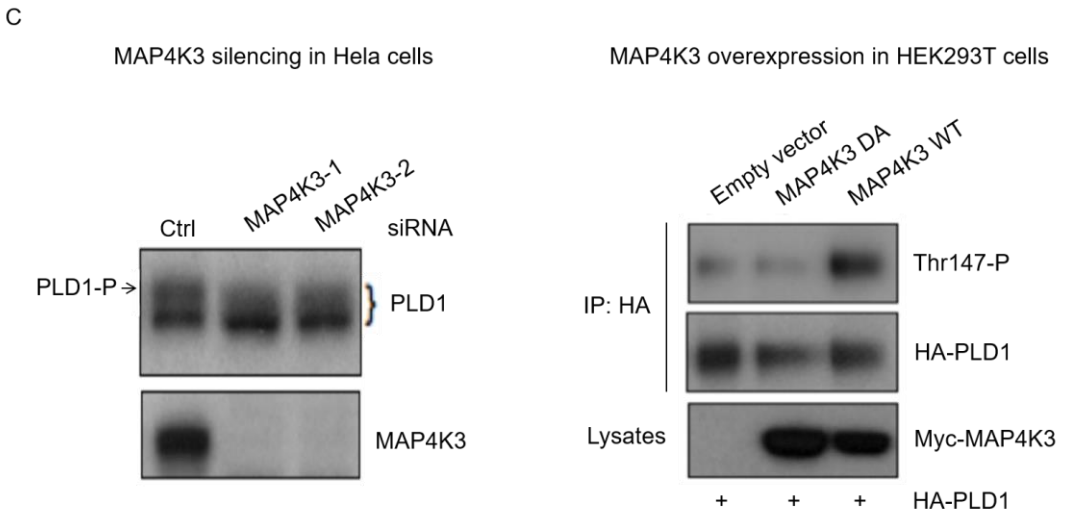

Figure 37. PLD1 is a potential substrate of MAP4K3.
A. MAP4K3 is an activator of mTORC1. Immunoblots of extracts from Hela cells transfected with control (Ctrl), Rheb and MAP4K3 siRNAs, and were probed for pS6K1 T389, total S6K1, Rheb and MAP4K3. Rheb siRNA was used here as a positive control for impaired mTORC1 activity. **B.** Left panel, the peptide array analysis of MAP4K3 substrate consensus shows specificity for the Threonine (Thr) motif; right panel, candidates containing the motif from searching Scansite including PLD1 Thr147 (red box). **C.** MAP4K3 potentially stimulates phosphorylation of PLD1 on Thr147. Left panel, immunoblots of extracts from Hela cells transfected with control or MAP4K3 siRNAs. MAP4K3 silencing resulted in smaller-size (dephosphorylating) shifts of PLD1 compared to that in control group; right panel, HA-PLD1 was co-expressed in HEK293T cells with empty vector, vectors expressing myc-MAP4K3 kinase inactive (DA) or myc-MAP4K3 wild-type (WT). Upper panels, HA-IP probed with phospho-PLD1 (Thr147) and HA antibodies; lower panel, immunoblots of cell lysates (Lysates) probed with the 9E10 antibody against the Myc epitope for Myc-MAP4K3.

3.2.1.2 MAP4K3 stimulates PLD1 phosphorylation on Thr147

To validate whether MAP4K3 mediated the phosphorylation of PLD1-Thr147, we analysed Thr147 phosphorylation of co-expressed HA-PLD1 induced by wild type MAP4K3 and by the kinase-inactive MAP4K3 mutant (DA). Overexpression of wild type MAP4K3, but not inactive MAP4K3, led to increased HA-PLD1 Thr147 phosphorylation (Figure 38), consistent with preliminary work demonstrating that MAP4K3 regulates phosphorylation of PLD1-Thr147, and the kinase activity of MAP4K3 is required. The phospho-PLD1 Thr147 band can only be detected when PLD1 is overexpressed probably because of its low cellular basal activity [209]. In addition, the overexpressed MAP4K3 could not be detected from the HA-IP samples, suggesting that there was no interaction between MAP4K3 and PLD1, or the

interaction was so weak that it had been interrupted during the lysis process. Thus, MAP4K3 stimulates the phosphorylation of PLD1-Thr147, likely in an indirect way.

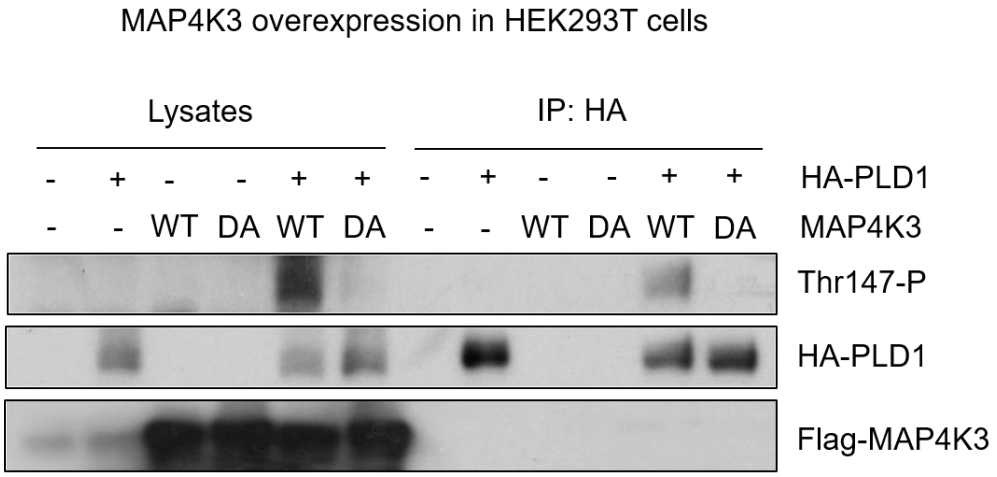

Figure 38. MAP4K3 stimulates phosphorylation of PLD1-Thr147.
HEK293T cells were co-transfected with pRK5-Flag-MAP4K3 wild type (WT) or kinase-inactive (DA), and HA-PLD1 plasmids. Lysates were collected 40 hours post transfection and subjected to HA-IP. Immunoblots were probed for phospho-PLD1 (Thr147) and re-probed with the HA antibody for HA-PLD1, as well as the Flag antibody for Flag-MAP4K3.

3.2.2. mTORC1 activation and lysosomal translocation are independent of PLD1

3.2.2.1 mTORC1 activation by amino acids is independent of PLD1

Following validation of PLD1 as a downstream effector of MAP4K3, we wanted to examine whether PLD1 played a role in activating mTORC1. Amino acids are known to be the indispensable stimuli of mTORC1 activation [46] and in support of this, the mTORC1 activity was complete inhibited following amino acid deprivation (-AA) for 60min in the control siRNA transfected cells, as demonstrated by the disappearance of pS6K1 T389 band on immunoblots (Figure 39A Ctrl siRNA). The mTORC1 activity was re-stimulated as soon as within 15min following amino acid re-addition (-/+AA). Previous publication has demonstrated that PLD1 is required for mTORC1 activation in Hela cells [110], however, when PLD1 was knocked-down using the two siRNAs with the same sequence as in the publication (PLD1 siRNA1 and 2) in our Hela cells, the level of phospho-S6K1 T389 in the presence of amino acids (-/+AA) did not seem to reduce on the immunoblots, compared to that

of the control siRNA transfected cells (Figure 39A). The results suggest that mTORC1 activation by amino acids seems to be independent of PLD1. The level of pS6K1 T389 was low in the normal medium (Figure 39A, +AA) most likely because the medium was not fresh prior to analysis and most nutrients including amino acids had been consumed. To avoid the possible off-target effects of the two PLD1 siRNAs, we have utilized another three independent siRNAs from Qiagen, PLD1 siRNA 3-5, and examined their effects on mTORC1 activity. As shown in Figure 39B, suppression of PLD1 in Hela cells using these five independent siRNAs, likewise, did not alter the level of pS6K1 T389 in the presence of amino acids, compared to that of control siRNA transfected cells. Therefore, it seems that the activation of mTORC1 by amino acids is independent of PLD1.

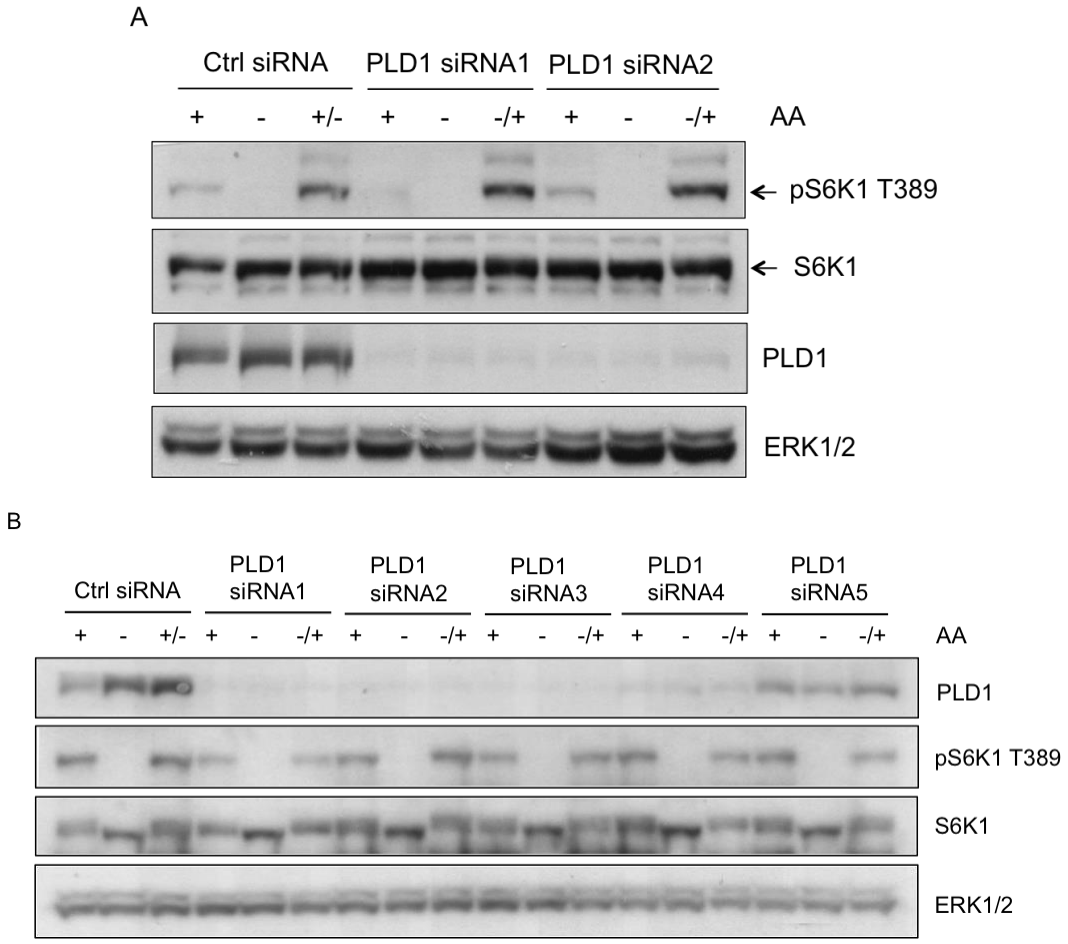

Figure 39. Amino acids activate mTORC1 in a PLD1-independent mechanism. Immunoblots of lysates from Hela cells transfected with control (Ctrl) siRNA or two (**A**) to five (**B**) PLD1-specific siRNAs followed by treatment with medium lacking amino acids with 10% d. FBS (-AA) for 60min, or deprived and stimulated with MEM amino acids for 15min (-/+AA). The condition where medium was not changed post transfection was labelled " +AA" in **A,** and the condition where

medium was changed to culture medium on the following day of transfection was labelled "+AA" in **B**. Cells lysates were prepared 72 hours post transfection in both **A** and **B**. Immunoblots were probed for PLD1, pS6K1 T389, total S6K1 and ERK1/2.

3.2.2.2 mTOR translocates to lysosomes independently of MAP4K3 and PLD1

In parallel to investigating whether suppression of PLD1 affected mTORC1 activity, we have also examined, using IF staining, whether PLD1 might regulate mTORC1 lysosomal translocation that is required for mTORC1 activation. As shown in Figure 40A, mTOR displayed a disperse pattern following amino acid deprivation for 60min in control siRNA transfected cells, whilst re-supplying the cells with amino acids immediately (15min) stimulated accumulation of mTOR onto lysosomes. This co-localization of mTOR with lysosomes induced by amino acids did not alter obviously when PLD1 and MAP4K3 were suppressed using siRNAs (Figure 40B), suggesting that neither MAP4K3 nor PLD1 seem to regulate the co-localization of mTOR with lysosomes. Since HA tagged PLD1 has been demonstrated, in the same publication [110], to undergo lysosomal translocation in response to amino acid sufficiency, we also examined the subcellular distribution of PLD1 using a recent commercially available IF antibody (clone F-12, mouse monoclonal) that detects endogenous human PLD1. The specificity of this antibody was firstly validated via PLD1 siRNA (Figure 40C). However, endogenous PLD1 displayed a disperse pattern and did not localize with lysosomes regardless of amino acids availability (Figure 40D). Therefore, it is unlikely that PLD1 regulates mTORC1 activity or its lysosomal translocation, and PLD1 itself does not seem to associate with lysosomes.

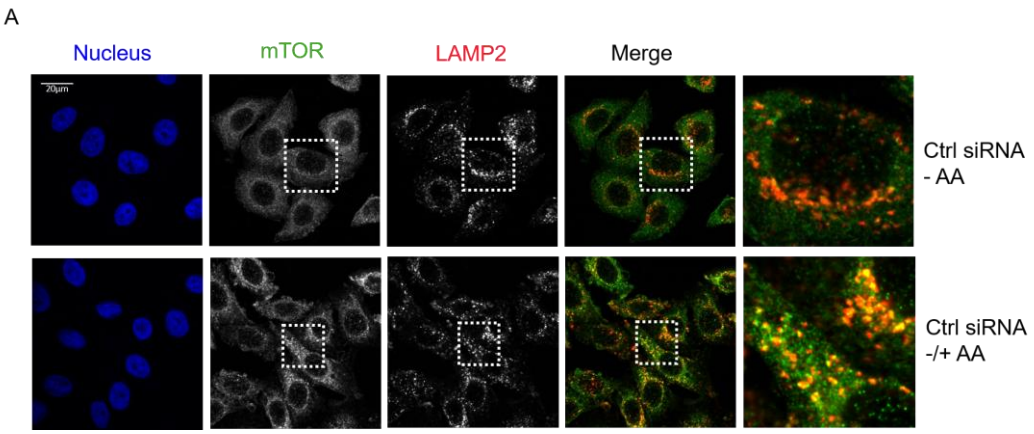

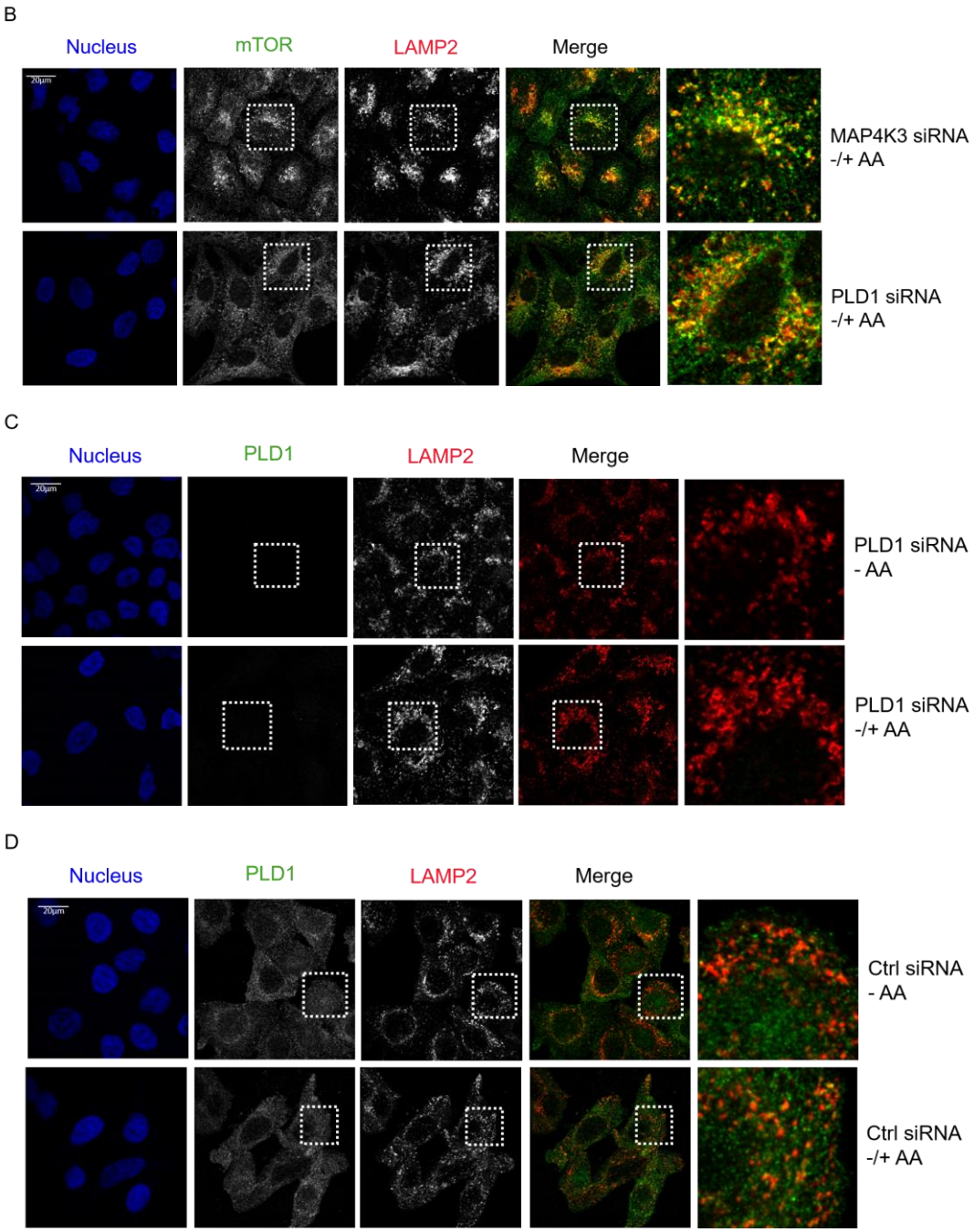

Figure 40. mTOR translocates to lysosomes in a PLD1-independent mechanism. Confocal immunofluorescence micrographs of Hela cells transfected with siRNAs targeting none (Ctrl), human PLD1 or MAP4K3, followed by treatment with medium lacking amino acids with 10% d.FBS (-AA) for 60min, or deprived and stimulated by MEM amino acids for 15min (-/+AA). Nucleus was stained in blue using Hoechst blue dye, mTOR (clone 7C10, rabbit monoclonal antibody in **A** and **B**) and PLD1 (clone F-12, mouse monoclonal antibody in **C** and **D**) in green, and LAMP2 (clone H4B4, mouse monoclonal antibody in **A** and **B**, clone GL2A7, rat monoclonal antibody in **C** and **D**) in red. Micrographs in the final lane are amplified from areas in the white dashed box. Two independent siRNAs were used in each

knockdown experiment and they exhibited similar effects, thereby only one group was displayed in this figure.

3.2.3 Characterization of cancer-associated MAP4K3 mutations

MAP4K3 has been implicated as an apoptosis inducer through the JNK signalling pathway [128], which suppresses cancer progression. An array of MAP4K3 mutations have been identified in human cancer and are collected in the Sanger Centre Cosmic Database, but their current relevance to MAP4K3 function and cancer development is unknown. Characterization of the MAP4K3 mutations may contribute to further understanding of the role of MAP4K3 in carcinogenesis and distinguish between cancer-promoting and cancer-suppressive functions of the MAP4K3 kinase. In this section, nine MAP4K3 mutations (Figure 41) from the Cosmic Database were sub-cloned into the pRK5-Flag vector, and their gain- and loss-of function was examined including activation of mTORC1 and the kinase activity.

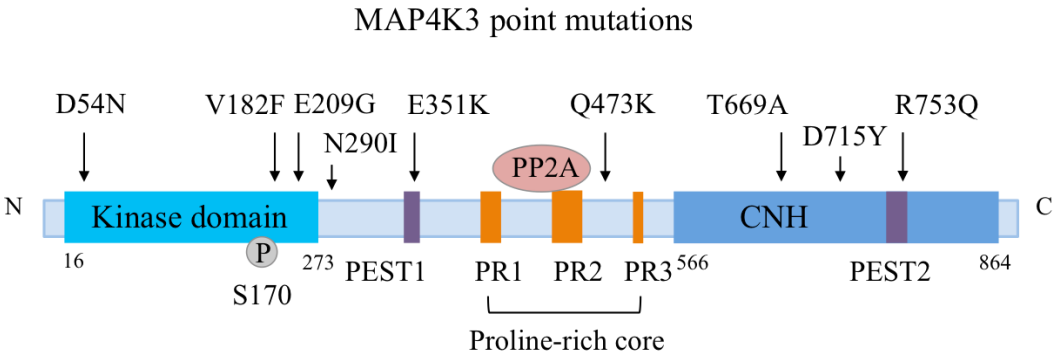

Figure 41. Linear schematic representation of MAP4K3 structure and mutations.
MAP4K3 consists of a kinase domain, a middle proline-rich core, two PEST domains and the CNH regulatory domain. S170 in the kinase domain is one of the trans-autophosphorylation sites. Positions of the nine MAP4K3 mutants in the linear structure are indicated by arrows.

3.2.3.1 Analysis of mTORC1 activation by MAP4K3 mutants

To investigate whether these MAP4K3 mutants displayed gain- and loss-of function in activating mTORC1, a S6K1-GST reporter was co-expressed with Flag-tagged MAP4K3 wild-type (WT), kinase-inactive (DA) or mutants in HEK293T cells (Figure 42). Transfected cells were starved from serum for 16 hours to avoid the

saturation of mTORC1 activity so that the increased activity due to active MAP4K3 were comparable on immunoblots. Two additional wells of cells were co-transfected with the empty vector pRK5-Myc and the S6K1-GST vector, both starved from serum for 16 hours, and one was stimulated with 10% FBS for 30min. These two wells served as controls for the inactive and activated mTORC1 respectively. As shown in Figure 42, serum starvation inhibited mTORC1 activity, as indicated by the level of phosphorylated S6K1-GST, which was remarkably restored by overexpressed wild type MAP4K3. The overexpressed kinase-inactive MAP4K3 (DA), as expected, failed to compensate for the inhibition of mTORC1 activity by serum starvation. These results are in accordance with kinase-active MAP4K3 being an activator of mTORC1 [108]. The kinase-domain mutants V182F and E209G continuously exhibited loss-of-function in activating mTORC1 in repeated experiments. Similar to the kinase-inactive MAP4K3, V182F mutant was unable to activate mTORC1. The level of phosphorylated S6K1-GST was barely detectable in cells transfected with the E209G mutant, suggesting that this mutant has somehow impaired the ability of endogenous MAP4K3 to activate mTORC1. One probable explanation could be that the E209G mutant formed a complex with the endogenous MAP4K3, which has compromised the kinase activity or led to degradation of the complex.

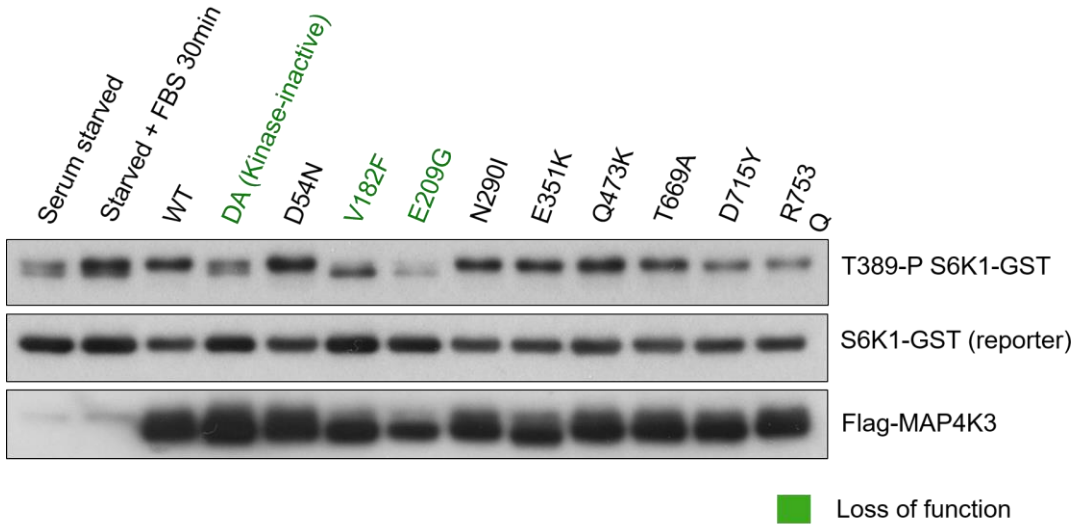

Figure 42. Analysis of mTORC1 activation by MAP4K3 mutants.
HEK293T cells were co-transfected with a S6K1-GST reporter vector and pRK5-Myc vector, pRK5-Flag MAP4K3 WT, kinase-inactive (DA), or nine mutants, followed by incubation in serum (FBS)-free medium for 16 hours, and one of the

Myc vector group was switched to medium containing 10% FBS for 30 min. Immunoblots were probed with antibodies detecting the GST tag for S6K1-GST expression, phosphorylated S6K1 T389 for the reporter and the Flag tag for Flag-MAP4K3 expression, respectively. The T389-P S6K1-GST has a molecular weight 26kDa higher than the endogenous phospho-S6K1 T389 due to the additional GST tag, thereby they were well separated on the immunoblots. The two loss-of-function mutants V182F and E209G are labelled in green.

3.2.3.2 Analysis of the kinase activity of MAP4K3 mutants

We also examined the kinase activity of these MAP4K3 mutants via the *in vitro* kinase assay using Flag-beads purified MAP4K3 and generic myelin basic protein (MBP) as the substrates (Figure 43). Ser170 within the kinase domain of MAP4K3 has been demonstrated as a transautophosphorylation site [109], and in support of this, the purified WT MAP4K3 displayed a high level of phosphorylated Ser170 on the immunoblots and conversely no phosphorylated Ser170 was detected with the DA MAP4K3. Phosphorylation of MBP followed the same pattern, as expected. The two mutants V182F and E209G that had displayed loss-of-function in mTORC1 activation also showed impaired kinase activity as demonstrated respectively by markedly lower and undetectable levels of phosphorylated MBP and Ser170. In addition, the binding efficiency of the inactive MAP4K3 including DA, V182F and E209G to the anti-Flag beads seemed significantly higher than that of WT and other seven mutants, indicating that these proteins may have become unfolded and thus the binding sites were more accessible by the anti-Flag beads.

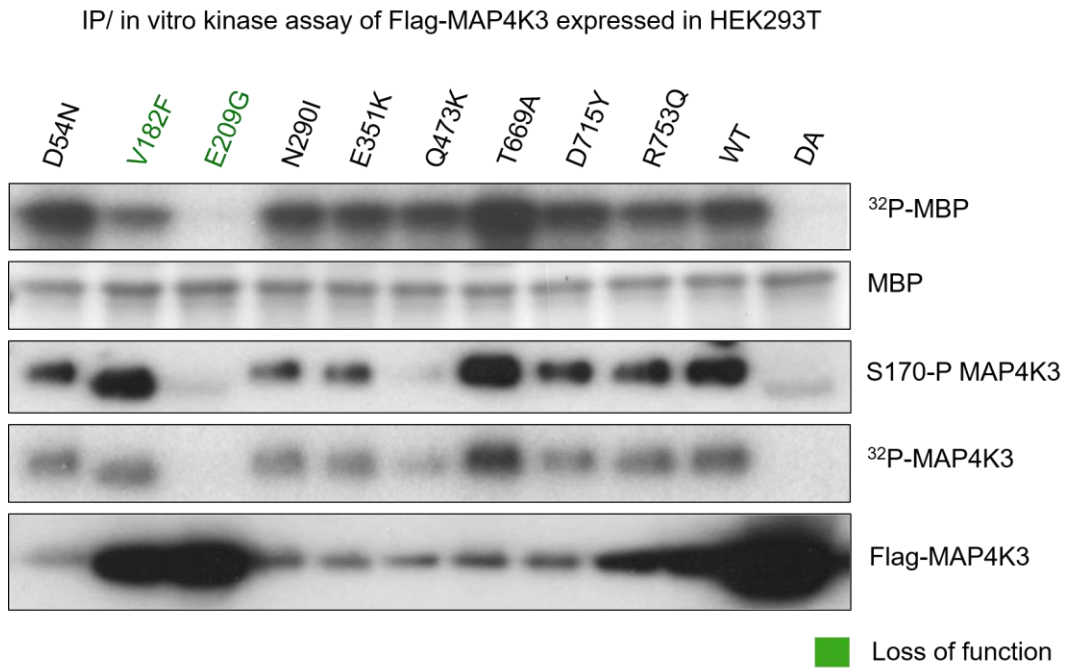

Figure 43. *In vitro* kinase assay of Flag-purified MAP4K3.
Flag tagged MAP4K3 (WT, DA and nine mutants) were overexpressed in HEK293T cells, purified using the anti-Flag beads and subjected to the kinase assay using MBP as substrates. Panel 1, autoradiograph displaying phosphorylated MBP. Panel 2, Ponceau S staining of total MBP. Panel 3, immunoblots of Ser170 auto-phosphorylation probed with a specific phospho-S170 peptide. Panel 4, autoradiograph displaying auto-phosphorylated MAP4K3. Panel 5, immunoblots of purified MAP4K3 probed against the Flag tag. The two loss-of-function mutants V182F and E209G are labelled in green.

3.2.3.3 Investigation of the subcellular distribution of MAP4K3 mutants

Subcellular localization of a kinase is closely correlated with its function and therefore we continued to examine the localization of these nine cancer-associated MAP4K3 mutants. Flag-tagged MAP4K3 (WT, DA and nine mutants) were expressed in HEK293T cells and the subcellular localization was analysed by immunofluorescence staining against the Flag epitope. As shown in Figure 44, WT MAP4K3 and the three kinase-inactive MAP4K3 (DA, V182F and E209G) exhibited two distinct patterns of localization. Unlike the WT MAP4K3, the inactive ones seemed to associate with microtubular structures. Cells overexpressing these MAP4K3 constructs were also co-stained with antibodies targeting perinuclear organelles including lysosome and also endoplasmic reticulum (ER), such as protein disulfide isomerase (PDI), KDEL (lysine-aspartic acid-glutamic acid-leucine, a

target peptide), and calreticulin, however, no co-localization was observed (data not shown).

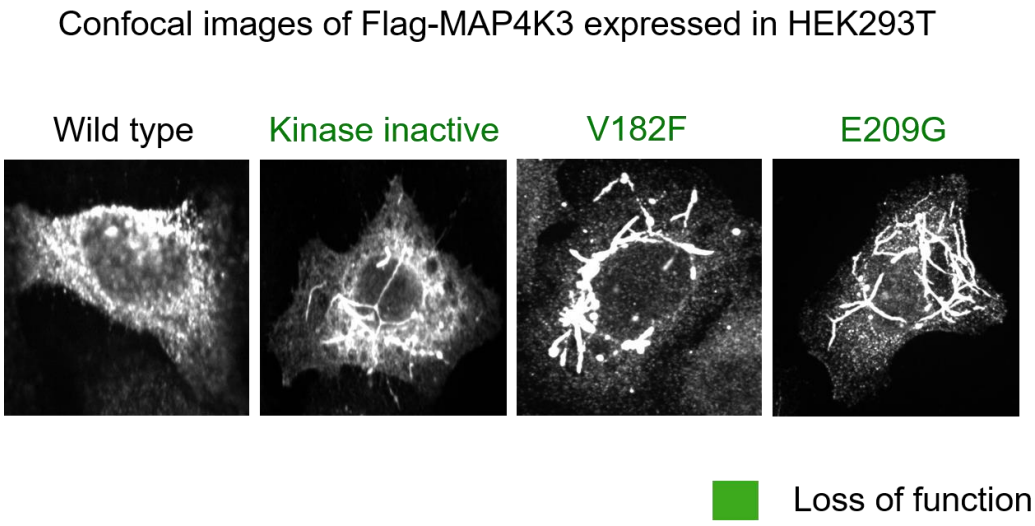

Figure 44. Investigation of MAP4K3 subcellular distribution.
Monochromic confocal micrographs of Flag-MAP4K3 (WT, DA and nine mutants) stained with the anti-Flag antibody following overexpression in HEK293T cells. The subcellular distribution of other seven mutants was also investigated and all exhibited the similar patterns to WT MAP4K3, thus the images are not displayed in this figure.

3.3 MAPK/ERK promotes ferroptosis in response to cystine deprivation

Results described in this section have been published in a paper that can be found in Appendix 6. Figures were generated based on the results from experiments performed by me, or my colleague Dr Ioannis Poursaitidis (a senior PhD student at the time), or together with colleagues from Glasgow or Austin, as indicated in figure legend.

Cancer cells reprogram their metabolism, altering both uptake and utilization of extracellular nutrients, to supply their rapid growth and proliferation. We therefore sought to investigate whether the high demands for nutrients, particularly amino acids, of cancer cells could be potentially exploited to identify cancer-specific vulnerabilities. In this study, we have taken advantages of the isogenic hTERT human mammary epithelial (HME) cell lines and the amino acid deprivation strategy. Four common oncogenic mutations including EGFR delE746-A750, KRAS G13D, BRAF V600E and PIK3CA H1047R had been individually knocked into the HME

cells and they have been demonstrated to activate the corresponding downstream signalling pathways [201]. In contrast to primary cancer cell lines that are extremely heterogeneous, such HME cell lines provide a much less complicated genetic context, which allows the gene-specific features to be characterized. By utilizing the amino acid deprivation strategy, synthetic lethal partners of the enumerated oncogenes could be potentially identified and exploited for cancer therapy.

3.3.1 Cystine deprivation selectively kills EGFR delE746-A750 HME cells

We firstly performed an amino acid dropout screen in the four HME cell lines, EGFR (delE746-A750), KRAS (G13D), BRAF (V600E) and PIK3CA (H1047R) (hereinafter referred to as EGFR, KRAS, BRAF, and PI3K mutant cells respectively for brevity), together with the wild type (WT) HME cell line. The media used for this screen were reconstituted according to the formulation of commercial media used to culture these cells, but to omit one specific amino acid, with 10% dialysed FBS to retain other growth supplements such as growth factors. Cells were maintained in normal medium for 24 hours before switched to media lacking the individual amino acid for 72 hours. Cell viability was then examined via CellTiter-Glo assay that detects ATP produced by viable cells. As shown in Figure 45A, among 15 amino acids deprived, deprivation of cystine (Cys) inhibited the viability of EGFR and BRAF mutant cells by more than 80% relative to control complete media (+AA, Chapter 2.1.10), whilst about 50% of WT cells remained alive under the same condition. This suggests that EGFR and BRAF mutant cells are more sensitive than WT cells to cysteine deprivation. As mentioned earlier, all of the four mutations are constitutively active due to the structural alterations. In support of this, these cell lines exhibited much higher levels of phosphorylated EGFR (pEGFR), Akt (pAKT) and ERK1/2 (ppERK) respectively than the WT cells, as examined by immunoblotting (Figure 45B). In addition, cystine deprivation did not seem to cause obvious changes of this pattern, supporting that both the MAPK/ERK and PI3K/Akt signalling pathways do not sense the conditions of amino acids [112]. Therefore, it was likely that cystine deprivation had triggered a certain cellular response that act synergistically with the activating MAPK/ERK signalling pathway to induce cell death.

A

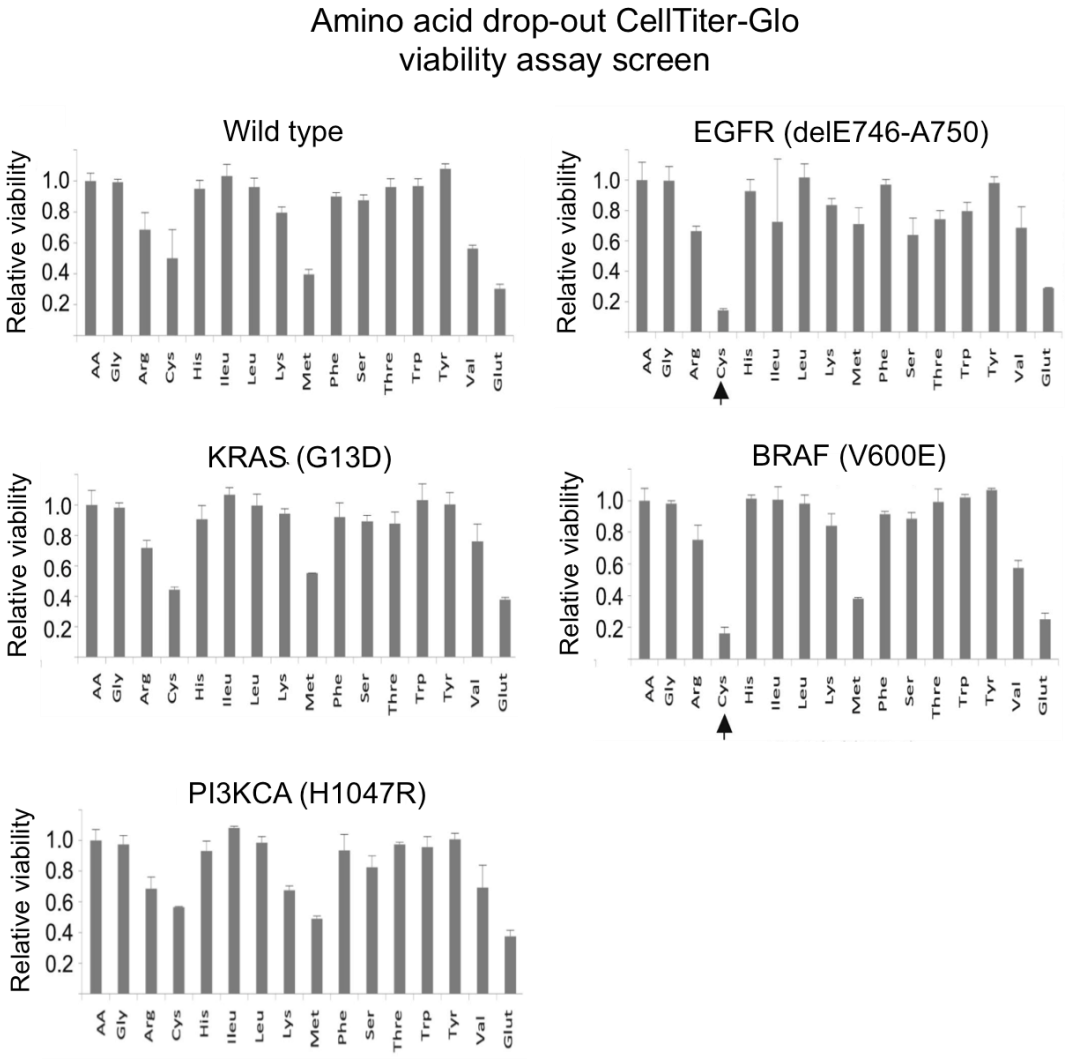
Amino acid drop-out CellTiter-Glo
viability assay screen
Wild type
EGFR (delE746-A750)
KRAS (G13D)
BRAF (V600E)
PI3KCA (H1047R)
Relative viability
1.0
0.8
0.6
0.4
0.2
AA
Gly
Arg
Cys
His
Ileu
Leu
Lys
Met
Phe
Ser
Thre
Trp
Tyr
Val
Glut

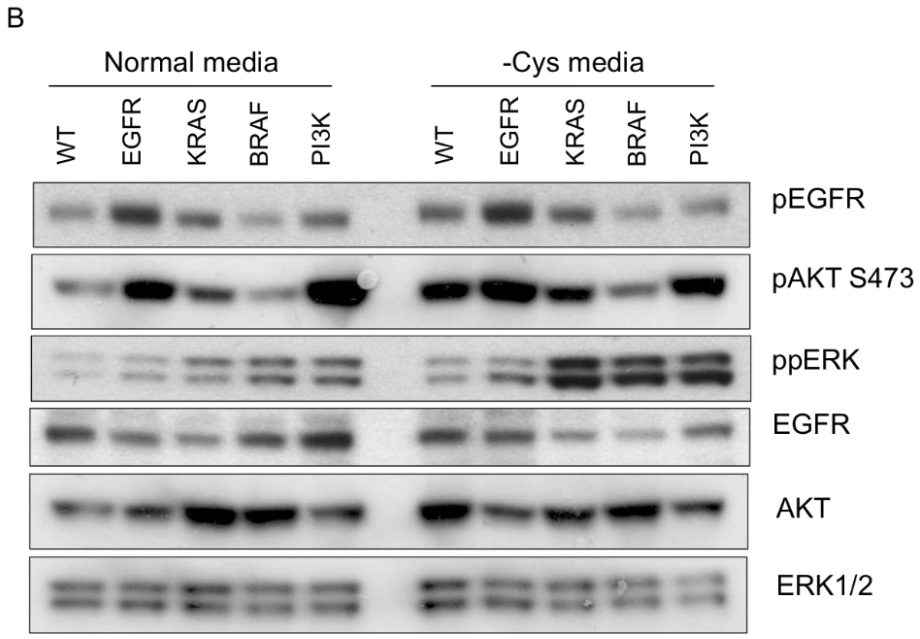

Figure 45. Cystine deprivation selectively kills EGFR delE746-A750 HME cells. **A.** Amino acid dropout screen in EGFR, KRAS, BRAF and PI3K mutant and WT HME cells. After seeding for 24 hours in normal media, cells were washed once in medium lacking all amino acids (-AA) and switched to media lacking specific amino acid for 72 hours, followed by Celltiter-Glo viability assay. Each amino acid is represented by its corresponding three- or four-letter abbreviation. Histograms represent the average viability ± SEM of three biological replicates relative to complete media (+AA) that was assigned a value of 1. Arrows indicate cystine (Cys) deprivation condition of EGFR and BRAF mutant cells. **B.** Immunoblots of lysates from EGFR, KRAS, BRAF and PI3K mutant and WT HME cells cultured in normal or cystine-free (-Cys) media for 12 hours. Immunoblots were probed with antibodies detecting phosphorylated EGFR (pEGFR), AKT (pAKT S473) and ERK (ppERK), and re-probed for total EGFR, AKT, and ERK (ERK1/2). Experiments shown in this figure have been performed by Ioannis Poursaitidis (Panel A) and me (Panel B).

3.3.2 Cystine deprivation induces ferroptosis in EGFR delE746-A750 HME cells

To determine whether such synchronous mechanisms exist, we needed to understand the nature of cell death in cystine-deprived EGFR mutant cells. We firstly asked whether the cell death occurred via apoptosis, a common form of programmed cell death with well-defined morphological features. Morphology of EGFR mutant and WT cells was analyzed by microscopy, and this has shown that cystine deprivation for 24 hours induced a widespread loss of viability in EGFR mutant, but not WT cells, with most EGFR mutant cells exhibiting a swollen morphology and loss of membrane integrity (Appendix 6). These morphological changes, however, were distinct from that during apoptosis, and therefore suggestive of an alternative form of

cell death. Since ferroptosis had previously been demonstrated to associate with the MAPK/ERK pathway (EGFR is the upstream activator) [147, 184, 187], it has been hypothesised that cell death in cystine-deprived EGFR mutant cells might occur by ferroptosis.

Because accumulation of ROS, particularly lipid ROS, is a key feature of ferroptosis, levels of total and lipid ROS were examined via fluorescence-activated cell sorting (FACS) analysis using the CMDCFDA and C11 BODIPY dyes respectively, and the results showed that levels of both total and lipid ROS in EGFR mutant cells indeed increased markedly following cystine deprivation whilst they were barely changed in WT cells (Figure 1E in Appendix 6). Further experiment using the iron chelator DFO suggested that this type of cell death was also dependent on cellular iron. Taken together with the data from ferroptosis inducer and inhibitor experiments, this has led to the conclusion that cell death in cystine-deprived EGFR mutant cells occurred by ferroptosis. Figures demonstrating this conclusion can be found in Figure 1 in Appendix 6.

3.3.3 Active MAPK/ERK cascade promotes cystine deprivation-induced cell death

Activation of EGFR stimulates multiple downstream signalling pathways, including MAPK/ERK and PI3K/Akt. We therefore asked whether inhibition of MAPK/ERK or PI3K/Akt signalling pathways by specific inhibitors could block ferroptosis in cystine-deprived EGFR mutant cells. To do this, we treated the cells with an EGFR inhibitor iressa, a MEK1/2 inhibitor selumetinib, and a PI3K inhibitor wortmannin (Figure 46). Iressa (ZD1839) is an effective drug for lung, breast and other cancers with activating mutation of or overexpressed EGFR [5]. Selumetinib (AZD6244) is a drug that specifically inhibits MEK1 and MEK2, and is currently being investigated for the treatment of various types of cancer, such as NSCLC [212]. Wortmannin is compound commonly used to inhibit PI3K in cell biology research.

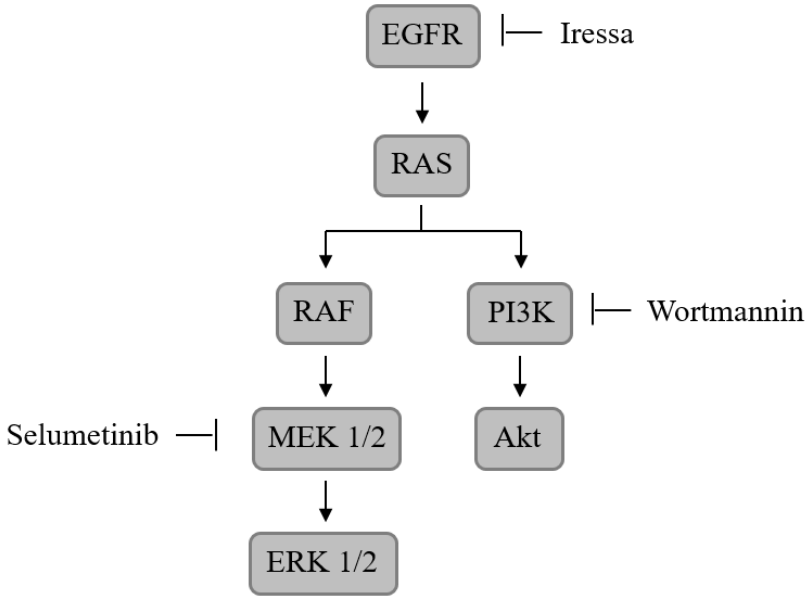

Figure 46. Inhibitors of MAPK/ERK and PI3K/Akt pathways.

Inhibition of the active EGFR (pEGFR), MEK1/2 (represented by ppERK) and PI3K (represented by pAKT) respectively by iressa, selumetinib and wortmannin in EGFR mutant cells were confirmed by immunoblots and not surprisingly their inhibitory effects displayed similar patterns under normal and cystine-deprived conditions (Figure 47A). As shown in the phase-contrast micrographs in Figure 47B, deprivation of cystine for 16 hours has caused dramatic cell death in DMSO-treated (vehicle control) EGFR mutant cells (Panel 2) whereas WT cells largely remained viable following deprivation of cystine for up to 24 hours (Panel 1). Cell death was markedly prevented by treatment with iressa and selumetinib, the inhibitors of EGFR and MEK1/2 respectively, but not with the PI3K inhibitor wortmannin. These observations were further supported by cell viability assay (Figure 47C) showing that treatment of cystine-deprived EGFR mutant cells with inhibitors of EGFR and MEK1/2, but not PI3K, significantly improved cell survival. In accordance with this, the FACS analysis of lipid ROS (Figure 47D) showed that iressa and selumetinib treatment in cystine-deprived EGFR mutant cells has led to a shift of lipid ROS back to that under the condition of normal medium, in contrast to that in control DMSO or wortmannin treated cells. Therefore, it seemed that the active MAPK/ERK signalling pathway in EGFR mutant cells has somehow promoted the accumulation of lipid ROS during cystine deprivation and rendered them highly sensitive to such stress, which has ultimately led to cell death.

A

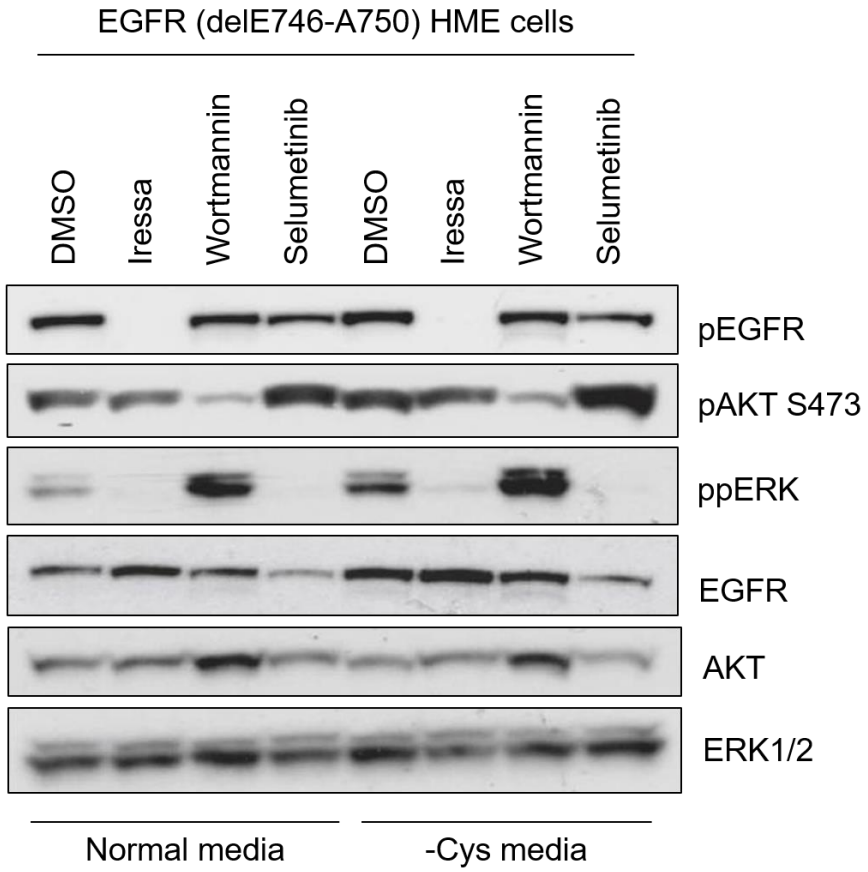
EGFR (delE746-A750) HME cells
DMSO
Iressa
Wortmannin
Selumetinib
DMSO
Iressa
Wortmannin
Selumetinib
pEGFR
pAKT S473
ppERK
EGFR
AKT
ERK1/2
Normal media
-Cys media

B

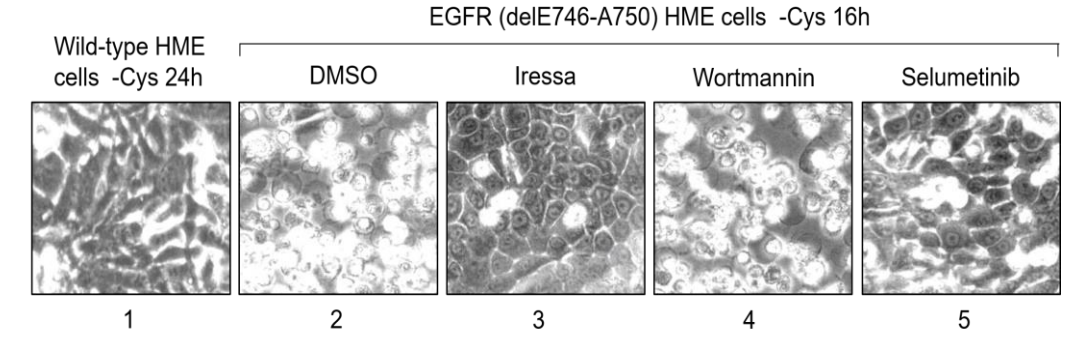
Wild-type HME cells -Cys 24h
EGFR (delE746-A750) HME cells -Cys 16h
DMSO
Iressa
Wortmannin
Selumetinib
1
2
3
4
5

C

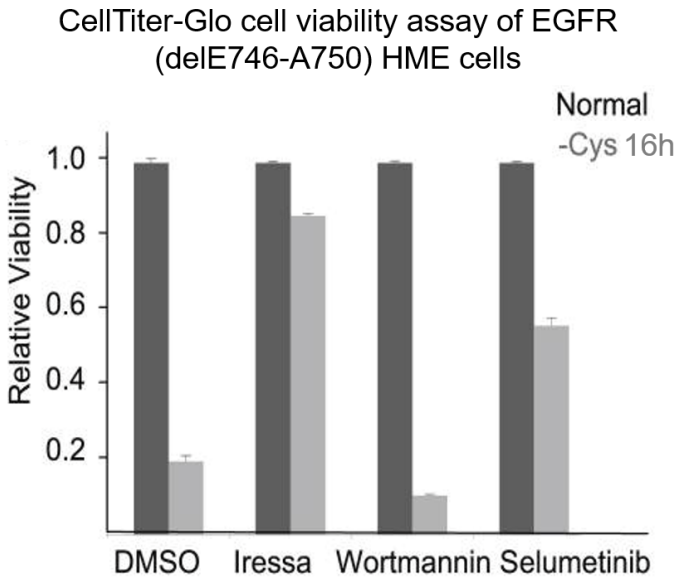

D

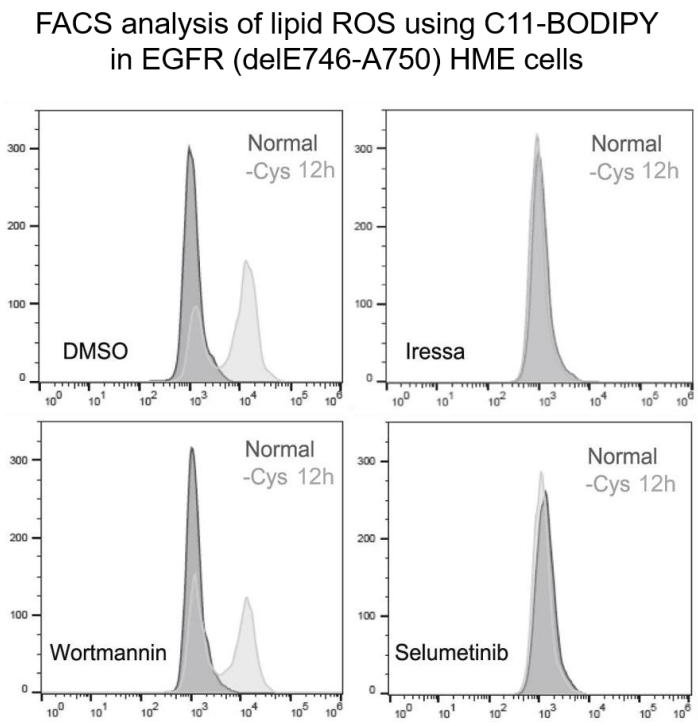

Figure 47. MAPK/ERK promotes cell death in response to cystine deprivation. EGFR mutant cells cultured in normal media (Normal) or cystine-free media (-Cys) for 12 hours (**A** and **D**) or 16 hours (**B** and **C**), in the absence (replaced with the vehicle control DMSO) or presence of inhibitors iressa, selumetinib and wortmannin for a total of 30 hours. **A.** Immunoblotting analysis of effects of the inhibitors on the MAPK/ERK cascade in EGFR mutant cells. Immunoblots were probed for pEGFR, pAKT and ppERK, and re-probed for total EGFR, AKT and ERK1/2. **B.** phase-contrast micrographs of EGFR mutant cells and WT cells maintained in cystine-free medium for 24 hours. Micrographs were captured using a 10X microscope objective.

C. CellTiter-Glo viability assay of EGFR mutant cells. Histograms represent the average viability ± SEM of three biological replicates relative to normal media that was assigned a value of 1. Dark and light bars indicate conditions of normal (Normal) and cystine-free media (-Cys) respectively. **D.** FACS analysis of lipid ROS using C11-BODIPY dyes (a membrane-targeted lipid ROS sensor) in EGFR mutant cells. Dark and light traces indicate conditions of normal (Normal) and cystine-free media (-Cys) respectively. Y-axis shows cell counts (events) and X-axis C11 fluorescence intensity using an emission channel of BL1. Experiments shown in this figure have been performed by Ioannis Poursaitidis.

3.3.4 Active MAPK/ERK cascade promotes lipid ROS independently of glutathione

Increased accumulation of lipid ROS can result from enhanced production of lipid ROS and/or decreased synthesis of cellular antioxidants. The reduced glutathione (GSH) is the major antioxidant in most mammalian cells and is biosynthesized from three amino acids: cysteine (reduced from cystine), glycine and glutamate, of which cysteine is the rate-limiting precursor [158]. We thus reasoned that one possible mechanism for WT cells to resist ferroptosis might be that they have preserved the intracellular abundance of either cysteine or GSH to counterbalance the toxicity of lipid ROS during cystine deprivation. To address this possibility, intracellular amino acids were extracted from WT and EGFR mutant cells cultured in normal and cystine-free media and subjected to LC-MS/MS analysis [183] to determine the quantity of 18 standard amino acids as well as cystine, reduced (GSH) and oxidized (GSSG) glutathione. Surprisingly, WT and EGFR mutant cells contained similar amounts of basal cystine under the normal-nutrient condition, and the amounts decreased to similar extents following extracellular cystine deprivation (Figure 48). The levels of glycine, glutamate and glutamine (converted to glutamate by glutaminase) were similar in WT and EGFR mutant cells, and they were scarcely altered when cystine was removed. These results indicated that WT and EGFR mutant cells are likely to harbour similar capacities to synthesize GSH. This was supported by the measurements of GSH and GSSG, both of which decreased dramatically and similarly following cystine deprivation in WT and EGFR mutant cells. Therefore, it seems that the active MAPK/ERK cascade promotes lipid ROS accumulation in a glutathione-independent mechanism.

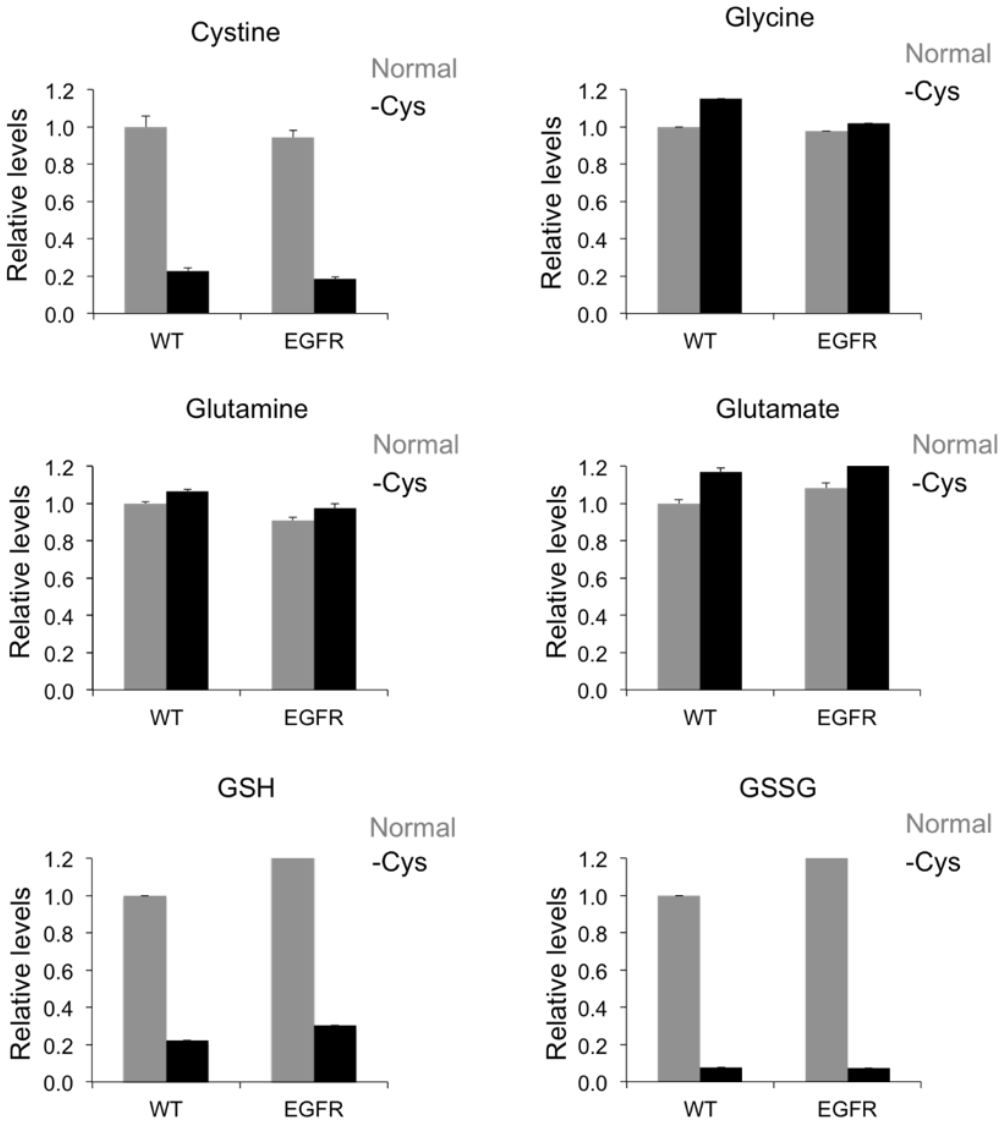

Figure 48. Analysis of the intracellular amino acids in EGFR delE746-A750 and WT HME cells.
Quantification of intracellular cystine, glycine, glutamine, glutamate, reduced (GSH) and oxidized (GSSG) glutathione using LC-MS. Metabolites were extracted from WT and EGFR mutant cells cultured in normal (Normal, light bars) or cystine-free (-Cys, dark bars) media for 4 hours. Histograms represent the average values ± SEM of three biological replicates and the level of WT cells in normal medium was assigned the value of 1.

3.3.5 The MAPK/ERK cascade promotes lipid ROS by regulating GPX4 and NOX4

Since the active MAPK/ERK cascade seems to promote lipid ROS in a glutathione-independent mechanism, we sought to identify potential mediators that act downstream of this cascade and are associated with the accumulation of lipid ROS.

As described in the introduction part, GPX4 catalyses the oxidation of GSH to GSSG, concomitantly detoxifying lipid ROS to corresponding alcohol. It has been demonstrated that loss of GPX4 activity can drive ferroptotic cancer cell death [183]. On the other hand, NOX4 is a membrane-bound enzyme that senses oxygen and promotes reactions to generate lipid ROS and it has also been reported to promote ferroptotic cell death [147]. We therefore hypothesized that the MAPK/ERK signalling pathway might promote the accumulation of lipid ROS by regulating GPX4 and NOX4 (Figure 49).

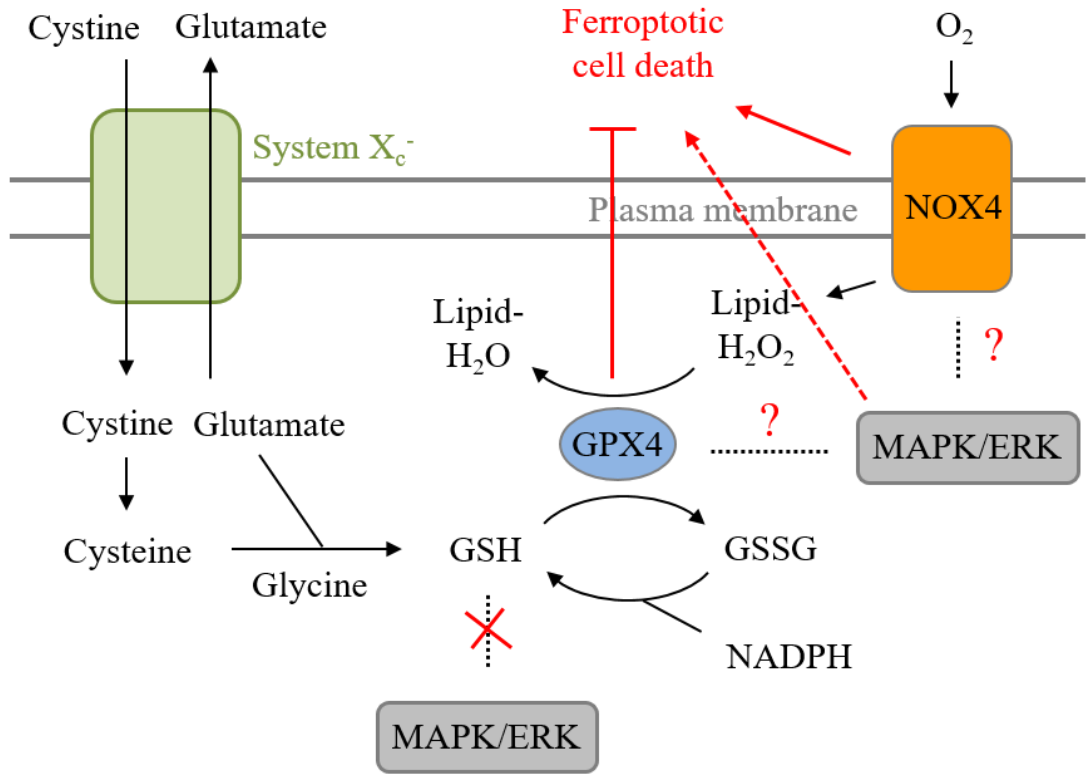

Figure 49. Hypothesized mechanisms of lipid ROS regulation by MAPK/ERK. GPX4 acts to scavenge lipid ROS and thus inhibit ferroptosis by catalysing the oxidation of GSH. NOX4 on the other hand promotes ferroptosis through stimulating the production of lipid ROS. Both GPX4 and NOX4 were hypothesized mediators downstream of the MAPK/ERK signalling pathway.

3.3.5.1 GPX4 is downregulated by the active MAPK/ERK cascade

Analysis of the level of endogenous GPX4 by western blot in WT and EGFR, KRAS, BRAF, or PI3K mutant cells has shown that EGFR and PI3K mutant cells harboured lower levels of GPX4 expression than WT, KRAS or BRAF mutant cells, and this pattern did not seem to change following cystine deprivation (Figure 49A). To

determine whether downregulation of GPX4 was a consequence of the activated MAPK/ERK cascade, we utilized selumetinib to disrupt the MAPK/ERK signalling in EGFR and BRAF mutant cells and examined the effect on GPX4 levels by western blot. As described previously, selumetinib is a selective inhibitor of MEK1/2, a downstream effector of EGFR and RAF. As shown previously in Figure 45, the MAPK/ERK signalling was activated in EGFR and BRAF mutant cells, and both lines were sensitive to cystine deprivation. Following selumetinib treatment, GPX4 expression was increased in EGFR mutant cells, to a comparable extent as in WT cells (Figure 50B). Selumetinib treatment did not alter the level of GPX4 expression in BRAF mutant cells, possibly because GPX4 in these cells was already expressed at a high level (Figure 50A), indicating the possibility that other mechanism(s) might counteract the downregulation of GPX4 by activated BRAF. Conversely, the PI3K mutant cells, although insensitive to cystine deprivation (Figure 45), has exhibited a decreased level of GPX4 (Figure 50A), relative to WT cells, indicating that GPX4 might not be the sole enzyme that protects these cells from ferroptotic death.

A

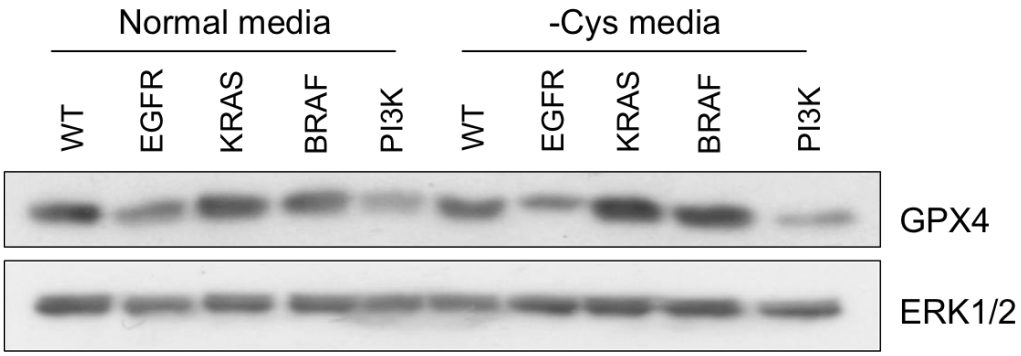

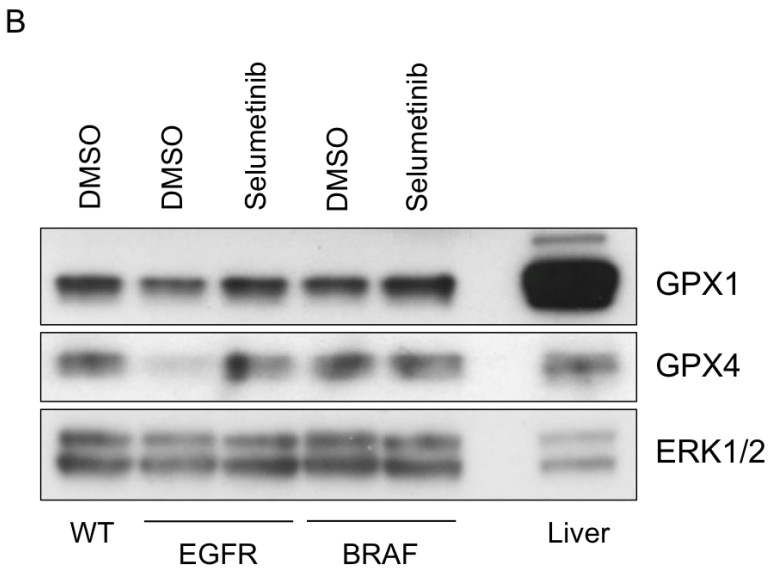

Figure 50. Analysis of GPX1 and GPX4 expression in HME cell lines.
A. Immunoblots of lysates from WT, EGFR, KRAS, BRAF and PI3K mutant cells cultured in normal (Normal) or cystine-free (-Cys) media for 24 hours were probed with antibodies detecting GPX4 and total ERK (ERK1/2, a loading control). **B.** Immunoblots of lysates from WT, EGFR and BRAF mutant cells cultured in normal medium in the presence of DMSO or MEK1/2 inhibitor selumetinib for 30 hours were probed with antibodies detecting GPX1, GPX4 and total EKR1/2. A sample of lysates from mouse liver (Liver) was loaded as a positive control for expression of GPX1 and GPX4.

In accordance with the previous inhibitor experiment (Figure 47), treatment with iressa and selumetinib, but not wortmannin, has increased the expression of GPX4 in EGFR mutant cells (Figure 51), suggesting that the downregulation of GPX4 in EGFR mutant cells was due to the active MAPK/ERK but not PI3K/AKT signalling pathways. Effects of other MAPK/ERK inhibitors on GPX4 expression in EGFR mutant cells have also been tested, to void potential off-target effects, and the level of GPX4 expression was increased by different extents under both normal-nutrient and cystine-deprivation conditions (Figure 52). Taken together, these data suggest that GPX4 lies downstream of the MAPK/ERK cascade and is downregulated by the active MAPK/ERK signalling.

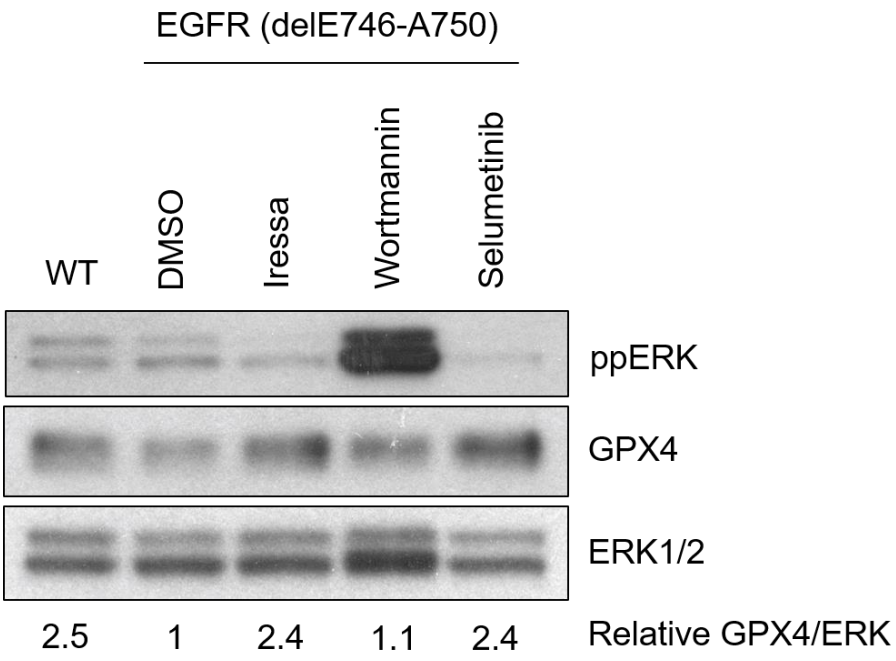

Figure 51. MAPK/ERK cascade downregulates GPX4 expression.
Immunoblots of lysates from WT and EGFR mutant cells cultured in normal medium in the presence of DMSO, iressa, selumetinib or wortmannin for a total of 30 hours were probed with antibodies detecting phosphorylated ERK (ppERK), GPX4 and total ERK1/2. Relative GPX4/ERK ratio was the average value from three biological repeats and was calculated using the ImageJ software from scanned autoradiographs, with the ratio in DMSO-treated EGFR mutant cells assigned the value of 1.

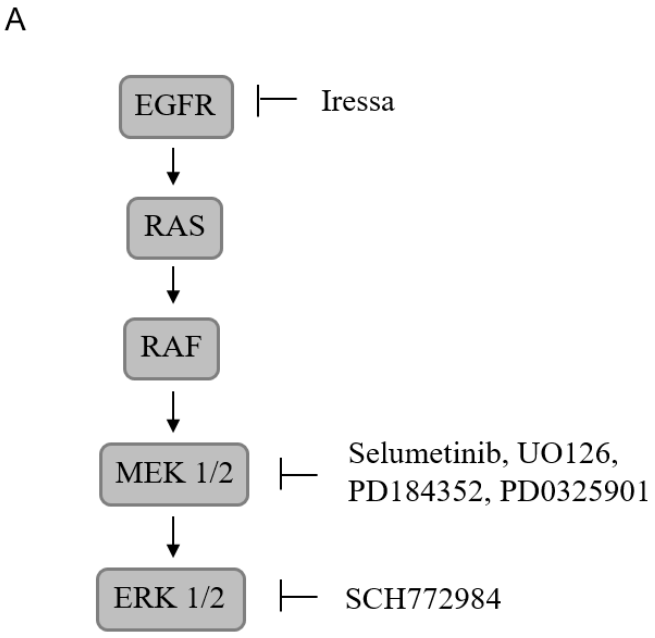

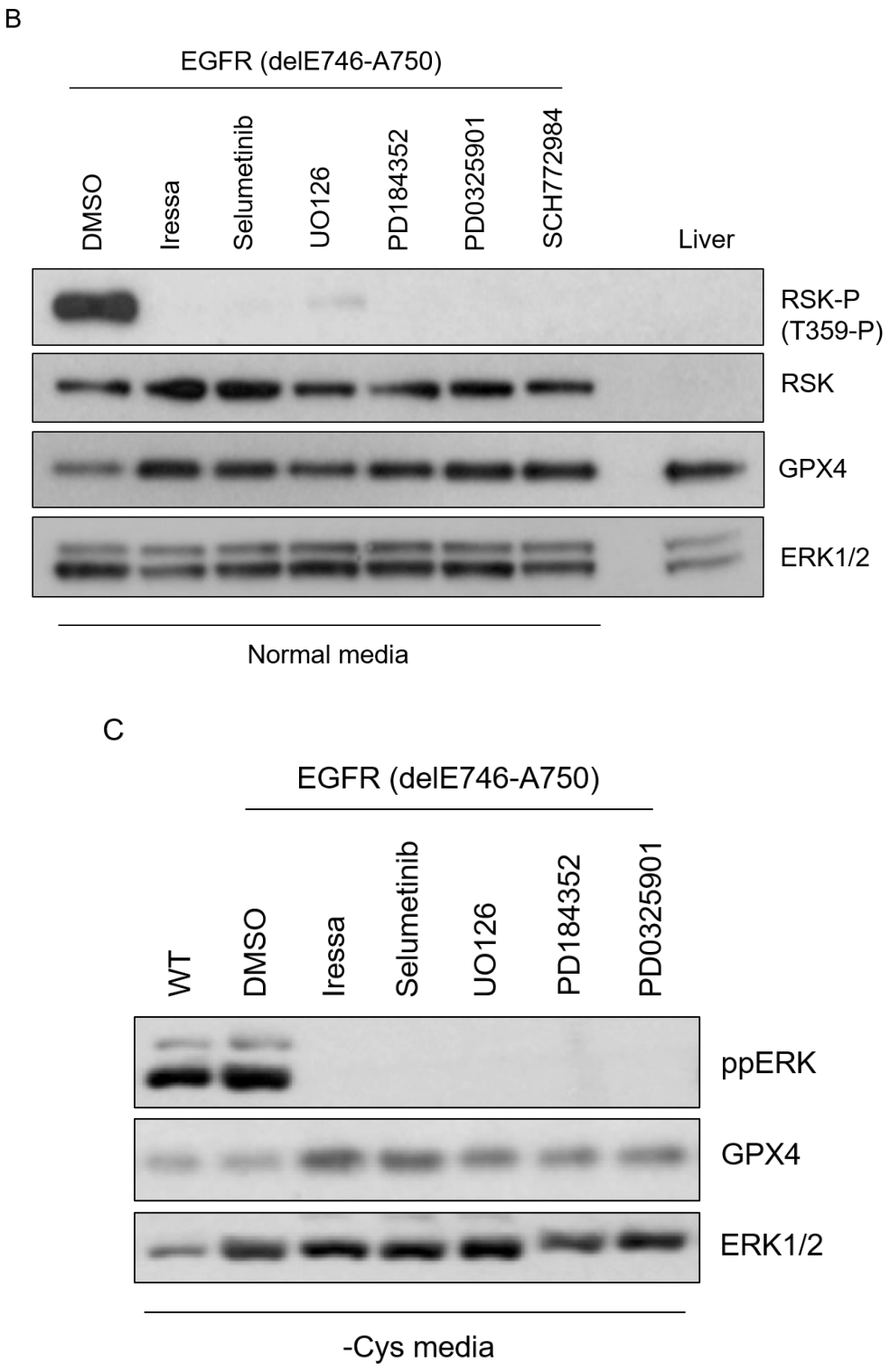

Figure 52. Inhibition of the MAPK/ERK cascade upregulates GPX4.
A. Schematic representation of the MAPK/ERK signalling pathway showing the targets of the five inhibitors. **B.** Immunoblots of EGFR mutant cell lysates probed with antibodies detecting phosphorylated RSK (T359-P), total RSK, GPX4 and total ERK1/2. A sample of lysates from mouse liver (Liver) was loaded as a positive control for expression of GPX4. **C.** Immunoblots of WT and EGFR mutant cell

lysates probed for phosphorylated ERK (ppERK), GPX4 and total ERK1/2. DMSO and inhibitors were added for 30 hours in **B** and **C,** and the cystine deprivation was for 12 hours in **C**.

To further investigate whether the MAPK/ERK cascade regulated GPX4 specifically, the expression of other isoforms of GPX, including GPX1, GPX2 and GPX3, was analyzed by western blot. A sample lysate from mouse liver was used in this experiment as a positive control for expression of GPX1, GPX2 and GPX4. GPX3 was not detected in either EGFR/WT cells or the liver sample. GPX2, although present in the liver lysate, was not expressed in either WT or EGFR mutant cells (Figure 53). GPX1 was detected in WT, EGFR and BRAF mutant cells, and no overt difference was observed between DMSO- and selumetinib-treated cells (Figure 50B). The various expression of these isoforms was not surprising, since GPX2 and GPX3 are differentially expressed in mammalian tissues and GPX1 is abundantly expressed in nearly all mammalian tissues [172].

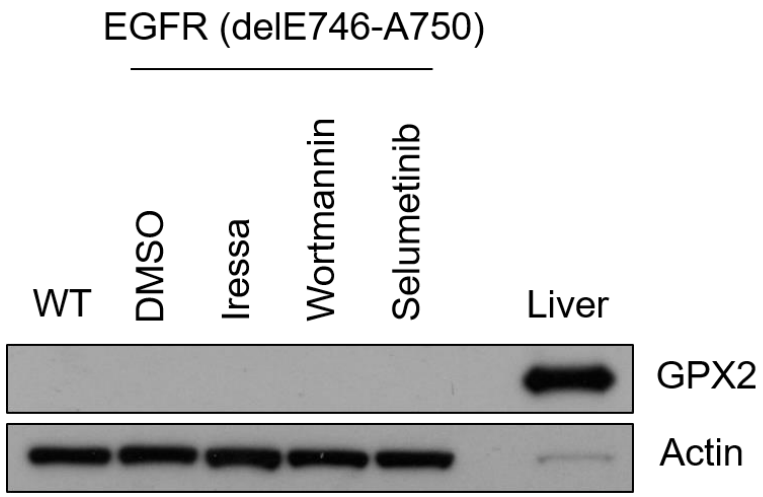

Figure 53. GPX2 is not expressed in WT or EGFR delE746-A750 HME cells. Immunoblots of WT and EGFR mutant cell lysates probed for GPX2 and Actin (a loading control). DMSO, iressa or selumetinib were added for 30 hours. A sample of lysates from mouse liver (Liver) was loaded as a positive control for expression of GPX2.

3.3.5.2 NOX4 is upregulated by the active MAPK/ERK cascade

The level of endogenous NOX4 in WT and EGFR mutant cells was also analyzed by western blot. In contrast to GPX4, NOX4 was highly expressed in EGFR mutant cells whereas it was barely detectable in WT cells (Figure 54A. left panel), and this high expression of NOX4 was significantly suppressed by inhibitors of EGFR and

MEK1/2 (Figure 52A. right panel), suggesting that NOX4 lies downstream of the MAPK/ERK cascade and is upregulated by the active MAPK/ERK signalling.

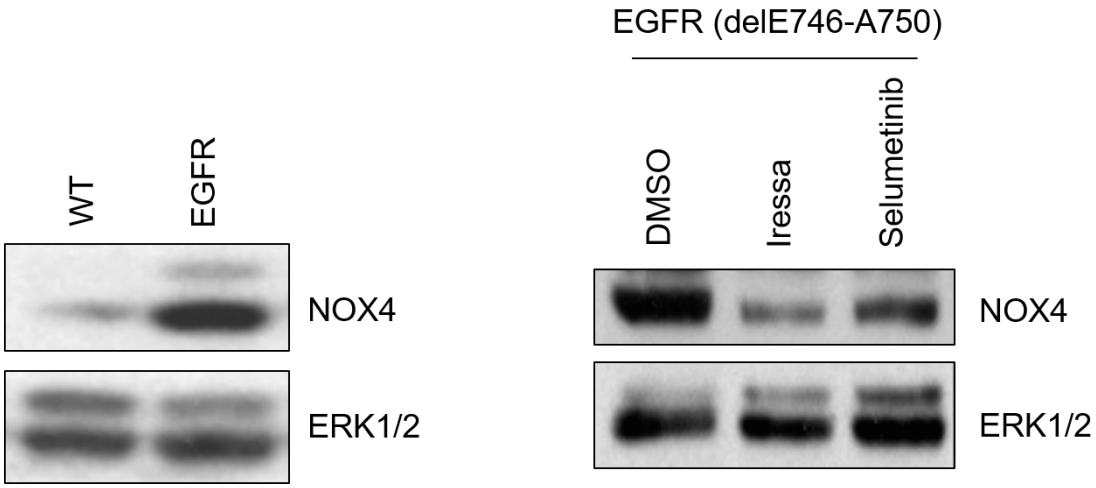

Figure 54. MAPK/ERK cascade upregulates NOX4 expression.
Immunoblots of WT and EGFR mutant cell lysates probed with antibodies detecting NOX4 and total ERK1/2. DMSO, iressa or selumetinib were added for 30 hours.

3.3.6 Cystine deprivation inhibits the viability of three NSCLC cell lines.

Based on the results described so far, it can be concluded that cystine/GSH is a synthetic lethal partner of the MAPK/ERK signalling pathway, which is associated with GPX4 and NOX4 that both are regulated by the pathway. These results were obtained in isogenic HME cell lines and we wanted to extend our analysis to NSCLC cell lines with multiple mutations. We have utilized a NSCLC cell line panel consisting of nine cell lines with various mutations in the MAPK/ERK cascade (Table 3) and examined whether they were sensitive to cystine deprivation.

Table 3
NSCLC cell lines

	Mutations in the MAPK/ERK cascade or PI3K
A549	KRAS G12S
Calu 6	KRAS Q61K
NCI-NH1650	EGFR delE746-A750, L858R, T790M
H1975	EGFR L858R, T790M
H727	KRAS G12V
H460	KRAS, PIK3CA

H322	WT
H3255	EGFR L858R
PC 9	EGFR delE746-A750

The MAPK/ERK activity of these cells was analyzed by western blot using the level of phosphorylated EGFR (pEGFR) and ERK (ppERK) as an indicator of activation, and cell viability was measured following cystine deprivation for 72 hours (Figure 55A and B). Although these nine cell lines possessed various activities in the MAPK/ERK signalling, as indicated by the levels of phosphorylated EGFR and ERK (Figure 55A), three cell lines NCI-NH1650 (EGFR delE746-A750), H3255 (EGFR L858R) and Calu-6 (KRAS Q61K) exhibited high sensitivity to cystine deprivation, as demonstrated by the significant loss of viability following cystine deprivation (Figure 55B). In accordance with this, cystine deprivation has induced massive cell death in those cells, and most cells displayed balloon-like membrane extensions, a morphological feature of the ferroptotic event (Figure 55C). Therefore, cystine deprivation seems to be a vulnerability specific to NSCLC cell lines NCI-NH1650 (EGFR delE746-A750), H3255 (EGFR L858R) and Calu-6 (KRAS Q61K).

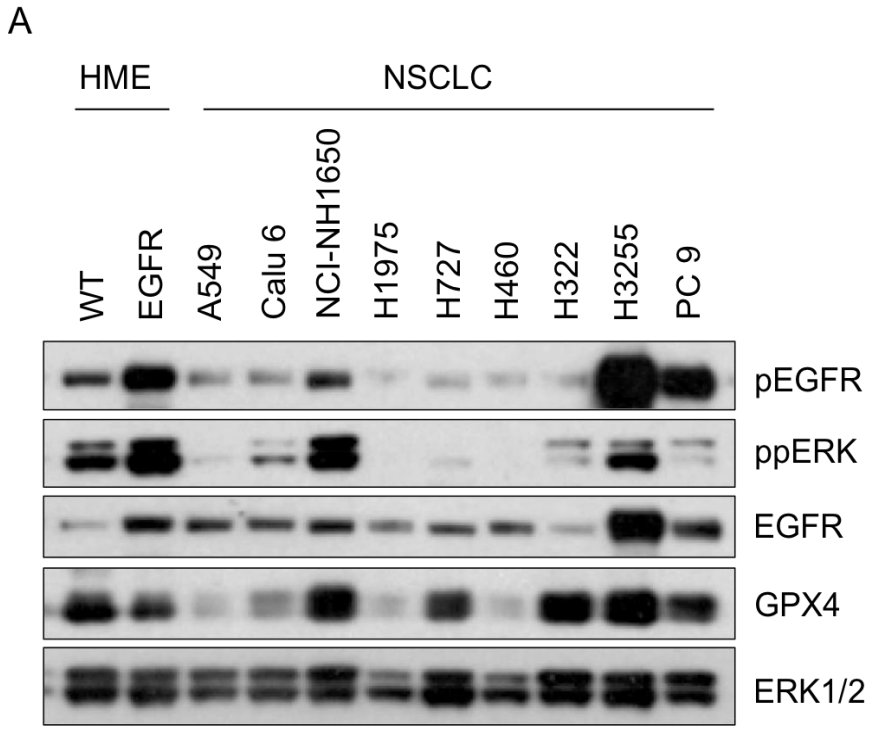

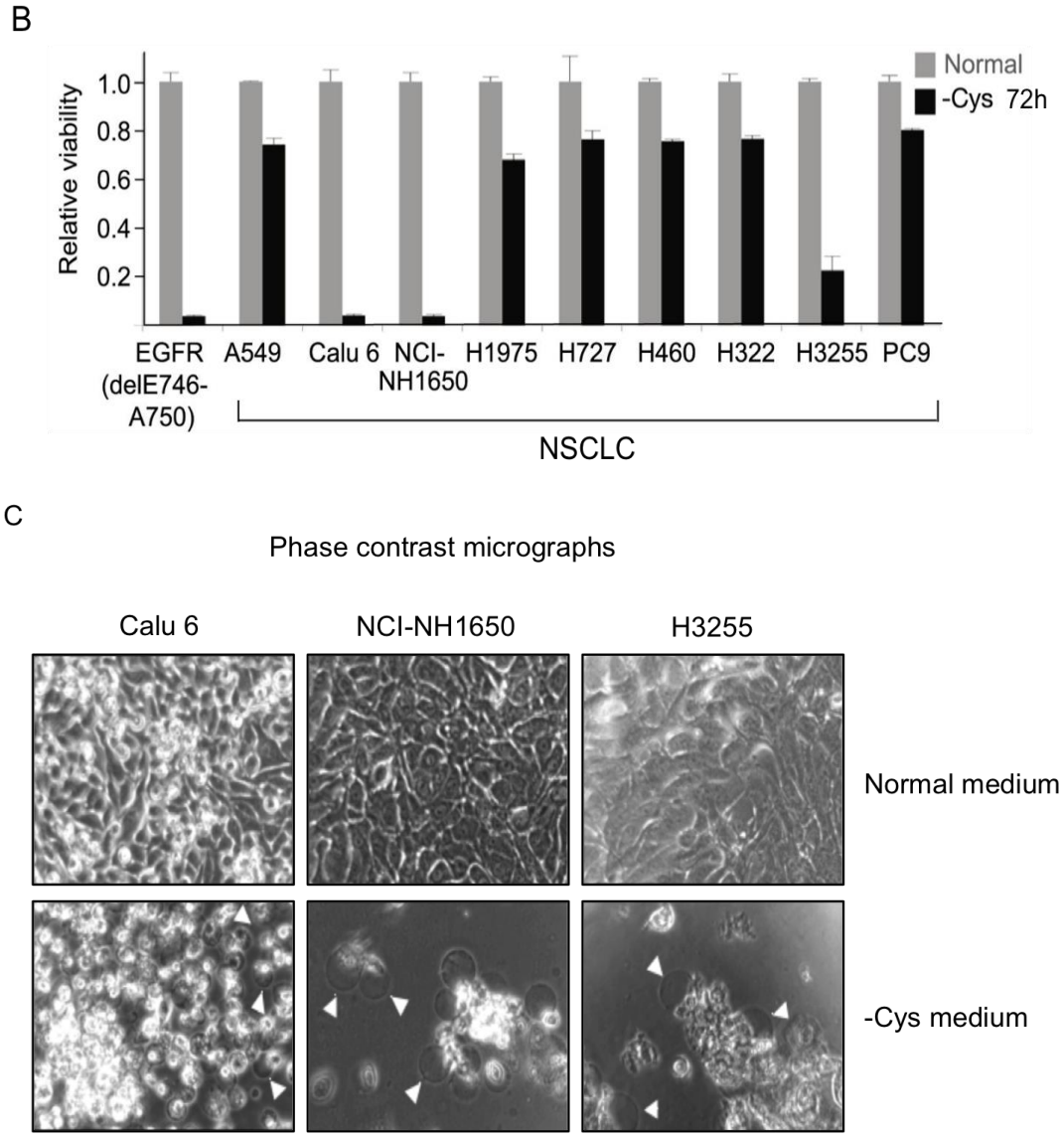

Figure 55. Cystine deprivation induces cell death in three NSCLC cell lines. **A.** Immunoblots of lysates from WT and EGFR (delE746-A750) HME cells and the nine NSCLC cell lines, probed with antibodies detecting pEGFR, ppERK, GPX4, total EGFR and ERK1/2. **B.** CellTiter-Glo viability assay of EGFR (delE746-A750) HME cells and the nine NSCLC cell lines cultured for 72 hours in normal (light bars) or cystine-free (dark bars) media. Histograms represent the average values ± SEM of three biological replicates and the viability in normal medium was assigned the value of 1 for each cell line. **C.** Phase-contrast micrographs of Calu-6, NCI-NH1650 and H3255 cells cultured in normal or cystine-free (-Cys) media for 72 hours. Micrographs were captured using a 10X microscope objective. Arrowheads indicate membrane extrusions. Experiments shown in this figure were performed by Ioannis Poursaitidis (Panels B and C) and me (Panel A).

Western blot analysis of GPX4 expression level in the nine NSCLC cell lines panel has demonstrated extremely variable expression patterns under both media

conditions (Figures 54A and 55A). GPX4, however, was highly expressed in NCI-NH1650 and H3255 cell lines, both of which have exhibited high levels of the MAPK/ERK signalling activity and been highly sensitive to cystine deprivation. The nine NSCLC cell lines generally have expressed high levels of NOX4 (Figure 56B), whereas only three cell lines exhibited high levels of the MAPK/ERK activity and sensitivity to cystine deprivation (Figure 55). Overall, it might not be reliable to determine the association of GPX4 and NOX4 to cystine deprivation-induced cell death in the NSCLC cell lines due to their complex genetic contexts.

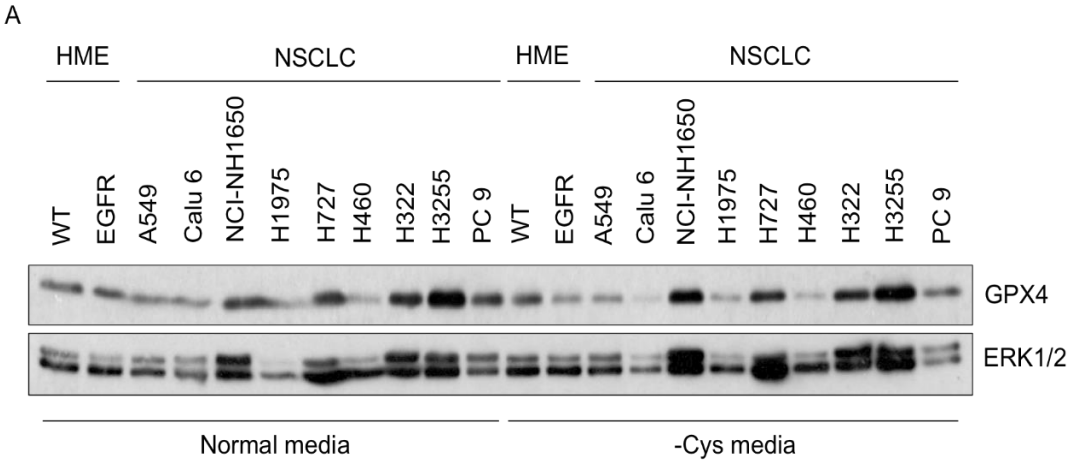

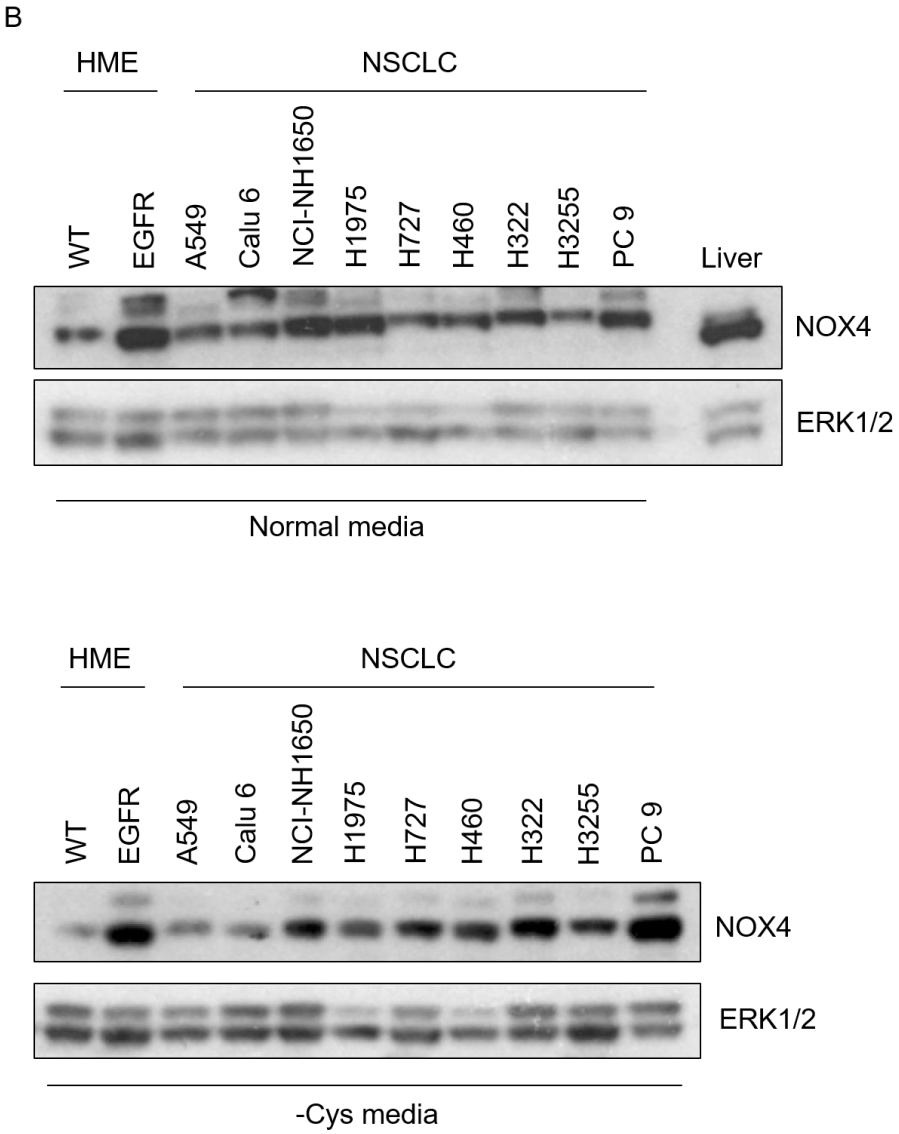

Figure 56. Analysis of GPX4 and NOX4 expression in a panel of NSCLC cell lines.
Immunoblots of lysates from HME and the nine NSCLC cell lines cultured in normal (Normal) or cystine-free (-Cys) media for 24 hours were probed with antibodies detecting GPX4 (**A**), NOX4 (**B**) and total ERK1/2.

3.3.7 Pharmacological depletion of intracellular cystine inhibits the growth of NCI-NHI1650 cells engrafted tumour

Of the three NSCLC cell lines that were sensitive to cystine deprivation (Figure 55), NCI-NHI1650 cell line was of particular interest, because this cell line expresses the same mutation EGFR delE746-A750 that was also present in EGFR mutant HME cell line. We thus examined whether NCI-NHI1650 cells might be responsive to pharmacological depletion of cystine and cysteine pools, potentially offering new

therapeutic opportunities. NCI-NHI1650 cells were treated with an engineered human cysteine/cystine-degrading enzyme, AECase [213], and cell proliferation was analyzed by CellTiter-Glo viability assay and microscopy. As expected, AECase treatment resulted in a significant loss of cell viability in both NCI-NHI1650 and EGFR mutant HME cells, to similar extents as upon cystine deprivation, and moreover cell viability was restored by the ferroptosis inhibitor (Fer-1) treatment (Figure 57A). Likewise, widespread cell death was observed in cells treated with AECase, and the morphological alterations were similar to those in cells deprived of cystine (Figure 57B). In addition, cyclooxygenase-2 (COX2), a prostaglandin-endoperoxide synthase that is upregulated during inflammation and development of certain types of cancer such as breast, pancreatic and lung cancers [214], has been recently identified as a marker for ferroptotic cell death [183]. As shown in Figure 57C, COX2 has been induced following AECase treatment in NCI-NHI1650 cells for 8 hours. Taken together, these data suggest that AECase is able to induce cell death in NCI-NHI1650 NSCLC cells and the cell death likely occurs via ferroptosis.

A

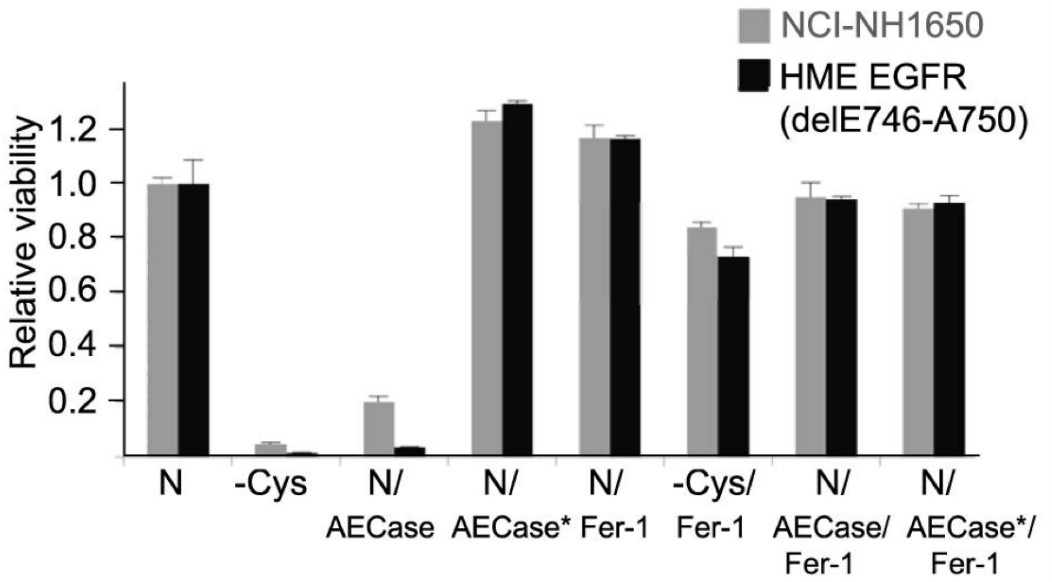

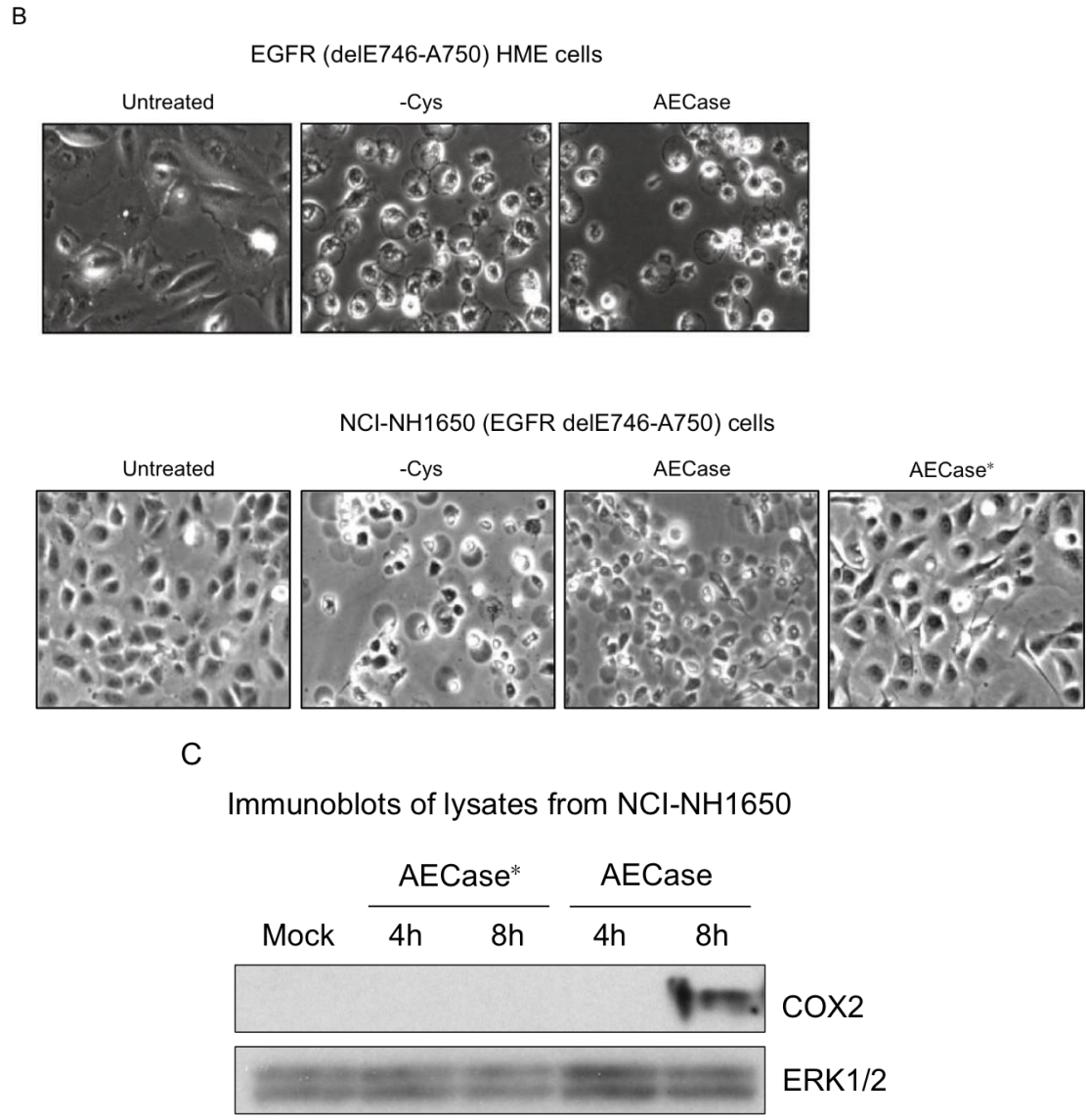

Figure 57. Cystine/cysteine-degrading enzyme AECase induces cell death in NCI-NHI1650 NSCLC cells.

A. CellTiter-Glo viability assay of EGFR mutant HME (dark bars) and NCI-NH1650 NSCLC (light bars) cells cultured for 48 hours in normal (N) or cystine-free (-Cys) media, in the presence or absence of 125nM AECase or heat-inactivated AECase (AECase∗) alone, or together with the ferroptosis inhibitor (Fer-1). The viability measurement of each cell line in the normal medium (N) was assigned the value of 1. The AECase enzyme activity was eliminated by heating at 65°C for 5min, and was used as a control [213]. **B.** Phase-contrast micrographs of EGFR mutant HME (upper panel) and NCI-NH1650 NSCLC (lower panel) cells cultured for 48 hours in normal (Untreated), cystine-free (-Cys) media, normal media containing AECase or heat-inactivated AECase. **C.** Immunoblots of lysates from NCI-NH1650 NSCLC cells treated with AECase or heat-inactivated AECase for 4 or 8 hours were probed with antibodies detecting COX2 and ERK1/2. Experiments shown in this figure were performed by Ioannis Poursaitidis (Panels A and B) and me (Panel C).

Since AECase treatment was shown to be effective in inducing cell death in NCI-NHI1650 NSCLC cells under cell culture conditions, we wanted to examine whether AECase would have the same effect *in vivo*, on engrafted cells. Immuno-deficient mice were injected with NCI-NH1650 NSCLC cells to develop tumours, and then injected with 30 mg/kg or 100 mg/kg of AECase. Tumour growth and mice survival were then monitored. As shown in Figure 58A, the tumour volume was significantly reduced in AECase-treated mice compared with the vehicle (PBS)-treated control group ($p = 0.0001$, $n=4$). Similarly, AECase treatment prolonged mice survival by around 15 day in a dose-dependent manner. Moreover, the inhibition of tumour growth by AECase was likely due to the induction of ferroptosis, as determined by the upregulation of COX2 expression in tumour lysates from AECase-treated mice, relative to the control groups treated with heat-inactivated AECase (HI AECase) (Figure 58B and C). Taken together, these data indicate that enzymatic depletion of cystine can be potentially applied to inhibit the growth of tumours that are sensitive to cystine deprivation.

A

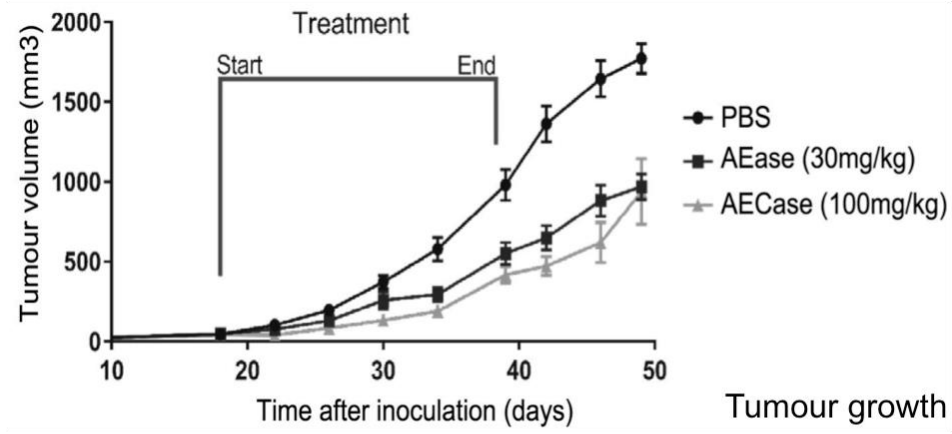

Tumour growth

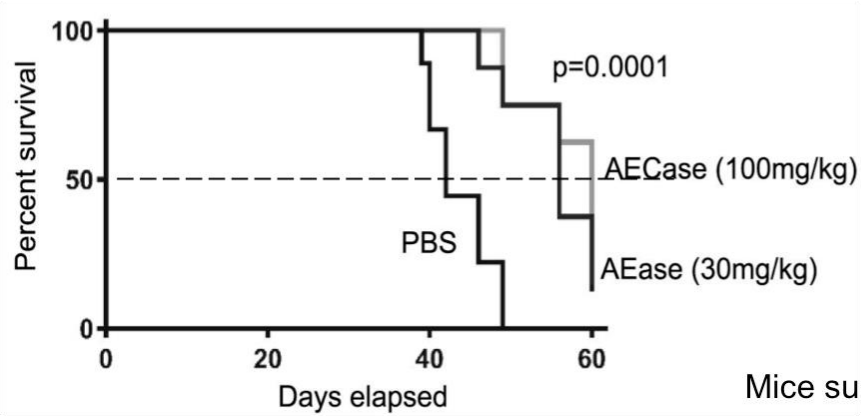

Mice survival

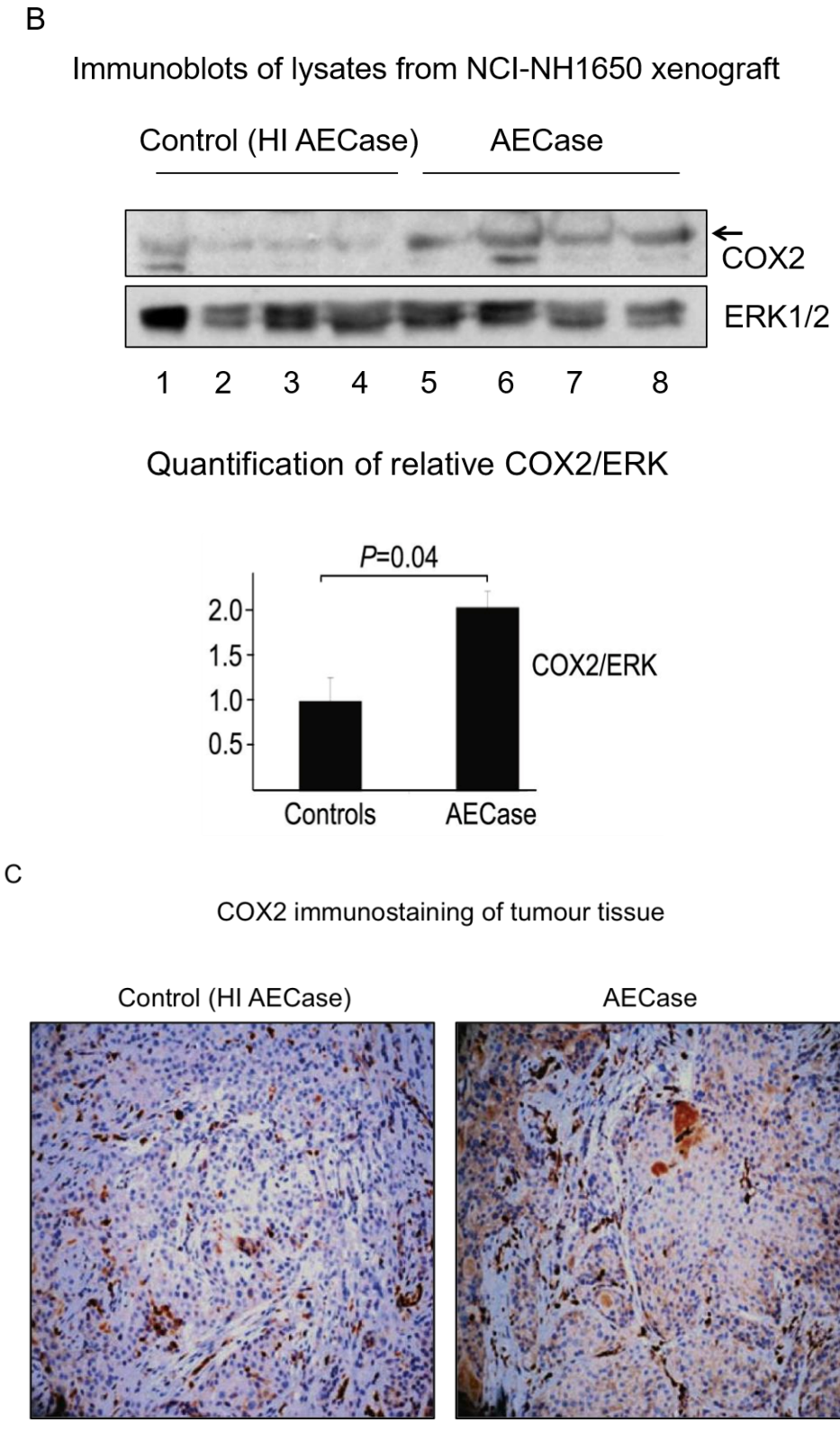

Figure 58. Cystine/cysteine-degrading enzyme AECase inhibits the growth of NCI-NHI1650 cells engrafted tumour.

A. Upper panel, Tumour volume curve following intraperitoneal injection of PBS control (dark circles), 30 mg/kg (dark squares) or 100 mg/kg (light triangles) AECase, up to 50 days after inoculation of NCI-NH1650 NSCLC cells. Lower panel,

Median survival curve of NCI-NH1650 NSCLC cells engrafted mice following intraperitoneal injection of PBS, 30 mg/kg or 100 mg/kg AECase. **B.** Upper panel, Immunoblots of lysates from NCI-NH1650 cells engrafted tumour tissues probed with antibodies detecting COX2 (arrow) and ERK1/2. NCI-NH1650 cells engrafted mice were treated with 100 mg/kg heat-inactivated AECase (Control HI AECase, 1-4) or AECase (5-8), n=4. Lower panel, Quantification of the relative COX2/ERK ratio (p=0.04, n=4) from the immunoblots shown in the upper panel using ImageJ. **C.** Images of immunohistochemical (IHC) staining of COX2 (brown) in control and AECase-treated tumours. Mice were treated with AECase for 4 days in A, B and C. Experiments shown in this figure were performed by Shira L. Cramer, Kenda Triplett, Everett Stone (Panels A and C) and me (Panel B).

3.4 P53 is activated by amino acid deprivation

Previously published studies suggest that activation of p53 can lead to inhibition of mTORC1 [215]. However, when mTORC1 activity was assessed using phosphorylated S6K1 T389 as an indicator, there was no increase in mTORC1 activity in p53 null (p53 -/-) HCT116 cells, compared to isogenic p53 wild type HCT116 cells (Figure 59A). Likewise, induction of p53 expression by etoposide did not seem to cause obvious alteration in mTORC1 activity. In accordance with this, although the activity of mTORC1 was inhibited by amino acid deprivation, the presence of p53 did not decrease mTORC1 activity, relative to that in cells lacking p53 (Figure 59B). On the contrary, absence of p53 seemed to weaken mTORC1 activation (Figure 59). One possible explanation for this might be that the inhibitory effect of p53 on mTORC1 activity is subtle and that it has been concealed by the high level of mTORC1 activity in p53 wild type cells cultured in the rich RPMI 1640 medium (Figure 59A). The reduced mTORC1 activity in p53 null cells might be a result of the higher proliferation, due to lack of p53, which has consumed nutrients and lowered mTORC1 activity. This has become clearer when the cells were cultured in the same medium for 48 hours before the media shifts in Figure 59B. The difference in mTOR1 activity (pS6K1 T389, +AA) between p53 wild type and null cells became more obvious presumably due to the increased difference of cell numbers between the two cell lines during the 48 hours. In addition, if the inhibitory effect of p53 on mTORC1 was fundamental, mTORC1 would have become unresponsive and remained active during amino acid deprivation in the p53 null cells, which was contrary to the almost complete suppression of mTORC1 activity under the same condition as shown in Figure 59B. Therefore, p53 seems to have no effect

on mTORC1 signalling, or subtle effect if there is any. On the other hand, the decreased mTORC1 activation in Figure 59A might result from the decreased mTORC1 expression in the p53 null cells, although it is currently unclear whether p53 affects mTORC1 expression.

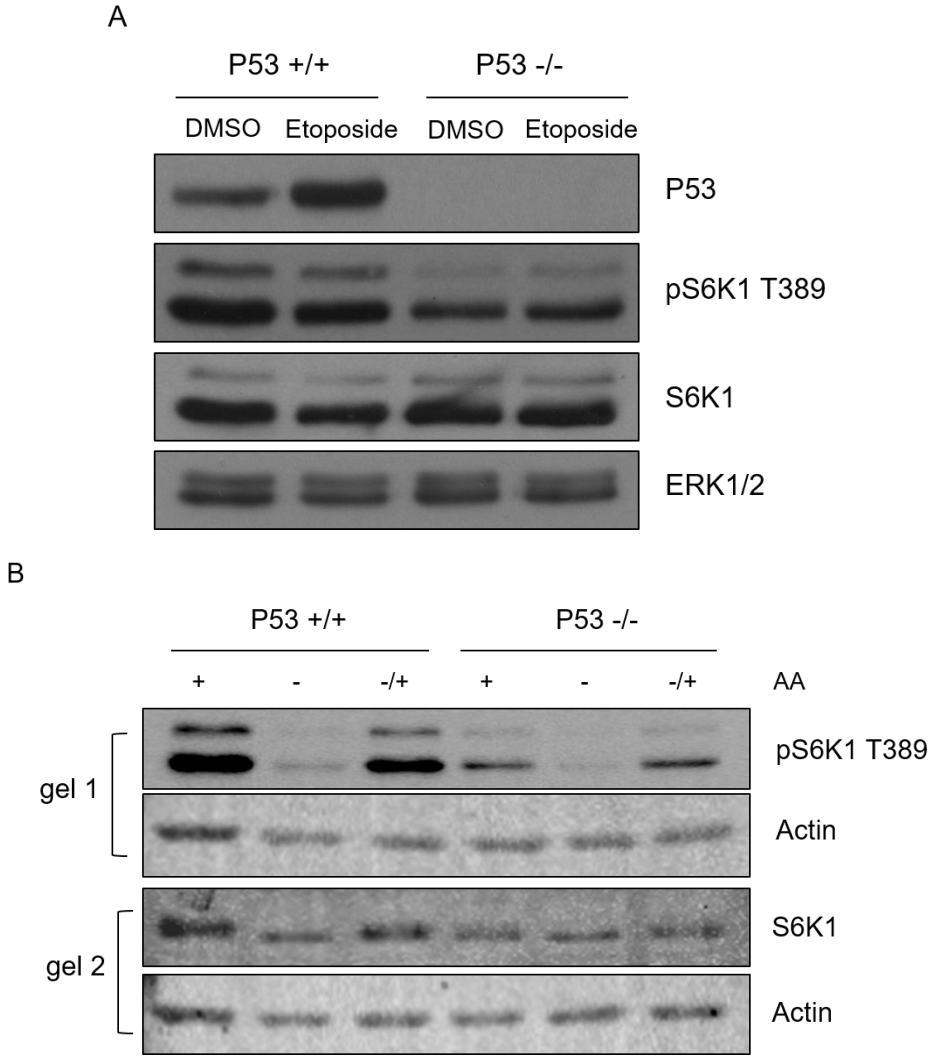

Figure 59. P53 does not seem to inhibit mTORC1 activity in HCT116 cells.
A. immunoblots of p53 wild type (p53 +/+) and null (p53 -/-) HCT116 cells treated with the vehicle control DMSO or 20µM etoposide for 24 hours. Immunoblots were probed with antibodies detecting p53, S6K1 T389 and ERK1/2 (a loading control), and re-probed for total S6K1. **B.** immunoblots of extracts from p53 wild type (p53 +/+) and null (p53 -/-) HCT116 cells cultured in media containing amino acids (+), lacking amino acids (-) for 60min, or deprived and stimulated with MEM amino acids for 15min. Identical gels and samples were used for gel 1-2 analysis. Immunoblots were probed for p53, S6K1 T389, total S6K1 and actin (a loading control).

Surprisingly, p53 seemed to be activated, represented by increased levels of phosphorylated Ser15 (Ser15 p-P53), following amino acid deprivation for 60min (-AA), and its activity might continue to increases during amino acid replenishment for 15min (-/+AA) (Figure 60). This alteration in p53 activation could potentially result from the shift from the relatively rich medium RPMI 1640 (the routine culture medium for HCT116 cells) to DMEM medium lacking AA as described in the Methods Chapter 2.1.10 and 2.2.4. Moreover, the continuous increase of p53 activation following amino acid replenishment could be a prolonged effect of amino acid deprivation. To address these two issues, the media shift experiment was repeated using the DMEM medium and a time-course of amino acid deprivation was conducted.

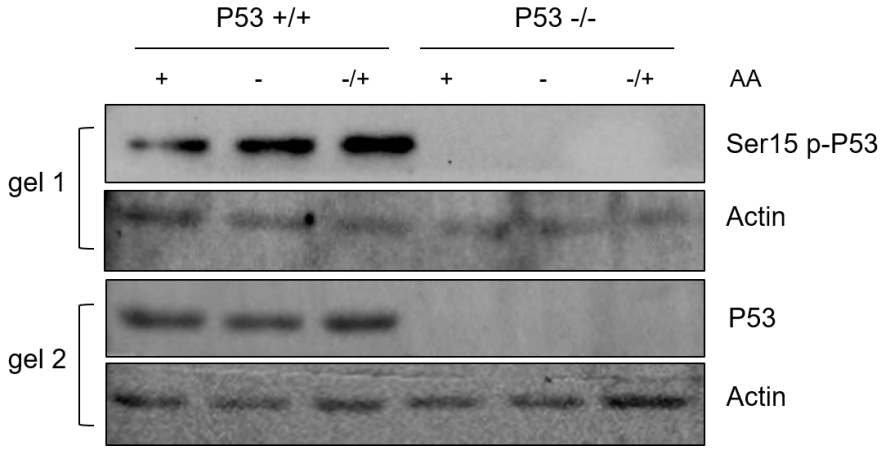

Figure 60. Amino acid deprivation seems to activate p53.
Immunoblots of extracts from p53 wild type and null HCT116 cells. Cells were seeded in RPMI medium supplemented with 10% d.FBS, 48 hours after seeding, for each cell line, one well was remained in the original medium (+AA), two wells were washed with and incubated in DMEM medium lacking amino acid with 10% d.FBS for 60min (-AA), and one of them was replenished with MEM amino acids for 15min (-/+AA). Immunoblots were probed for phosphorylated Ser15 of p53 (Ser15 p-P53), total p53 and actin. Identical gels and samples were used for gel 1-2 analysis.

As shown in Figure 61, the level of p53 phosphorylation seemed to increase similarly with both media shift treatments, the shift from normal DMEM to DMEM lacking amino acids and from RPMI to DMEM lacking amino acids. Thus, the activation of p53 did not seem to result from different types of media used. In addition, the level of phospho-Ser15 was barely detectable in cells seeded in DMEM medium, compared to that in RPMI medium, thus the media shift for the subsequent experiments followed the shift from normal RPMI to DMEM lacking amino acids.

As a positive control for p53 phosphorylation and activation, two wells of HCT116 cells (p53 wild type) were exposed to 10Gy of γ-irradiation to induce DNA damage and incubated for 1 hour and 3 hour respectively. The level of phosphorylated Ser15 of p53 was indeed massively increased following irradiation exposure.

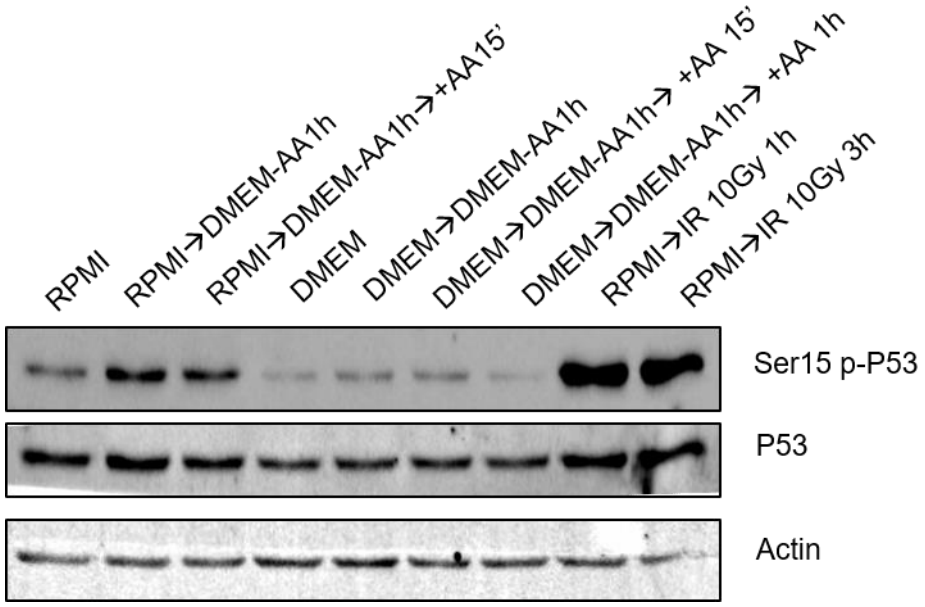

Figure 61. Activation of p53 in response to amino acid deprivation.
Immunoblots of extracts from p53 wild type HCT116 cells. Cells were seeded in RPMI/DMEM media supplemented with 10% d.FBS, 48 hours after seeding, for each media shift, one well was remained in the original RPMI or DMEM media, two wells were washed with and incubated in DMEM medium lacking amino acid with 10% d.FBS for 60min (DMEM –AA 1h), and one of them was replenished with MEM amino acids for 15min (DMEM –AA 1h --> +AA). Separately, two wells were exposed to 10Gy of γ-irradiation, and one was incubated for 1 hours and the other 3 hours. Immunoblots were probed for Ser15 p-P53, total p53 and actin.

To address the second issue, a time course experiment was performed in which cells were deprived of amino acids for different times up to 4 hours, or deprived for 1 hour and stimulated with amino acids for different times up to 1 hour, and p53 activation was analyzed by immunoblotting (Figure 62). The level of p53 expression and probably phosphorylated Ser15 indeed increased, although slightly, following amino acid deprivation for up to 4 hours (Figure 62A). In accordance with this, amino acid replenishment for up to 1 hour did not increase p53 expression or phosphorylation (Figure 62B). However, the changes in p53 expression and activity following amino acid deprivation were subtle and thus require further investigation.

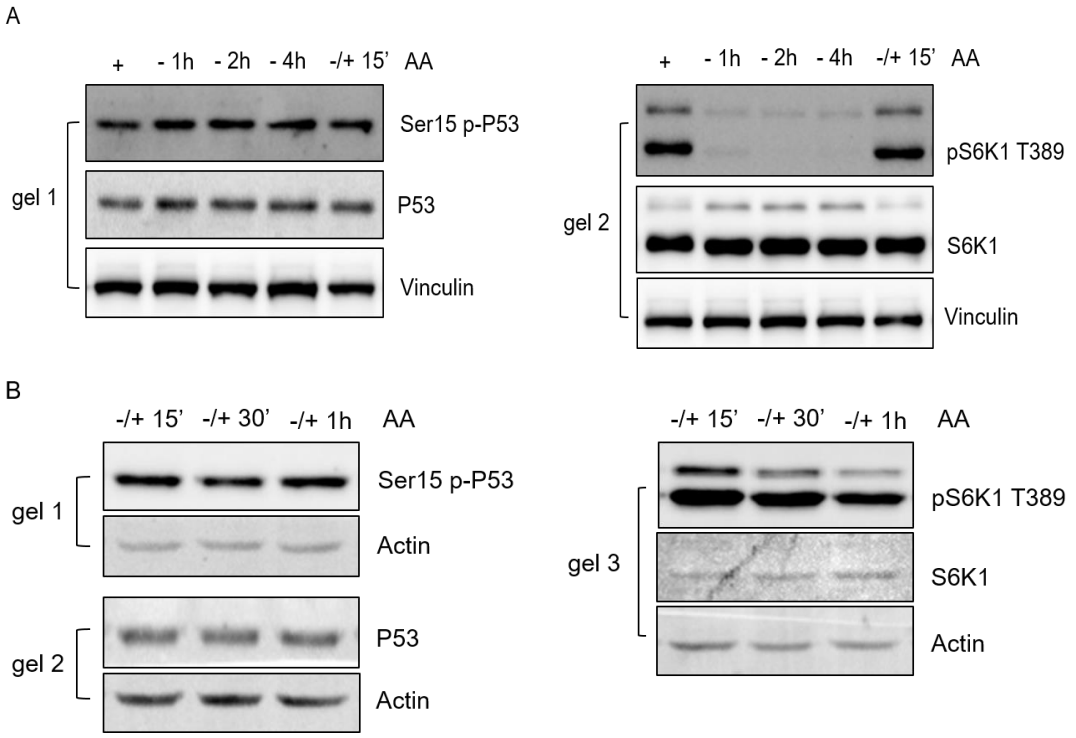

Figure 62. A time-course of p53 activation following amino acid deprivation or replenishment in HCT116 cells.
A. A time-course of amino acid deprivation. Immunoblots of extracts from cells cultured in normal medium (+AA), or medium lacking amino acids for 1h, 2h and 4h (-AA), or medium lacking amino acid for 1h followed by re-addition of MEM amino acids for 15min (-/+AA). **B.** a time-course of amino acid replenishment. Immunoblots of extracts from cells cultured in medium lacking amino acid for 1h followed by re-addition of MEM amino acids for 15min, 30min and 1h (-/+AA). Immunoblots were probed for Ser15 p-P53, pS6K1 T389, total p53 and S6K1, vinculin (**A**) and actin (**B**) as loading controls. Identical gels and samples were used for panel A and B respectively.

Similarly and in accordance with the upregulation of p53 by amino acid deprivation, inhibition of mTORC1 activity by rapamycin seems to enhance p53 expression and phosphorylation, as displayed in Figure 63. This has raised the possibility that activated mTORC1 might inhibit p53 activation. Again, the alteration in p53 activation observed was slight and requires further investigation.

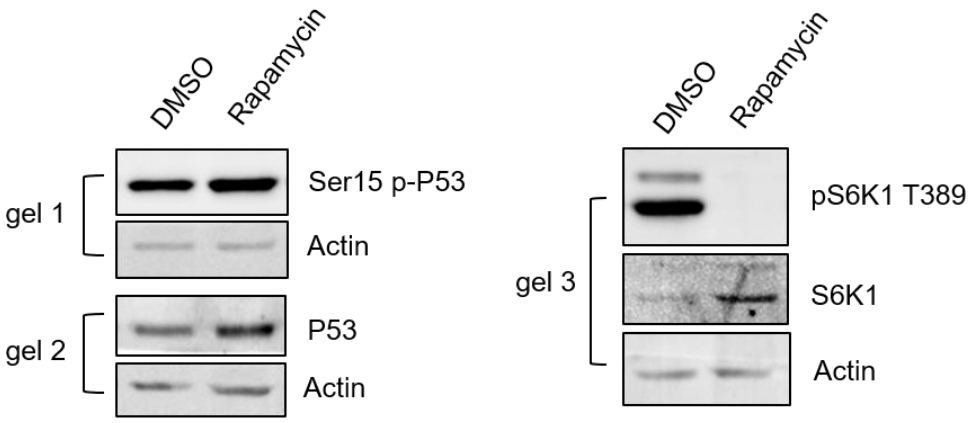

Figure 63. Inhibition of mTORC1 by rapamycin induced an increase in p53 overall levels and activity.
Immunoblots of extracts from HCT116 cells cultured in normal medium in the presence of DMSO or 100nM rapamycin for 1h. Immunoblots were probed for Ser15 p-P53, pS6K1 T389, total p53 and S6K1, and actin. Identical gels and samples were used for gel 1-3 analysis.

Chapter 4

Discussion

Chapter 4-Discussion

Cancer cells are capable of growing and proliferating constitutively and rapidly, primarily due to activation of oncogenes and inactivation of tumour suppressor genes [1, 216]. Many proteins encoded by these genes are critical components of signalling pathways that regulate cell survival, such as the p53, PI3K/Akt, MAPK/ERK and mTORC1 signalling pathways [47, 217, 218]. Dysregulation of these pathways has been implicated in a large number of cancer types, indicating the importance of these signalling pathways for cancer formation and/or maintenance. In addition, cancer cells exhibit extremely high demands for glucose and amino acids to sustain rapid proliferation and growth [219, 220]. Therefore, understanding of the mechanisms by which cells sense extracellular signals, stimulating the corresponding cellular responses that mediate metabolism and cell growth, is essential for developing a well-targeted chemotherapy.

This study has centred on amino acid nutrients and their association with the oncogenic signalling pathways including PI3K/Akt, MAPK/ERK and mTORC1, as well as the tumour suppressor p53, all of which play a role in mediating metabolism and cell survival [47, 132, 217, 218]. The mTORC1 signalling pathway coordinates the availability of amino acid nutrients and growth factors with the biosynthesis of proteins, lipids and nucleotides required for cell proliferation and growth [46]. The MAPK/ERK signalling pathway is known to sense growth factors and promotes cell proliferation and survival, and members in this pathway are frequently mutated in cancer [5, 6, 38]. We have thereby particularly focused on understanding the mechanism of mTORC1 inactivation in response to amino acid deprivation in a variety of tissue-culture cells, and on understanding the role of MAPK/ERK in cellular response to deprivation of amino acid cystine in isogenic HME cells and further in a panel of NSCLC cell lines.

4.1 Mechanisms of mTORC1 inactivation following amino acid depletion

4.1.1 GCN2 is a novel inhibitor of mTORC1

Activation of mTORC1 requires the presence of growth factors and amino acids [67, 112]. This is consistent with the notion that to be activated mTORC1 needs to be translocated to the lysosomes, a process regulated by amino acids through the Rag GTPase heterodimer [96, 97]. In addition, mTORC1 activation requires the presence of GTP-bound Rheb that is controlled by growth factors through TSC2, the master inhibitor of mTORC1 [46]. Previous studies have also suggested that TSC2 undergoes lysosomal translocation by interacting with the Rag GTPase heterodimer in the absence of amino acids, a process that is required for mTORC1 inactivation [99]. However, the regulator/mechanism of the translocation remains elusive.

In this study, we present a novel mechanism by which mTORC1 becomes inactive following amino acid deprivation. This mechanism links a known effect of amino acid depletion, accumulation of uncharged tRNAs, to cellular response regulated by the mTORC1 signalling pathway. Through a high-throughput quantitative cell imaging siRNA screen of around 975 protein kinases/phosphatases to identify mediators of TSC2 localization in Hela cells, GCN2, a kinase that senses amino acid deficiency and represses protein synthesis, has been identified as a novel regulator of TSC2 lysosomal localization (Figure 25). In accordance with this, GCN2 is required for mTORC1 inactivation in response to amino acid deprivation (Figure 27). Our finding that GCN2 inhibits mTORC1 is consistent with a very recent publication, suggesting that GCN2 contributes to mTORC1 inhibition through a mechanism that is independent of ATF4, one of the downstream effectors of eIF2α [111]. GCN2 is known to be activated by uncharged tRNAs and acts to suppress translation initiation via phosphorylation on Ser51 of its only known substrate eIF2α [118-120]. Using the two novel GCN2-specific inhibitors, we further determined that the kinase activity of GCN2 is required to promote TSC2 lysosomal translocation (Figure 28), however, eIF2α does not seem to be necessary for TSC2 subcellular localization (Figure 29), which is also consistent with previously mentioned publication [111].

It is unlikely that TSC2 itself is the substrate of GCN2, since no interaction has been detected between TSC2 and GCN2 (Figure 30). Therefore, future work will firstly involve identification and characterization of new substrates of GCN2 that potentially act as mediators to regulate TSC2 lysosomal translocation in response to amino acid deprivation, and secondly investigation of negative regulators of TSC2 lysosomal localization. Our data suggest that GCN2 potentially inhibits mTORC1 at least in part through promoting the lysosomal translocation of TSC2 independently of eIF2α phosphorylation. In addition, GCN2 inhibitors are likely to prevent TSC2 from associating with lysosomes, indicating the kinase activity of GCN2 is required to regulate TSC2 lysosomal translocation. However, a recent publication also suggests that the protein-protein interactions can be structurally destabilized by protein binding to compounds [221, 222]. Similarly, it might be possible that the dissociation of TSC2 from lysosomes is a result of structural alteration of inhibitor-bound GCN2. Therefore, identification and characterization of critical residues within the kinase domain of GCN2 involved in its effect on TSC2-lysosome association will help to clarify this issue. Furthermore, it might be also interesting in the future to investigate the other candidates (apart from GCN2) from the imaging-based high-throughput siRNA screen displayed in Figure 25, however, these kinases do not seem relevant to the mTORC1 pathway.

4.1.2. Alternative model of mTORC1 regulation by TSC/Rheb axis

It is well established that GTP-bound Rheb directly binds to mTORC1 and activates its catalytic activity in response to growth factors, and the master inhibitor TSC2 inhibits mTORC1 by deactivating GTP-bound Rheb when growth factors are scarce (reviewed in reference [45]). However, whether the TSC/Rheb axis is associated with the lysosomal localization of mTORC1 and the Rag GTPases in response to amino acid conditions remained elusive. In addition to identifying GCN2 that inhibits mTORC1 potentially via regulating the lysosomal localization of TSC2, our studies also demonstrate that Rheb indirectly activates mTORC1 via promoting the lysosomal localization of mTOR and RagC, and it also contributes to mTORC1 inactivation by stabilizing TSC2-lysosome association. Moreover, TSC2 is found to promote mTORC1 inactivation via stimulating the dissociation of RagA from

lysosomes. Therefore, our findings provide a more complete mechanistic framework for regulation of mTORC1 by the TSC2/Rheb axis in response to amino acid conditions.

The lysosomal translocation of TSC2 seems to be mediated by the Rag GTPase heterodimer [99], and in accordance with this, RagA is required for TSC2 lysosomal translocation (Figure 30). In addition to the Rag GTPases, we have also identified Rheb, the substrate of TSC2 and a critical activator of mTORC1 [84], as a mediator that promotes the lysosomal translocation of both TSC2 and mTORC1 in response to amino acid deficiency and sufficiency respectively (Figures 30 and 33). Furthermore, Rheb is not only required for RagC to localize with lysosomes (Figure 33) but also for the association of RagA with the lysosomal protein Ragulator (Figure 34). Therefore, our findings suggest that Rheb is more important than it has been thought, and have positioned Rheb in the mTORC1 signalling pathway in response to amino acids due to the identified ability of Rheb to mediate the lysosomal localization of mTORC1, TSC2, RagC and RagA. However, whether Rheb interacts with the Rag GTPases requires further investigation.

Consistent with previous findings [99], TSC2 was found to indeed interact with the RagA/RagC heterodimer and this interaction is enhanced by amino acid deprivation (Figure 31). However, TSC2 seems to interact preferentially with RagC (Figure 31), instead of RagA as has been suggested [99]. This discrepancy may have been caused by different experimental procedures including different plasmids that were used for the pull down assay, lysis and pull down conditions. The cell lines used might also be a concern although HEK293T and HEK293FT (a fast growing variant of HEK293T) cell lines were used in both our experiments and the cited article.

Currently it is difficult to detect the subcellular distribution of endogenous RagA due to lack of antibody detecting endogenous RagA by immunofluorescence. However, TSC2 seems to prevent HA-tagged RagA from associating with lysosomes in response to amino acid deprivation, but it does not affect RagC co-localization with lysosomes under the same condition (Figure 35). This suggests an alternative model of mTORC1 inhibition by TSC2 in response to amino acid deficiency that lysosome-

localized TSC2 likely inhibits mTORC1 indirectly by dissociating RagA from lysosomes. Endogenous RagC is found to localize on lysosomes regardless of amino acid conditions, which is consistent with the findings previously reported in reference [95]. It is worth noticing that HA-tagged RagA appears to dissociate from lysosomes upon amino acid deprivation, a finding different from suggestion that RagA localizes with lysosomes under the same condition that was proposed in the same publication. This statement was based on the results of IP experiments showing that RagA co-immunoprecipitates with RagC and that endogenous RagC localizes on lysosomes, regardless of amino acid conditions. An antibody that specifically detects endogenous RagA by immunofluorescence will certainly clarify whether the association of endogenous RagA with lysosomes is dependent on amino acids.

It has been debated for many years whether Rheb is localized on the lysosomal membrane, due to lack of suitable reagents, including an antibody that can be used for detecting endogenous Rheb at that time [95, 101, 102]. By utilizing an antibody (recently established at Institute of Cancer Research) that specifically detects endogenous Rheb by immunofluorescence, it has been demonstrated in our studies that Rheb does not co-localize with lysosomes (Figure 32). Whether Rheb co-localizes with mTORC1, as well as the compartment that retains Rheb need to be further investigated.

Nevertheless, a very recent publication from 2018 suggests that endogenous Rheb localizes with Golgi apparatus in proximity to lysosomes in an amino acid-independent manner [103], which is in accordance with our findings. On the other hand, another publication from 2015 suggests that endogenous Rheb localizes with lysosomes in the presence of amino acids [223]. It is interesting that in both of these studies a commercial antibody from Abnova has been used to detect Rheb. However, whether these two antibodies were from the same clone cannot be confirmed due to lack of information. In addition, the discrepancy might be caused by different cell lines were used in both studies, which are HEK293T and HCT116 cell lines. The differences between our findings and some of the published studies might be a result of a number of things. For example, the antibodies used for detection of endogenous Rheb by immunofluorescence in the published studies and the one used for

experiments described here were from different clones. In addition, Rheb might have differential expression and localization patterns in different cell lines or tissues. HCT116 cells [223] and HEK293T [103] cells used in the two studies were derived from colon cancer and human embryonic kidney respectively, whilst Hela cells used in our experiments were derived from cervical cancer and are also infected with HPV. Another reason might be different experimental procedures including culturing cells and media shift, and reagents used to culture or treat cells that might be from different companies or batches. Moreover, this discrepancy might result from the highly dynamic subcellular distribution of Rheb [102]. Overall, the subcellular localization of Rheb seems to be more complicated than what was initially proposed, and will require further investigation with approaches that allow the endogenous Rheb to be "tracked" in order to understand the dynamics of its subcellular trafficking.

Our studies therefore support an alternative model by which mTORC1 is regulated by the TSC/Rheb axis in response to amino acid conditions (Figure 64). In the presence of amino acids, mTORC1 translocates onto lysosomal membrane via interacting with the RagA-RagC heterodimer, and this association is stabilized by Rheb via unknown mechanism(s). TSC is cytosolic and unable to inhibit Rheb. GTP-bound Rheb then activates lysosome-localized mTORC1. Upon amino acid deprivation, GCN2 is activated and promotes the association of TSC with the RagA-RagC heterodimer. TSC is then recruited onto lysosomal surface likely via interacting with RagC. Rheb stabilizes the association via unknown mechanism(s). Lysosome-localized TSC2 not only deactivates Rheb but also promotes RagA to dissociate from lysosomes, leading to release of mTORC1 from lysosomes and thus inactivation of mTORC1.

①

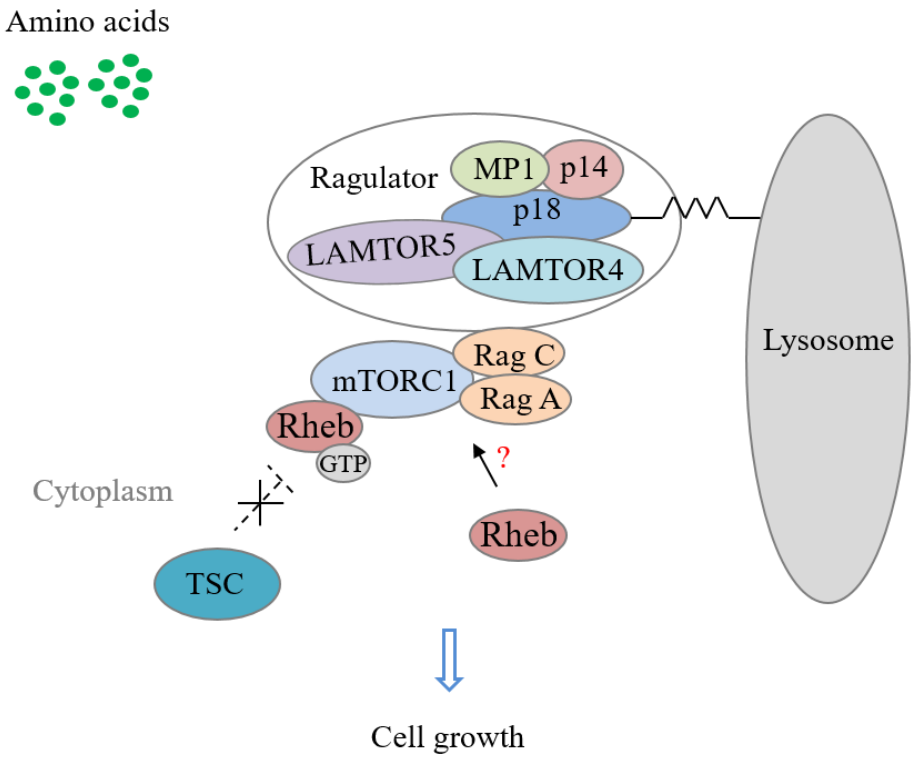
Amino acids
Ragulator
MP1
p14
p18
LAMTOR5
LAMTOR4
Lysosome
Rag C
mTORC1
Rag A
Rheb
GTP
?
Cytoplasm
Rheb
TSC
Cell growth

②

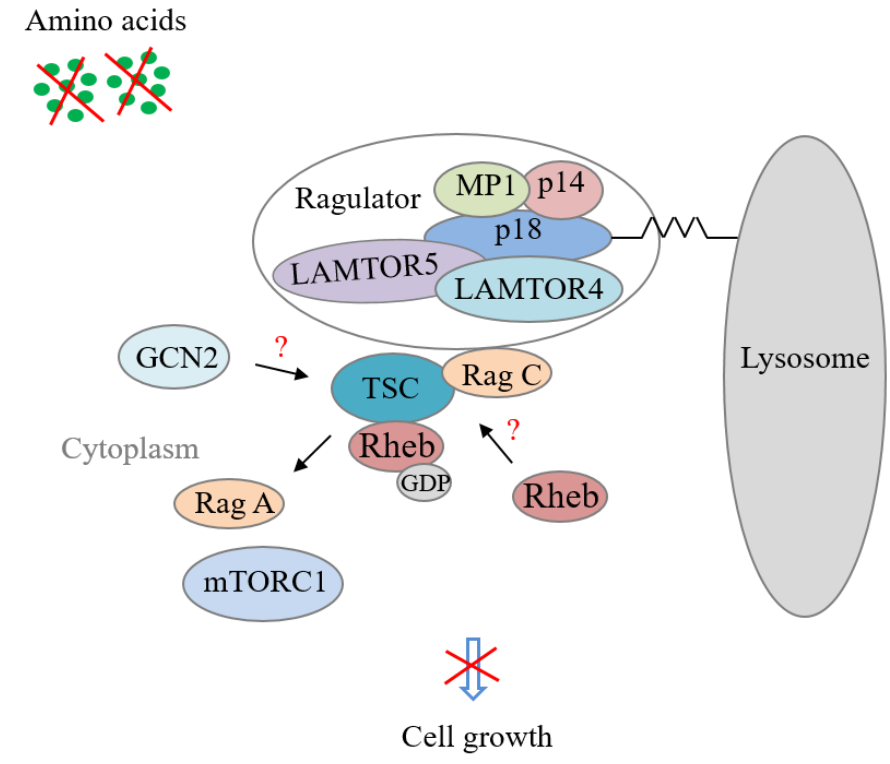
Amino acids
Ragulator
MP1
p14
p18
LAMTOR5
LAMTOR4
Lysosome
GCN2
?
TSC
Rag C
Cytoplasm
Rheb
GDP
?
Rag A
Rheb
mTORC1
Cell growth

Figure 64. A suggested model of mTORC1 regulation by TSC/Rheb in response to amino acid deprivation
Panel 1, in the presence of amino acids, mTORC1 is recruited to lysosomal membrane via interacting with the RagA/RagC heterodimer that binds to the lysosomal protein complex Ragulator. TSC, in contrast, residues in the cytosol and is unable to deactivates Rheb. GTP-bound Rheb, localized in proximity to lysosomes, not only activate the catalytic function of mTORC1 but also stabilizes the association of mTORC1 with the Rag heterodimer via an unknown mechanism. Activated mTORC1 stimulates a series of subcellular processes, ultimately promoting cell growth. **Panel 2**, upon amino acid deprivation, the kinase GCN2 is activated and promotes the lysosomal translocation of TSC via an unknown mechanism. TSC is recruited to lysosomal membrane by interacting with the RagA/RagC heterodimer, likely with RagC. Rheb stabilizes the lysosome-TSC association also via an unknown mechanism. Lysosome-localized TSC inhibits mTORC1 via inducing the GTP hydrolysis of Rheb. In addition, TSC seems to promote the dissociation of RagA from lysosomes, which destabilizes the interaction of mTORC1 with the RagA/RagC heterodimer and thus results in release of mTORC1 into cytosol. Inactive mTORC1 is unable to stimulate cell growth or repress autophagy. The processes indicated by arrows are novel findings compared to the proposed model in Figure 12.

4.2. The MAPK/ERK cascade promotes cell death in response to cystine deprivation

Anticancer therapies that affect cancer cells but spare normal cells are most beneficial for cancer patients. The concept of synthetic lethality opens opportunities to identify cancer-specific vulnerabilities that can be exploited to selectively eliminate cancer cells [224-227]. Instead of targeting a second gene which is the conventional way to identify synthetic lethality of cancer [224], we have focused on the reprogrammed metabolism of cancer cells, to identify metabolic vulnerabilities targeting the oncogenes in the MAPK/ERK cascade. Cancer cells universally exhibit reprogramming of glucose and amino acids metabolism [219, 220] to sustain their rapid cell division and growth. Many cancer types are found to strongly dependent on specific amino acids from either exogenous or endogenous sources [220, 228]. Amino acid deprivation therefore provides a potential approach to identify novel cancer-specific vulnerabilities.

We have utilized isogenic breast cell lines (HME) that express a number of mutated oncogenic proteins (oncoproteins) resulting in activation of specific signalling pathways that have been established by Prof Alberto Bardelli [201]. Utilizing such

isogenic cell line confers an advantage of avoiding the highly heterogeneous context within cancer cells and allowing the oncogenic mutation-specific features to be characterized. These four mutations: EGFR delE746-A750, KRAS G13D, BRAF V600E, and PI3KCA H1047R, have been frequently implicated in a variety of cancer types, such as NSCLC, melanomas, pancreatic and breast cancer [27, 37, 38]. Particularly, EGFR delE746-A750 mutant is the most common EGFR mutation in NSCLCs [5].

Through an amino acid dropout screen on HME cell lines containing isogenic knock-in mutations, EGFR delE746-A750, KRAS G13D, BRAF V600E, and PI3KCA H1047R, we have identified amino acid cystine as a vulnerability specific to EGFR delE746-A750 HME cell line (Figure 45). Deprivation of cystine, but not of any other amino acids from the culture medium, has caused lethality in EGFR delE746-A750 but not EGFR wild-type HME cells, and the induced cell death exhibits non-apoptotic morphological features (Figure 45 and Appendix 6). Based on morphological characteristics observed, the cell death is likely to occurs via ferroptosis since we have also found that it is accompanied by elevated accumulation of lipid ROS and is strictly dependent on iron (Appendix 6). Furthermore, this cystine deprivation-induced cell death requires the activating MAPK/ERK cascade, since inhibition of this cascade using specific inhibitors prevents accumulation of lipid ROS and cell death (Figure 47). This suggests that cystine/GSH is likely to act as a synthetic lethal partner of the EGFR delE746-A750 mutant. It seems that deprivation of cystine has triggered a certain cellular stress, most likely oxidative stress, which is aggravated by the activating MAPK/ERK cascade as in the case of EGFR delE746-A750 HME cells, and results in severe loss of cell viability.

Cancer cells experience higher oxidative stress from ROS than non-malignant cells due to genetic alterations and abnormal growth and as a result, maintenance of the antioxidant glutathione (GSH) is essential for their survival and proliferation [229-231]. Wild-type HME cells might maintain the intracellular level of antioxidants, mainly cystine and GSH [229-231], to scavenge ROS and survive cystine deprivation. However, this does not seem to be the case since the intracellular levels of cystine and GSH decline to similar extends in wild-type and EGFR delE746-A750

cells (Figure 48). Another possibility is that EGFR delE746-A750 cells already produce high amounts of lipid ROS, but under the normal-nutrient condition the lipid ROS is scavenged by cellular antioxidants and thus the damage is eliminated. However, during deprivation of cystine, the cellular antioxidants are declined and incapable of scavenging the original high level of ROS, which results in dramatic damage to the cells. In accordance with this, inhibition of the MAPK/ERK cascade has lowered lipid ROS and thus protects these cells from cystine deprivation (Figure 47).

We further identified that the MAPK/ERK cascade promotes lipid ROS accumulation through regulating two enzymes, GPX4 and NOX4. These two enzymes act to remove and produce lipid ROS respectively, thereby tightly control the cellular level of lipid ROS [183, 232]. The activating MAPK/ERK cascade in the EGFR delE746-A750 HME cells downregulates the cellular level of GPX4 and upregulates that of NOX4 (Figures 50, 51 and 53), which render these cells rather susceptible to oxidative stress resulting from cystine deprivation. Therefore, a model of MAPK/ERK promoting cell death in response to cystine deprivation in the EGFR delE746-A750 HME cells has been proposed (Figure 65). The persistently active MAPK/ERK cascade, due to the EGFR delE746-A750 mutation, increases the production of lipid ROS by upregulating NOX4 and downregulating GPX4. Under normal-nutrient condition, this high level of lipid ROS is scavenged by cellular antioxidants mainly glutathione (GSH) that is synthesized from cysteine. In the absence of cystine, the cellular level of GSH has been depleted, resulting in excessive accumulation of lipid ROS and thus severe oxidative damages to the cell membrane and other compartments. These damages ultimately leads to cell death likely via ferroptosis. In addition, it is likely that cystine/cysteine is a synthetic lethal partner of the EGFR delE746-A750 mutation in HME cells, by targeting the intracellular cystine/cysteine pool using AECase, the EGFR mutant cells become vulnerable and inviable whereas the wild type HME cells survive (Figure 66).

①

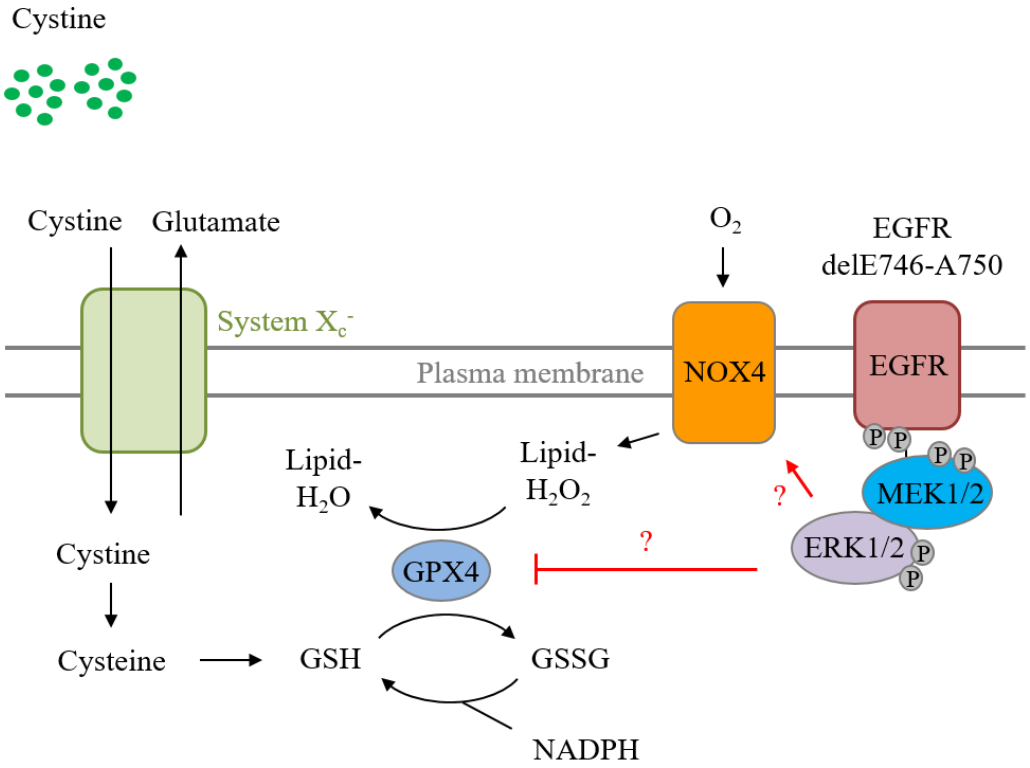
Cystine
Cystine
Glutamate
System X_c^-
Plasma membrane
O_2
NOX4
EGFR
delE746-A750
EGFR
P
P
P
P
MEK1/2
ERK1/2
P
P
?
?
Lipid-
H_2O
Lipid-
H_2O_2
GPX4
Cystine
Cysteine
GSH
GSSG
NADPH

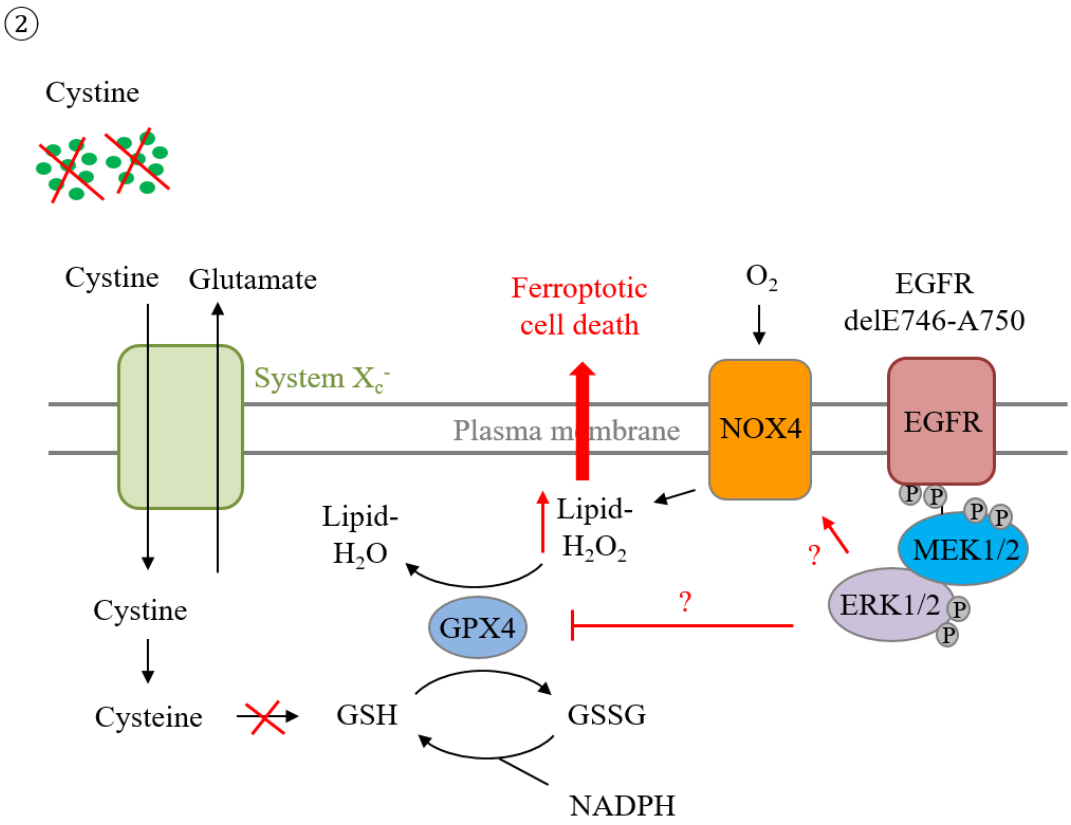

Figure 65. MAPK/ERK cascade promotes cell death in response to cystine deprivation.
In EGFR delE746-A750 HME cells, the MAPK/ERK cascade is continuously active, which upregulates the expression of NOX4 and downregulates that of GPX4 via unknown mechanisms. The lipid ROS is thus produced at a high level in these cells but they are scavenged by cellular antioxidants mainly GSH under the normal-nutrient condition (**Panel 1**). During cystine deprivation, the GSH pool has been depleted due to lack of cysteine and cystine, and the lipid ROS is thus accumulated at high levels, which cause oxidative damages to the cells and ultimately leads to cell death likely via ferroptosis (**Panel 2**). The mechanism that the MAPK/ERK cascade promotes ferroptosis via downregulating GPX4 and upregulating NOX4 is a novel finding compared to the model in Figure 49.

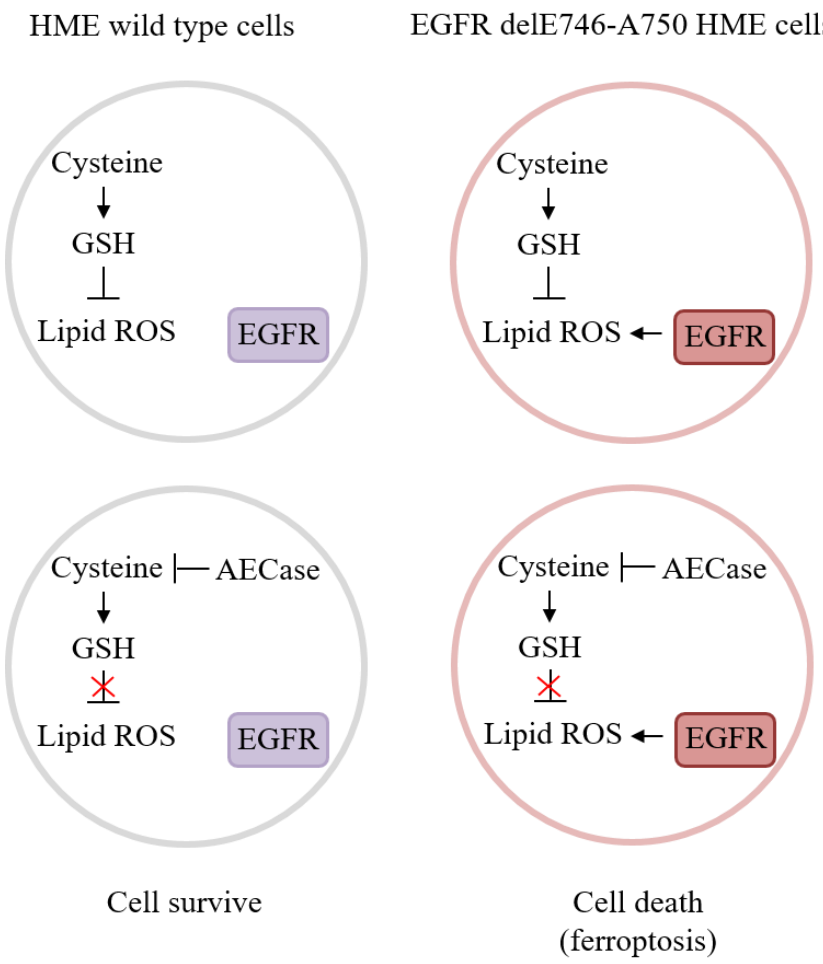

Figure 66. Schematic representation of cystine/cysteine as a synthetic lethal target of EGFR delE746-A750 mutation.
Depletion of cystine/cysteine pool by AECase causes cell death (likely ferroptosis) in EGFR delE746-A750 HME cells whereas wild type cells stay viable.

Through the cystine deprivation experiments conducted using nine NSCLC cell lines obtained from Liverpool cell line repository, we identify that the NCI-NH1650 cell line is vulnerable to cystine depletion (Figure 55). This cell line contains the two most common EGFR mutations, delE746-A750 and L858R [5, 6], as well as the EGFR T790M mutation that is associated with resistance to EGFR inhibitor therapy [20]. Our *in vitro* work demonstrates that the NCI-NH1650 cells are susceptible to pharmacological depletion of cystine/cysteine pools by AECase, an engineered cysteine/cystine-degrading enzyme (Figure 57). Moreover, our study on a mouse tumour model engrafted with NCI-NH1650 NSCLC cells suggests that AECase and its analogues might be potentially used in preclinical studies and clinical application to inhibit the growth of tumours that are susceptible to cystine depletion. In addition,

our study has demonstrated an approach to screen for synthetic lethality of oncogenes based on amino acid metabolism reprogramming of cancer cells. This approach can be potentially used to screen for metabolic synthetic lethality of cancer-associated genes, which might contribute to novel cancer therapeutics.

Appendix - Supplementary Tables and Figures

Appendix 1. Sites of point mutations in human MAP4K3 sequence.

A. MAP4K3 opening reading frame (ORF, 2685bp) obtained from the website of GenScript. **B**. MAP4K3 amino acid sequence (894 amino acids) obtained from the website of UniProt. DNA and amino acid sequence of the nine MAP4K3 point mutations are highlighted in red in **A** and **B**.

A

5’ 1 atgaaccccg gcttcgattt gtcccgccgg aacccgcagg aggacttcga gctgattcag
61 cgcatcggca gcggcaccta cggcgacgtc tacaaggcac ggaatgttaa cactggtgaa
121 ttagcagcaa ttaaagtaat aaaattggaa ccaggagaa**g ac**tttgcagt tgtgcagcaa
181 gaaattatta tgatgaaaga ctgtaaacac ccaaatattg ttgcttattt tggaagctat
241 ctcaggcgag ataagctttg gatttgcatg gagttttgtg gaggtggttc tttacaggat
301 atttatcacg taactggacc tctgtcagaa ctgcaaattg catatgttag cagagaaaca
361 ctgcagggat tatattatct tcacagtaaa ggaaaaatgc acagagatat aaagggagct
421 aacattctat taacggataa tggtcatgtg aaattggctg attttggagt atctgcacag
481 ataacagcta caattgccaa acggaagtct ttcattggca caccatattg gatggctcca
541 gaa**gtt**gcag ctgttgagag gaaggggggt tacaatcaac tctgtgatct ctgggcagtg
601 ggaatcactg ccatagaact tgca**gag**ctt cagcctccta tgtttgactt acacccaatg
661 agagcattat ttctaatgac aaaaagcaat tttcagcctc ctaaactaaa ggataaaatg
721 aaatggtcaa atagttttca tcactttgtg aaaatggcac ttaccaaaaa tccgaaaaaa
781 agacctactg ctgaaaaatt attacagcat ccttttgtaa cacaacattt gacacggtct
841 ttggcaatcg agctgttgga taaagta**aat** aatccagatc attccactta ccatgatttc
901 gatgatgatg atcctgagcc tcttgttgct gtaccacata gaattcactc aacaagtaga
961 aacgtgagag aagaaaaaac acgctcagag ataacctttg gccaagtgaa atttgatcca
1021 cccttaagaa aggagacaga accacatcat **gaa**cttcccg acagtgatgg ttttttggac
1081 agttcagaag aaatatacta cactgcaaga tctaatctgg atctgcaact ggaatatgga
1141 caaggacacc aaggtggtta ctttttaggt gcaaacaaga gtcttctcaa gtctgttgaa
1201 gaagaattgc atcagcgagg acacgtcgca catttagaag atgatgaagg agatgatgat
1261 gaatctaaac actcaactct gaaagcaaaa attccacctc ctttgccacc aaagcctaag
1321 tctatcttca taccacagga aatgcattct actgaggatg aaaatcaagg aacaatcaaG

1381 agatgtccca tgtcagggag cccagcaaag ccatcc**caa**g ttccacctag accaccacct

1441 cccagattac ccccacacaa acctgttgcc ttaggaaatg gaatgagctc cttccagtta

1501 aatggtgaac gagatggctc attatgtcaa caacagaatg aacatagagg cacaaacctt

1561 tcaagaaaag aaaagaaaga tgtaccaaag cctattagta atggtcttcc tccaacacct

1621 aaagtgcata tgggtgcatg tttttcaaaa gtttttaatg ggtgtccctt gaaaattcac

1681 tgtgcatcat catggataaa cccagataca agagatcagt acttgatatt tggtgccgaa

1741 gaagggattt ataccctcaa tcttaatgaa cttcatgaaa catcaatgga acagctattc

1801 cctcgaaggt gtacatggtt gtatgtaatg aacaattgct tgctatcaat atctggtaaa

1861 gcttctcagc tttattccca taatttacca gggctttttg attatgcaag acaaatgcaa

1921 aagttacctg ttgctattcc agcacacaaa ctccctgaca gaatactgcc aaggaaattt

1981 tctgtatcag caaaaatccc tgaa**acc**aaa tggtgccaga agtgttgtgt tgtaagaaat

2041 ccttacacgg gccataaata cctatgtgga gcacttcaga ctagcattgt tctattagaa

2101 tgggttgaac caatgcagaa atttatgtta attaagcaca ta**gat**tttcc tataccatgt

2161 ccacttagaa tgtttgaaat gctggtagtt cctgaacagg agtacccttt agtttgtgtt

2221 ggtgtcagta gaggtagaga cttcaaccaa gtggtt**cga**t ttgagacggt caatccaaat

2281 tctacctctt catggtttac agaatcagat accccacaga caaatgttac tcatgtaacc

2341 caactggaga gagataccat ccttgtatgc ttggactgtt gtataaaaat agtaaatctc

2401 caaggaagat taaaatctag caggaaattg tcatcagaac tcacctttga tttccagatt

2461 gaatcaatag tgtgcctaca agacagtgtg ctagctttct ggaaacatgg aatgcaaggt

2521 agaagtttta gatctaatga ggtaacacaa gaaatttcag atagcacaag aattttcagg

2581 ctgcttggat ctgacagggt cgtggttttg gaaagtaggc caactgataa ccccacagca

2641 aatagcaatt tgtacatcct ggcgggtcat gaaaacagtt actga 3’

B

10 20 30 40 50

MNPGFDLSRR NPQEDFELIQ RIGSGTYGDV YKARNVNTGE LAAIKVIKLE

60 70 80 90 100

PGEDFAVVQQ EIIMMKDCKH PNIVAYFGSY LRRDKLWICM

EFCGGGSLQD

110 120 130 140 150

IYHVTGPLSE LQIAYVSRET LQGLYYLHSK GKMHRDIKGA NILLTDNGHV

160 170 180 190 200

KLADFGVSAQ ITATIAKRKS FIGTPYWMAP EVAAVERKGG YNQLCDLWAV

210 220 230 240 250

GITAIELAEL QPPMFDLHPM RALFLMTKSN FQPPKLKDKM KWSNSFHHFV

260 270 280 290 300

KMALTKNPKK RPTAEKLLQH PFVTQHLTRS LAIELLDKVN NPDHSTYHDF

310 320 330 340 350

DDDDPEPLVA VPHRIHSTSR NVREEKTRSE ITFGQVKFDP PLRKETEPHH

360 370 380 390 400

ELPDSDGFLD SSEEIYYTAR SNLDLQLEYG QGHQGGYFLG ANKSLLKSVE

410 420 430 440 450

EELHQRGHVA HLEDDEGDDD ESKHSTLKAK IPPPLPPKPK SIFIPQEMHS

460 470 480 490 500

TEDENQGTIK RCPMSGSPAK PSQVPPRPPP PRLPPHKPVA LGNGMSSFQL

510 520 530 540 550

NGERDGSLCQ QQNEHRGTNL SRKEKKDVPK PISNGLPPTP KVHMGACFSK

560 570 580 590 600

VFNGCPLKIH CASSWINPDT RDQYLIFGAE EGIYTLNLNE LHETSMEQLF

610 620 630 640 650

PRRCTWLYVM NNCLLSISGK ASQLYSHNLP GLFDYARQMQ KLPVAIPAHK

660 670 680 690 700

LPDRILPRKF SVSAKIPETK WCQKCCVVRN PYTGHKYLCG ALQTSIVLLE

710 720 730 740 750

WVEPMQKFML IKHIDFPIPC PLRMFEMLVV PEQEYPLVCV GVSRGRDFNQ

760 770 780 790 800

VVRFETVNPN STSSWFTESD TPQTNVTHVT QLERDTILVC LDCCIKIVNL

810 820 830 840 850

QGRLKSSRKL SSELTFDFQI ESIVCLQDSV LAFWKHGMQG RSFRSNEVTQ

860 870 880 890

EISDSTRIFR LLGSDRVVVL ESRPTDNPTA NSNLYILAGH ENSY

Appendix 2. Primers for MAP4K3 mutagenesis and sequencing

Appendix 2-1 Primers for mutagenesis		
Site	Forward (F) / Reverse (R)	Sequence 5' to 3'
D54N (g160a)	F	ggaaccaggagaaaactttgcagttgtgc
	R	gcacaactgcaaagttttctcctggttcc
V182F (g544t)	F	ggatggctccagaatttgcagctgttgag
	R	ctcaacagctgcaaattctggagccatcc
E209G (a626g)	F	gccatagaacttgcagggcttcagcctcctatg
	R	cataggaggctgaagccctgcaagttctatggc
N290I (a869)	F	gctgttggataaagtaattaatccagatcattcc
	R	ggaatgatctggattaattactttatccaacagc
E351K (g1051a)	F	gacagaaccacatcataaacttcccgacagtg
	R	caatgtcgggaagtttatgatgtggttctgtc
Q473K (c1417a)	F	ccagcaaagccatccaaagttccacctagacc
	R	ggtctaggtggaactttggatggctttgctgg
T669A (a2005g)	F	gcaaaaatccctgaagccaaatggtgccag
	R	ctggcaccatttggcttcagggatttttgc
D715Y (g2143t)	F	gttaattaagcacatatattttcctataccatg
	R	catggtataggaaaatatatgtgcttaattaac
R753Q (g2258a)	F	caaccaagtggttcaatttgagacggtc
	R	gaccgtctcaaattgaaccacttggttg

Appendix 2-2 Primers for sequencing		
Site	Forward (F) / Reverse (R)	Sequence 5' to 3'
D54N (g160a)	F	cggctacaattaatacataacc
	R	cagccaatttcacatgacca
V182F (g544t)	F	gtggaggtggttctttacagg
	R	ctacttgttgagtgaattc
E209G (a626g)	F	gtggaggtggttctttacagg
	R	ctacttgttgagtgaattc
N290I (a869)	F	ggcacttaccaaaaatccg
	R	ctacttgttgagtgaattc
E351K (g1051a)	F	ggcacttaccaaaaatccg
	R	ctccctgacatgggacatctc
Q473K (c1417a)	F	gaaggagatgatgatgaatct
	R	ccctggtaaattatgggaat
T669A (a2005g)	F	gccgaagaagggatttatacc
	R	caacagtccaagcatacaagg
D715Y (g2143t)	F	gccgaagaagggatttatacc
	R	caacagtccaagcatacaagg
R753Q (g2258a)	F	gaacaggagtacccttagt
	R	caacagtccaagcatacaagg

Appendix 3. PCR conditions for mutagenesis of human MAP4K3

Appendix 3-1 50µl PCR reaction setup	
10X reaction buffer	5µl
QuikSolution reagent	3µl
DNA template	10ng
forward primer	125ng
reverse primer	125ng
10mM dNTP Mix	1µl
DNA polymerase	2.5U
ddH_2O	to a final volume of 50µl

Appendix 3-2 Thermol cycle for PCR reaction			
Step	Cycles	Temperature	Time
1	1	95°C	1min
2	18	95°C	50s
		60°C	50s
		68°C	8.5min
3	1	68°C	7min

Appendix 4. Rheb promotes the co-localization of mTOR and RagC with lysosomes.

Confocal immunofluorescence micrographs of Hela cells stained with antibodies to mTOR (green in A) or RagC (green in B) and LAMP2 (red). Cells were treated with medium lacking amino acids for 60min (-AA) or deprived and stimulated with MEM amino acids for 15min (+AA) following transfection with control (Ctrl) and Rheb-specific siRNAs.

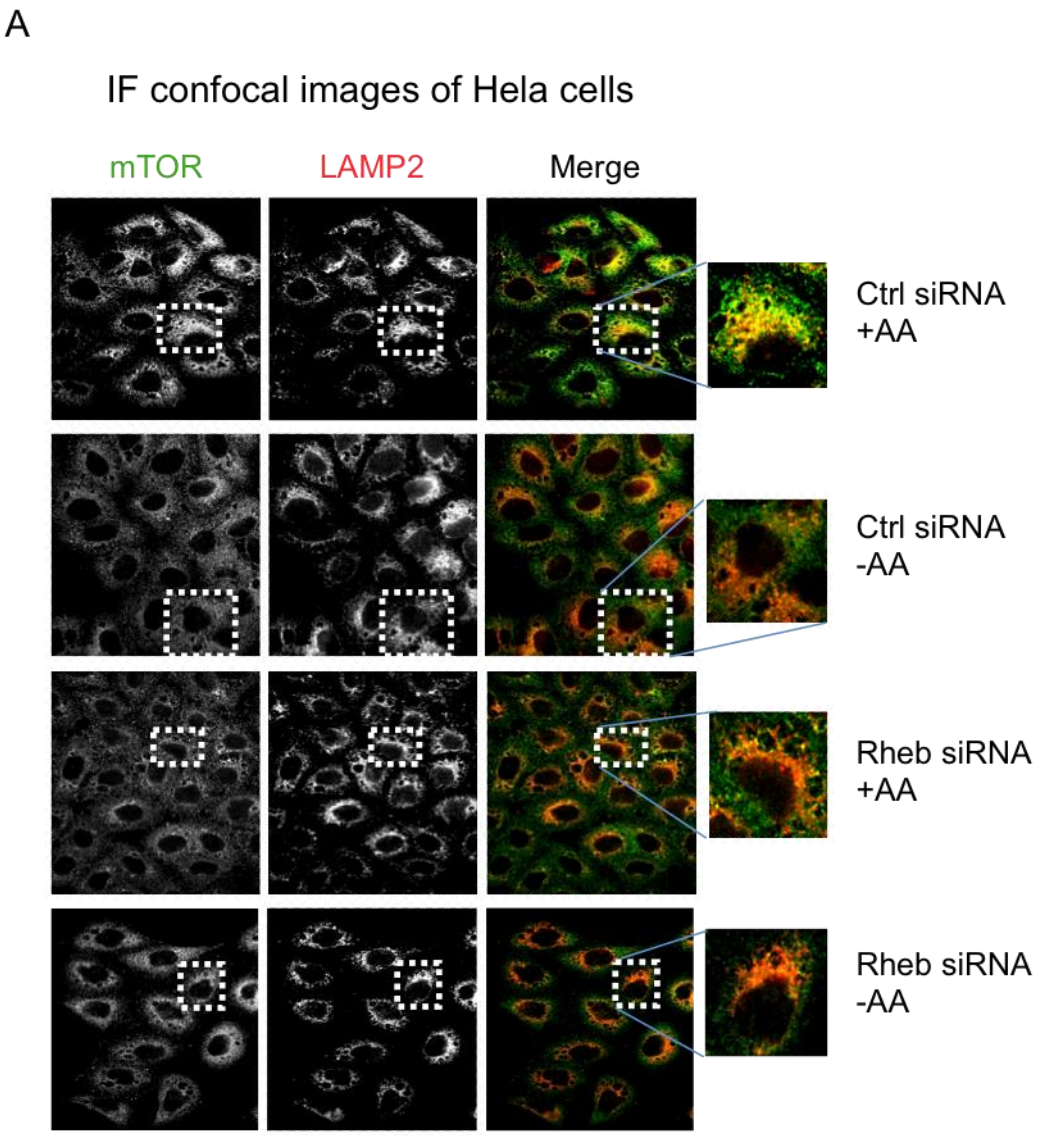

B

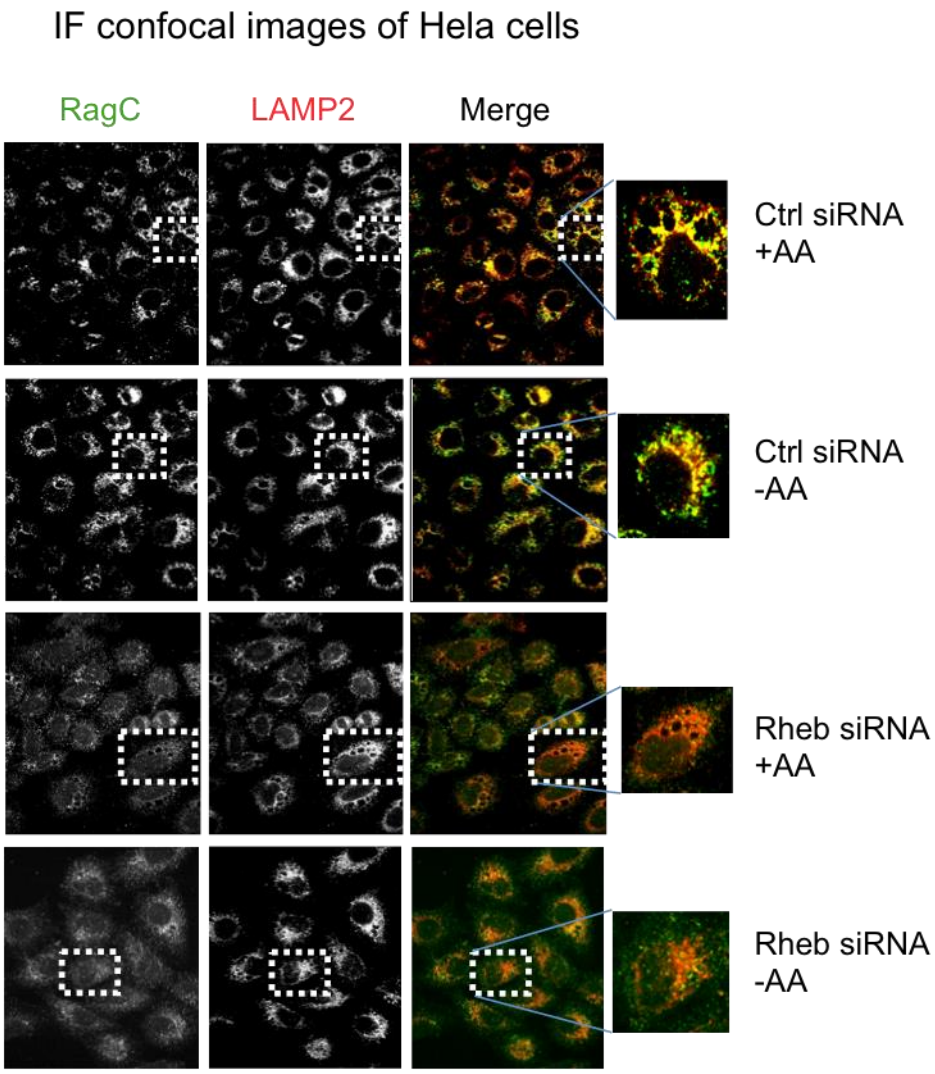
IF confocal images of Hela cells
RagC
LAMP2
Merge
Ctrl siRNA
+AA
Ctrl siRNA
-AA
Rheb siRNA
+AA
Rheb siRNA
-AA

Appendix 5. Inhibition of the MAPK/ERK cascade by the specific inhibitors.

A. Schematic representation of MAPK/ERK cascade with the five inhibitors. **B.** Immunoblots of EGFR mutant cell lysates probed with antibodies detecting phosphorylated EGFR (pEGFR), ERK (ppERK), total EGFR and ERK1/2. Cells were cultured in normal medium in the presence of DMSO (vehicle control) and inhibitors for 30 hours.

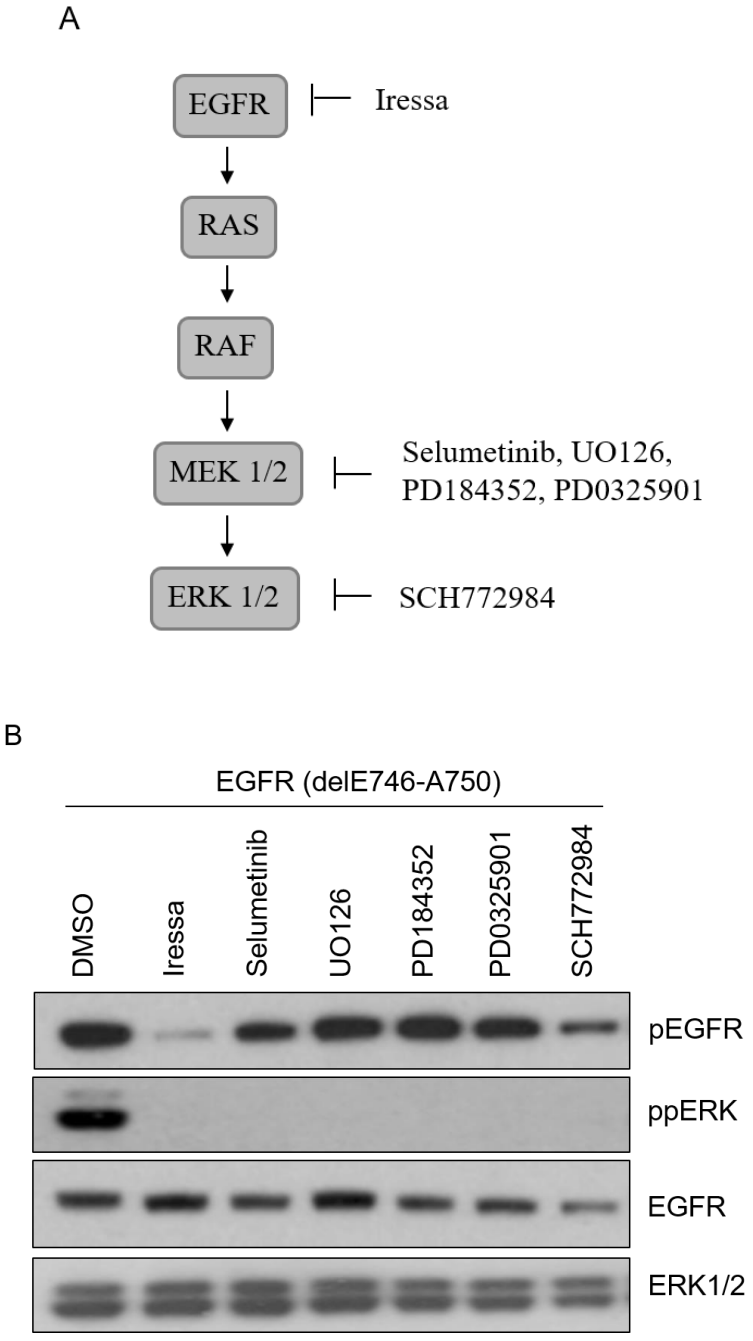

Appendix 6. Publication

See next page

Cell Reports

Report

Oncogene-Selective Sensitivity to Synchronous Cell Death following Modulation of the Amino Acid Nutrient Cystine

Graphical Abstract

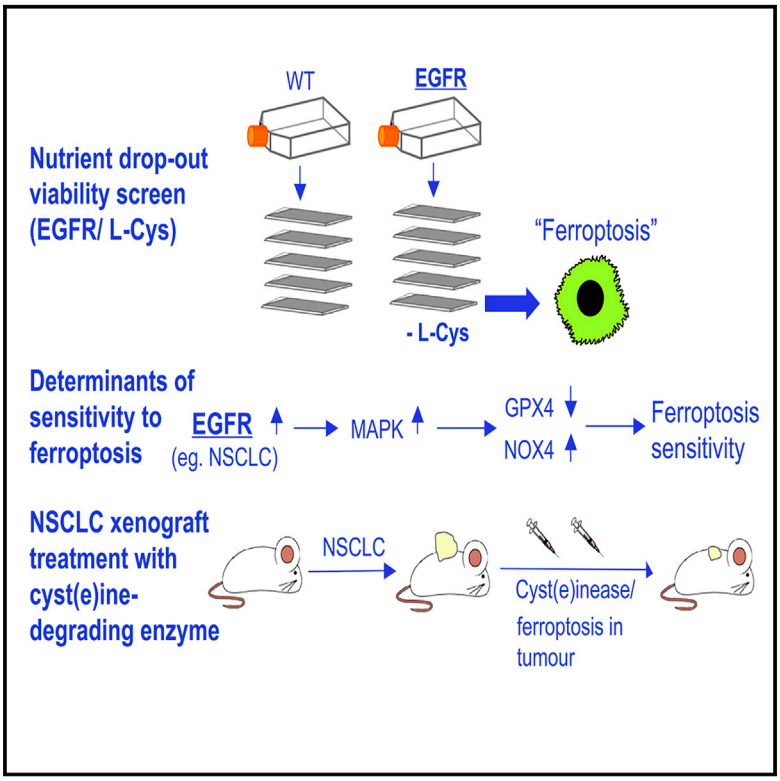

Highlights

- A nutrient depletion screen revealed a selective role for cystine in promoting viability
- Cystine was shown to promote viability by preventing ferroptosis
- Sensitivity to depletion of cystine was related to activation of MAPK
- Depletion of cystine inhibited tumor growth in a NSCLC xenograft model

Authors

Ioannis Poursaitidis, Xiaomeng Wang, Thomas Crighton, ..., Scott W. Rowlinson, Everett Stone, Richard F. Lamb

Correspondence

lambr@hope.ac.uk

In Brief

Poursaitidis et al. show that EGFR and BRAF mutant cells are sensitive to ferroptosis. Sensitivity was related to activation of MAPK signaling and the generation and release of hydrogen peroxide. To show that this sensitivity can be exploited therapeutically, growth of an EGFR mutant NSCLC xenograft was inhibited by a cyst(e)ine-degrading enzyme.

Poursaitidis et al., 2017, Cell Reports *18*, 2547–2556
March 14, 2017
http://dx.doi.org/10.1016/j.celrep.2017.02.054

CellPress

Cell Reports
Report

Oncogene-Selective Sensitivity to Synchronous Cell Death following Modulation of the Amino Acid Nutrient Cystine

Ioannis Poursaitidis,[2,9] Xiaomeng Wang,[2,9] Thomas Crighton,[2] Christiaan Labuschagne,[3] David Mason,[4] Shira L. Cramer,[5] Kendra Triplett,[5] Rajat Roy,[6] Olivier E. Pardo,[6] Michael J. Seckl,[6] Scott W. Rowlinson,[7] Everett Stone,[8] and Richard F. Lamb[1,10,*]

[1]School of Health Sciences, Liverpool Hope University, Hope Park Campus, Liverpool L16 9JD, UK
[2]Department of Molecular and Clinical Cancer Medicine, University of Liverpool North West Cancer Research Centre, University of Liverpool, 200 London Road, Liverpool L69 7ZB, UK
[3]Cancer Research UK Beatson Institute, Switchback Road, Bearsden, Glasgow G61 1BD, UK
[4]Centre for Cell Imaging, Institute of Integrative Biology, University of Liverpool, Biosciences Building, Crown Street, Liverpool L69 7ZB, UK
[5]Department of Chemical Engineering, The University of Texas at Austin, Austin, TX 78712, USA
[6]Division of Cancer CRUK Laboratories, 1st Floor ICTEM Building, Hammersmith Hospital Campus of Imperial College London, Du Cane Road, London W120NN, UK
[7]Aeglea BioTherapeutics, Austin, TX 78746, USA
[8]Department of Molecular Biosciences, The University of Texas at Austin, Austin, TX 78712, USA
[9]Co-first author
[10]Lead Contact
*Correspondence: lambr@hope.ac.uk
http://dx.doi.org/10.1016/j.celrep.2017.02.054

SUMMARY

Cancer cells reprogram their metabolism, altering both uptake and utilization of extracellular nutrients. We individually depleted amino acid nutrients from isogenic cells expressing commonly activated oncogenes to identify correspondences between nutrient supply and viability. In HME (human mammary epithelial) cells, deprivation of cystine led to increased cell death in cells expressing an activated epidermal growth factor receptor (EGFR) mutant. Cell death occurred via synchronous ferroptosis, with generation of reactive oxygen species (ROS). Hydrogen peroxide promoted cell death, as both catalase and inhibition of NADPH oxidase 4 (NOX4) blocked ferroptosis. Blockade of EGFR or mitogen-activated protein kinase (MAPK) signaling similarly protected cells from ferroptosis, whereas treatment of xenografts derived from EGFR mutant non-small-cell lung cancer (NSCLC) with a cystine-depleting enzyme inhibited tumor growth in mice. Collectively, our results identify a potentially exploitable sensitization of some EGFR/MAPK-driven tumors to ferroptosis following cystine depletion.

INTRODUCTION

Synthetic lethal screens have led to the identification of specific cancer cell vulnerabilities (Barbie et al., 2009; Possik et al., 2014; Scholl et al., 2009). One such vulnerability has previously been exploited therapeutically in acute lymphoblastic leukemia (ALL), where leukemic cells lacking asparagine synthase are known to require the amino acid asparagine and apoptose following administration of asparaginase (Holleman et al., 2003; Tallal et al., 1970). Overall amino acid abundance itself may be higher in cancerous tissue, suggesting an increased need for amino acids in some tumors (Hirayama et al., 2009; Kami et al., 2013). In pancreatic ductal adenocarcinoma (PDAC), KRAS is thought to induce a genetic program that favors metabolism of glutamine, rendering these cells particularly sensitive to glutamine withdrawal (Son et al., 2013). Some tumor cell lines (Scott et al., 2000) and primary tumors (Gonzalez and Byus, 1991) require exogenous arginine, indicating some selectivity in amino acid requirements. Here, we have explored the extracellular amino acid nutrient requirements of cells gene edited to introduce common oncogenic mutations. We identify a selective sensitivity to synchronous cell death by ferroptosis following deprivation of the amino acid nutrient cystine. Sensitization was found to be related to elevated mitogen-activated protein kinase (MAPK) signaling, with synchronous cell death involving hydrogen peroxide generation and release. Finally, we show that enzymatic cystine deprivation in vivo results in an inhibition of tumor growth in an EGFR mutant NSCLC xenograft model, suggesting that, by promoting ferroptosis, cystine depletion provides therapeutic benefit in some tumors.

RESULTS

EGFR Mutant HME Cells Undergo Cell Death when Deprived of the Amino Acid Nutrient Cystine

Human mammary epithelial (HME) cells were gene edited to introduce common oncogenic driver mutations (epidermal

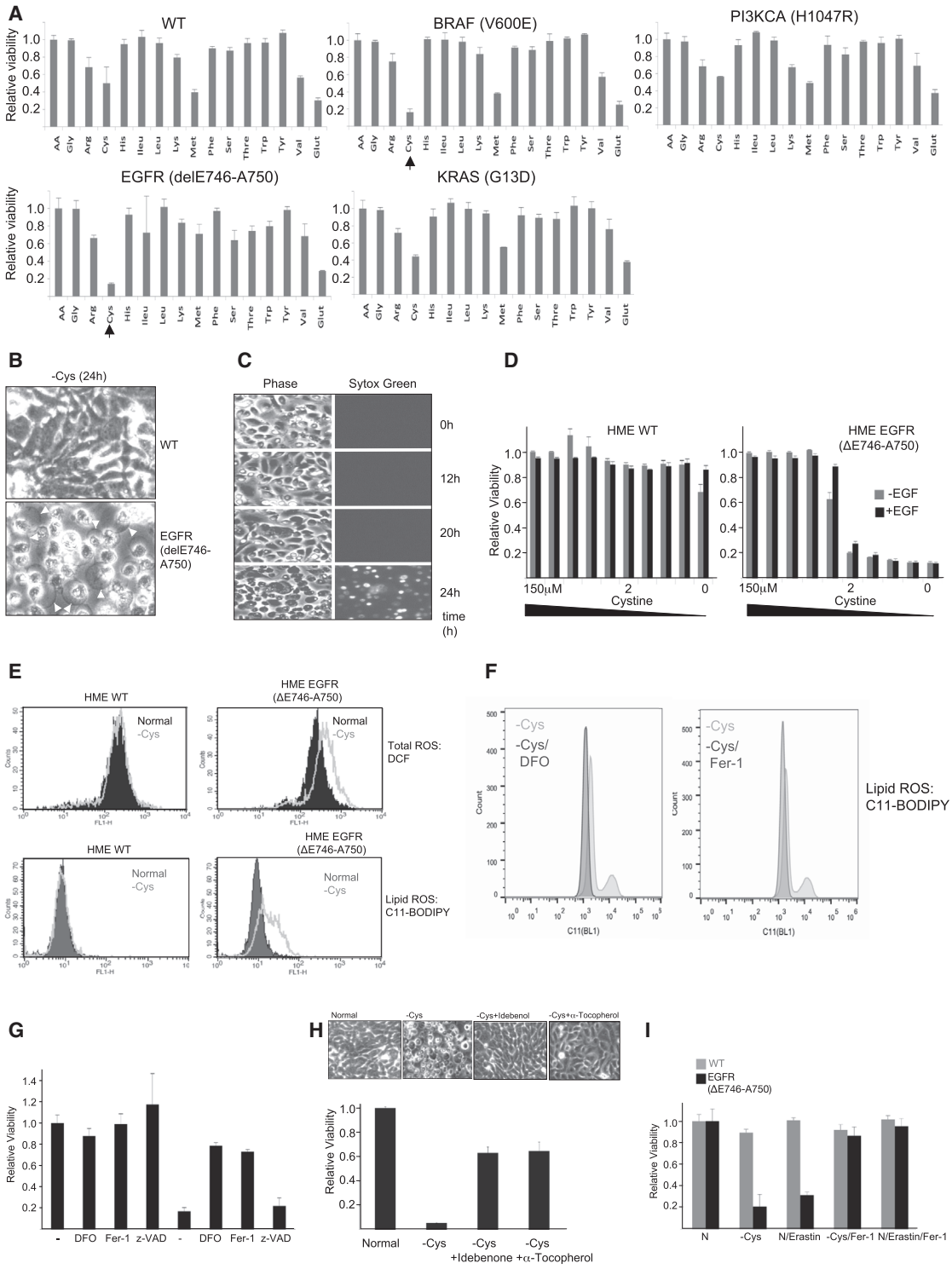

Figure 1. Deprivation of Cystine Induces Selective Cell Death by Ferroptosis in EGFR Mutant HME Cells

(A) Cell viability screen of HME cell lines deprived of individual amino acids for 72 hr. Histograms represent the average viability ± SD of three biological replicates relative to complete media assigned a value of 1 (+AA).

(B) Phase contrast micrographs of wild-type (WT) and EGFR (delE746-A750) HME cells deprived of cystine for 24 hr. Arrowheads indicate membrane extrusions.

(C) Time-lapse phase contrast (left) and Sytox Green (right) micrographs of live EGFR (delE746-A750) cells deprived of cystine for various times up to 24 hr.

(legend continued on next page)

growth factor receptor [EGFR] [delE746-A750], KRAS [G13D], BRAF [V600E], and PIK3CA [H1047R]) in an otherwise diploid genetic background (Di Nicolantonio et al., 2008). Following culture in media deficient in specific amino acids, we measured cell viability. All lines deprived of L-cystine (cystine) exhibited some loss of viability ranging from 40% to >80%. However, EGFR and BRAF mutant HME cells were especially sensitive, with viability inhibited by >80% (Figure 1A). Cystine deprivation induced a widespread loss of viability in EGFR mutant, but not wild-type HME, cells, with the majority of cells exhibiting a swollen or burst morphology (Figure 1B).

Next, we monitored EGFR mutant HME cells deprived of cystine by video time-lapse microscopy and observed rapid and synchronous cell swelling/bursting (Figure 1C; Movie S1). Sytox Green, a cell-impermeant nuclear stain, synchronously entered cells after cystine depletion (Figure 1C), indicating loss of plasma membrane integrity at <2 μM cystine (Figure 1D). Death was reversible upon re-supplementation of cystine for up to 10 hr but declined progressively thereafter and was not prevented by addition of D-cystine (Figure S1A).

Cell Death in Cystine-Deprived EGFR Mutant HME Cells Exhibits Hallmarks of Ferroptosis

This type of death resembled ferroptosis, an iron-dependent non-apoptotic cell death (Dixon et al., 2012). Because lipid reactive oxygen species (ROS) accumulation characterizes ferroptosis (Dixon et al., 2012), we measured ROS. Fluorescence-activated cell sorting (FACS) analysis indicated increased ROS accumulation in EGFR mutant HME cells following cystine deprivation (Figure 1E). EGFR mutant HME cells treated with known ferroptosis inhibitors inhibited lipid ROS generation (Figure 1F) and protected EGFR mutant (and BRAF mutant; Figure S1B) cells from cell death (Figure 1G), as did treatment with two other antioxidants (Figure 1H). Finally, erastin, an inhibitor of the system x_c-cystine/glutamate antiporter (Dixon et al., 2012), also induced selective loss of viability in EGFR mutant cells (Figure 1H). Collectively, these data indicate that cell death in EGFR mutant cells occurs by ferroptosis.

MAPK Signaling Sensitizes EGFR Mutant Cells to Cell Death following Cystine Deprivation

EGFR activation results in activation of downstream signaling cascades (Pines et al., 2010). Ferroptosis had previously been shown to require MAPK signaling (Yagoda et al., 2007; Dixon et al., 2012). Treatment of EGFR mutant cells for >24 hr with EGFR or MAPK (MEK and ERK1/2) inhibitors inhibited EGFR and MAPK signaling (Figures 2A and S2A), restored normal adherens junction formation and gap junctional intercellular communication (GJIC) (Figures 2B and 2C), and rescued cell viability following cystine withdrawal (Figures 2D and S2B). Likewise, EGFR and MAPK inhibition in EGFR mutant cells inhibited ROS generation (Figures 2E, S2C, and S2D).

Cystine Promotes Viability in EGFR Mutant HME Cells via a Glutathione-Independent Mechanism

HME cells might resist ferroptosis by maintaining intracellular levels either of cystine or glutathione, the major cystine-derived antioxidant. To address the former possibility, we deprived cells of cystine and measured activation of GCN2, a sensor of amino acid depletion (Hinnebusch, 2005). However, in both wild-type and EGFR mutant HME cells, GCN2 was equivalently activated following cystine deprivation (Figure 3A). Basal cystine levels were also equivalent and declined similarly in wild-type and EGFR mutant cells following extracellular cystine depletion (Figure S3A). Recent data have suggested a role for glutaminolysis in promoting ferroptosis (Gao et al., 2015). However, both wild-type and EGFR mutant HME cells contained similar steady-state intracellular levels of glutamine that were largely unaltered by deprivation of cystine (Figure S3A). Similarly, total levels of glutathione declined equivalently in wild-type and EGFR mutant HME cells following cystine deprivation (Figure 3B). However, Iressa-treated EGFR mutant cells accumulated more oxidized glutathione (GSSG) in comparison to untreated EGFR mutant HME cells following deprivation of cystine, suggesting that EGFR inhibition increased ROS detoxification (Figure 3C). Surprisingly, an inhibitor of glutathione synthesis (buthionine sulfoximine [BSO]), although also depleting glutathione levels, did not induce cell death (Figure 3D) nor increase ROS in EGFR mutant HME cells, unlike deprivation of cystine (Figure S3B). We therefore asked whether short-term deprivation of cystine, or inhibition of cystine import, acted synergistically with glutathione depletion to induce cell death. Indeed, short-term deprivation of cystine or treatment with inhibitors of the system x_c-antiporter induced significantly increased cell death when combined with glutathione depletion (Figure 3E). Treatment with auranofin, an inhibitor of the thioredoxin reductase/thioredoxin (TRX) system (Gromer et al., 1998) implicated in reduction of cystine to cysteine (Mandal et al., 2010; Pader et al., 2014), also synergized with glutathione depletion to promote loss of viability and lipid ROS induction (Figures S3B and S3C). Thus, EGFR mutant cells

(D) Cell viability following titration of cystine in WT and EGFR (delE746-A750) HME cells. Histogram represents the average viability ± SD of cells cultured in various concentrations of cystine ± EGF, relative to complete media (150 μM cystine; assigned an arbitrary value of 1).
(E) ROS in WT HME and EGFR (delE746-A750). (Upper panels) Total ROS measured using CMDCFDA (DCF) is shown; (lower panels) lipid ROS measured using C11 BODIPY 581/591 (C11-BODIPY) is shown. Dark traces, cells cultured in normal media for 12 hr; light traces, cells cultured in media lacking cystine for 12 hr.
(F) Lipid ROS in WT and EGFR (delE746-A750) HME cells. Dark traces, cells cultured in media lacking cystine in the presence of deferoxamine (DFO; 100 μM) or ferrostatin (Fer-1; 2 μM) for 12 hr; light traces, cells cultured in media lacking cystine for 12 hr.
(G) Cell viability of EGFR (delE746-A750) HME cells. Histogram is average viability ± SD cells cultured in normal media (left four bars, untreated [–] assigned an arbitrary value of 1) or media lacking cystine for 24 hr (right four bars) in the presence or absence of DFO, Fer-1, and z-VAD-fMK.
(H) Cell viability (bottom histogram) and phase-contrast microscopy (upper panels) of EGFR (delE746-A750) HME cells. Histogram is average viability ± SD of three biological replicates cultured in normal media (assigned an arbitrary value of 1) or media lacking cystine for 24 hr in the presence or absence of ROS scavengers idebenone and α-tocopherol.
(I) Cell viability of WT (gray bars) and EGFR (delE746-A750; black bars) HME cells. Histogram represents the average viability ± SD cells cultured in normal media or media lacking cystine for 24 hr in the presence or absence of erastin and Fer-1.

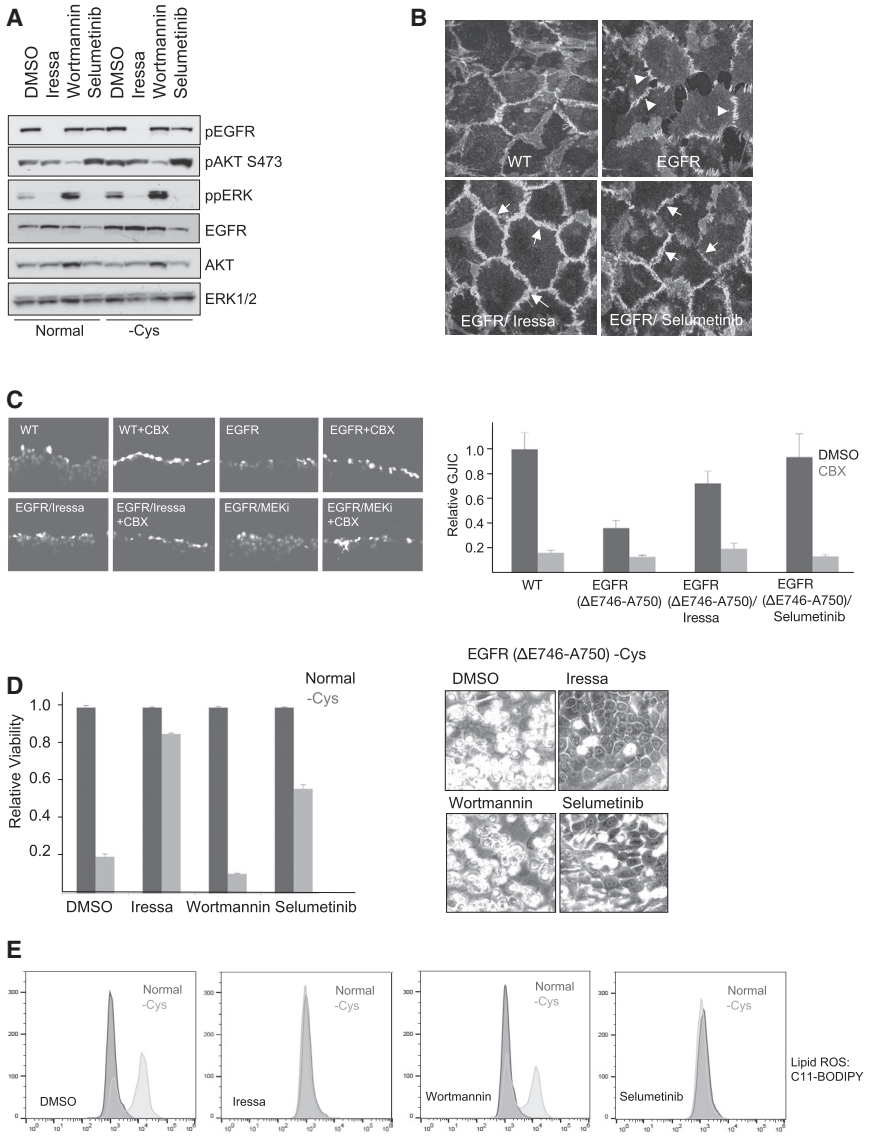

Figure 2. Active MAPK Signaling Promotes Sensitivity to Cystine Deprivation

(A) Immunoblots of EGFR (delE746-A750) HME cell lysates probed to detect phosphorylated EGFR, ERK, and AKT from cells cultured in normal media (normal) or media lacking cystine for 12 hr (−Cys) in the presence or absence of inhibitors added for a total of 30 hr.

(B) Confocal micrographs of adherens junctions stained with β-catenin antibody of WT or EGFR (delE746-A750) HME cells treated with vehicle (EGFR) or following treatment with inhibitors for 30 hr. Arrows indicate linear staining for β-catenin at intercellular junctions; arrowheads indicate presence of discontinuous adherens junctions.

(C) (Left panels) Fluorescence micrographs of GJIC measured by lucifer yellow infiltration in WT, EGFR (delE746-A750), Iressa-treated EGFR (delE746-A750; EGFR/Iressa), and selumetinib-treated EGFR (delE746-A750; EGFR/MEKi) in the presence or absence of carbenoxolone (CBX). (Right histogram) Quantification of GJIC is shown. Each condition was analyzed in six random 20× fields in three biological replicates with the values shown representing the mean and SEM and expressed relative to GJIC in WT HME cells assigned an arbitrary value of 1. Light bars represent GJIC in the presence of CBX.

(D) Cell viability (left histogram) and phase-contrast micrographs (right panels) of EGFR (delE746-A750) HME cells treated with inhibitors. Histogram is viability ± SD of cells cultured in normal media (dark bars) or media lacking cystine for 16 hr (light bars) in the presence or absence of inhibitors. Results were expressed for each condition separately, with viability in normal media assigned the arbitrary value of 1.

(E) FACS analyses of lipid ROS in EGFR (delE746-A750) cells following treatment with inhibitors. Dark traces, cells cultured in normal media; light traces, cells cultured in media lacking cystine for 12 hr.

oxidize less glutathione during cystine deprivation, contributing to ROS accumulation, whereas intracellular cysteine appears to play an additional role, aside from glutathione synthesis, in counteracting ROS and ferroptosis.

GPX4 Is Downregulated in EGFR Mutant HME Cells via MAPK Signaling and Modulates Sensitivity to Cell Death upon Cystine Deprivation

Glutathione peroxidases (GPXs) are good candidates for mediating sensitivity to ferroptosis. GPX4 has previously been implicated in ferroptosis (Friedmann Angeli et al., 2014; Yang et al., 2014), whereas GPX4 is induced following treatment with a BRAF inhibitor (Parmenter et al., 2014). By immunoblotting, GPX4, but not GPX1, expression was upregulated following either EGFR or MAPK (MEK and ERK; Figure S3D) inhibition, whereas GPX2 was not expressed in these cells (Figure 3E) and GPX3 is a secreted GPX expressed in the kidney (Maser et al., 1994). Suppression of GPX4 strongly promoted cell death in both wild-type (Figure 3G) and Iressa-treated EGFR mutant cells (Figure 3H). Lipid ROS similarly increased after suppression of GPX4 (Figure 3I). Thus, downregulation of GPX4 in EGFR mutant HME cells conferred increased sensitivity to ferroptosis following cystine deprivation. To determine whether loss of viability was related to low levels of GPX4, we expressed Flag-GPX4 in EGFR mutant cells. Indeed, ectopic expression of GPX4 significantly increased viability following deprivation of cystine (Figure 3J). Thus, downregulation of GPX4 plays a key role in sensitizing EGFR mutant HME cells to ferroptosis.

Synchronous Cell Death in EGFR Mutant HME Cells Involves Generation and Release of Hydrogen Peroxide

Hydrogen peroxide is implicated in synchronous ferroptosis in kidney tubule epithelia (Linkermann et al., 2014). Media

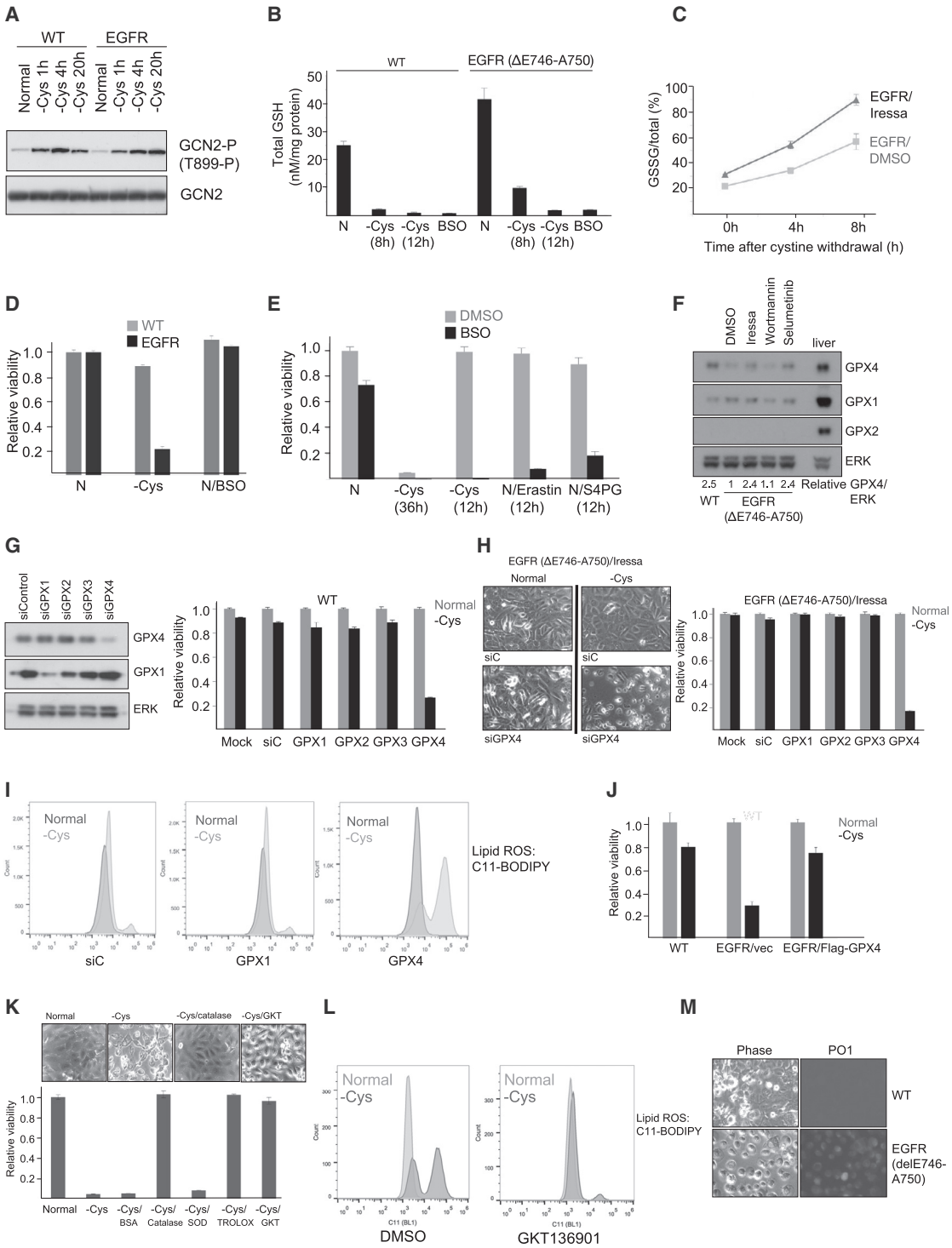

Figure 3. Involvement of Intracellular Cysteine, GPX4, and Hydrogen Peroxide in Sensitivity to Ferroptosis

(A) Immunoblots of cell lysates probed with an antibody to active GCN2 (T899-P). Cells were cultured in normal media for 24 hr (normal) or media lacking cystine for various times.

(B) Histogram of total glutathione levels in WT and EGFR (delE746-A750) cells cultured in normal media for 12 hr (N) or media lacking cystine for 8 or 12 hr. As a positive control, BSO was added to cells for 12 hr to deplete the glutathione pool by inhibiting glutathione synthesis.

(C) Time course of glutathione oxidation (GSSG/total) in EGFR (delE746-A750) treated with vehicle (EGFR/DMSO) or Iressa for 30 hr (EGFR/Iressa). Cells were cultured in media lacking cystine for 4 or 8 hr. Chart displays the average ratio of oxidized glutathione (GSSG) to total glutathione (GSH+GSSG) of three biological replicates.

(legend continued on next page)

containing soluble catalase similarly rescued viability of EGFR mutant HME cells (Figure 3K). Hydrogen peroxide is produced by NADPH oxidase 4 (NOX4) (Takac et al., 2011). A NOX4 inhibitor (GKT136901; Laleu et al., 2010) also rescued viability, to the same degree as addition of catalase (Figure 3K), and inhibited lipid ROS generation (Figure 3L). NOX4 expression was also increased in EGFR mutant HME cells and downregulated by both EGFR and MAPK inhibition (Figure S3E). Finally, increased accumulation of hydrogen peroxide was detected following deprivation of cystine in EGFR mutant cells (Dickinson et al., 2010; Figure 3M). Thus, hydrogen peroxide contributes to loss of viability of EGFR mutant HME cells deprived of cystine.

NSCLC Tumor Cell Lines Exhibit a Targetable Sensitivity to Ferroptosis

Mutations in the EGF receptor are found in non-small-cell lung cancers (NSCLCs) (Pao et al., 2004) that are sensitive to tyrosine kinase inhibitors (TKIs) (Paez et al., 2004). We removed cystine from NSCLC cell lines and measured viability and MAPK activation. Of nine NSCLC cell lines tested, three with the highest MAPK signaling (Figure S4A) demonstrated significant loss of viability following withdrawal of cystine (Figures 4A and S4B). In H3255 cells (EGFR L858R mutant), sensitivity was reversed by either EGFR or MAPK inhibition, whereas in Calu-6 cells (KRAS Q61K mutant), sensitivity was reversed by MAPK, but not EGFR, inhibition (Figure S4C). Thus, in NSCLC cell lines, the magnitude of MAPK activation is an important determinant in sensitization to ferroptosis, rather than the nature of the specific oncogenic driver that promotes MAPK signaling. In NCI-NH1650 cells (EGFR delE746-A750), viability was restored by addition of either α-tocopherol, the ferroptosis inhibitor Fer-1 (Figure 4B), or Iressa (data not shown) following cystine depletion, indicating that ferroptosis and EGFR signaling were responsible for loss of viability. Surprisingly, however, MEK inhibition in these cells did not rescue viability following cystine depletion (data not shown). Thus, MAPK activation may not invariably promote sensitivity to ferroptosis, and other unknown EGFR-dependent signaling pathway(s) can substitute.

Survival after treatment with TKIs in NSCLC is typically less than 1 year, with patients developing secondary EGFR mutations (Stewart et al., 2015). We therefore sought to determine whether EGFR mutant NSCLC cells might be responsive to low levels of cystine, potentially offering additional therapeutic options utilizing a novel cystine/cysteine-degrading enzyme (cyst(e)inase; AECase) engineered from cystathionine-γ-lyase (Cramer et al., 2017). Addition of AECase reduced viability in both HME delE746-A750 EGFR or NCI-NH1650 cells (Figures 4C and 4D) and induced widespread uptake of Sytox Green (Figure 4D; Movie S2). Finally, we injected mice bearing established NCI-NH1650 xenografts with AECase. Mirroring the in vitro results, tumor growth was significantly retarded in AECase-treated groups ($p = 0.0001$; Figure 4E). AECase-treated mice were also found to upregulate expression of COX2 (Figure 4F), indicating that they had experienced cystine depletion and initiated ferroptosis within the tumor (Yang et al., 2014). Thus, inhibition of tumor growth can be achieved in tumors sensitive to ferroptosis by enzymatic degradation of cystine/cysteine in vivo.

DISCUSSION

Cell death by ferroptosis has been implicated in diverse processes (Yang and Stockwell, 2016). Previous data indicated that ferroptosis could be induced preferentially in cells overexpressing mutant RAS oncoproteins (Dixon et al., 2012; Dolma et al., 2003; Yang and Stockwell, 2008) and in some sensitive cell lines could be blocked by MAPK inhibition (Yagoda et al., 2007).

(D) Cell viability of WT (light bars) or EGFR (delE746-A750; dark bars) HME cells. Histogram represents the average viability ± SD of cells cultured for 24 hr in normal media (N), normal media containing 200 μM BSO (N/BSO), or media lacking cystine (−Cys).

(E) Cell viability of EGFR (delE746-A750) pre-treated for 18 hr with DMSO vehicle (light bars) or 200 μM BSO (dark bars) in normal media (N), in normal media containing erastin (N/Erastin), or S4PG (N/S4PG) for 12 hr or following removal of cystine for 36 or 12 hr. Histogram represents the average viability ± SD of cells cultured in normal media (assigned a value of 1).

(F) Immunoblots of WT and EGFR (delE746-A750) cell lysates probed for GPX4, GPX1, GPX2, and ERK in the presence or absence of inhibitors. Relative GPX4/ERK was calculated using ImageJ from scanned autoradiographs of three biological replicates, with the ratio in EGFR (delE746-A750) cells assigned a value of 1.

(G) (Left panels) Immunoblots of WT HME lysates probed for GPX4, GPX1, and ERK1/2. (Right) Histogram of cell viability of HME cells cultured in normal media (light bars) or media lacking cystine (dark bars) for 24 hr. Histogram represents the average viability ± SD following knockdown GPX1–4. Results were expressed for each condition separately, with viability in normal media assigned a value of 1.

(H) (Left panels) Phase-contrast micrographs of EGFR (delE746-A750) HME cells following transfection with control (siC) or GPX4 small interfering RNAs (siRNAs) (siGPX4) and treated with Iressa for 30 hr followed by culture in normal media or media lacking cystine for 24 hr. (Right) Histogram is viability ± SD after knockdown of GPX1–4 in Iressa-treated EGFR (delE746-A750) cells. Viability of cells cultured in normal media (light bars) or media lacking cystine (dark bars) were determined. Results were expressed for each condition separately, with viability in normal media assigned the arbitrary value of 1.

(I) FACS analyses of lipid ROS in WT HME cells following knockdown of GPX1 and GPX4. Dark traces, cells cultured in normal media; light traces, cells cultured in media lacking cystine for 12 hr.

(J) Histogram is shown representing the average viability ± SD following overexpression of Flag-GPX4 (Mannes et al., 2011) in EGFR (delE746-A750) cells. Viability of WT HME cells or vector- or GPX4-transfected EGFR (delE746-A750) cells cultured in normal media (light bars) or media lacking cystine (dark bars) for 16 hr is shown. Results were expressed for each condition separately, with viability in normal media assigned a value of 1.

(K) (Top panels) Phase-contrast micrographs of EGFR (delE746-A750) HME cells in normal media or media deprived of cystine alone or containing catalase or GKT136901. (Bottom) Histogram representing the average viability ± SD of EGFR (delE746-A750) HME cells cultured for 24 hr in normal media (normal; assigned a value of 1) or media lacking cystine alone (−Cys) or with BSA, catalase, superoxide dismutase (SOD), Trolox, or GKT136901 added is shown.

(L) FACS analyses of lipid ROS in EGFR (delE746-A750) HME cells following treatment with the NOX4 inhibitor GKT136901. Dark traces, cells cultured in media lacking cystine; light traces, cells cultured in normal media.

(M) Live images of hydrogen peroxide detected with PO1. (Left) Phase-contrast images of WT and EGFR (delE746-A750) cells deprived of cystine for 24 hr and incubated with PO1 (right panels) are shown.

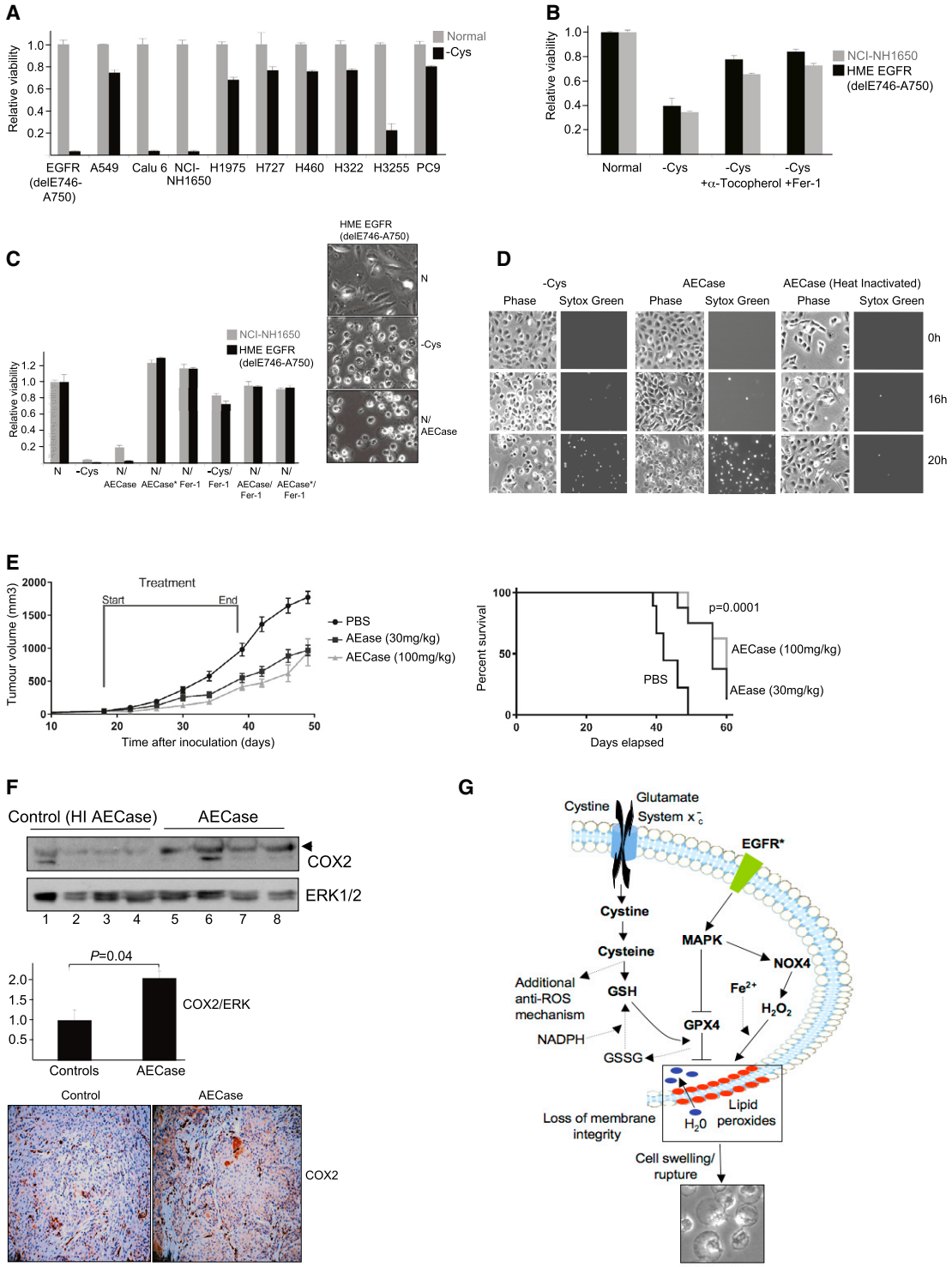

Figure 4. Ferroptosis Is Induced in Some NSCLC Cell Lines and Inhibits Tumor Growth

(A) Histogram of viability ± SD of EGFR (delE746-A750) HME and NSCLC cell lines cultured for 72 hr in normal media (light bars) or media lacking cystine (dark bars). Results were expressed for each cell line separately, with viability in normal media assigned a value of 1.

(B) Histogram representing the average viability ± SD of EGFR (delE746-A750) HME (dark bars) or NCI-NH1650 (light bars) cultured for 72 hr in normal media (N), normal media containing ferrostatin (N/Fer-1), media lacking cystine (−Cys), or media lacking cystine in the presence of α-tocopherol or Fer-1. Results were expressed for each cell line separately, with viability in normal media assigned a value of 1.

(legend continued on next page)

We identify here a selective cell death of EGFR mutant cells deprived of the amino acid cystine. Death was associated with synchronous loss of plasma membrane integrity. By a variety of criteria, this mode of cell death is ferroptosis. In our model (Figure 4G), active MAPK signaling downstream of active EGFR can sensitize cells to ferroptosis upon cystine depletion. Sensitization involves both impaired detoxification of lipid peroxides, due to reduced expression of GPX4, and generation of hydrogen peroxide, via NOX4. A major consequence of lipid peroxidation is loss of impermeability to water (Lis et al., 2011; Wong-Ekkabut et al., 2007), providing an explanation for the characteristic cell swelling and rupture we observe.

Sensitivity to induction of ferroptosis or cystine deprivation is likely to be modulated by additional, and possibly MAPK-independent, mechanisms, such as the utilization of the sulfur-containing amino acid methionine via the transsulfuration pathway (Hayano et al., 2016). Our results suggest, however, the possibility of exploiting ferroptosis sensitivity in a translational manner. Tumors with sustained MAPK activation, as found in NSCLC, are likely to respond to cystine depletion in vivo by inducing ferroptosis. Our results indicate that an enzymatic approach (Cramer et al., 2017) may be effective in reducing cystine levels in vivo, inducing ferroptosis. Collectively, our work indicates that it might therefore be possible both to identify tumors exhibiting increased sensitivity to ferroptosis and to treat them via cycles of cystine depletion.

EXPERIMENTAL PROCEDURES

Cell Culture and Treatments

The hTERT-HME cell lines were a kind gift from Prof. Alberto Bardelli (Institute for Cancer Research and Treatment, IRCC). Cells were grown in DMEM media as described (Di Nicolantonio et al., 2008). To deprive individual amino acids, cells were washed once in DMEM media lacking all amino acids (−AA) and switched to specific amino-acid-free media. DMEM media used for deprivation were made from powdered AA-free DMEM (US Biological), with 10% dialyzed fetal bovine serum (FBS) and additives (Di Nicolantonio et al., 2008). Amino acids (Sigma) at 50× concentrations in water were added at 1× concentration. All amino acids were added for complete media (+AA), with individual DMEM amino acids omitted to generate single amino-acid-deficient media. For the initial screen, 30,000 cells were plated per well in a 96-well plate and switched after 24 hr to depleted amino acid media for 72 hr. Viability was assessed in the initial screen using Calcein AM (Molecular Probes; ThermoFisher) at 1 μM for 2 hr and cells fixed for 15 min with 4% paraformaldehyde prior to analysis on a Genios plate reader and in all other experiments using the CellTiter-Glo luminescence assay (Promega).

FACS Analysis

To detect ROS, 200,000 cells were plated in 6-well plates and switched to cystine-deprived media for 12 hr prior to FACS analysis. CMDCFDA and C11-BODIPY581/591 (Molecular Probes; Thermo Fisher) were used to detect total and lipid ROS, respectively. Following deprivation of cystine for 12 hr, cells were washed with PBS, loaded with either CMDCFDA (10 μM) or C11 BODIPY (2 μM) in DPBS for 30 min, trypsinized with 0.25% Trypsin-EDTA, resuspended in PBS with 1% FBS, and analyzed using an Attune NxT flow cytometer (Thermo Fisher). Dyes were excited using a blue 488-nm laser, and emission was recorded on BL1 (530/30) for a minimum of 5,000 cells per sample.

Xenograft Tumor Model

2.5× 105 NCI-H1650 cells were inoculated 1:1 in Matrigel: PBS (100 mL) by subcutaneous injection into eight non-obese diabetic (NOD) severe combined immunodeficiency (SCID) gamma male mice. Tumors were allowed to engraft and grow for 30 days (tumor volume averaged ~200 mm3) and mice treated by intraperitoneal (i.p.) injection with 100 mg/kg cyst(e)inase or 100 mg/kg heat-inactivated cyst(e)inase (n = 4 ea.) on day 30, with a second dose given on day 33. Mice were necropsied 24 hr after the second dose. For analyses of COX2, control and treated tumors were excised and one-half preserved in 10% neutral buffered formalin for immunohistochemistry (IHC) and the remaining half frozen in liquid nitrogen for protein extraction. For IHC, anti-COX2 from Abcam (ab15191) was used with DAB detection.

Statistical Analyses

Data were analyzed using Microsoft Excel or GraphPad Prism software (GraphPad) and are presented as mean values ± SEM. All viability data represent the mean of three biological replicates/condition. Statistical analyses were performed using two-sided Student's t test. For Kaplan-Meier plots, statistical significance was analyzed by the log rank (Mantel-Cox) test. Sample variance was not significant between control and treatment groups prior to study onset. Significance was set at $p < 0.05$. All data are representative of at least two independent experiments.

SUPPLEMENTAL INFORMATION

Supplemental Information includes Supplemental Experimental Procedures, four figures, and two movies and can be found with this article online at http://dx.doi.org/10.1016/j.celrep.2017.02.054.

(C) (Left) Histogram of viability ± SD of EGFR (delE746-A750) HME (dark bars) or NCI-NH1650 (light bars) cells cultured for 48 hr in normal media (N) (assigned a value of 1), media lacking cystine (−Cys), normal media containing 125 nM cyst(e)inase (AECase) on its own (N/AECase) or with Fer-1 (N/AECase/Fer-1), or normal media containing 125 nM heat-inactivated AECase on its own (N/AECase*) or with Fer-1 (N/AECase*/Fer-1). (Right) Phase-contrast micrographs of EGFR (delE746-A750) HME cells in normal media, media deprived of cysteine, or normal media containing 125 nM AECase (N/AECase) for 48 hr are shown.

(D) Phase contrast (left), and Sytox Green (right) micrographs of H1650 cells deprived of cystine (left panels), treated with 125 nM AECase (middle panels), or treated with heat-inactivated AECase (right panels) for various times up to 20 hr.

(E) Cyst(e)inase (AECase) administration inhibits tumor growth in a NCI-NH1650 xenograft mouse model. (Left panel) Increase in tumor volume following i.p. administration of PBS control (dark circles) or 30 mg/kg (dark squares) or 100 mg/kg (light triangles) AECase is shown. Start and end of treatment times are also shown. (Right panel) Kaplan-Meier plots of median survival of PBS- or AECase-treated tumor-bearing mice are shown.

(F) (Top panels) Immunoblots of lysates from control (lanes 1–4) or AECase-treated (lanes 5–8) NCI-NH1650 xenograft lysates probed to detect COX2 (arrowhead). (Middle histogram) Quantification of relative COX2/ERK in control or AECase-treated groups is shown. $p = 0.04$; $n = 4$. (Bottom micrographs) Images of COX2 staining in control and AECase-treated tumors are shown.

(G) Model depicting role of activated EGFR in determining sensitivity to ferroptosis. Activated EGFR (EGFR*) stimulates MAPK signaling, reducing expression of GPX4 and inducing expression of NOX4. GPX4 utilizes reduced glutathione (GSH) derived from cystine transported via the System x_c^- cystine-glutamate exchanger to detoxify membrane lipid peroxides (red), generating oxidized glutathione (GSSG). GSSG is recycled to GSH using reducing equivalents derived from NADPH (dashed line). Cystine can be reduced to generate cysteine that can independently detoxify ROS and may have additional functions (e.g., Briggs et al., 2016). Lipid peroxides are generated from hydrogen peroxide (H_2O_2, derived from NOX4) and iron (Fe^{2+}), producing hydroxyl radicals that initiate lipid peroxidation. Lipid peroxidation leads to loss of membrane integrity, allowing uptake of water, cell swelling, and rupture.

AUTHOR CONTRIBUTIONS

I.P. and X.W. performed cell viability assays, inhibitor and siRNA treatments, FACS analyses, and immunoblotting experiments; T.C. performed immunofluorescence and assays of GJIC; C.L. performed amino acid analyses; D.M. assisted with methods of quantification; S.L.C., K.T., and E.S. designed and performed the xenograft experiments; R.R., O.E.P., and M.J.S. provided NSCLC cell lines; and S.W.R. provided AECase. R.F.L. conceived the study and wrote the paper.

ACKNOWLEDGMENTS

The p442-PL1 Flag-Strep-HA-GPx4 (Flag-GPX4) was from Marcus Konrad. We are grateful for the support of John Neoptolemos and to Cancer Research UK and the Liverpool Pancreatic Biomedical Research Unit for funding (to I.P. and R.F.L.). R.R. was supported by the Cancer Treatment and Research Trust and M.J.S. by the Imperial National Institute for Health Research (NIHR) Biomedical Research Centre and Imperial CRUK/NIHR Experimental Cancer Medicine Centre. X.W. and R.F.L. acknowledge support from North West Cancer Research and D.M. from the Medical Research Council. E.S. is an inventor on intellectual property related to part of this work, and E.S. and S.W.R. have an equity interest in Aeglea Biotherapeutics.

Received: August 8, 2016
Revised: November 30, 2016
Accepted: February 16, 2017
Published: March 14, 2017

REFERENCES

Barbie, D.A., Tamayo, P., Boehm, J.S., Kim, S.Y., Moody, S.E., Dunn, I.F., Schinzel, A.C., Sandy, P., Meylan, E., Scholl, C., et al. (2009). Systematic RNA interference reveals that oncogenic KRAS-driven cancers require TBK1. Nature *462*, 108–112.

Briggs, K.J., Koivunen, P., Cao, S., Backus, K.M., Olenchock, B.A., Patel, H., Zhang, Q., Signoretti, S., Gerfen, G.J., Richardson, A.L., et al. (2016). Paracrine Induction of HIF by Glutamate in Breast Cancer: EglN1 Senses Cysteine. Cell *166*, 126–139.

Cramer, S.L., Saha, A., Liu, J., Tadi, S., Tiziani, S., Yan, W., Triplett, K., Lamb, C., Alters, S.E., Rowlinson, S., et al. (2017). Systemic depletion of L-cyst(e)ine with cyst(e)inase increases reactive oxygen species and suppresses tumor growth. Nat. Med. *23*, 120–127.

Di Nicolantonio, F., Arena, S., Gallicchio, M., Zecchin, D., Martini, M., Flonta, S.E., Stella, G.M., Lamba, S., Cancelliere, C., Russo, M., et al. (2008). Replacement of normal with mutant alleles in the genome of normal human cells unveils mutation-specific drug responses. Proc. Natl. Acad. Sci. USA *105*, 20864–20869.

Dickinson, B.C., Huynh, C., and Chang, C.J. (2010). A palette of fluorescent probes with varying emission colors for imaging hydrogen peroxide signaling in living cells. J. Am. Chem. Soc. *132*, 5906–5915.

Dixon, S.J., Lemberg, K.M., Lamprecht, M.R., Skouta, R., Zaitsev, E.M., Gleason, C.E., Patel, D.N., Bauer, A.J., Cantley, A.M., Yang, W.S., et al. (2012). Ferroptosis: an iron-dependent form of nonapoptotic cell death. Cell *149*, 1060–1072.

Dolma, S., Lessnick, S.L., Hahn, W.C., and Stockwell, B.R. (2003). Identification of genotype-selective antitumor agents using synthetic lethal chemical screening in engineered human tumor cells. Cancer Cell *3*, 285–296.

Friedmann Angeli, J.P., Schneider, M., Proneth, B., Tyurina, Y.Y., Tyurin, V.A., Hammond, V.J., Herbach, N., Aichler, M., Walch, A., Eggenhofer, E., et al. (2014). Inactivation of the ferroptosis regulator Gpx4 triggers acute renal failure in mice. Nat. Cell Biol. *16*, 1180–1191.

Gao, M., Monian, P., Quadri, N., Ramasamy, R., and Jiang, X. (2015). Glutaminolysis and transferrin regulate ferroptosis. Mol. Cell *59*, 298–308.

Gonzalez, G.G., and Byus, C.V. (1991). Effect of dietary arginine restriction upon ornithine and polyamine metabolism during two-stage epidermal carcinogenesis in the mouse. Cancer Res. *51*, 2932–2939.

Gromer, S., Arscott, L.D., Williams, C.H., Jr., Schirmer, R.H., and Becker, K. (1998). Human placenta thioredoxin reductase. Isolation of the selenoenzyme, steady state kinetics, and inhibition by therapeutic gold compounds. J. Biol. Chem. *273*, 20096–20101.

Hayano, M., Yang, W.S., Corn, C.K., Pagano, N.C., and Stockwell, B.R. (2016). Loss of cysteinyl-tRNA synthetase (CARS) induces the transsulfuration pathway and inhibits ferroptosis induced by cystine deprivation. Cell Death Differ. *23*, 270–278.

Hinnebusch, A.G. (2005). Translational regulation of GCN4 and the general amino acid control of yeast. Annu. Rev. Microbiol. *59*, 407–450.

Hirayama, A., Kami, K., Sugimoto, M., Sugawara, M., Toki, N., Onozuka, H., Kinoshita, T., Saito, N., Ochiai, A., Tomita, M., et al. (2009). Quantitative metabolome profiling of colon and stomach cancer microenvironment by capillary electrophoresis time-of-flight mass spectrometry. Cancer Res. *69*, 4918–4925.

Holleman, A., den Boer, M.L., Kazemier, K.M., Janka-Schaub, G.E., and Pieters, R. (2003). Resistance to different classes of drugs is associated with impaired apoptosis in childhood acute lymphoblastic leukemia. Blood *102*, 4541–4546.

Kami, K., Fujimori, T., Sato, H., Sato, M., Yamamoto, H., Ohashi, Y., Sugiyama, N., Ishihama, Y., Onozuka, H., Ochiai, A., et al. (2013). Metabolomic profiling of lung and prostate tumor tissues by capillary electrophoresis time-of-flight mass spectrometry. Metabolomics *9*, 444–453.

Laleu, B., Gaggini, F., Orchard, M., Fioraso-Cartier, L., Cagnon, L., Houngninou-Molango, S., Gradia, A., Duboux, G., Merlot, C., Heitz, F., et al. (2010). First in class, potent, and orally bioavailable NADPH oxidase isoform 4 (Nox4) inhibitors for the treatment of idiopathic pulmonary fibrosis. J. Med. Chem. *53*, 7715–7730.

Linkermann, A., Skouta, R., Himmerkus, N., Mulay, S.R., Dewitz, C., De Zen, F., Prokai, A., Zuchtriegel, G., Krombach, F., Welz, P.S., et al. (2014). Synchronized renal tubular cell death involves ferroptosis. Proc. Natl. Acad. Sci. USA *111*, 16836–16841.

Lis, M., Wizert, A., Przybylo, M., Langner, M., Swiatek, J., Jungwirth, P., and Cwiklik, L. (2011). The effect of lipid oxidation on the water permeability of phospholipids bilayers. Phys. Chem. Chem. Phys. *13*, 17555–17563.

Mandal, P.K., Seiler, A., Perisic, T., Kölle, P., Banjac Canak, A., Förster, H., Weiss, N., Kremmer, E., Lieberman, M.W., Bannai, S., et al. (2010). System x(c)- and thioredoxin reductase 1 cooperatively rescue glutathione deficiency. J. Biol. Chem. *285*, 22244–22253.

Mannes, A.M., Seiler, A., Bosello, V., Maiorino, M., and Conrad, M. (2011). Cysteine mutant of mammalian GPx4 rescues cell death induced by disruption of the wild-type selenoenzyme. FASEB J. *25*, 2135–2144.

Maser, R.L., Magenheimer, B.S., and Calvet, J.P. (1994). Mouse plasma glutathione peroxidase. cDNA sequence analysis and renal proximal tubular expression and secretion. J. Biol. Chem. *269*, 27066–27073.

Pader, I., Sengupta, R., Cebula, M., Xu, J., Lundberg, J.O., Holmgren, A., Johansson, K., and Arnér, E.S. (2014). Thioredoxin-related protein of 14 kDa is an efficient L-cystine reductase and S-denitrosylase. Proc. Natl. Acad. Sci. USA *111*, 6964–6969.

Paez, J.G., Jänne, P.A., Lee, J.C., Tracy, S., Greulich, H., Gabriel, S., Herman, P., Kaye, F.J., Lindeman, N., Boggon, T.J., et al. (2004). EGFR mutations in lung cancer: correlation with clinical response to gefitinib therapy. Science *304*, 1497–1500.

Pao, W., Miller, V., Zakowski, M., Doherty, J., Politi, K., Sarkaria, I., Singh, B., Heelan, R., Rusch, V., Fulton, L., et al. (2004). EGF receptor gene mutations are common in lung cancers from "never smokers" and are associated with sensitivity of tumors to gefitinib and erlotinib. Proc. Natl. Acad. Sci. USA *101*, 13306–13311.

Parmenter, T.J., Kleinschmidt, M., Kinross, K.M., Bond, S.T., Li, J., Kaadige, M.R., Rao, A., Sheppard, K.E., Hugo, W., Pupo, G.M., et al. (2014). Response

of BRAF-mutant melanoma to BRAF inhibition is mediated by a network of transcriptional regulators of glycolysis. Cancer Discov. *4*, 423–433.

Pines, G., Köstler, W.J., and Yarden, Y. (2010). Oncogenic mutant forms of EGFR: lessons in signal transduction and targets for cancer therapy. FEBS Lett. *584*, 2699–2706.

Possik, P.A., Müller, J., Gerlach, C., Kenski, J.C.N., Huang, X., Shahrabi, A., Krijgsman, O., Song, J.-Y., Smit, M.A., Gerritsen, B., et al. (2014). Parallel in vivo and in vitro melanoma RNAi dropout screens reveal synthetic lethality between hypoxia and DNA damage response inhibition. Cell Rep. *9*, 1375–1386.

Scholl, C., Fröhling, S., Dunn, I.F., Schinzel, A.C., Barbie, D.A., Kim, S.Y., Silver, S.J., Tamayo, P., Wadlow, R.C., Ramaswamy, S., et al. (2009). Synthetic lethal interaction between oncogenic KRAS dependency and STK33 suppression in human cancer cells. Cell *137*, 821–834.

Scott, L., Lamb, J., Smith, S., and Wheatley, D.N. (2000). Single amino acid (arginine) deprivation: rapid and selective death of cultured transformed and malignant cells. Br. J. Cancer *83*, 800–810.

Son, J., Lyssiotis, C.A., Ying, H., Wang, X., Hua, S., Ligorio, M., Perera, R.M., Ferrone, C.R., Mullarky, E., Shyh-Chang, N., et al. (2013). Glutamine supports pancreatic cancer growth through a KRAS-regulated metabolic pathway. Nature *496*, 101–105.

Stewart, E.L., Tan, S.Z., Liu, G., and Tsao, M.S. (2015). Known and putative mechanisms of resistance to EGFR targeted therapies in NSCLC patients with EGFR mutations-a review. Transl. Lung Cancer Res. *4*, 67–81.

Takac, I., Schröder, K., Zhang, L., Lardy, B., Anilkumar, N., Lambeth, J.D., Shah, A.M., Morel, F., and Brandes, R.P. (2011). The E-loop is involved in hydrogen peroxide formation by the NADPH oxidase Nox4. J. Biol. Chem. *286*, 13304–13313.

Tallal, L., Tan, C., Oettgen, H., Wollner, N., McCarthy, M., Helson, L., Burchenal, J., Karnofsky, D., and Murphy, M.L. (1970). E. coli L-asparaginase in the treatment of leukemia and solid tumors in 131 children. Cancer *25*, 306–320.

Wong-Ekkabut, J., Xu, Z., Triampo, W., Tang, I.M., Tieleman, D.P., and Monticelli, L. (2007). Effect of lipid peroxidation on the properties of lipid bilayers: a molecular dynamics study. Biophys. J. *93*, 4225–4236.

Yagoda, N., von Rechenberg, M., Zaganjor, E., Bauer, A.J., Yang, W.S., Fridman, D.J., Wolpaw, A.J., Smukste, I., Peltier, J.M., Boniface, J.J., et al. (2007). RAS-RAF-MEK-dependent oxidative cell death involving voltage-dependent anion channels. Nature *447*, 864–868.

Yang, W.S., and Stockwell, B.R. (2008). Synthetic lethal screening identifies compounds activating iron-dependent, nonapoptotic cell death in oncogenic-RAS-harboring cancer cells. Chem. Biol. *15*, 234–245.

Yang, W.S., and Stockwell, B.R. (2016). Ferroptosis: death by lipid peroxidation. Trends Cell Biol. *26*, 165–176.

Yang, W.S., SriRamaratnam, R., Welsch, M.E., Shimada, K., Skouta, R., Viswanathan, V.S., Cheah, J.H., Clemons, P.A., Shamji, A.F., Clish, C.B., et al. (2014). Regulation of ferroptotic cancer cell death by GPX4. Cell *156*, 317–331.

Cell Reports, Volume *18*

Supplemental Information

Oncogene-Selective Sensitivity to Synchronous Cell Death following Modulation of the Amino Acid Nutrient Cystine

Ioannis Poursaitidis, Xiaomeng Wang, Thomas Crighton, Christiaan Labuschagne, David Mason, Shira L. Cramer, Kendra Triplett, Rajat Roy, Olivier E. Pardo, Michael J. Seckl, Scott W. Rowlinson, Everett Stone, and Richard F. Lamb

Supplemental Figures and Legends, Tables, Experimental Procedures, and References

Figure S1 (related to Figure 1).

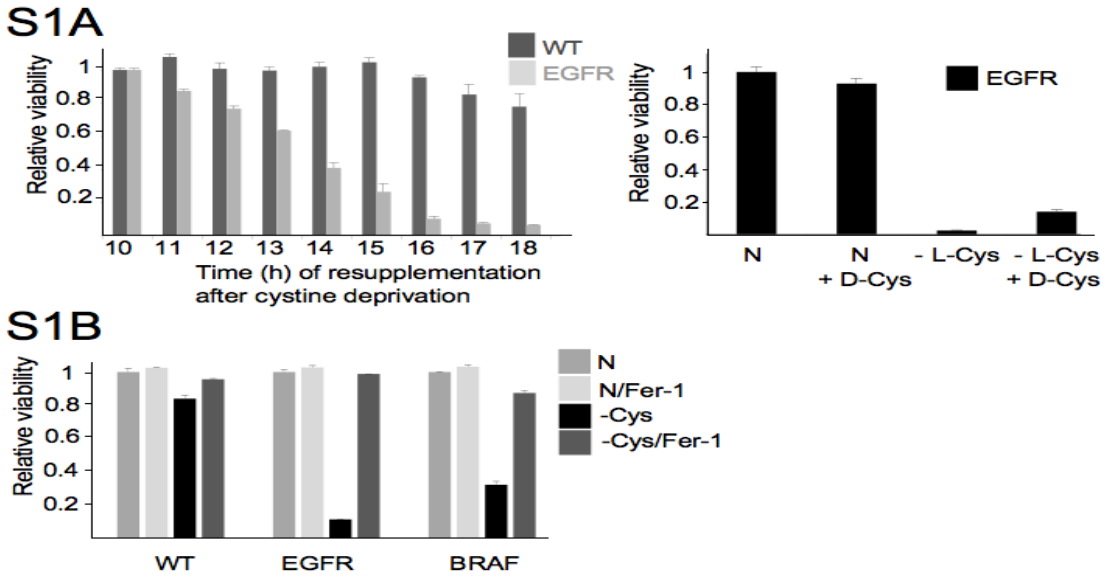

A, Left, cell viability following deprivation of cystine, followed by cystine resupplmentation, in wild type (WT) and EGFR (delE746-A750) HME cells. Histogram represents the average viability ± standard deviation (SD) of three biological replicates using CellTitre-Glo, relative to removal of cystine for 10 hours (assigned an arbitrary value of 1). Results are typical of experiments performed twice. Right, cell viability in normal media (N) or following deprivation of cystine (- L-Cys), followed by D-cystine addition (+ D-Cys, added at 150μM), in EGFR (delE746-A750) HME cells. Histogram represents the average viability ± standard deviation (SD) of three biological replicates using CellTitre-Glo with viability in normal media assigned an arbitrary value of 1. Results are typical of experiments performed twice.
B, Cell viability in normal media or following deprivation of cystine in the presence or absence of Fer-1 (2μM), in wild type (WT), EGFR (delE746-A750) and BRAF-mutant HME cells. Histogram represents the average viability ± standard deviation (SD) of three biological replicates using CellTitre-Glo, relative to normal media (N, assigned an arbitrary value of 1). Results are typical of experiments performed twice.

Figure S2 (related to Figure 2).

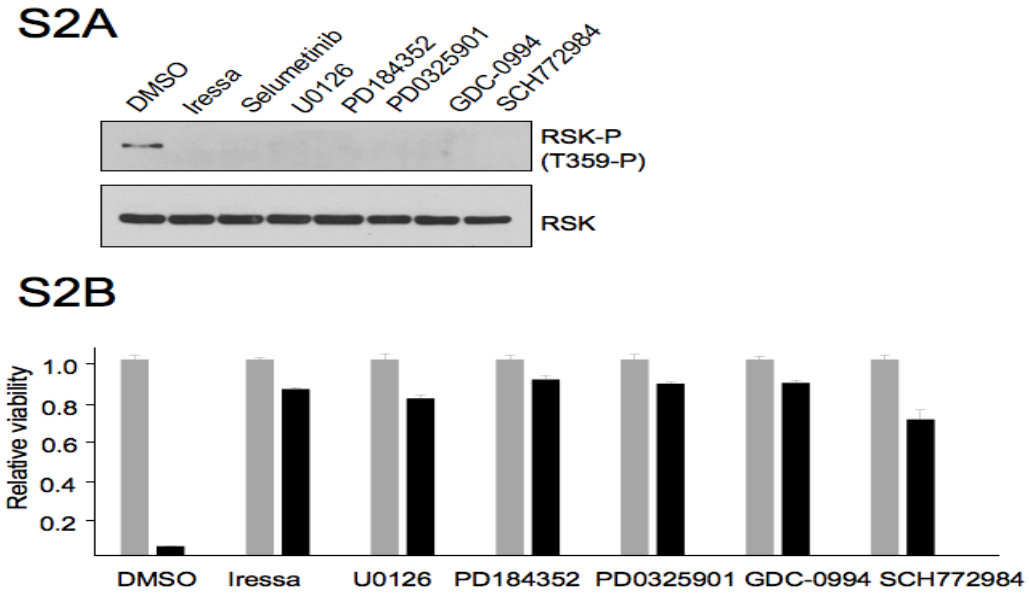

S2C

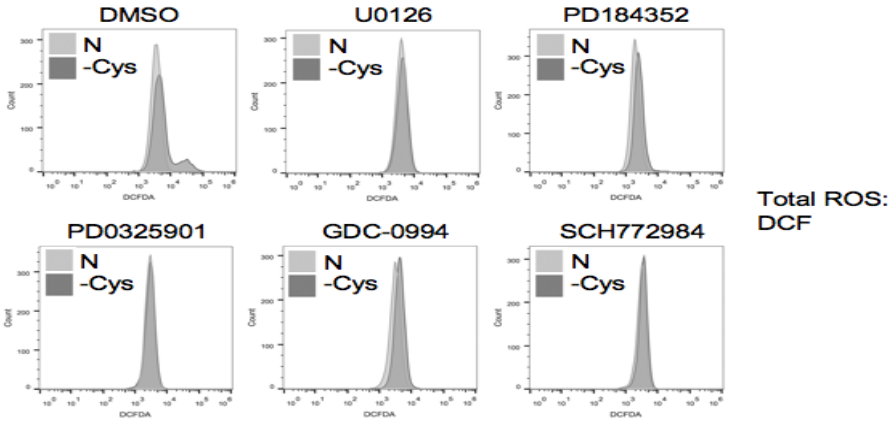

S2D

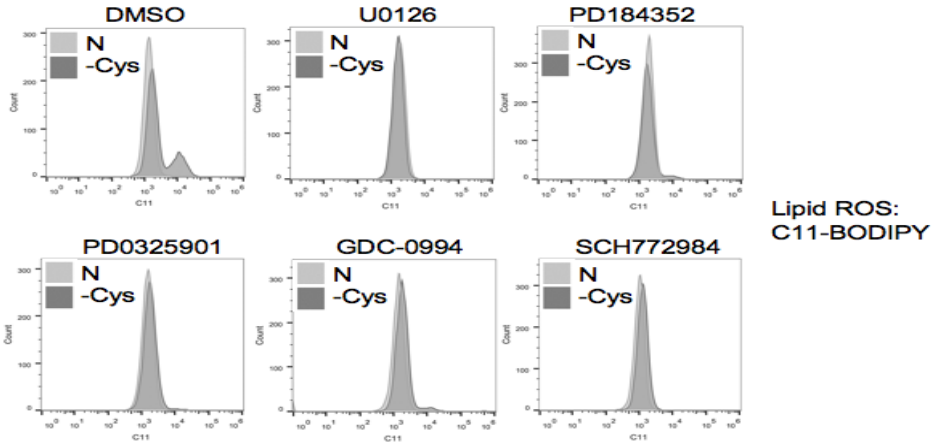

A, Immunoblots of EGFR (delE746-A750) HME cell lysates probed with antibodies detecting phosphorylated RSK (T359-P), and total RSK from cells cultured in normal media in the presence of vehicle (DMSO), Iressa, and the indicated MEK and ERK signalling inhibitors added for a total of 30 hours.
B, Cell viability of EGFR (delE746-A750) HME cells. Histogram represents the average viability ± standard deviation (SD) of three biological replicates cultured in normal media (assigned an arbitrary value of 1), or media lacking cystine for 24 hours measured using CellTitre-Glo, in the presence or absence of Iressa, and the indicated MEK and ERK signalling inhibitors added for a total of 30 hours prior to cystine deprivation. Results were expressed for each inhibitor condition separately, with viability in normal media assigned the arbitrary value of 1. Results are typical of experiments performed twice.
C, FACS analyses of total ROS in EGFR (delE746-A750) cells following treatment with MEK and ERK inhibitors. Dark traces, cells cultured in normal media; light traces, cells cultured in media lacking cystine for 12 hours. Results are typical of experiments performed twice.
D, FACS analyses of lipid ROS in EGFR (delE746-A750) cells following treatment with MEK and ERK inhibitors. Dark traces, cells cultured in normal media; light traces, cells cultured in media lacking cystine for 12 hours. Results are typical of experiments performed twice.

Figure S3 (related to Figure 3).

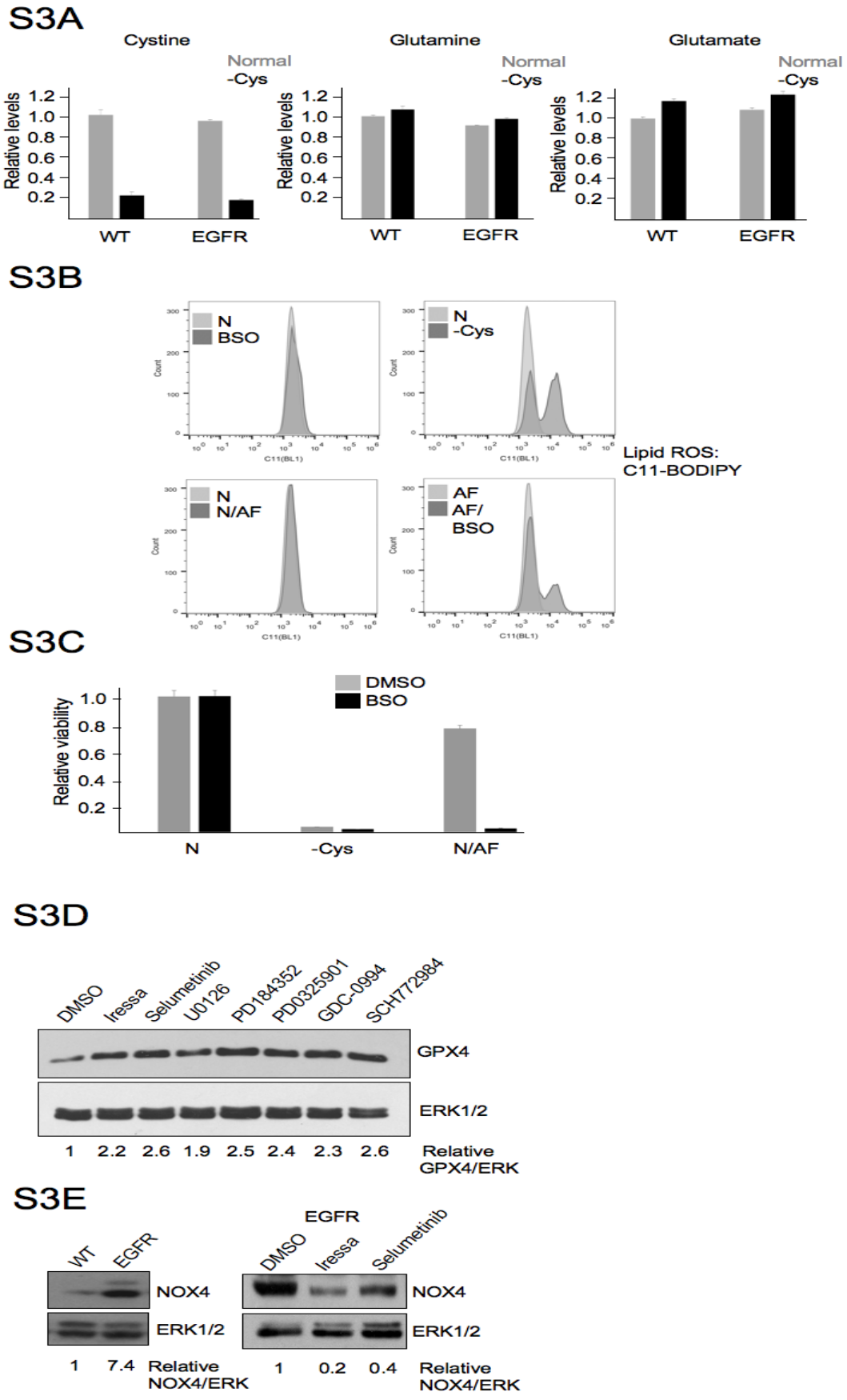

A, Amino acid analysis of steady-state levels of cystine, glutamine and glutamate measured by LC-MS in wild type and EGFR (delE746-A750) cells cultured in normal media (Normal, light bars) or media lacking cystine for for 8 hours. Histogram represents the average values ± standard deviation (SD) of three biological replicates with the level in normal media of wild type HME cells assigned the arbitrary value of 1. Results are typical of experiments performed twice.
B, FACS analyses of lipid ROS in EGFR (delE746-A750) cells following treatment for 14 hours with BSO alone or with auranofin. Light traces, cells cultured in normal media or normal media containing auranofin for 14 hours (N or N+AF); dark traces, cells treated for 14 hours with BSO alone (BSO), or cultured in media lacking cystine for 14 hours (-Cys) or treated with auranofin for 14h (N+AF) or treated auranofin for 6 hours following pretreatment with BSO for 14h. Results are typical of experiments performed twice.
C, Cell viability of EGFR (delE746-A750) HME cells. Viability of cells cultured for 18 hours in normal media containing DMSO vehicle (light bars), or containing 200μM BSO (BSO, dark bars), followed by deprivation of cystine, or treatment with auronofin for 24 hours, with viability measured using CellTitre-Glo. Histogram represents the average values ± standard deviation (SD) of three biological replicates with the level in normal media assigned the arbitrary value of 1. Results are typical of experiments performed twice.
D, Immunoblots of EGFR (delE746-A750) HME cell lysates probed with antibodies detecting GPX4, and ERK1/2 from cells cultured in normal media in the presence of vehicle (DMSO), Iressa, and the indicated MEK and ERK signalling inhibitors added for a total of 30 hours. Relative GPX4 was calculated using ImageJ from scanned autoradiographs with the ratio in DMSO-treated EGFR (delE746-A750) HME cells assigned the arbitrary value of 1.
E, Left, Immunoblots of wild type and EGFR (delE746-A750) HME cell lysates probed with antibodies detecting NOX4 and ERK1/2; right, from EGFR (delE746-A750) cells cultured in normal media in the presence of vehicle (DMSO), Iressa, or Selumetinib for a total of 30 hours. Relative NOX4 was calculated using ImageJ from scanned autoradiographs with the ratio in wild type or DMSO-treated EGFR (delE746-A750) HME cells assigned the arbitrary value of 1 in each case.

Figure S4 (related to Figure 4).

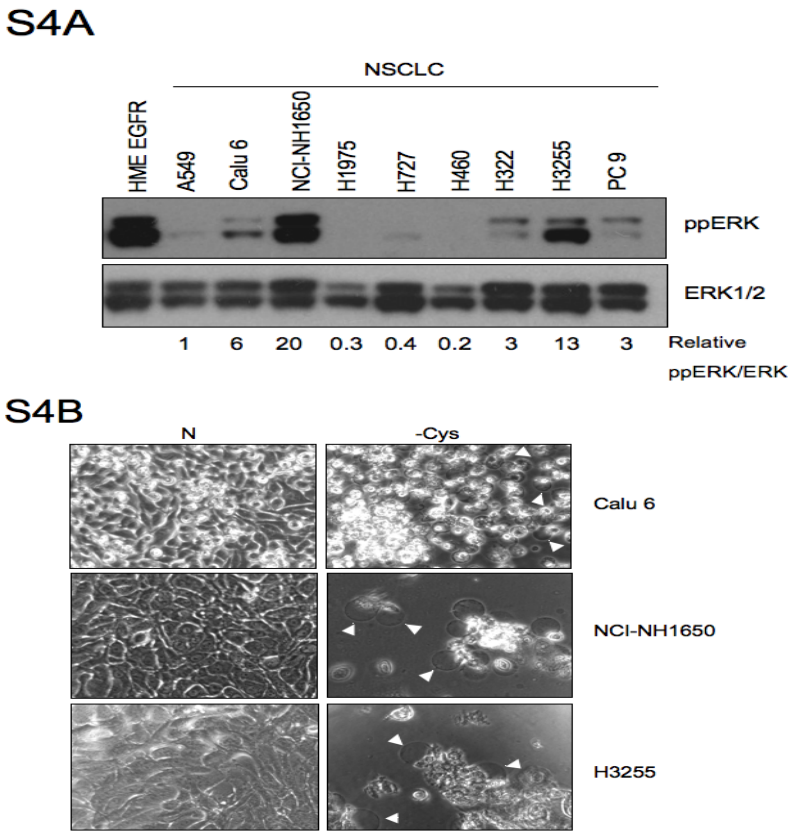

S4C

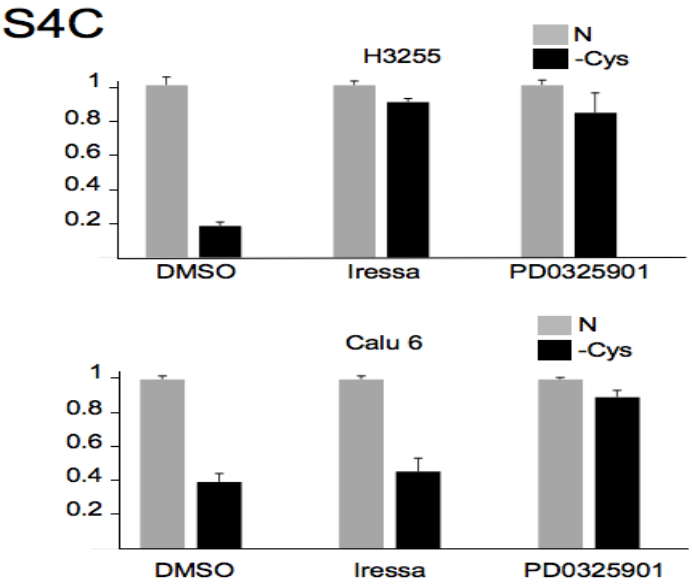

S4D

			Allred Score		
	Sample #	IHC	Intensity	Proportion	Global
controls	1	COX2	1	1	2
	2	COX2	1	1	2
	3	COX2	1	1	2
	4	COX2	1	1	2
AECase	5	COX2	1	2	3
	6	COX2	1	2	3
	7	COX2	1	5	6
	8	COX2	1	2	3

A, Immunoblots of EGFR (delE746-A750) HME and various NSCLC cell lysates probed with antibodies detecting ppERK and ERK1/2 Relative ppERK was calculated using ImageJ from scanned autoradiographs with the ratio in A549 assigned the arbitrary value of 1.
B, Left panels, phase contrast micrographs of Calu 6, NCI-NH1650 and H3255 cells followed by culture in normal media (left) or media lacking cystine for 72 hours (right). Arrowheads indicate balloon-like membrane extensions of cells that have undergone ferroptosis.
C, Histogram representing the average viability ± standard deviation (SD) of three biological replicates of Calu 6 and H3255 cells cultured for 30 hours in normal media containing DMSO, Iressa or PD0325901 (light bars) or media lacking cystine for 48 hours (dark bars). Results were expressed for each condition separately, with viability in normal media assigned the arbitrary value of 1. Results are typical of experiments performed twice.
D, Pathological evaluation of COX2 immunostaining in mice treated with heat-inactivated AECase (Controls 1-4) or AECase (5-8).

Supplemental Movies S1, S2
Movie S1 (related to Figure 1).
Withdrawal of cystine leads to synchronous cell death. EGFR (delE746-A750) HME cells grown to confluency in normal media were switched to media lacking cystine from which point images were collected by time-lapse phase contrast microscopy. Frames were taken every 5 mins for 24 hrs and saved for playback at 100ms intervals.
Movie S2 (related to Figure 4):
Withdrawal of cystine leads to synchronous cell death in NSCLC cells. NCI-NH1650 cells grown to confluency in normal media were switched to media lacking cystine and containing Sytox Green, from which point images were collected. Individual frames were obtained every 5 minutes in phase contrast and green fluorescence channels with Sytox Green used at 0.5μM concentration (Molecular Probes, Thermofisher) for 24 hrs and saved for dual-channel playback at 100ms interval.

Supplemental Experimental Procedures

siRNA knockdown and plasmid transfection

Lipofectamine 2000 (Invitrogen, ThermoFisher) was used for siRNA transfection of HME cells. 500,000 cells were plated in 6-well plates and either mock-transfected or transfected with either siCtrl or siGenome Smartpool siRNAs (Dharmacon, GE Lifesciences) to GPX1, GPX2, GPX3 and GPX4 at a final concentration of 50nM. A day after transfection cells were trypsinized and split between a 12-well plate well, with 250,000 cells, and 6 96-well plate wells, with 25,000 cells per well, for immunoblotting and viability assay respectively 3 days post transfection. For plasmid transfections, 5x105 EGFR-mutant cells were transfected in 3cm dishes with 5μg of Flag-GPX4 (p442-PL1 Flag-Strep-HA-GPX4, (Mannes et al., 2011)) or control vector using Lipofectamine 2000 (Invitrogen, ThermoFisher). 48h after transfection wild type or transfected cells were trypsinised and replated in a 96 well plate at 20,000 cells per well and the viability experiment performed following 16h of cystine deprivation.

Western Blotting

Cells were lysed in lysis buffer (50 mM Tris-HCl, pH 7.5, 1mM EGTA, 1 mM EDTA, 1% Triton X-100, 1mM Na3VO4, 50 mM NaF, 50 mM β-glycerolphosphate, 0.27M sucrose, 0.1% beta-mercaptoethanol, Complete protease inhibitors (Roche). Protein concentration was determined using Bradford assay reagent (Biorad) and 25 μg of total protein was loaded per sample.

Commercial antibodies used were: pEGFR Y1068 (Cell Signalling Technologies) #3777, EGFR (Cell Signalling Technologies) #2232, pAKT S473 (Cell Signalling Technologies) #9271, AKT (Upstate, EMD Millipore) 07-416, ppERK (Cell Signalling Technologies) #4370, ERK1/2 (Santa Cruz Biotech) sc-94, GCN2-P T899 (Epitomics, Abcam) 2425-1, GCN2 (Cell Signalling Technologies) #3302, GPX1 (R&D systems, Biotechne) AF3798, GPX2 (R&D systems, Biotechne) MAB5470, GPX4 (Abcam) ab125066, COX2 (Cayman Chemicals) #160112, NOX4 (Abcam) #, RSK-P Thr 359-P and RSK (Cell Signaling Technologies) 133303 and b-catenin (Transduction Labs) C19220.

GJIC scrape loading dye transfer assay

Confluent EGFR-mutant cells growing in 24-well plates were incubated with 1μM Iressa, 1μM Wortmannin, 5μM Selumetinib or 1μM DMSO (control) for 30h. Cells were then washed in Ca++-deficient PBS and transferred to PBS containing 0.5mg/mL Lucifer yellow (Sigma), 10mM glucose, 30mM HEPES buffer (Thermofisher), 0.1% BSA, 0.5 mg/mL rhodamine-dextran (Molecular Probes) and either vehicle (100mM DMSO) or 100mM carbenoxolone (Sigma). Wells were wounded via two perpendicular scratches to the monolayer and incubated for 15 minutes before being washed with PBS and fixed in 4% paraformaldehyde. Areas close to the wound margin were imaged for green fluorescence at 20X magnification using an AMG EVOS digital inverted microscope and the extent of Lucifer yellow infiltration into the monolayer was analysed using ImageJ software.

Confocal immunofluorescence microscopy

Confluent HME WT and EGFR-mutant cells growing on glass coverslips were incubated with 1μM Iressa, 1μM Wortmannin, 5μM Selumetinib or 1μM DMSO for 30h. Immunofluorescence labelling of β-catenin was undertaken as previously described (Menon et al.) and cells were imaged at 63X magnification with a confocal laser scanning microscope (Zeiss 3I LSM 800).

Additional cell treatments and microscopy

The timelapse microscope used was a Nikon TE-300 [motorised with Sutter filter wheels and a Conix block changer] equipped with a 10X phase contrast [PC] objective, encased in a Perspex 37°C incubation chamber with an insert for multi-well plates flushed with humidified, 5% CO2 air. Green fluorescence was acquired through a Nikon B-2A block split into Sutter filter wheels and a Conix block changer. Images were collected using a Hamamatsu Orca AG camera, with MicroManager software (Edelstein et al., 2010), converting time series to an ImageJ readable format using in-house software. Cells were plated in a 6-well plate at 500,000 cells per well and grown for 3 days prior to media switch to cystine-deprived media. The plates were then transferred in the microscope stage maintained at 37°C with 5% CO2. Individual frames were obtained every 5 minutes in phase contrast and green fluorescence channels for detection of nonviable cells by Sytox Green nuclear staining used at 0.5μM concentration (Molecular Probes, Thermofisher). Apoptosis inhibitor z-VAD-fMK (Selleck) was

used at 50μM. ROS scavengers Idebenone and α-Tocopherol (Sigma) were used at 1μM and 30μM respectively. Induction of ferroptotic death by erastin (Cayman Chemical) was achieved at a concentration of 2.5μg/ml. Other inhibitors used were catalase used at 1000U/ml (Sigma), superoxide dismutase used at 100U/ml (Sigma), NOX4 inhibitor GKT136901 (Aobious) at 20μM and the water-soluble vitamin E analogue Trolox at 5μM (Sigma). To determine ferroptotic cell death 10,000 EGFR HME cells were plated in a 96-well plate and allowed to grow for 3 days prior to a media shift in the presence of inhibitors of ferroptotic or apoptotic death or scavengers of reactive oxygen species. Ferroptosis inhibitor Ferrostatin1 (Fer-1, Sigma) was used at 2μM and iron chelator deferroxamine (DFO, Sigma) was used at 100μM.

To image H2O2 confluent cells were transferred to cystine-deficient media for 24 hours. Cells were then incubated with 10μM Peroxy Orange 1 (PO1, Tocris Bioscience) for 60 minutes before being washed three times in dPBS and imaged immediately at 20X magnification using an AMG EVOS digital inverted microscope. To inhibit signal transduction downstream of EGFR cells were treated for 24h prior to media switch with EGFR inhibitor Iressa (Tocris) at 1μM, MEK inhibitor Selumetinib (Selleckchem) at 5μM, PI3K inhibitor Wortmannin (Sigma) at 1μM. DMSO (Sigma) was used as a vehicle control. Additional MEK and ERK inhibitors used were U0126 (Calbiochem, 10μM), PD184352 (Sigma, 10μM), PD0325901 (Selleckchem, 1μM), GDC-0994 (ERK inhibitor, Selleckchem, 5μM) and SCH772984 (ERK inhibitor, Cayman Chemicals, 5μM). Following pre-treatment for 24h cells were switched to either complete or cysteine deficient media containing the same concentration of inhibitors for 12h prior to analysis. Wortmannin was re-added at the same concentration 1hour before collection. Auranofin and S4PG were from Santa Cruz and used at 1 and 100μM, respectively. NOX4 inhibitor GKT136901 (Aobious) was used at 20μM. PEGylated AECase was used at a final concentration of 125nM, heat inactivation was performed by incubation at 95 ^{0}C for 7 minutes, followed by brief centrifugation for 5 mins at 13,000 rpm.

For cystine titration cells were plated in triplicate cells at a final concentration of 30,000 per well in a 96-well plate (NUNC, Thermofisher) and the following day complete synthetic media containing or lacking EGF was serially diluted with DMEM lacking cystine to achieve a range of decreasing cystine concentrations. After 24h of treatment viability was determined using the CellTitre-Glo assay (Promega). An equal volume of CellTitre-Glo reagent was added and the plate was vortexed at 1000 rpm for 2 minutes to allow cell lysis. The plates were then analysed on a Tecan Genios plate reader.

GSH/GSSG quantification

For the quantification of cellular reduced (GSH) and oxidised (GSSG) glutathione the method described by Rahman et al (Rahman et al., 2006) was used, which utilises the reaction of GSH with 5,5′-Dithiobis (2-nitrobenzoic acid) (DTNB) that leads to the production of the 5′-thio-2-nitrobenzoic acid (TNB) chromophore measured at 412nm (Tietze, 1969). $1x10^{6}$ cells were plated in 6-well plates (Greiner) and the following day treated with 200μM of BSO or switched to cystine deficient media for 8h. Cells were then washed in cold PBS, trypsinised and resuspended in 0.2ml of ice-cold extraction buffer (0.1% Triton-X and 0.6% sulfosalicylic acid in 0.1 potassium phosphate buffer with 5 mM EDTA disodium salt, pH 7.5 (KPE)). Cells were then freeze-thawed four times (liquid nitrogen - 37°C water bath) and lysates subsequently centrifuged at 3000g for 5 min at 4 °C and supernatants collected. Protein concentrations were measured using a Bradford assay in order to express GSH and GSSG levels as nM/mg of total protein. Total glutathione (Total [GSH] = [GSH] + 2 × [GSSG]) was measured via a kinetic assay based on the reaction of DTNB with GSH and the recycling reaction by the enzyme glutathione reductase (GR) (Sigma) which in the presence of β-Nicotinamide adenine dinucleotide 2′-phosphate (β-NAPDH, Sigma) can reduce GSSG to GSH (Guntherb.H and Rost, 1966). The rate of TNB formation was calculated by measuring 415nm absorbance in a plate reader every 30sec. GSH standards of known concentration were made from stock GSH (Sigma) and their rate of formation used to create a standard curve. For measurement of GSSG, 2-vinylpyridine (Aldrich) is added to cell lysates at 18.5 mM for 1h creating a covalent bond with GSH therefore allowing measurement only of GSSG. Excess 2-vinylpyridine was then neutralised with 75mM triethanolamine (Sigma) for 30 min (Griffith, 1980). Levels of GSSG were determined by applying the recycling assay and measuring rate of formation of TNB as described above but using GSSG standard samples (Sigma) to create a standard curve. Reduced glutathione (GSH) could be then determined by subtraction of oxidised (GSSG) from Total glutathione (Total [GSH] = [GSH] + 2 × [GSSG]). All measurements were done in triplicate. Glutathione synthesis inhibitor buthionine sulfoximine (BSO, Santa Cruz Biotechnologies) was used at 200μM.

COX2 immunostaining

After immunostaining the slides were evaluated by a pathologist (Precision Pathology) for percentage of postive tumor cells in the sample and intensity of the staining after excluding all non-tumor cells and non-specific staining of any background stroma or other components. Each sample was assessed using the Allred scoring matrix that generates a global score ranging from 0 to 8. The global score was composed of stain intensity from 1 to 3+ and a proportion score of 0 to 5 (5 being the highest) that was apportioned based on the raw percentge of positive target cells in the sample. The percent of positive target cells is an average of at least 5 fields examined at 200X. The system was originally developed for scoring intensity and proportion of staining estimation of samples using a matrix of scores over a range of both intensity and proportion of positive cells in a given sample. Scores range from 0 to 3 for intensity and from 0 to 5 for proportion with the global score being intensity + proportion. Thus a sample where the staining is weak and is present in 15% of the target cells on the slide, the score would be 1 (intensity) + 1 (proportion) for a global score of 2. Conversely, a sample that showed strong diffuse staining of 98% of target cells would have a score of 8 (3 intensity + 5 proportion).

Amino acid anayses by Liquid Chromatography-Mass Spectrometry (LC-MS)

Wild type and EGFR-mutant HME cells were seeded in seven dishes at $5x10^6$/10cm dish for each cell line and the next day washed 3 times using DPBS. Three dishes of each cell line were then switched to –cys media, or normal media for 4h. The last dish was used to count cells from both cell lines to ensure similar cell number per volume of extraction buffer. Metabolites were extracted in a polar solvent (50% methanol, 30% acetonitrile, 20% water) and centrifuged to precipitate and remove any proteins present, in preparation for LC-MS analysis. The volume of extraction solution was calculated from the cell count with 1-2 x 10^6 cells/ml. The cell metabolites were extracted from the samples by placing the cell culture plates on a rocking shaker at 0-4°C for 5 minutes. The extraction solution from each well was then pipetted into a microcentrifuge tube and shaken in the Thermomixer (Thermomixer comfort, Eppendorf AG, Hamburg, Germany) at high speed of 1400rpm at 0-4°C for 10 minutes. The microcentrifuge tubes were then centrifuged at 16,100 x g for 10 minutes at 0-4°C. The supernatants are transferred to glass HPLC vials and kept at -75°C prior to LC-MS analysis. Hydrophilic Interaction Liquid Chromatography with a Sequant ZIC-pHILIC column (2.1 × 150 mm, 5 μm) (Merck) was used to separate amino acids before detection with high-resolution, accurate-mass (HR/AM) Mass Spectrometry using an Orbitrap Exactive in line with an Accela autosampler and an Accela 600 pump (Thermo Scientific). The elution buffers used to elute the analytes were Acetonitrile (ACN) for A and 20 mM $(NH_4)_2CO_3$, 0.1% NH_4OH in H_2O for B. A linear gradient was programed starting from 80% A and ending at 20% A after 20 min at a flow rate of 200ul/min, followed by wash (20% A) and re-equilibration (80% A) steps at a flow rate of 400 μl/min. An Electrospray Ionization (ESI) probe was used to achieve ionization and the mass spectrometer operated in full-scan and polar-switching mode with the positive voltage at 4.5 kV and negative voltage at 3.5 kV. Metabolite identification and data analysis were done using TraceFinder ^{TM} software (Thermo Scientific).

Supplemental References

Edelstein, A., Amodaj, N., Hoover, K., Vale, R., and Stuurman, N. (2010). Computer control of microscopes using Manager. Current protocols in molecular biology / edited by Frederick M Ausubel [et al] *Chapter 14*, Unit 14.20.

Griffith, O.W. (1980). Determination of glutathione and glutathione disulfide using glutathione-reductase and 2-vinylpyridine. Analytical Biochemistry *106*, 207-212.

Guntherb H., and Rost, J. (1966). True oxidized glutathione content of red blood cells obtained by new enzymic and paper chromatographic methods. Analytical biochemistry *15*, 205-&.

Rahman, I., Kode, A., and Biswas, S.K. (2006). Assay for quantitative determination of glutathione and glutathione disulfide levels using enzymatic recycling method. Nature Protocols *1*, 3159-3165.

Tietze, F. (1969). Enzymic method for quantitative determination of nanogram amounts of total and oxidized glutathione - applications to mammalian blood and other tissues. Analytical Biochemistry *27*, 502.

References

1. Hanahan, D. and R.A. Weinberg, *Hallmarks of cancer: the next generation.* Cell, 2011. **144**(5): p. 646-74.
2. Hennessy, B.T., et al., *Exploiting the PI3K/AKT pathway for cancer drug discovery.* Nat Rev Drug Discov, 2005. **4**(12): p. 988-1004.
3. Lemmon, M.A. and J. Schlessinger, *Cell signaling by receptor tyrosine kinases.* Cell, 2010. **141**(7): p. 1117-34.
4. Sharma, S.V., et al., *Epidermal growth factor receptor mutations in lung cancer.* Nat Rev Cancer, 2007. **7**(3): p. 169-81.
5. Shigematsu, H., et al., *Clinical and biological features associated with epidermal growth factor receptor gene mutations in lung cancers.* J Natl Cancer Inst, 2005. **97**(5): p. 339-46.
6. Maheswaran, S., et al., *Detection of mutations in EGFR in circulating lung-cancer cells.* N Engl J Med, 2008. **359**(4): p. 366-77.
7. Wilson, C.Y. and P. Tolias, *Recent advances in cancer drug discovery targeting RAS.* Drug Discov Today, 2016. **21**(12): p. 1915-1919.
8. Leonetti, A., et al., *BRAF in non-small cell lung cancer (NSCLC): Pickaxing another brick in the wall.* Cancer Treat Rev, 2018. **66**: p. 82-94.
9. Nicholson, K.M. and N.G. Anderson, *The protein kinase B/Akt signalling pathway in human malignancy.* Cell Signal, 2002. **14**(5): p. 381-95.
10. Bailey, M.H., et al., *Comprehensive Characterization of Cancer Driver Genes and Mutations.* Cell, 2018. **173**(2): p. 371-385 e18.
11. Fumarola, C., et al., *Targeting PI3K/AKT/mTOR pathway in non small cell lung cancer.* Biochem Pharmacol, 2014. **90**(3): p. 197-207.
12. Zimmermann, S. and K. Moelling, *Phosphorylation and regulation of Raf by Akt (protein kinase B).* Science, 1999. **286**(5445): p. 1741-4.
13. Mayer, I.A. and C.L. Arteaga, *The PI3K/AKT Pathway as a Target for Cancer Treatment.* Annu Rev Med, 2016. **67**: p. 11-28.
14. Martini, M., et al., *PI3K/AKT signaling pathway and cancer: an updated review.* Ann Med, 2014. **46**(6): p. 372-83.

15. Zhang, X., et al., *An allosteric mechanism for activation of the kinase domain of epidermal growth factor receptor.* Cell, 2006. **125**(6): p. 1137-49.
16. Du, Z. and C.M. Lovly, *Mechanisms of receptor tyrosine kinase activation in cancer.* Mol Cancer, 2018. **17**(1): p. 58.
17. Nicholson, R.I., J.M. Gee, and M.E. Harper, *EGFR and cancer prognosis.* Eur J Cancer, 2001. **37 Suppl 4**: p. S9-15.
18. Lynch, T.J., et al., *Activating mutations in the epidermal growth factor receptor underlying responsiveness of non-small-cell lung cancer to gefitinib.* N Engl J Med, 2004. **350**(21): p. 2129-39.
19. Sequist, L.V., et al., *Genotypic and histological evolution of lung cancers acquiring resistance to EGFR inhibitors.* Sci Transl Med, 2011. **3**(75): p. 75ra26.
20. Balak, M.N., et al., *Novel D761Y and common secondary T790M mutations in epidermal growth factor receptor-mutant lung adenocarcinomas with acquired resistance to kinase inhibitors.* Clin Cancer Res, 2006. **12**(21): p. 6494-501.
21. Hobbs, G.A., C.J. Der, and K.L. Rossman, *RAS isoforms and mutations in cancer at a glance.* J Cell Sci, 2016. **129**(7): p. 1287-92.
22. Bos, J.L., H. Rehmann, and A. Wittinghofer, *GEFs and GAPs: critical elements in the control of small G proteins.* Cell, 2007. **129**(5): p. 865-77.
23. Yan, J., et al., *Ras isoforms vary in their ability to activate Raf-1 and phosphoinositide 3-kinase.* J Biol Chem, 1998. **273**(37): p. 24052-6.
24. Prior, I.A., P.D. Lewis, and C. Mattos, *A comprehensive survey of Ras mutations in cancer.* Cancer Res, 2012. **72**(10): p. 2457-67.
25. McCormick, F., *K-Ras protein as a drug target.* J Mol Med (Berl), 2016. **94**(3): p. 253-8.
26. Engelman, J.A., *Targeting PI3K signalling in cancer: opportunities, challenges and limitations.* Nat Rev Cancer, 2009. **9**(8): p. 550-62.
27. Samuels, Y., et al., *High frequency of mutations of the PIK3CA gene in human cancers.* Science, 2004. **304**(5670): p. 554.
28. Stambolic, V., et al., *Regulation of PTEN transcription by p53.* Mol Cell, 2001. **8**(2): p. 317-25.

29. Siempelkamp, B.D., et al., *Molecular mechanism of activation of class IA phosphoinositide 3-kinases (PI3Ks) by membrane-localized HRas.* J Biol Chem, 2017. **292**(29): p. 12256-12266.
30. Vanhaesebroeck, B. and D.R. Alessi, *The PI3K-PDK1 connection: more than just a road to PKB.* Biochem J, 2000. **346 Pt 3**: p. 561-76.
31. Sarbassov, D.D., et al., *Phosphorylation and regulation of Akt/PKB by the rictor-mTOR complex.* Science, 2005. **307**(5712): p. 1098-101.
32. Mayo, L.D. and D.B. Donner, *A phosphatidylinositol 3-kinase/Akt pathway promotes translocation of Mdm2 from the cytoplasm to the nucleus.* Proc Natl Acad Sci U S A, 2001. **98**(20): p. 11598-603.
33. Manning, B.D., et al., *Identification of the tuberous sclerosis complex-2 tumor suppressor gene product tuberin as a target of the phosphoinositide 3-kinase/akt pathway.* Mol Cell, 2002. **10**(1): p. 151-62.
34. Cargnello, M. and P.P. Roux, *Activation and function of the MAPKs and their substrates, the MAPK-activated protein kinases.* Microbiol Mol Biol Rev, 2011. **75**(1): p. 50-83.
35. Karoulia, Z., E. Gavathiotis, and P.I. Poulikakos, *New perspectives for targeting RAF kinase in human cancer.* Nat Rev Cancer, 2017. **17**(11): p. 676-691.
36. Khan, A.Q., et al., *RAS-mediated oncogenic signaling pathways in human malignancies.* Semin Cancer Biol, 2018.
37. Dhillon, A.S., et al., *MAP kinase signalling pathways in cancer.* Oncogene, 2007. **26**(22): p. 3279-90.
38. Davies, H., et al., *Mutations of the BRAF gene in human cancer.* Nature, 2002. **417**(6892): p. 949-54.
39. Roskoski, R., *MEK1/2 dual-specificity protein kinases: structure and regulation.* Biochem Biophys Res Commun, 2012. **417**(1): p. 5-10.
40. Roskoski, R., *ERK1/2 MAP kinases: structure, function, and regulation.* Pharmacol Res, 2012. **66**(2): p. 105-43.
41. Raman, M., W. Chen, and M.H. Cobb, *Differential regulation and properties of MAPKs.* Oncogene, 2007. **26**(22): p. 3100-12.

42. Ma, L., et al., *Phosphorylation and functional inactivation of TSC2 by Erk implications for tuberous sclerosis and cancer pathogenesis.* Cell, 2005. **121**(2): p. 179-93.
43. Zhang, W. and H.T. Liu, *MAPK signal pathways in the regulation of cell proliferation in mammalian cells.* Cell Res, 2002. **12**(1): p. 9-18.
44. Roux, P.P., et al., *Tumor-promoting phorbol esters and activated Ras inactivate the tuberous sclerosis tumor suppressor complex via p90 ribosomal S6 kinase.* Proc Natl Acad Sci U S A, 2004. **101**(37): p. 13489-94.
45. von Manteuffel, S.R., et al., *4E-BP1 phosphorylation is mediated by the FRAP-p70s6k pathway and is independent of mitogen-activated protein kinase.* Proc Natl Acad Sci U S A, 1996. **93**(9): p. 4076-80.
46. Saxton, R.A. and D.M. Sabatini, *mTOR Signaling in Growth, Metabolism, and Disease.* Cell, 2017. **169**(2): p. 361-371.
47. Guertin, D.A. and D.M. Sabatini, *Defining the role of mTOR in cancer.* Cancer Cell, 2007. **12**(1): p. 9-22.
48. Martelli, A.M., F. Buontempo, and J.A. McCubrey, *Drug discovery targeting the mTOR pathway.* Clin Sci (Lond), 2018. **132**(5): p. 543-568.
49. Guertin, D.A., et al., *Ablation in mice of the mTORC components raptor, rictor, or mLST8 reveals that mTORC2 is required for signaling to Akt-FOXO and PKCalpha, but not S6K1.* Dev Cell, 2006. **11**(6): p. 859-71.
50. Peterson, T.R., et al., *DEPTOR is an mTOR inhibitor frequently overexpressed in multiple myeloma cells and required for their survival.* Cell, 2009. **137**(5): p. 873-86.
51. Kaizuka, T., et al., *Tti1 and Tel2 are critical factors in mammalian target of rapamycin complex assembly.* J Biol Chem, 2010. **285**(26): p. 20109-16.
52. Hara, K., et al., *Raptor, a binding partner of target of rapamycin (TOR), mediates TOR action.* Cell, 2002. **110**(2): p. 177-89.
53. Kim, D.H., et al., *mTOR interacts with raptor to form a nutrient-sensitive complex that signals to the cell growth machinery.* Cell, 2002. **110**(2): p. 163-75.
54. Nojima, H., et al., *The mammalian target of rapamycin (mTOR) partner, raptor, binds the mTOR substrates p70 S6 kinase and 4E-BP1 through their TOR signaling (TOS) motif.* J Biol Chem, 2003. **278**(18): p. 15461-4.

55. Vander Haar, E., et al., *Insulin signalling to mTOR mediated by the Akt/PKB substrate PRAS40.* Nat Cell Biol, 2007. **9**(3): p. 316-23.
56. Sancak, Y., et al., *PRAS40 is an insulin-regulated inhibitor of the mTORC1 protein kinase.* Mol Cell, 2007. **25**(6): p. 903-15.
57. Wang, L., et al., *PRAS40 regulates mTORC1 kinase activity by functioning as a direct inhibitor of substrate binding.* J Biol Chem, 2007. **282**(27): p. 20036-44.
58. Oshiro, N., et al., *Dissociation of raptor from mTOR is a mechanism of rapamycin-induced inhibition of mTOR function.* Genes Cells, 2004. **9**(4): p. 359-66.
59. Sarbassov, D.D., et al., *Rictor, a novel binding partner of mTOR, defines a rapamycin-insensitive and raptor-independent pathway that regulates the cytoskeleton.* Curr Biol, 2004. **14**(14): p. 1296-302.
60. Jacinto, E., et al., *SIN1/MIP1 maintains rictor-mTOR complex integrity and regulates Akt phosphorylation and substrate specificity.* Cell, 2006. **127**(1): p. 125-37.
61. Yang, Q., et al., *Identification of Sin1 as an essential TORC2 component required for complex formation and kinase activity.* Genes Dev, 2006. **20**(20): p. 2820-32.
62. Pearce, L.R., et al., *Identification of Protor as a novel Rictor-binding component of mTOR complex-2.* Biochem J, 2007. **405**(3): p. 513-22.
63. Sciarretta, S., et al., *New Insights Into the Role of mTOR Signaling in the Cardiovascular System.* Circ Res, 2018. **122**(3): p. 489-505.
64. Sarbassov, D.D., et al., *Prolonged rapamycin treatment inhibits mTORC2 assembly and Akt/PKB.* Mol Cell, 2006. **22**(2): p. 159-68.
65. Laplante, M. and D.M. Sabatini, *mTOR signaling in growth control and disease.* Cell, 2012. **149**(2): p. 274-93.
66. Lamming, D.W., et al., *Rapamycin-induced insulin resistance is mediated by mTORC2 loss and uncoupled from longevity.* Science, 2012. **335**(6076): p. 1638-43.
67. Zoncu, R., A. Efeyan, and D.M. Sabatini, *mTOR: from growth signal integration to cancer, diabetes and ageing.* Nat Rev Mol Cell Biol, 2011. **12**(1): p. 21-35.

68. Ma, X.M. and J. Blenis, *Molecular mechanisms of mTOR-mediated translational control.* Nat Rev Mol Cell Biol, 2009. **10**(5): p. 307-18.
69. Burnett, P.E., et al., *RAFT1 phosphorylation of the translational regulators p70 S6 kinase and 4E-BP1.* Proc Natl Acad Sci U S A, 1998. **95**(4): p. 1432-7.
70. Porstmann, T., et al., *SREBP activity is regulated by mTORC1 and contributes to Akt-dependent cell growth.* Cell Metab, 2008. **8**(3): p. 224-36.
71. Duvel, K., et al., *Activation of a metabolic gene regulatory network downstream of mTOR complex 1.* Mol Cell, 2010. **39**(2): p. 171-83.
72. Ben-Sahra, I., et al., *mTORC1 induces purine synthesis through control of the mitochondrial tetrahydrofolate cycle.* Science, 2016. **351**(6274): p. 728-733.
73. Robitaille, A.M., et al., *Quantitative phosphoproteomics reveal mTORC1 activates de novo pyrimidine synthesis.* Science, 2013. **339**(6125): p. 1320-3.
74. Iadevaia, V., R. Liu, and C.G. Proud, *mTORC1 signaling controls multiple steps in ribosome biogenesis.* Semin Cell Dev Biol, 2014. **36**: p. 113-20.
75. Rabinowitz, J.D. and E. White, *Autophagy and metabolism.* Science, 2010. **330**(6009): p. 1344-8.
76. Hosokawa, N., et al., *Nutrient-dependent mTORC1 association with the ULK1-Atg13-FIP200 complex required for autophagy.* Mol Biol Cell, 2009. **20**(7): p. 1981-91.
77. Ganley, I.G., et al., *ULK1.ATG13.FIP200 complex mediates mTOR signaling and is essential for autophagy.* J Biol Chem, 2009. **284**(18): p. 12297-305.
78. Jung, C.H., et al., *ULK-Atg13-FIP200 complexes mediate mTOR signaling to the autophagy machinery.* Mol Biol Cell, 2009. **20**(7): p. 1992-2003.
79. Kim, J., et al., *AMPK and mTOR regulate autophagy through direct phosphorylation of Ulk1.* Nat Cell Biol, 2011. **13**(2): p. 132-41.
80. García-Martínez, J.M. and D.R. Alessi, *mTOR complex 2 (mTORC2) controls hydrophobic motif phosphorylation and activation of serum- and glucocorticoid-induced protein kinase 1 (SGK1).* Biochem J, 2008. **416**(3): p. 375-85.
81. Cantley, L.C., *The phosphoinositide 3-kinase pathway.* Science, 2002. **296**(5573): p. 1655-7.

82. Inoki, K., et al., *TSC2 is phosphorylated and inhibited by Akt and suppresses mTOR signalling.* Nat Cell Biol, 2002. **4**(9): p. 648-57.
83. Potter, C.J., L.G. Pedraza, and T. Xu, *Akt regulates growth by directly phosphorylating Tsc2.* Nat Cell Biol, 2002. **4**(9): p. 658-65.
84. Tee, A.R., et al., *Tuberous sclerosis complex gene products, Tuberin and Hamartin, control mTOR signaling by acting as a GTPase-activating protein complex toward Rheb.* Curr Biol, 2003. **13**(15): p. 1259-68.
85. Dibble, C.C., et al., *TBC1D7 is a third subunit of the TSC1-TSC2 complex upstream of mTORC1.* Mol Cell, 2012. **47**(4): p. 535-46.
86. European Chromosome 16 Tuberous Sclerosis, C., *Identification and characterization of the tuberous sclerosis gene on chromosome 16.* Cell, 1993. **75**(7): p. 1305-15.
87. Inoki, K., et al., *Rheb GTPase is a direct target of TSC2 GAP activity and regulates mTOR signaling.* Genes Dev, 2003. **17**(15): p. 1829-34.
88. Long, X., et al., *Rheb binds and regulates the mTOR kinase.* Curr Biol, 2005. **15**(8): p. 702-13.
89. Inoki, K., T. Zhu, and K.L. Guan, *TSC2 mediates cellular energy response to control cell growth and survival.* Cell, 2003. **115**(5): p. 577-90.
90. Menon, S., et al., *Spatial control of the TSC complex integrates insulin and nutrient regulation of mTORC1 at the lysosome.* Cell, 2014. **156**(4): p. 771-85.
91. Carriere, A., et al., *Oncogenic MAPK signaling stimulates mTORC1 activity by promoting RSK-mediated raptor phosphorylation.* Curr Biol, 2008. **18**(17): p. 1269-77.
92. Carracedo, A., et al., *Inhibition of mTORC1 leads to MAPK pathway activation through a PI3K-dependent feedback loop in human cancer.* J Clin Invest, 2008. **118**(9): p. 3065-74.
93. Gwinn, D.M., et al., *AMPK phosphorylation of raptor mediates a metabolic checkpoint.* Mol Cell, 2008. **30**(2): p. 214-26.
94. Feng, Z., et al., *The regulation of AMPK beta1, TSC2, and PTEN expression by p53: stress, cell and tissue specificity, and the role of these gene products in modulating the IGF-1-AKT-mTOR pathways.* Cancer Res, 2007. **67**(7): p. 3043-53.

95. Sancak, Y., et al., *Ragulator-Rag complex targets mTORC1 to the lysosomal surface and is necessary for its activation by amino acids.* Cell, 2010. **141**(2): p. 290-303.
96. Kim, E., et al., *Regulation of TORC1 by Rag GTPases in nutrient response.* Nat Cell Biol, 2008. **10**(8): p. 935-45.
97. Sancak, Y., et al., *The Rag GTPases bind raptor and mediate amino acid signaling to mTORC1.* Science, 2008. **320**(5882): p. 1496-501.
98. Bar-Peled, L., et al., *Ragulator is a GEF for the rag GTPases that signal amino acid levels to mTORC1.* Cell, 2012. **150**(6): p. 1196-208.
99. Demetriades, C., N. Doumpas, and A.A. Teleman, *Regulation of TORC1 in response to amino acid starvation via lysosomal recruitment of TSC2.* Cell, 2014. **156**(4): p. 786-99.
100. Demetriades, C., M. Plescher, and A.A. Teleman, *Lysosomal recruitment of TSC2 is a universal response to cellular stress.* Nat Commun, 2016. **7**: p. 10662.
101. Buerger, C., B. DeVries, and V. Stambolic, *Localization of Rheb to the endomembrane is critical for its signaling function.* Biochem Biophys Res Commun, 2006. **344**(3): p. 869-80.
102. Saito, K., et al., *Novel role of the small GTPase Rheb: its implication in endocytic pathway independent of the activation of mammalian target of rapamycin.* J Biochem, 2005. **137**(3): p. 423-30.
103. Hao, F., et al., *Rheb localized on the Golgi membrane activates lysosome-localized mTORC1 at the Golgi-lysosome contact site.* J Cell Sci, 2018. **131**(3).
104. Sato, T., et al., *Rheb protein binds CAD (carbamoyl-phosphate synthetase 2, aspartate transcarbamoylase, and dihydroorotase) protein in a GTP- and effector domain-dependent manner and influences its cellular localization and carbamoyl-phosphate synthetase (CPSase) activity.* J Biol Chem, 2015. **290**(2): p. 1096-105.
105. Bar-Peled, L., et al., *A Tumor suppressor complex with GAP activity for the Rag GTPases that signal amino acid sufficiency to mTORC1.* Science, 2013. **340**(6136): p. 1100-6.

106. Zheng, X., et al., *Current models of mammalian target of rapamycin complex 1 (mTORC1) activation by growth factors and amino acids.* Int J Mol Sci, 2014. **15**(11): p. 20753-69.
107. Zoncu, R., et al., *mTORC1 senses lysosomal amino acids through an inside-out mechanism that requires the vacuolar H(+)-ATPase.* Science, 2011. **334**(6056): p. 678-83.
108. Findlay, G.M., et al., *A MAP4 kinase related to Ste20 is a nutrient-sensitive regulator of mTOR signalling.* Biochem J, 2007. **403**(1): p. 13-20.
109. Yan, L., et al., *PP2A T61 epsilon is an inhibitor of MAP4K3 in nutrient signaling to mTOR.* Mol Cell, 2010. **37**(5): p. 633-42.
110. Yoon, M.S., et al., *Class III PI-3-kinase activates phospholipase D in an amino acid-sensing mTORC1 pathway.* J Cell Biol, 2011. **195**(3): p. 435-47.
111. Averous, J., et al., *GCN2 contributes to mTORC1 inhibition by leucine deprivation through an ATF4 independent mechanism.* Sci Rep, 2016. **6**: p. 27698.
112. Hara, K., et al., *Amino acid sufficiency and mTOR regulate p70 S6 kinase and eIF-4E BP1 through a common effector mechanism.* J Biol Chem, 1998. **273**(23): p. 14484-94.
113. Li, Z. and H. Zhang, *Reprogramming of glucose, fatty acid and amino acid metabolism for cancer progression.* Cell Mol Life Sci, 2016. **73**(2): p. 377-92.
114. Sood, R., et al., *A mammalian homologue of GCN2 protein kinase important for translational control by phosphorylation of eukaryotic initiation factor-2alpha.* Genetics, 2000. **154**(2): p. 787-801.
115. Dever, T.E. and A.G. Hinnebusch, *GCN2 whets the appetite for amino acids.* Mol Cell, 2005. **18**(2): p. 141-2.
116. Wek, S.A., S. Zhu, and R.C. Wek, *The histidyl-tRNA synthetase-related sequence in the eIF-2 alpha protein kinase GCN2 interacts with tRNA and is required for activation in response to starvation for different amino acids.* Mol Cell Biol, 1995. **15**(8): p. 4497-506.
117. Dong, J., et al., *Uncharged tRNA activates GCN2 by displacing the protein kinase moiety from a bipartite tRNA-binding domain.* Mol Cell, 2000. **6**(2): p. 269-79.

118. Dever, T.E., et al., *Phosphorylation of initiation factor 2 alpha by protein kinase GCN2 mediates gene-specific translational control of GCN4 in yeast.* Cell, 1992. **68**(3): p. 585-96.

119. Colthurst, D.R., D.G. Campbell, and C.G. Proud, *Structure and regulation of eukaryotic initiation factor eIF-2. Sequence of the site in the alpha subunit phosphorylated by the haem-controlled repressor and by the double-stranded RNA-activated inhibitor.* Eur J Biochem, 1987. **166**(2): p. 357-63.

120. Pathak, V.K., D. Schindler, and J.W. Hershey, *Generation of a mutant form of protein synthesis initiation factor eIF-2 lacking the site of phosphorylation by eIF-2 kinases.* Mol Cell Biol, 1988. **8**(2): p. 993-5.

121. Wek, R.C., H.Y. Jiang, and T.G. Anthony, *Coping with stress: eIF2 kinases and translational control.* Biochem Soc Trans, 2006. **34**(Pt 1): p. 7-11.

122. Vattem, K.M. and R.C. Wek, *Reinitiation involving upstream ORFs regulates ATF4 mRNA translation in mammalian cells.* Proc Natl Acad Sci U S A, 2004. **101**(31): p. 11269-74.

123. Lopez, A.B., et al., *A feedback transcriptional mechanism controls the level of the arginine/lysine transporter cat-1 during amino acid starvation.* Biochem J, 2007. **402**(1): p. 163-73.

124. Siu, F., et al., *ATF4 is a mediator of the nutrient-sensing response pathway that activates the human asparagine synthetase gene.* J Biol Chem, 2002. **277**(27): p. 24120-7.

125. Chuang, H.C., et al., *The kinase GLK controls autoimmunity and NF-κB signaling by activating the kinase PKC-θ in T cells.* Nat Immunol, 2011. **12**(11): p. 1113-8.

126. Zhao, B., et al., *MicroRNA let-7c inhibits migration and invasion of human non-small cell lung cancer by targeting ITGB3 and MAP4K3.* Cancer Lett, 2014. **342**(1): p. 43-51.

127. Lam, D., et al., *MAP4K3 modulates cell death via the post-transcriptional regulation of BH3-only proteins.* Proc Natl Acad Sci U S A, 2009. **106**(29): p. 11978-83.

128. Diener, K., et al., *Activation of the c-Jun N-terminal kinase pathway by a novel protein kinase related to human germinal center kinase.* Proc Natl Acad Sci U S A, 1997. **94**(18): p. 9687-92.

129. Ramjaun, A.R., et al., *Endophilin regulates JNK activation through its interaction with the germinal center kinase-like kinase.* J Biol Chem, 2001. **276**(31): p. 28913-9.
130. Hsu, C.P., et al., *GLK/MAP4K3 overexpression associates with recurrence risk for non-small cell lung cancer.* Oncotarget, 2016. **7**(27): p. 41748-41757.
131. Simabuco, F.M., et al., *p53 and metabolism: from mechanism to therapeutics.* Oncotarget, 2018. **9**(34): p. 23780-23823.
132. Kruiswijk, F., C.F. Labuschagne, and K.H. Vousden, *p53 in survival, death and metabolic health: a lifeguard with a licence to kill.* Nat Rev Mol Cell Biol, 2015. **16**(7): p. 393-405.
133. Fridman, J.S. and S.W. Lowe, *Control of apoptosis by p53.* Oncogene, 2003. **22**(56): p. 9030-40.
134. Deng, Y., S.S. Chan, and S. Chang, *Telomere dysfunction and tumour suppression: the senescence connection.* Nat Rev Cancer, 2008. **8**(6): p. 450-8.
135. Aloni-Grinstein, R., et al., *p53: the barrier to cancer stem cell formation.* FEBS Lett, 2014. **588**(16): p. 2580-9.
136. Lane, D.P., *Cancer. p53, guardian of the genome.* Nature, 1992. **358**(6381): p. 15-6.
137. Puzio-Kuter, A.M., *The Role of p53 in Metabolic Regulation.* Genes Cancer, 2011. **2**(4): p. 385-91.
138. Liberti, M.V. and J.W. Locasale, *The Warburg Effect: How Does it Benefit Cancer Cells?* Trends Biochem Sci, 2016. **41**(3): p. 211-218.
139. Levine, A.J., J. Momand, and C.A. Finlay, *The p53 tumour suppressor gene.* Nature, 1991. **351**(6326): p. 453-6.
140. Vogelstein, B., D. Lane, and A.J. Levine, *Surfing the p53 network.* Nature, 2000. **408**(6810): p. 307-10.
141. Haupt, Y., et al., *Mdm2 promotes the rapid degradation of p53.* Nature, 1997. **387**(6630): p. 296-9.
142. Shieh, S.Y., et al., *DNA damage-induced phosphorylation of p53 alleviates inhibition by MDM2.* Cell, 1997. **91**(3): p. 325-34.
143. Vassilev, L.T., et al., *In vivo activation of the p53 pathway by small-molecule antagonists of MDM2.* Science, 2004. **303**(5659): p. 844-8.

144. Ekshyyan, O., A. Anandharaj, and C.A. Nathan, *Dual PI3K/mTOR inhibitors: does p53 modulate response?* Clin Cancer Res, 2013. **19**(14): p. 3719-21.
145. Elmore, S., *Apoptosis: a review of programmed cell death.* Toxicol Pathol, 2007. **35**(4): p. 495-516.
146. Mishra, A.P., et al., *Programmed Cell Death, from a Cancer Perspective: An Overview.* Mol Diagn Ther, 2018. **22**(3): p. 281-295.
147. Dixon, S.J., et al., *Ferroptosis: an iron-dependent form of nonapoptotic cell death.* Cell, 2012. **149**(5): p. 1060-72.
148. Saraste, A. and K. Pulkki, *Morphologic and biochemical hallmarks of apoptosis.* Cardiovasc Res, 2000. **45**(3): p. 528-37.
149. Lowe, S.W. and A.W. Lin, *Apoptosis in cancer.* Carcinogenesis, 2000. **21**(3): p. 485-95.
150. Czabotar, P.E., et al., *Control of apoptosis by the BCL-2 protein family: implications for physiology and therapy.* Nat Rev Mol Cell Biol, 2014. **15**(1): p. 49-63.
151. Gimenez-Cassina, A. and N.N. Danial, *Regulation of mitochondrial nutrient and energy metabolism by BCL-2 family proteins.* Trends Endocrinol Metab, 2015. **26**(4): p. 165-75.
152. Shamas-Din, A., et al., *BH3-only proteins: Orchestrators of apoptosis.* Biochim Biophys Acta, 2011. **1813**(4): p. 508-20.
153. Westphal, D., et al., *Molecular biology of Bax and Bak activation and action.* Biochim Biophys Acta, 2011. **1813**(4): p. 521-31.
154. Tsujimoto, Y. and S. Shimizu, *Role of the mitochondrial membrane permeability transition in cell death.* Apoptosis, 2007. **12**(5): p. 835-40.
155. Circu, M.L. and T.Y. Aw, *Reactive oxygen species, cellular redox systems, and apoptosis.* Free Radic Biol Med, 2010. **48**(6): p. 749-62.
156. Labi, V. and M. Erlacher, *How cell death shapes cancer.* Cell Death Dis, 2015. **6**: p. e1675.
157. Halliwell, B. and C.E. Cross, *Oxygen-derived species: their relation to human disease and environmental stress.* Environ Health Perspect, 1994. **102 Suppl 10**: p. 5-12.

158. Birben, E., et al., *Oxidative stress and antioxidant defense.* World Allergy Organ J, 2012. **5**(1): p. 9-19.
159. Görlach, A., et al., *Reactive oxygen species, nutrition, hypoxia and diseases: Problems solved?* Redox Biol, 2015. **6**: p. 372-85.
160. Dent, P., et al., *MAPK pathways in radiation responses.* Oncogene, 2003. **22**(37): p. 5885-96.
161. Meyer, M., R. Schreck, and P.A. Baeuerle, *H2O2 and antioxidants have opposite effects on activation of NF-kappa B and AP-1 in intact cells: AP-1 as secondary antioxidant-responsive factor.* EMBO J, 1993. **12**(5): p. 2005-15.
162. Chandel, N.S., et al., *Mitochondrial reactive oxygen species trigger hypoxia-induced transcription.* Proc Natl Acad Sci U S A, 1998. **95**(20): p. 11715-20.
163. Valko, M., et al., *Free radicals, metals and antioxidants in oxidative stress-induced cancer.* Chem Biol Interact, 2006. **160**(1): p. 1-40.
164. Cadet, J. and J.R. Wagner, *DNA base damage by reactive oxygen species, oxidizing agents, and UV radiation.* Cold Spring Harb Perspect Biol, 2013. **5**(2).
165. Berlett, B.S. and E.R. Stadtman, *Protein oxidation in aging, disease, and oxidative stress.* J Biol Chem, 1997. **272**(33): p. 20313-6.
166. Halliwell, B. and S. Chirico, *Lipid peroxidation: its mechanism, measurement, and significance.* Am J Clin Nutr, 1993. **57**(5 Suppl): p. 715S-724S; discussion 724S-725S.
167. Murphy, M.P., *How mitochondria produce reactive oxygen species.* Biochem J, 2009. **417**(1): p. 1-13.
168. Paravicini, T.M. and R.M. Touyz, *NADPH oxidases, reactive oxygen species, and hypertension: clinical implications and therapeutic possibilities.* Diabetes Care, 2008. **31 Suppl 2**: p. S170-80.
169. Nauseef, W.M., *Biological roles for the NOX family NADPH oxidases.* J Biol Chem, 2008. **283**(25): p. 16961-5.
170. Huang, Y., et al., *Cystine-glutamate transporter SLC7A11 in cancer chemosensitivity and chemoresistance.* Cancer Res, 2005. **65**(16): p. 7446-54.
171. Miyamoto, Y., et al., *Oxidative stress caused by inactivation of glutathione peroxidase and adaptive responses.* Biol Chem, 2003. **384**(4): p. 567-74.

172. Imai, H. and Y. Nakagawa, *Biological significance of phospholipid hydroperoxide glutathione peroxidase (PHGPx, GPx4) in mammalian cells.* Free Radic Biol Med, 2003. **34**(2): p. 145-69.
173. Stockwell, B.R., et al., *Ferroptosis: A Regulated Cell Death Nexus Linking Metabolism, Redox Biology, and Disease.* Cell, 2017. **171**(2): p. 273-285.
174. Yang, W.S., et al., *Peroxidation of polyunsaturated fatty acids by lipoxygenases drives ferroptosis.* Proc Natl Acad Sci U S A, 2016. **113**(34): p. E4966-75.
175. Hayano, M., et al., *Loss of cysteinyl-tRNA synthetase (CARS) induces the transsulfuration pathway and inhibits ferroptosis induced by cystine deprivation.* Cell Death Differ, 2016. **23**(2): p. 270-8.
176. Angeli, J.P.F., et al., *Ferroptosis Inhibition: Mechanisms and Opportunities.* Trends Pharmacol Sci, 2017. **38**(5): p. 489-498.
177. Cao, J.Y. and S.J. Dixon, *Mechanisms of ferroptosis.* Cell Mol Life Sci, 2016. **73**(11-12): p. 2195-209.
178. Bannai, S., H. Tsukeda, and H. Okumura, *Effect of antioxidants on cultured human diploid fibroblasts exposed to cystine-free medium.* Biochem Biophys Res Commun, 1977. **74**(4): p. 1582-8.
179. Gao, M., et al., *Glutaminolysis and Transferrin Regulate Ferroptosis.* Mol Cell, 2015. **59**(2): p. 298-308.
180. Gaschler, M.M. and B.R. Stockwell, *Lipid peroxidation in cell death.* Biochem Biophys Res Commun, 2017. **482**(3): p. 419-425.
181. Magtanong, L., P.J. Ko, and S.J. Dixon, *Emerging roles for lipids in non-apoptotic cell death.* Cell Death Differ, 2016. **23**(7): p. 1099-109.
182. Fearnhead, H.O., P. Vandenabeele, and T. Vanden Berghe, *How do we fit ferroptosis in the family of regulated cell death?* Cell Death Differ, 2017. **24**(12): p. 1991-1998.
183. Yang, W.S., et al., *Regulation of ferroptotic cancer cell death by GPX4.* Cell, 2014. **156**(1-2): p. 317-331.
184. Lee, Y.S., et al., *Ferroptosis-induced Endoplasmic Reticulum Stress: Crosstalk Between Ferroptosis and Apoptosis.* Mol Cancer Res, 2018.
185. Tarangelo, A., et al., *p53 Suppresses Metabolic Stress-Induced Ferroptosis in Cancer Cells.* Cell Rep, 2018. **22**(3): p. 569-575.

186. Ursini, F., et al., *Purification from pig liver of a protein which protects liposomes and biomembranes from peroxidative degradation and exhibits glutathione peroxidase activity on phosphatidylcholine hydroperoxides.* Biochim Biophys Acta, 1982. **710**(2): p. 197-211.
187. Dhingra, R., A. Ravandi, and L.A. Kirshenbaum, *Ferroptosis: Beating on Death's Door.* Am J Physiol Heart Circ Physiol, 2017.
188. Jiang, L., et al., *Ferroptosis as a p53-mediated activity during tumour suppression.* Nature, 2015. **520**(7545): p. 57-62.
189. Baba, Y., et al., *Protective effects of the mechanistic target of rapamycin against excess iron and ferroptosis in cardiomyocytes.* Am J Physiol Heart Circ Physiol, 2018. **314**(3): p. H659-H668.
190. Bayeva, M., et al., *mTOR regulates cellular iron homeostasis through tristetraprolin.* Cell Metab, 2012. **16**(5): p. 645-57.
191. Pagliarini, R., W. Shao, and W.R. Sellers, *Oncogene addiction: pathways of therapeutic response, resistance, and road maps toward a cure.* EMBO Rep, 2015. **16**(3): p. 280-96.
192. Bridges, C.B., *The Origin of Variations.* 1922.
193. DOBZHANSKY, T., *Genetics of natural populations; recombination and variability in populations of Drosophila pseudoobscura.* Genetics, 1946. **31**: p. 269-90.
194. O'Neil, N.J., M.L. Bailey, and P. Hieter, *Synthetic lethality and cancer.* Nat Rev Genet, 2017. **18**(10): p. 613-623.
195. Lord, C.J. and A. Ashworth, *PARP inhibitors: Synthetic lethality in the clinic.* Science, 2017. **355**(6330): p. 1152-1158.
196. WARBURG, O., *On the origin of cancer cells.* Science, 1956. **123**(3191): p. 309-14.
197. Kaye, S.B., *New antimetabolites in cancer chemotherapy and their clinical impact.* Br J Cancer, 1998. **78 Suppl 3**: p. 1-7.
198. Tsun, Z.Y. and R. Possemato, *Amino acid management in cancer.* Semin Cell Dev Biol, 2015. **43**: p. 22-32.
199. Zecchini, V. and C. Frezza, *Metabolic synthetic lethality in cancer therapy.* Biochim Biophys Acta, 2017. **1858**(8): p. 723-731.

200. Nijman, S.M., *Synthetic lethality: general principles, utility and detection using genetic screens in human cells.* FEBS Lett, 2011. **585**(1): p. 1-6.
201. Di Nicolantonio, F., et al., *Replacement of normal with mutant alleles in the genome of normal human cells unveils mutation-specific drug responses.* Proc Natl Acad Sci U S A, 2008. **105**(52): p. 20864-9.
202. Schneider, C.A., W.S. Rasband, and K.W. Eliceiri, *NIH Image to ImageJ: 25 years of image analysis.* Nat Methods, 2012. **9**(7): p. 671-5.
203. Bolte, S. and F.P. Cordelieres, *A guided tour into subcellular colocalization analysis in light microscopy.* J Microsc, 2006. **224**(Pt 3): p. 213-32.
204. Wek, R.C., B.M. Jackson, and A.G. Hinnebusch, *Juxtaposition of domains homologous to protein kinases and histidyl-tRNA synthetases in GCN2 protein suggests a mechanism for coupling GCN4 expression to amino acid availability.* Proc Natl Acad Sci U S A, 1989. **86**(12): p. 4579-83.
205. Zaborske, J.M., et al., *Genome-wide analysis of tRNA charging and activation of the eIF2 kinase Gcn2p.* J Biol Chem, 2009. **284**(37): p. 25254-67.
206. Fang, Y., et al., *Phosphatidic acid-mediated mitogenic activation of mTOR signaling.* Science, 2001. **294**(5548): p. 1942-5.
207. English, D., Y. Cui, and R.A. Siddiqui, *Messenger functions of phosphatidic acid.* Chem Phys Lipids, 1996. **80**(1-2): p. 117-32.
208. Chen, Y., Y. Zheng, and D.A. Foster, *Phospholipase D confers rapamycin resistance in human breast cancer cells.* Oncogene, 2003. **22**(25): p. 3937-42.
209. Exton, J.H., *Regulation of phospholipase D.* Biochim Biophys Acta, 1999. **1439**(2): p. 121-33.
210. Fang, Y., et al., *PLD1 regulates mTOR signaling and mediates Cdc42 activation of S6K1.* Curr Biol, 2003. **13**(23): p. 2037-44.
211. Sun, Y., et al., *Phospholipase D1 is an effector of Rheb in the mTOR pathway.* Proc Natl Acad Sci U S A, 2008. **105**(24): p. 8286-91.
212. Casaluce, F., et al., *Selumetinib for the treatment of non-small cell lung cancer.* Expert Opin Investig Drugs, 2017. **26**(8): p. 973-984.

213. Cramer, S.L., et al., *Systemic depletion of L-cyst(e)ine with cyst(e)inase increases reactive oxygen species and suppresses tumor growth.* Nat Med, 2017. **23**(1): p. 120-127.
214. Sobolewski, C., et al., *The role of cyclooxygenase-2 in cell proliferation and cell death in human malignancies.* Int J Cell Biol, 2010. **2010**: p. 215158.
215. Agarwal, S., et al., *p53 Deletion or Hotspot Mutations Enhance mTORC1 Activity by Altering Lysosomal Dynamics of TSC2 and Rheb.* Mol Cancer Res, 2016. **14**(1): p. 66-77.
216. Vogelstein, B., et al., *Cancer genome landscapes.* Science, 2013. **339**(6127): p. 1546-58.
217. Vivanco, I. and C.L. Sawyers, *The phosphatidylinositol 3-Kinase AKT pathway in human cancer.* Nat Rev Cancer, 2002. **2**(7): p. 489-501.
218. Roberts, P.J. and C.J. Der, *Targeting the Raf-MEK-ERK mitogen-activated protein kinase cascade for the treatment of cancer.* Oncogene, 2007. **26**(22): p. 3291-310.
219. Koppenol, W.H., P.L. Bounds, and C.V. Dang, *Otto Warburg's contributions to current concepts of cancer metabolism.* Nat Rev Cancer, 2011. **11**(5): p. 325-37.
220. Ananieva, E., *Targeting amino acid metabolism in cancer growth and anti-tumor immune response.* World J Biol Chem, 2015. **6**(4): p. 281-9.
221. Richards, M.W., et al., *Structural basis of N-Myc binding by Aurora-A and its destabilization by kinase inhibitors.* Proc Natl Acad Sci U S A, 2016. **113**(48): p. 13726-13731.
222. Arkin, M.R., Y. Tang, and J.A. Wells, *Small-molecule inhibitors of protein-protein interactions: progressing toward the reality.* Chem Biol, 2014. **21**(9): p. 1102-14.
223. Fawal, M.A., M. Brandt, and N. Djouder, *MCRS1 binds and couples Rheb to amino acid-dependent mTORC1 activation.* Dev Cell, 2015. **33**(1): p. 67-81.
224. Kaelin, W.G., *The concept of synthetic lethality in the context of anticancer therapy.* Nat Rev Cancer, 2005. **5**(9): p. 689-98.
225. Barbie, D.A., et al., *Systematic RNA interference reveals that oncogenic KRAS-driven cancers require TBK1.* Nature, 2009. **462**(7269): p. 108-12.

226. Possik, P.A., et al., *Parallel in vivo and in vitro melanoma RNAi dropout screens reveal synthetic lethality between hypoxia and DNA damage response inhibition.* Cell Rep, 2014. **9**(4): p. 1375-86.
227. Scholl, C., et al., *Synthetic lethal interaction between oncogenic KRAS dependency and STK33 suppression in human cancer cells.* Cell, 2009. **137**(5): p. 821-34.
228. Dillon, B.J., et al., *Incidence and distribution of argininosuccinate synthetase deficiency in human cancers: a method for identifying cancers sensitive to arginine deprivation.* Cancer, 2004. **100**(4): p. 826-33.
229. Trachootham, D., J. Alexandre, and P. Huang, *Targeting cancer cells by ROS-mediated mechanisms: a radical therapeutic approach?* Nat Rev Drug Discov, 2009. **8**(7): p. 579-91.
230. Dixon, S.J. and B.R. Stockwell, *The role of iron and reactive oxygen species in cell death.* Nat Chem Biol, 2014. **10**(1): p. 9-17.
231. Harris, I.S., et al., *Glutathione and thioredoxin antioxidant pathways synergize to drive cancer initiation and progression.* Cancer Cell, 2015. **27**(2): p. 211-22.
232. Nisimoto, Y., et al., *Nox4: a hydrogen peroxide-generating oxygen sensor.* Biochemistry, 2014. **53**(31): p. 5111-20.